Negative microfilm received from university

66–5071

GAD EL–MAWLA, Ahmed El–Said Mohamed, 1933–
A STUDY OF HYDROCARBON CONCENTRATION AND TEMPERATURE PROFILES THROUGH A STEADY–STATE FLAME ADJACENT TO A WALL.

The University of Michigan, Ph.D., 1965
Engineering, mechanical

University Microfilms, Inc., Ann Arbor, Michigan

A STUDY OF HYDROCARBON CONCENTRATION AND TEMPERATURE PROFILES THROUGH A STEADY-STATE FLAME ADJACENT TO A WALL

by
Ahmed El-Said Mohamed Gad El-Mawla

A dissertation submitted in partial fulfillment
of the requirements for the degree of
Doctor of Philosophy in The
University of Michigan
1965

Doctoral Committee:

Professor William Mirsky, Chairman
Professor Vedat S. Arpaci
Professor Jay A. Bolt
Mr. Wayne A. Daniel, General Motors Corporation
Professor James A. Nicholls
Professor Gordon J. Van Wylen

ACKNOWLEDGMENTS

The author wishes to express his gratitude to Professor William Mirsky, Chairman of his doctoral committee. Appreciation is also expressed to the other members of the committee, Professor Gordon Van Wylen, Chairman of the Department of Mechanical Engineering, Professors Vedat Arpaci, Jay Bolt, James Nicholls, and Mr. Wayne Daniel from General Motors Corporation.

The financial support of General Motors' Engineering Staff is gratefully acknowledged.

Also, I wish to thank the Delco Moraine Division of General Motors Corporation for the supply of the porous plates.

Finally, I am extremely grateful to my wife and family for their sacrifices and patience.

DEDICATION

To my lovely Mother in gratitude for her sacrifice and patience.

TABLE OF CONTENTS

	Page
LIST OF TABLES	v
LIST OF FIGURES	vi
NOMENCLATURE	viii
INTRODUCTION	1
Chapter	
I. BRIEF SUMMARY OF PREVIOUS WORKS ON WALL QUENCHING	4
A. Thermal Theory	4
B. Diffusion Theory	6
II. ANALYSIS OF THE WALL EFFECT IN THE POROUS PLATE MODEL	9
III. EXPERIMENTAL EQUIPMENT	16
A. Air and Propane Supply Flow Systems	18
B. Burner Assembly	19
C. Instruments and Accessories	23
IV. TEST PROCEDURE	30
A. Operation of the Equipment	30
B. Data Collection	31
1. Sampling and Analysis	31
2. Temperature Measurement	33
3. Location of the Luminous Zone	33
C. Data Corrections	34
1. Flame Temperature	34
2. Hydrocarbon Concentration	35
D. Data Processing	37
V. DATA AND RESULTS	39
A. Flame Structure	39
B. Quench Distance	90
C. Mass of Unburned Hydrocarbons	
D. Effect of Pressure, Temperature, and Mixture Ratio on the Mass of the Unburned Hydrocarbons	100

TABLE OF CONTENTS (Concluded)

Chapter		Page
VI.	DISCUSSION	103
	A. Discussion of Results Obtained with Porous Plate Burner	103
	B. Comparison of Results with Engine Data	114
	1. Single Cylinder	116
	2. Multicylinder Engine	118
	3. Summary of Correlations	120
VII.	CONCLUSIONS AND RECOMMENDATIONS	121
	A. Conclusions	121
	B. Recommendations	121
Appendix		
A.	CALIBRATION OF GAS CHROMATOGRAPH	123
B.	FLOW RATE MEASUREMENTS AND CALIBRATION OF ORIFICES	148
C.	CALIBRATION CURVES FOR PRESSURE GAGES, IRON-CONSTANTAN THERMOCOUPLE, AND ROTAMETER	153
D.	LOCATION OF SAMPLING REGION WITH RESPECT TO PROBE TIP	159
E.	CHOICE OF SAMPLING PROBE	161
REFERENCES		162

LIST OF TABLES

Table		Page
I.	Figure Numbers Corresponding to Each Set of Wall and Flame Conditions	40
II.	Masses of Unburned Hydrocarbons per Unit Surface Area of Wall at Various Mixture Ratios and Wall Temperatures and Chamber Pressure of 1.0 Atmosphere	95
III.	Masses of Unburned Hydrocarbons per Unit Surface Area of Wall at Various Mixture Ratios and Wall Temperatures and Chamber Pressure of 2.0 Atmospheres	96
IV.	Mass of Unburned Hydrocarbons per Unit Area of Wall at Constant Plate Temperatures and Various Mixture Ratios and Chamber Pressures	100
V.	Values of Constant of Proportionality and Exponents Used in Eqn. (5.1)	102
VI.	Species and Their Mass Fractions in the Standard Sample	130
VII.	Relation Between Hydrocarbon Concentrations and Peak Heights	132
VIII.	Data for Orifice Calibration—Air	149
IX.	Data for Orifice Calibration—Propane	150

LIST OF FIGURES

Figure		Page
1.	Assumed quenching process when a flame propagates through a stagnant mixture to a solid wall.	11
2.	Qualitative flame temperature and concentration profiles in the model.	13
3.	Photograph of experimental equipment.	16
4.	Schematic diagram of experimental equipment.	17
5.	Close-up photograph showing flame, sampling probe and thermocouple.	19
6.	Porous-plate, flat-flame burner.	20
7.	Burner assembly.	22
8.	Sampling probe.	24
9.	Platinum, platinum-10% rhodium thermocouple.	27
10.	Schematic diagram for sampling procedure.	32
11.	Temperature correction factor for radiation losses.	36
12-35.	Flame structure. (a) Temperature profile. (b) Hydrocarbon concentration profiles.	42-88
36.	Effect of wall temperature on quench distance at various mixture ratios at a chamber pressure of 1.0 atmosphere.	91
37.	Effect of mixture ratio and plate temperature on the quench distance at a chamber pressure of 1.0 atmosphere.	92
38.	Three-dimensional representation of quench distance resulting from variations in both plate temperature and mixture ratio at a chamber pressure of 1.0 atmosphere.	94
39.	Three-dimensional representation of mass of unburned hydrocarbons per unit surface area at different plate temperatures and mixture ratios and chamber pressure of 1.0 atmosphere.	98

LIST OF FIGURES (Concluded)

Figure		Page
40.	Three-dimensional representation of mass of unburned hydrocarbons per unit surface area at different plate temperatures and mixture ratios and chamber pressure of 2.0 atmospheres.	99
41.	Effect of chamber pressure on mass of unburned hydrocarbons at various ratios and plate temperatures.	101
42.	Hydrocarbon concentration profiles based on a uniform temperature.	105
43.	Comparison of porous plate model quench distance and dead space with dead space measurments by Kaskan.	107
44.	Relation between quench distance and burning velocity.	109
45.	Effect of engine deposits on instantaneous heat transfer through engine walls.	112
46.	Schematic diagram showing system for standard sample preparation.	124
47.	Relation between peak height and peak area for different hydrocarbon species.	128
48.	Relation between sample pressure and concentrations of different hydrocarbon species.	133
49-55.	Calibration curves for gas chromatograph.	134-146
56.	Discharge coefficient for propane flow.	151
57.	Discharge coefficient for air flow.	152
58-59.	Calibration curves for pressure gages.	154-155
60.	Calibration curve for iron-constantan thermocouples.	156
61.	Calibration curve for rotameter.	157
62.	Calibration curve for iron-constantan thermocouple used to measure plate temperature.	158

NOMENCLATURE

A	Area
a	General exponent
B	Fraction of molecules which must react for flame to continue to propagate, in Eqn. (6.1) due to Simon and Belles
B_i	Term arising from radical recombination in gas phase, in Eqn. (6.2) due to Tanford and Pease
b	General exponent
C	Concentration
C_D	Orifice discharge coefficient
C.F.	Temperature correction factor
C_p	Specific heat
D	Diffusion coefficient
d	Diameter
d*	Quench diameter, distance in Eqn. (1.1) due to Potter and Berlad. Quench diameter, distance in Eqn. (1.4) due to Simon and Belles
e	Efficiency of the wall to prevent active particles which collide with it from returning to gas phase as chain carriers
F	View factor
F_1	Factor in Eqn. (1.1)
F_2	Factor in Eqn. (1.2)
G	Geometric factor in Eqn. (1.1)
h	Convective coefficient of heat transfer, Btu/hr°F-ft^2
K	Constant of proportionality, Eqn. (5.1)
k	Conductive coefficient of heat transfer, Btu/hr°F-ft
k_i	Specific rate constant for the reaction of the active particle
M	Mass, lb

NOMENCLATURE (Continued)

$\dot{M}$	Rate of mass production of hydrocarbons, lb/hr
M_F	Mole fraction
M_W	Molecular weight
m	Mass per unit surface area, lb/ft^2
$\dot{m}$	Mass flow rate, lb/hr
N	Avogadro's number
N_F	Number of fuel molecules
n	Moles of combustion products per mole of fuel
P	Pressure
p	Partial pressure
Q	Mole fraction of potential combustion product in Eqn. (6.2)
Qd	Quench distance as used in the present work
R	Gas constant
T	Temperature
U	Velocity
V	Volume
$\dot{V}$	Volume flow rate
w	Rate of disappearance of fuel (molecules/cc-sec)
x	distance
x*	Quench distance in Eqn. (1.2) due to Friedman
Y	Mole fraction
Δ	Finite difference
δ	Dead space, distance
ϵ	Emissivity
ρ	Mass density
σ	Boltzmann constant

τ	Frequency of collision
ϕ	Equivalence ratio

SUBSCRIPTS

B	Barometric condition
c	Condition at thermocouple
DS	Downstream
f	Condition at flame
F	Designation for fuel
i	Designation for species
ig	Ignition conditions
m	Mixture
o	Initial condition
p	Condition at the plate
UP	Upstream condition
v	Condition in sampling valve
w	Condition at the wall
1,2	Reference to locations

ABBREVIATIONS

AC	Alternating current
cc	Cubic centimeter
F/A	Fuel-air ratio
ID	Inside diameter
mv	Millivolt
NBS	National Bureau of Standards
Nu	Nusselt number
OD	Outside diameter
psi	Pounds per square inch
μv	Microvolt

INTRODUCTION

Air pollution in some cities of the United States has long been both a nuisance and a health hazard. Until recently the pollution was largely the result of factory fumes and smoke from homes and buildings using bituminous coal for heating. Exhaust emission from motor vehicles was a relatively insignificant contributor. In recent years, however, the rapidly increasing number of motor vehicles and concentration of population in urban areas have made the automobile a major factor in air pollution.

Automobile manufacturers have been conducting intense research to reduce the quantity of unburned hydrocarbons emitted in the exhaust gases. Perhaps the most important phase of the research is the study of the combustion conditions which result in the hydrocarbon residues.

In one such study, Daniel[9] noted that the unburned hydrocarbons which he found in the exhaust of a spark-ignited engine were likely due to the flame quenching at the relatively cool walls of the combustion chamber. The phenomenon of flame quenching, which will herein after be called "wall quenching" may be defined as the effect of the wall in suppressing flame propagation and retarding chemical reaction in a thin layer along the wall. Visual evidence of wall quenching is manifested by a dark zone between the luminous part of the flame and the wall.

The evidence that wall quenching is one of the major sources of hydrocarbon emission led to the present study. Because of the complex-

ities involved in the use of an engine for studying wall quenching, a model was used. The model was chosen to simulate, with a steady state process, the transient process which occurs when a flame approaches a solid wall and is quenched. The model consisted of a porous-plate, flat flame burner enclosed in a cylindrical chamber. This model produced a one-dimensional, steady-state flame propagating towards a relatively cool wall.

In selecting the model it was assumed that:

1. Chemical reactions that might occur as the mixture passes through the porous plate are negligible.

2. The effect of mixture velocity on the flame structure could be made negligible by using a mixture velocity much lower than the flame velocity which would occur in the mixture if no wall were present.

It was believed that with these two assumptions the model would permit a study of the wall effect on flame propagation.

Propane was used as a fuel to permit comparison with earlier studies using the same fuel. It also simplified the measurement of hydrocarbons because of the relatively small number of intermediates resulting from its reaction with air. In addition, there is a similarity between it and the higher saturated hydrocarbons with regard to burning velocity, minimum ignition energy, flame temperature, and low oxidation characteristics.

The objectives of this study were:

1. To devise a method for measuring the quantities of unburned hydrocarbons resulting from the influence of the wall on the flame in a porous-plate, flat-flame burner.

2. To study the quantity and distribution of unburned hydrocarbons in the vicinity of the wall under controlled variations of wall temperatures, mixture ratio, and chamber pressure.

3. To gain a better understanding of the phenomenon of wall quenching.

The quantity of unburned hydrocarbons in the quench zone in the porous plate burner is presented as mass per unit area of wall surface. The results were obtained for a range of equivalence ratios from 0.945 to 1.26, wall temperatures between 190 and 600°F, and for chamber pressures of 1.0 and 2.0 atmospheres.

CHAPTER I

BRIEF SUMMARY OF PREVIOUS WORKS ON WALL QUENCHING

Wall quenching has been studied by many research workers from both theoretical and experimental approaches. Although their interests arose from various fields of application, they were primarily studying wall quenching as a natural phenomenon.

Various methods were used to indicate the extent of the quenching effect. Two of the principal methods were linear measurement of the dark zone, or "dead space," between the wall and the luminous part of the flame, and measurement of the minimum opening through which a flame will propagate. There were also two theories regarding the mechanism by which a flame is presumed to be quenched: the thermal theory, in which the cooling effect of the wall is the principal deterrent to propagation, and the diffusion theory, in which free radical chain carriers necessary to propagation are said to be deactivated by the wall.

Since many of the earlier studies assumed either the thermal theory or the diffusion theory, the literature is presented under those two headings.

A. THERMAL THEORY

In the studies of Von Karman[52] on laminar flames near a cold wall, a flame temperature profile was computed from a hypothetical situation in which a flame was assumed to be propagating in a large tube filled

with a combustible gaseous mixture. In these studies "dead space" was defined as the distance between the wall and a point in the flame front corresponding to the "ignition temperature." Using the properties of three different fuels, methane, propane, and propylene, it was found that the ratio of the dead space to the flame thickness remained approximately the same. From this, it was concluded that thermal conduction is the fundamental process which determines the behavior of the flame near the wall. It was also stated that the computed values of the dead space agreed with Kaskan's[32] measured values of the distance between the visible part of the flame and the wall in a similar model.

In the study of wall quenching by Wohl[54] a flame was assumed to be established parallel to a cool wall by igniting a combustible gaseous mixture passed through a cooled porous wall. In this study it was found that the distance from the wall at which a flame can be maintained is a function of the amount of heat transferred to the wall; that is, should the heat transfer increase a greater distance would be necessary to reduce the heat transfer and maintain the flame, otherwise the flame would be extinguished.

In Potter and Berlad's[44] study of flame quenching in tubes, it was assumed that the flame was quenched when the amount of heat retained by the flame is equal to or less than a constant fraction of the total heat produced by the flame. From this study the following equation for quench distance was derived.*

*Symbols are defined in the Nomenclature.

$$d^* = \left[\frac{F_1 G N k Y}{C_p w}\right]^{1/2} \qquad (1.1)$$

Friedman[15] derived an equation for quench distance in a rectangular opening between two plates based on the assumption that quenching occurs when the rate of heat generation in the flame is equal to or less than the rate of heat transfer to the walls. The distance between the two plates at the quenching condition which Friedman called the quench distance, is expressed as follows:

$$x^* = \frac{2k}{U_f C_p}\left[\frac{1}{F_2}\frac{T_f - T_{ig}}{T_{ig} - T_o}\right]^{1/2} \qquad (1.2)$$

The effect of wall temperature and mixture pressure on the quench distance was studied experimentally by Friedman[16] and the following relation was obtained,

$$x^* \propto \frac{1}{p^a T^b} \qquad (1.3)$$

where

a and b equal 0.76 and 0.85, respectively, for lean mixtures

and 0.91 and 0.50, respectively, for rich mixtures.

B. DIFFUSION THEORY

Simon and Belles[49] examined a simple active particle mechanism of quenching, in which active particles are considered to be generated in the flame and destroyed on the container walls. The following equation

for the quench diameter was derived from the assumption that in order for the flame to propagate through a tube, the number of effective collisions per unit volume necessary for the flame to propagate must be less than the total number of effective collisions per unit volume before the chain carriers are destroyed at the wall.

$$d^* = \left[\frac{32 A P}{\sum_i \frac{p_i}{D_i \tau_i e_i}} \right]^{1/2} \qquad (1.4)$$

In this equation the quench distance depends partly on the nature of the wall surface through the coefficient "e." Simon and Belles attempted to determine experimentally the effect of the nature of the wall, but found the results conflicting. Either no effect or a very slight effect was observed.

To compare the thermal and diffusion theories with experimental results, Potter and Berlad,[46] using an argon-oxygen-propane flame, replaced the argon with helium. It was found that the thermal quenching equation satisfactorily predicted the effect of the replacement of argon with helium on quench distance, while a similar equation for the diffusion effect did not; however, the authors stated that the success of the thermal equation should not be interpreted as conclusive evidence that flame quenching is an entirely thermal process, since many approximations were made in deriving the expressions for both theories.

Although neither the thermal theory nor the diffusion theory is es-

tablished as the exclusive process by which wall quenching occurs, these earlier studies provided some information useful to the present work. They showed that wall quenching is affected by the properties and temperature of the wall, free flame speed, initial mixture temperature, and the geometry of the wall surface.

In these earlier studies the hydrocarbons resulting from wall quenching were not measured. The present study arose from the need for a measurement of the quantity of hydrocarbons resulting from wall quenching. Such data is of interest to researchers working on the air pollution problem.

CHAPTER II

ANALYSIS OF THE WALL EFFECT IN THE POROUS PLATE MODEL

At present, theoretical work concerning wall quenching involves many assumptions which arise from the fact that very little is known either about the structure of a flame or about the mechanism by which a flame is quenched. In order to determine the amounts and types of hydrocarbons resulting from wall quenching by theoretical methods it would be necessary to have the following information:

a. The mechanism by which reaction occurs in the flame.

b. The rates of all the reactions occurring in the flame and their dependence on temperature and concentration.

c. The transport properties of all components of the mixture and their dependence on temperature.

d. The effect of the wall in breaking chain carriers.

e. The "environmental conditions" for which the information is desired.

Very little of this information is available for any actual system, and even if it were, the derivation of a mathematical solution to obtain the desired results would be quite difficult. Consequently, an experimental approach was used.

Experimental approaches also encounter some difficulties; studying wall quenching in an internal combustion engine, which is of current practical interest, is complicated by the fact that the quenching occurs during a short-time period and in a very thin layer along the wall[9]

(about 0.005 in.). Outside the engine a flame approaching a solid wall is also quenched in a relatively short time. To simplify experimental measurements a model was designed for the present study to produce a steady-state, flat, laminar flame propagating towards a flat, smooth-surfaced porous plate which serves as a quench wall.

This model was chosen in the attempt to elucidate what happens in the actual transient wall-quenching process in which a propane-air flame propagates through a stagnant mixture toward a solid, relatively cool wall and is finally quenched by that wall. In the latter system, as long as the flame is at a sufficiently large distance from the wall, unreacted propane and air exist ahead of the flame, and burned products, which likely include only a negligible amount of unoxidized hydrocarbons, exist behind the flame. As the flame approaches the wall, heat is transferred to the wall and active particles may be destroyed by the wall, until the flame is quenched and chemical reaction stops.

This transient process is qualitatively represented in Fig. 1. The curve in this figure represents the location of the flame with respect to the wall at various instances. Its slope at any point represents the flame speed at that point. As the flame approaches the wall its speed decreases until the flame is completely quenched. Between the region where the free flame exists and the point where quenching is complete there is a region in which partial quenching may be assumed to exist. Within this region the degree of quenching varies from zero to full quenching.

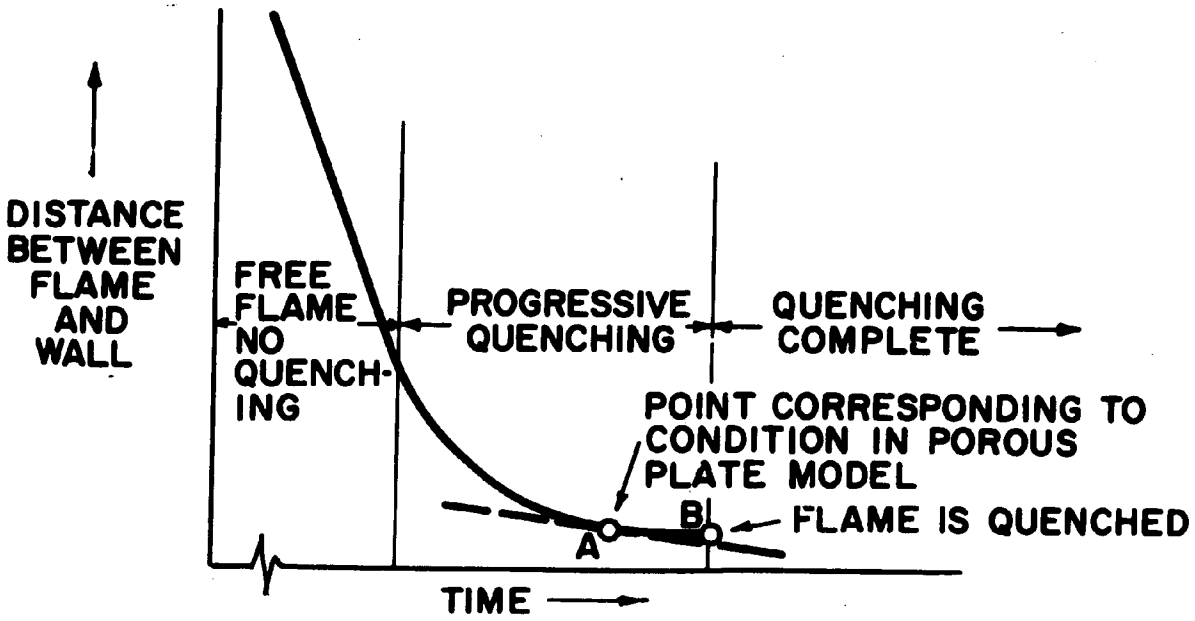


Fig. 1. Assumed quenching process when a flame propagates through a stagnant mixture to a solid wall.

In the model, the mixture passing through the porous plate opposes the flame motion and keeps it at a distance from the plate at which the modified flame speed equals the mixture velocity. Since the ratio of mixture velocity to the flame velocity equals the ratio of the slope at this distance to the slope for the free flame, at any given mixture velocity the point at which the modified flame speed equals the mixture velocity can be located on the curve.

The location of the point relates the mixture velocity to the degree of quenching, and it can be seen that as the ratio of mixture velocity to free flame velocity decreases the location of the point approaches that of complete quenching. Consequently it was necessary to maintain a low mixture velocity in the model in order to approach the

point of complete quenching. In general, the ratio of mixture velocity to free flame velocity was about 1:16. The point for this ratio is indicated by A on the curve in Fig. 1.

Obviously a flame approaching a solid wall and being quenched is a transient process. The porous plate model used in the present study is an attempt to simulate this transient system with a steady-state system.

How well the model simulates the system for which it was intended depends upon how well the gas composition profiles in the vicinity of the porous plate under steady-state conditions (point A, Fig. 1) agree with the gas composition profiles in the vicinity of a solid wall at the instant a flame is quenched (point B, Fig. 1). Such a comparison was outside the scope of the present investigation.

Qualitative flame temperature and concentration profiles in the model are shown in Fig. 2. The model permitted quantitative measurements of the unburned hydrocarbons resulting from the wall effect at various flame and wall conditions. The flame condition was controlled by varying the fuel-air ratio and the chamber pressure while the wall condition was varied by cooling the porous plate. Gas samples were withdrawn from the flame and analyzed, and the quantity of the different hydrocarbon species determined. The samples were taken at measured distances from the wall through the flame up to a point where no hydrocarbons were detected. Concentration profiles for each hydrocarbon were constructed and were used to compute the total mass of unburned hydrocarbons

per unit area of wall surface.

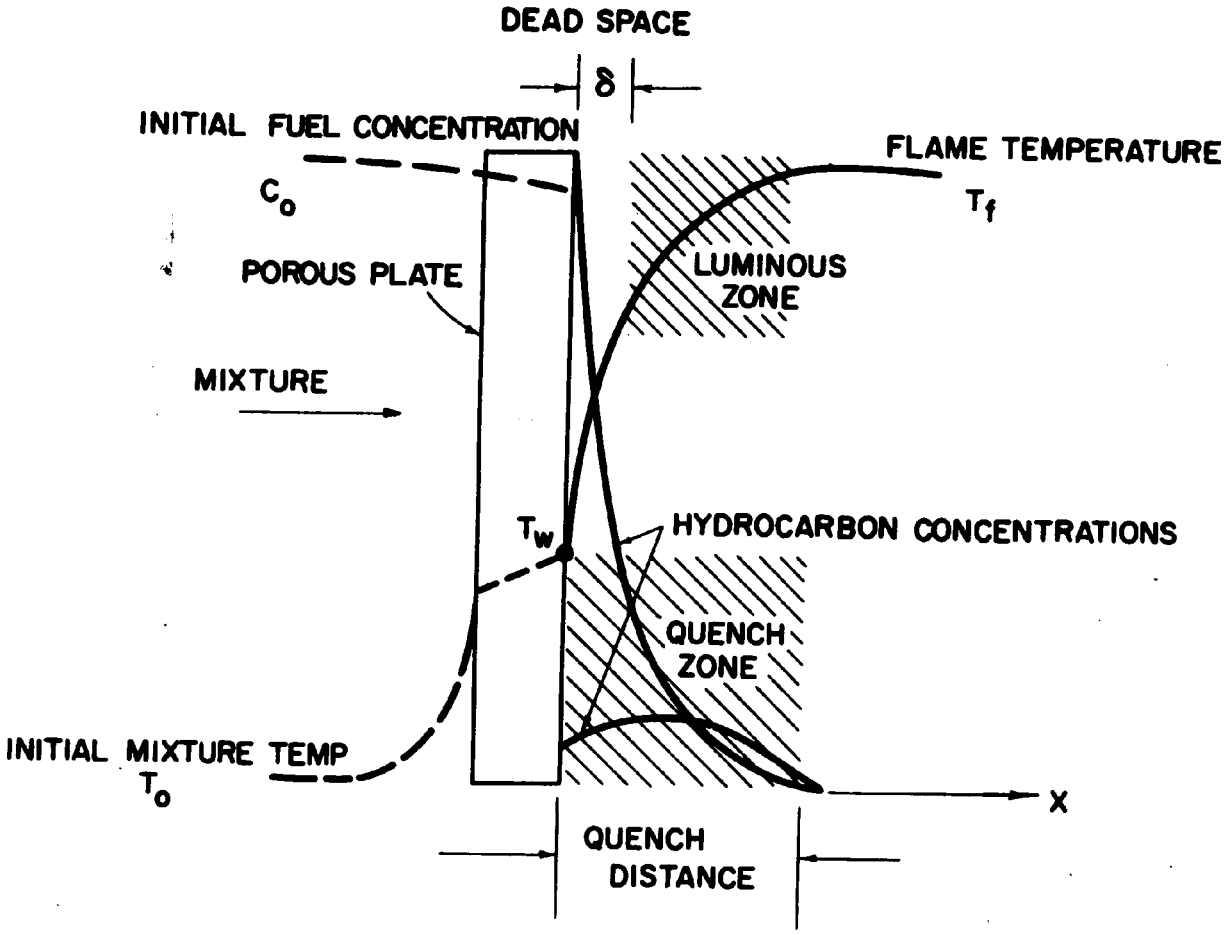


Fig. 2. Qualitative flame temperature and concentration profiles in the model.

The quench zone was taken to be the zone containing all of the detectable quantities of unburned hydrocarbons. The quench distance, therefore, was taken to be the distance between the wall and the end of the quench zone as shown in Fig. 2. This is not synonymous with the term quench distance as used by other investigators in the earlier studies. For the present work, however, this new definition is more significant because of the interest in the hydrocarbon residue resulting from wall quenching.

The distance from the wall at which the gas sample was taken was measured by optically locating the tip of the sampling probe. In addition to the hydrocarbon measurements, the model permitted optical measurements of the luminous zone thickness and dead space (distance between luminous zone and wall). Locating the luminous zone on the plotted hydrocarbon profiles provides a means for comparing the amount of unburned hydrocarbons in the dead space with the total amount of unburned hydrocarbons contained in the quench zone. In discussing the results, quench distance is used as a measure of the wall quenching effect. The effect of the wall in quenching the flame is expressed in mass of unburned hydrocarbons per unit area of wall surface.

Temperature profiles were constructed for the different flame and wall conditions. These were used to correct for the change in density between the various regions of the flame and the sampling valve. In addition they were used to locate the region where quenching occurs with respect to the preheating and the reaction zones in the flame front. The preheating zone is defined as the region where the second derivative of the temperature with respect to distance is positive, i.e., $\frac{\partial^2 T}{\partial x^2} > 0$, which means that a mass element in this region gains thermal energy by conduction from the hotter gas element downstream faster than it loses energy to the cooler elements upstream. The reaction zone is defined as the zone where the temperature curve has a negative second derivative which results from thermal energy generation.

In earlier studies,[15,16,44,49] it was found that variations in wall

temperature and free flame speed affected the extent of the quenching process. The thermal theory of quenching is based on the fact that the wall is a heat sink which absorbs some of the thermal energy necessary to sensitize the approaching gases so that they may join in the reaction when a suitably high temperature is reached. The thermal conductivity and the surface temperature of the wall affect the amount of heat transfer from the flame to the wall. In the model the surface temperature of the wall was varied while the conductivity remained constant.

Variations in free flame speed were produced by varying the chamber pressure and the fuel-air mixture ratio. Changes in mixture ratio cause changes in the reaction rates (i.e., flame speed) which are manifested by changes in flame thickness. The quench distance being related to flame thickness (see Fig. 2) as the flame expands or contracts the quench distance increases or decreases and the total mass of unburned hydrocarbons for the same pressure becomes greater or smaller.

The results obtained from the study of the wall quenching process in the porous-plate, flat-flame burner provided the following data, some of which were not previously available:

a. Concentration profiles of the unburned hydrocarbons;

b. flame temperature profiles;

c. position of the luminous zone; and

d. measurement of quench distances.

CHAPTER III

EXPERIMENTAL EQUIPMENT

The experimental equipment was composed of:

a. Air and fuel supply flow systems;

b. burner assembly; and

c. measuring and recording instruments.

The complete test equipment is shown in Fig. 3. A schematic diagram of the equipment is shown in Fig. 4.

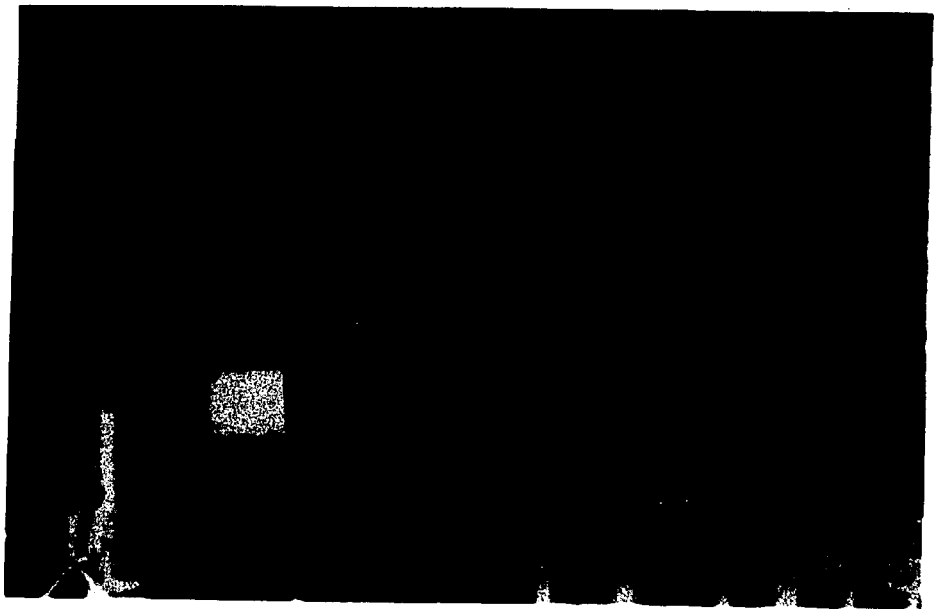


Fig. 3. Photograph of experiment equipment.

Homogeneous mixtures of air and propane were fed to a porous-plate, flat-flame burner placed in a cylindrical, thick-walled chamber. The gases emerging from the surface of the porous plate were ignited by an ignition coil suspended above the burner.

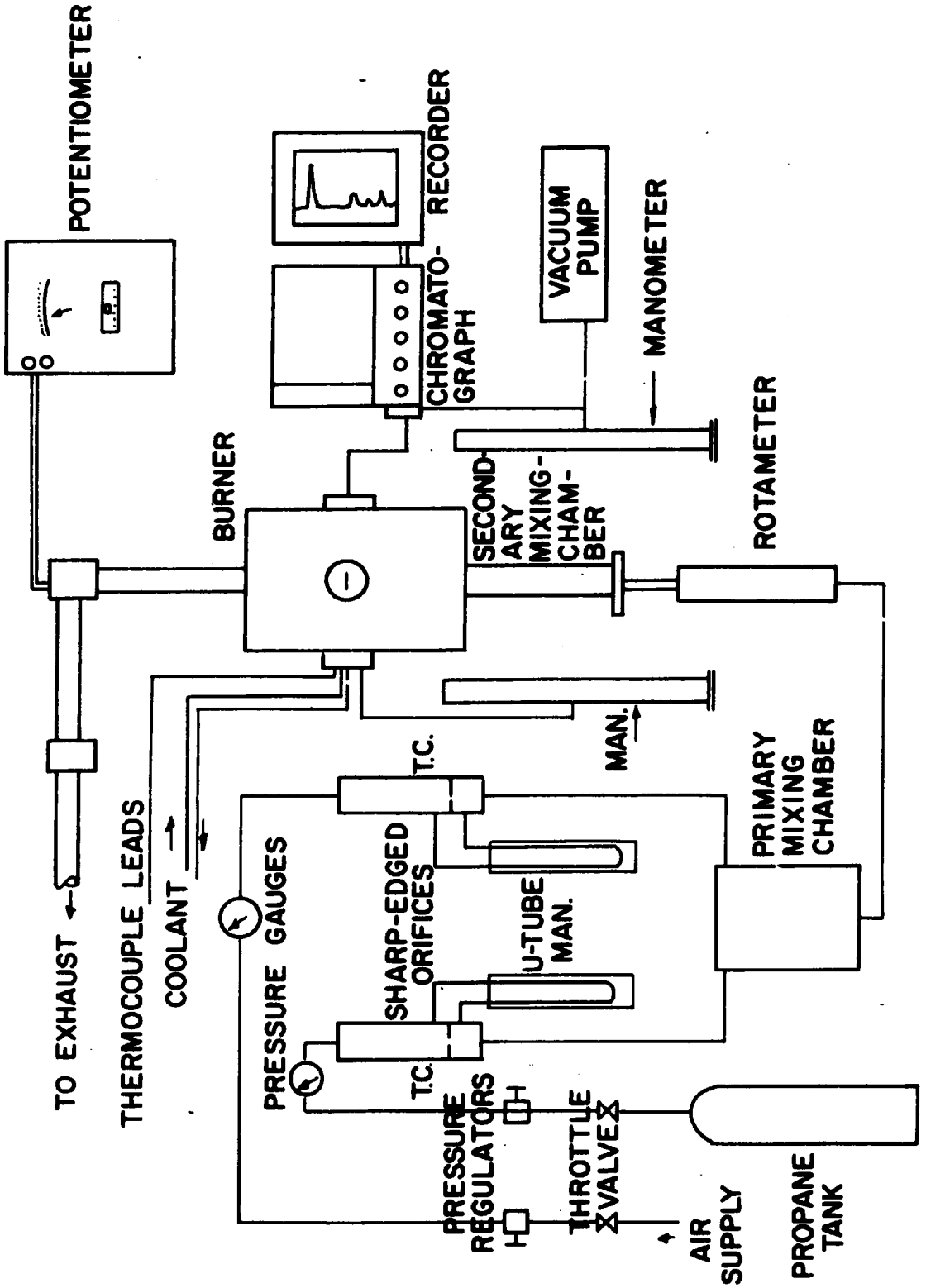


Fig. 4. Schematic diagram of experimental equipment

A sampling probe was mounted solidly to the wall of the chamber and positioned to take gas samples through the flame close to the center of the burner. Samples were taken at various distances from the top of the burner and conducted through stainless steel tubing to a gas chromatograph which analyzed the hydrocarbon constituents of the sample.

A fine, platinum, platinum-10% rhodium thermocouple (0.001 in. diameter) was used to measure the flame temperature.

Flame and quench wall conditions were varied by varying plate temperature, propane-air mixture ratio, and chamber pressure.

A. AIR AND PROPANE SUPPLY FLOW SYSTEM

Air for the mixture was obtained from the laboratory supply header at about 90 psig and 76°F. It was fed to the system through a shut-off valve. Air pressure in the conducting tube was controlled by a regulator located downstream from the shut-off valve. The air passed into a cylinder in which there were two chambers separated by a sharp-edged orifice. A U-tube manometer was attached to both chambers in the cylinder to measure the pressure drop across the orifice. From the cylinder the air passed through a variable-area, critical-flow orifice, formed by a small needle valve, to a primary mixing chamber. This needle valve was used to control the flow rate. The propane, 99.5% pure, was obtained from a bottle and reached the primary mixing chamber through a line similar to that used for air.

The air and propane were partially mixed in the primary mixing

chamber. This chamber was an aluminum cylinder of 8 in. diameter and 18 in. long in which four baffles were equally spaced. Holes in the baffles were arranged to promote mixing of the gases.

From the primary mixing chamber the mixture passed to a secondary mixing chamber located at the bottom of the burner assembly. This chamber was a tube 2 in. in diameter and 20 in. long filled with 1/4 in. diameter glass beads. This improved the possibility of a homogeneous mixture of air and propane immediately prior to entering the burner.

B. BURNER ASSEMBLY

The porous-plate, flat-flame burner head shown in Figs. 5 and 6 was

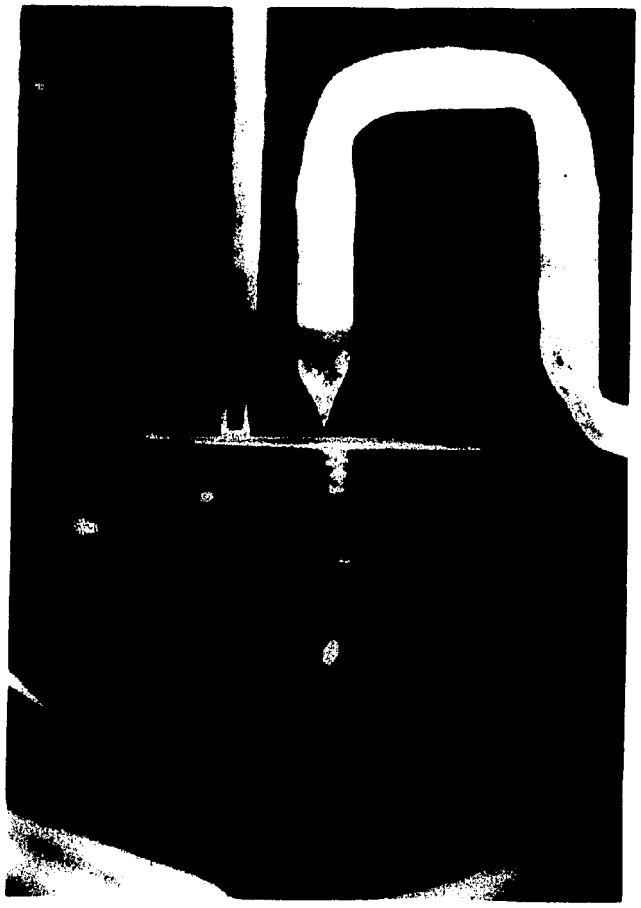


Fig. 5. Close-up photograph showing flame, sampling probe, and thermocouple.

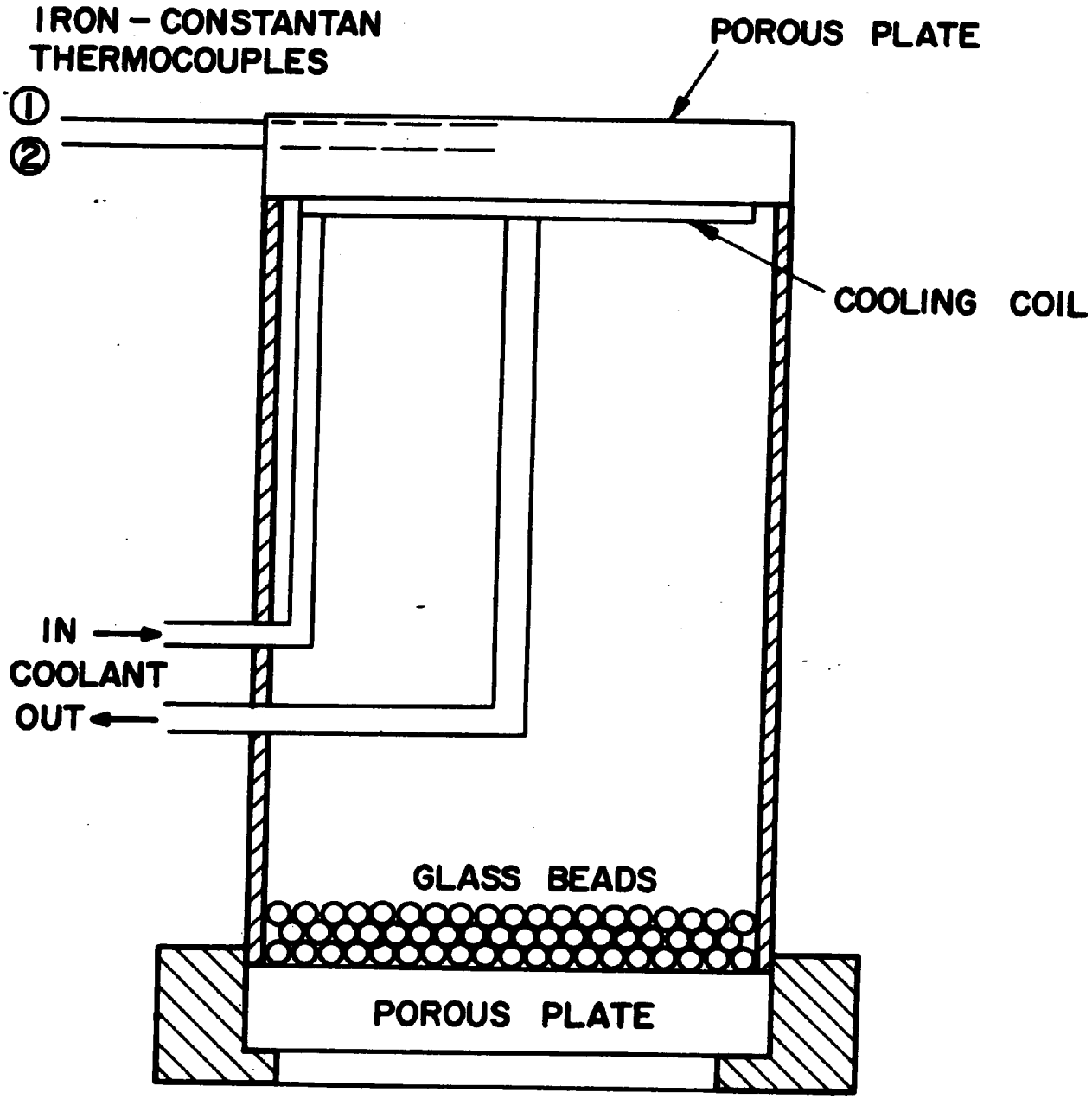


Fig. 6. Porous-plate, flat-flame burner.

constructed of a 2 in. diameter, 6 in. long copper tube having at the upper and lower ends two 1/4 in. thick porous discs. These porous discs were made of sintered brass, 90% copper and 10% tin. (Grade fine, produced by Delco-Moraine Division of General Motors.) The space between these discs was filled with 3 mm diameter glass beads to provide additional mixing and to produce an even flow to the top of the burner. In the top plate two 0.024 in. diameter iron-constantan thermocouples were inserted parallel to the surface. One was used to measure the surface temperature and the other the temperature at a distance 1/8 in. below the first thermocouple.

The burner top plate was cooled by a 1/8 in. diameter cooling coil soldered along the edge of the bottom surface. Air and water were used as coolants in order to give two distinctive cooling rates to the plate. The rate of flow of either coolant was controlled by a needle valve.

The ignition system used to start the flame was a nichrome wire heating coil connected to a variable AC electrical power source.

The burner was housed in a thick-walled, cylindrical iron-chamber 10 in. in diameter, 18 in. long, and 3/4 in. thick which was designed for internal pressures up to 1000 psi (Fig. 7). This chamber was provided with four identical 3-in. diameter viewing and access ports equally spaced around the chamber wall. In one pair of in-line ports there were pyrex windows used for viewing the flame. The other two ports were covered with plates which provided access for the sampling probe, the electrical ignition coil, and the thermocouple and the cool-

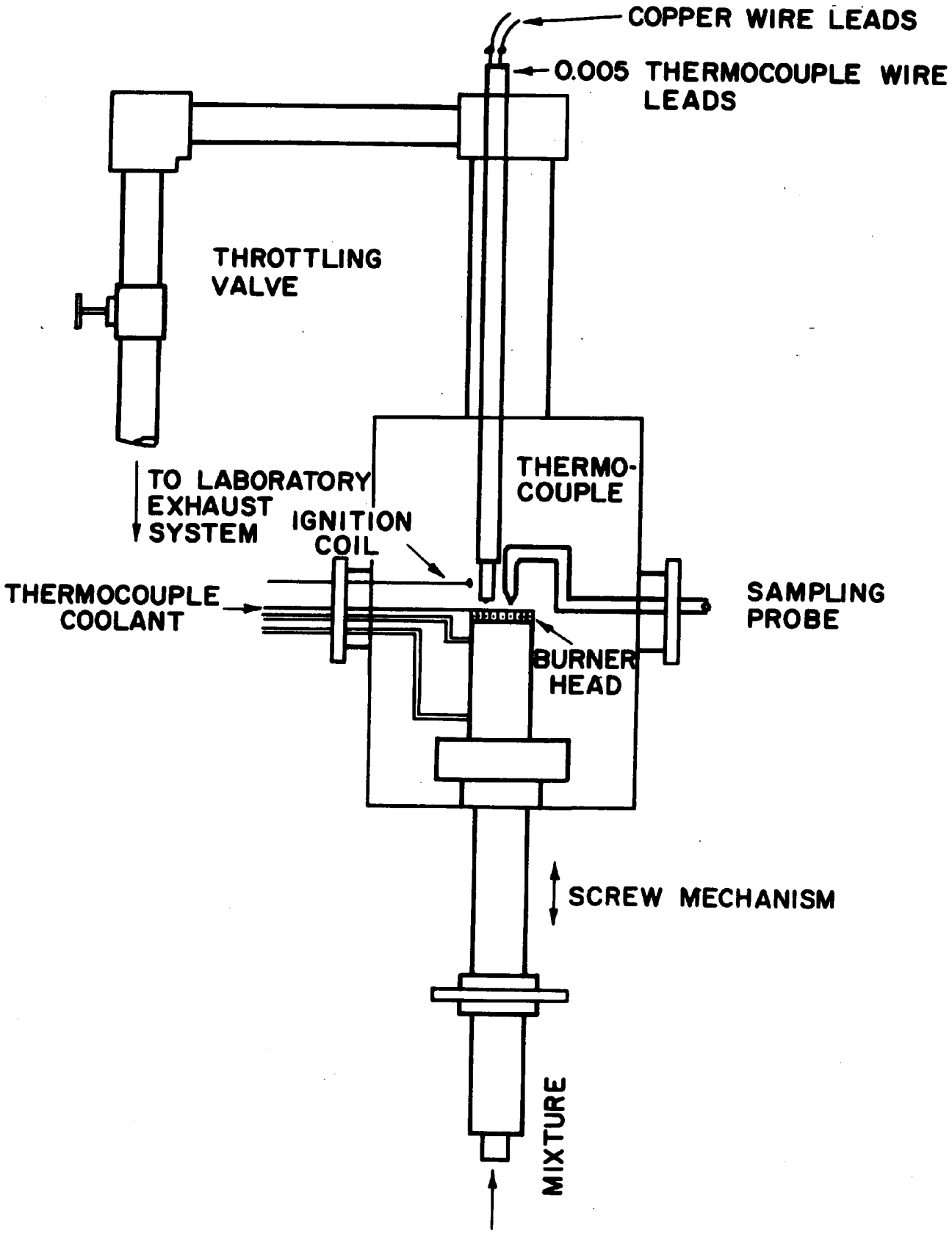


Fig. 7. Burner assembly.

ing coil leads to the burner top plate.

The burner head could be adjusted vertically without rotation, to vary the distance between the sampling probe and the porous plate, by a screw mechanism located at the bottom of the chamber. This mechanism permitted continuous vertical movement of the burner through a distance of about 1/2 in.

The exhaust from the burner was removed through a 3-in. diameter tube attached to the top of the chamber and connected to the laboratory main exhaust system.

C. INSTRUMENTS AND ACCESSORIES

The instruments and accessories were divided into two groups.

The first group included instruments to control and measure the propane and air flow rate, plate temperature, and chamber pressure.

The flow rates of air and propane were obtained by measuring the pressure drop across each of the sharp-edged orifices, and the pressure and temperature upstream from each orifice. Calibrations of the sharp-edged orifices were performed by a soap-bubble flowmeter technique (Appendix B).

Pressures of air and propane were measured upstream from the orifice with calibrated pressure gauges having a range of 0-60 psi (Figs. 58 and 59). Temperatures upstream were measured by calibrated iron-constantan thermocouples (Fig. 60) attached to a Brown multiple-point potentiometer. The pressure drop across each orifice was measured with

an 18-in. U-tube manometer filled with manometer fluid having a specific gravity of 1.025.

A calibrated rotameter (Fig. 61) was used to monitor the flow of the mixture to the burner. Calibration curves are shown in Appendix C.

The burner plate thermocouples were connected to the Brown potentiometer, model No. Y 153X62 (PSD12)-(W7)-(60)(G)(U).

The pressure in the burner chamber was controlled by a throttling valve on the exhaust pipe and was measured by a 36-in. U-tube mercury manometer.

The second group of instruments included those for taking gas samples from the flame and measuring the amounts of hydrocarbon constituents, measuring flame temperatures at different levels from the plate, and locating the sampling probe tip and luminous part of the flame with respect to the burner plate.

Gas samples were taken from the flame using a fine quartz probe (Fig. 8). This probe was made of 8 mm OD clear quartz tube, drawn down

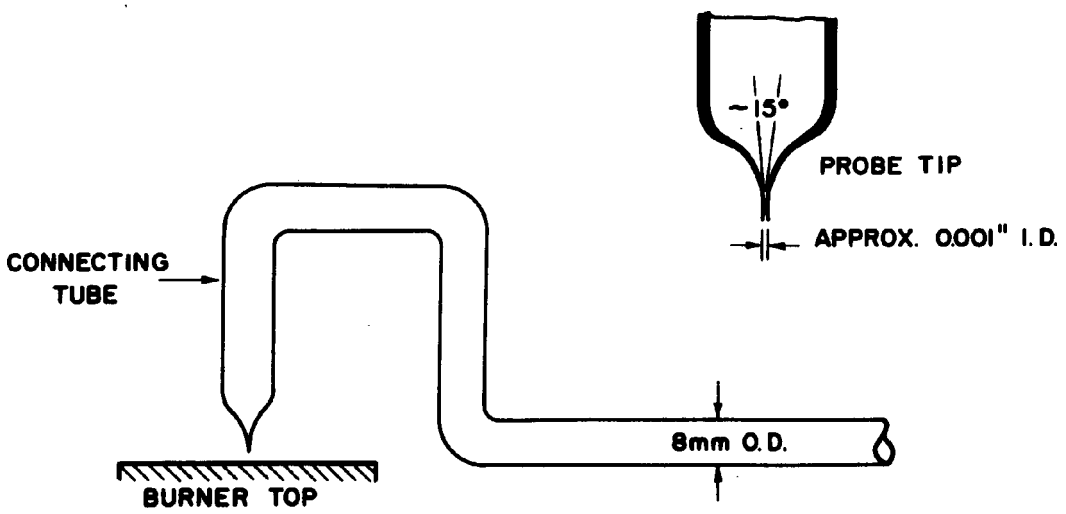


Fig. 8. Sampling probe.

to a conical tip of approximately 0.001 in. ID. The small size of the tip minimized any interference with the flame. Also, the rapidly expanding diameter of the tip promoted freezing of the gas sample. The conducting tube from the probe tip was designed to minimize the effect of exposure to the flame. The sampling probe was attached directly to the gas chromatograph through a temperature-controlled stainless steel tube.

A Model 800 Perkin-Elmer gas chromatograph, employing dual columns, was used to analyze and measure the hydrocarbon constituents in the gas samples. The chromatograph was used with a gas sampling valve of 1/4 cc volume. This valve introduced the gaseous samples into the carrier gas entering the sensing column. Perkin-Elmer Type "S" columns were used in this study. The columns were constructed of stainless steel tubing 1/8 in. in diameter and 2 m long. The separating agent, or fixed phase, in this column was di-2-ethylhexyl sebacate, which was mixed with silica gel. The silica gel acted both as an adsorbent and a support for the sebacate oil. Column "S" makes use of a modified adsorbent to increase column reproducibility and stability.

A flame ionization detector was used with this chromatograph. It employs a hydrogen flame as a means for ionizing the gas sample. By measuring the electrical conductivity of the ionized gas flame, the detector signals the passage of the various components of a sample. This kind of detector has many desirable features including wide dynamic range, linear response, high hydrocarbon sensitivity, no response to

CO, CO_2, H_2O, H_2, and N_2, low effective volume and resistance to contamination.

The output from the detector was recorded on a Leeds and Northrup Type "S" recorder. A microswitch was added to the gas sampling valve of the chromatograph to provide a mark on the recorder chart paper at the beginning of a run.

Nitrogen was used as a carrier gas at a pressure of 30 psig and a flow rate of 30 cc/min. The pressures of the air and hydrogen for the detector flame were maintained at 30 and 16.5 psig, respectively. These conditions gave adequate retention times for well separated, moderately sharp peaks. Under these conditions calibration curves were made to give a relation between hydrocarbon peak heights and their corresponding concentrations. Since under the test conditions the peak height was found to be directly proportional to the area under the peak (Appendix A), it was used as a measure of the mass of the different hydrocarbon species in the gas sample.

For calibration, a standard sample mixed in the laboratory was used (Appendix A).

To measure flame temperature profiles a thermocouple was constructed of 0.001 in. diameter platinum, platinum-10% rhodium wire (Fig. 9). The thermocouple bead was formed by fusing the wires in a tiny flame. The thermocouple wires were stretched between two quartz tubes 1.0 mm ID and 2.0 mm OD in such a way that the bead was centered between the quartz tubes. The thermocouple wires were held parallel to the flame

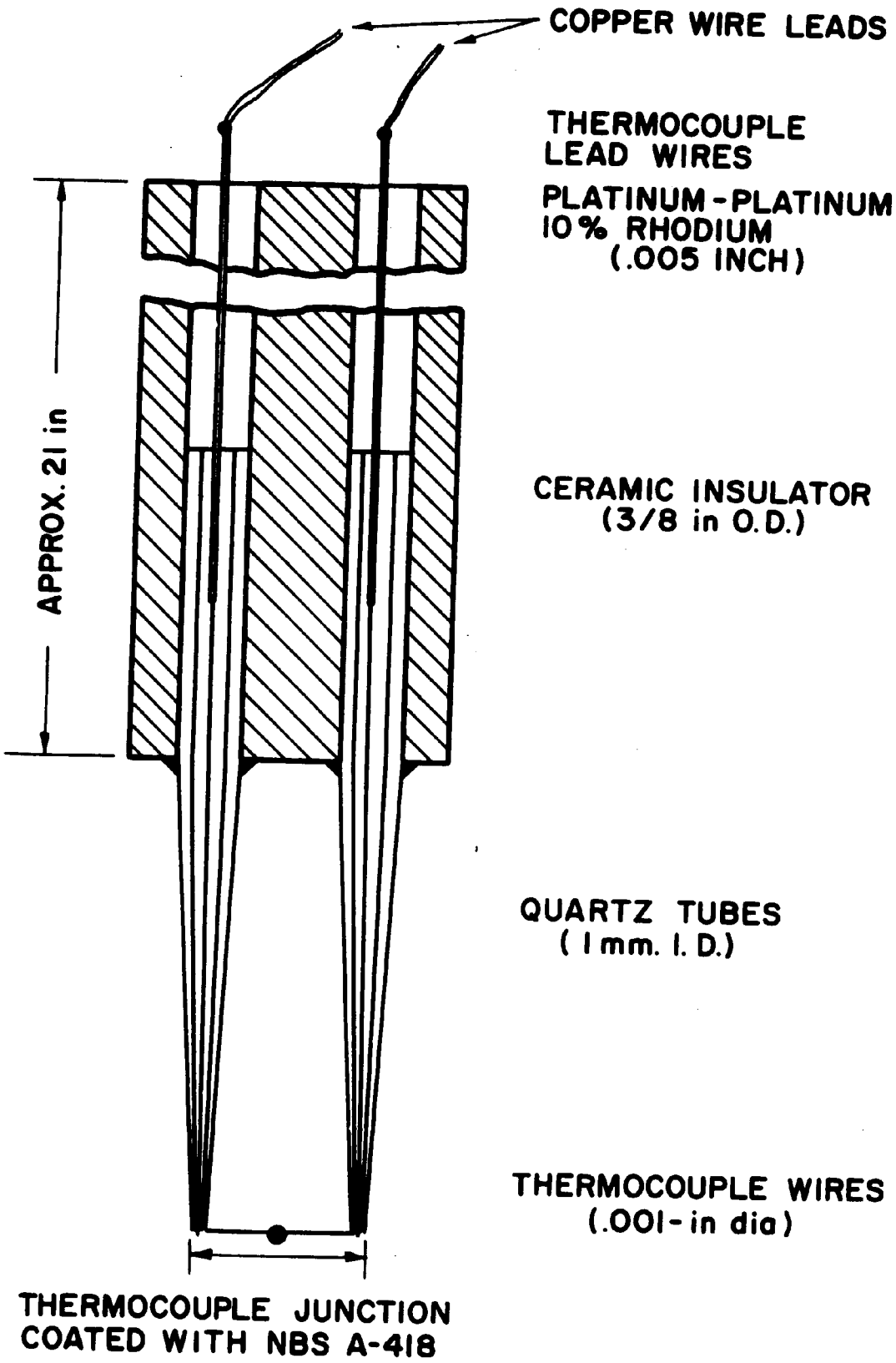


Fig. 9. Platinum, platinum-10% rhodium thermocouple.

to minimize heat conduction from the bead. Each quartz tube was drawn to a fine tip to minimize flame disturbance. These quartz tubes were cemented in a 3/8 in. diameter two-hole ceramic insulator. The insulator was supported at the top of the burner chamber and positioned so that the thermocouple bead was at the same level as the probe tip. In order to improve the resolution of the temperature profile measurements, the diameter of the bead was made small, less than 1/15 the thickness of the flame. This also reduced the radiation losses from the bead. To relieve internal stresses and structural changes due to welding, the thermocouple junction was electrically heated to high temperatures (not measured) for about one hour. (NBS recommended 1450°C for one hour.) The thermocouple junction was also coated with NBS A-418 ceramic coating to eliminate the catalytic effect.[41]

Copper wire was used to connect the 0.005 in. thermocouple leads to a Leeds and Northrup Model 8686 potentiometer which measured the EMF caused by the temperature difference between the thermocouple bead and the reference junction in the potentiometer. The potentiometer had a compensator which compensates for the temperature of the reference junction. The manufacturer gives the limit of error as $\pm$ 0.05% of the reading + 6 μv with the reference junction compensator.

A Kueffel and Esser optical micrometer was used to measure the distance of the thermocouple and the probe tip from the top of the burner. The same instrument was used to locate the luminous zone of the flame with respect to the burner.

This optical micrometer consisted of a plane-parallel plate, so arranged that it could be precisely tilted by the movement of a graduated drum. When the plate was tilted, the line of sight was moved parallel to itself. The micrometer drum was graduated in both directions to provide measurements from 0 to $\pm$ 0.100 in. with an accuracy of 0.001 in. In operation, this micrometer is attached to a Kueffel and Esser Paragon tilting level which consists of 12-3/4 in. telescope with 30X magnification, resolving 4 sec of arc.

CHAPTER IV

TEST PROCEDURE

A. OPERATION OF THE EQUIPMENT

The procedures listed below were followed for each day's test runs.

1. Make sure pressure regulators and throttle valves in propane and air supplies are closed.
2. Open shut-off valves.
3. Regulate air pressure to 60 psig.
4. Measure temperature of air upstream from the orifice.
5. Compute the pressure drop across the orifice required to get the desired flow rate.
6. Open the throttle valve until the required pressure is reached.
7. Repeat items 3-6 for the propane.
8. Ignite mixture emerging from the porous plate.
9. Allow the system to operate until plate temperature remains constant.
10. Adjust plate temperature by applying coolant.

While the plate is being brought to a constant temperature, the chromatograph may be prepared for operation as follows:

1. Adjust nitrogen pressure to 30 psig and check flow rates in the columns using a soap-bubble flowmeter.
2. Start the chromatograph.
3. Gradually increase oven temperature to 100°C.
4. Open hydrogen and air inlets to the detector.

5. Adjust air pressure to 30 psig and hydrogen to 16.5 psig.

6. Ignite detector flames.

7. Allow to stabilize for 1/2 hour.

8. Pass samples from atmosphere through chromatograph to saturate column with water vapor.

9. To calibrate, pass through the chromatograph different sized samples from the standard sample supply and record the peak heights corresponding to the concentrations of the various hydrocarbons.

The equipment is now ready for a test run.

B. DATA COLLECTION

1. Sampling and Analysis

For these tests it was found that there was no noticeable flame movement due to drift or acoustic oscillations. It was also assumed that the gas samples were obtained from the immediate location of the probe tip (Appendix D).

The procedure for taking gas samples was as follows:

1. Adjust burner level to give required distance between probe tip and burner plate.

2. Adjust plate temperature.

3. Adjust to required chamber pressure.

4. Rotate sampling valve to position I (Fig. 10).

5. Start vacuum pump.

6. Shut valve (1) and open valve (2).

7. Adjust the zero level on the manometer.

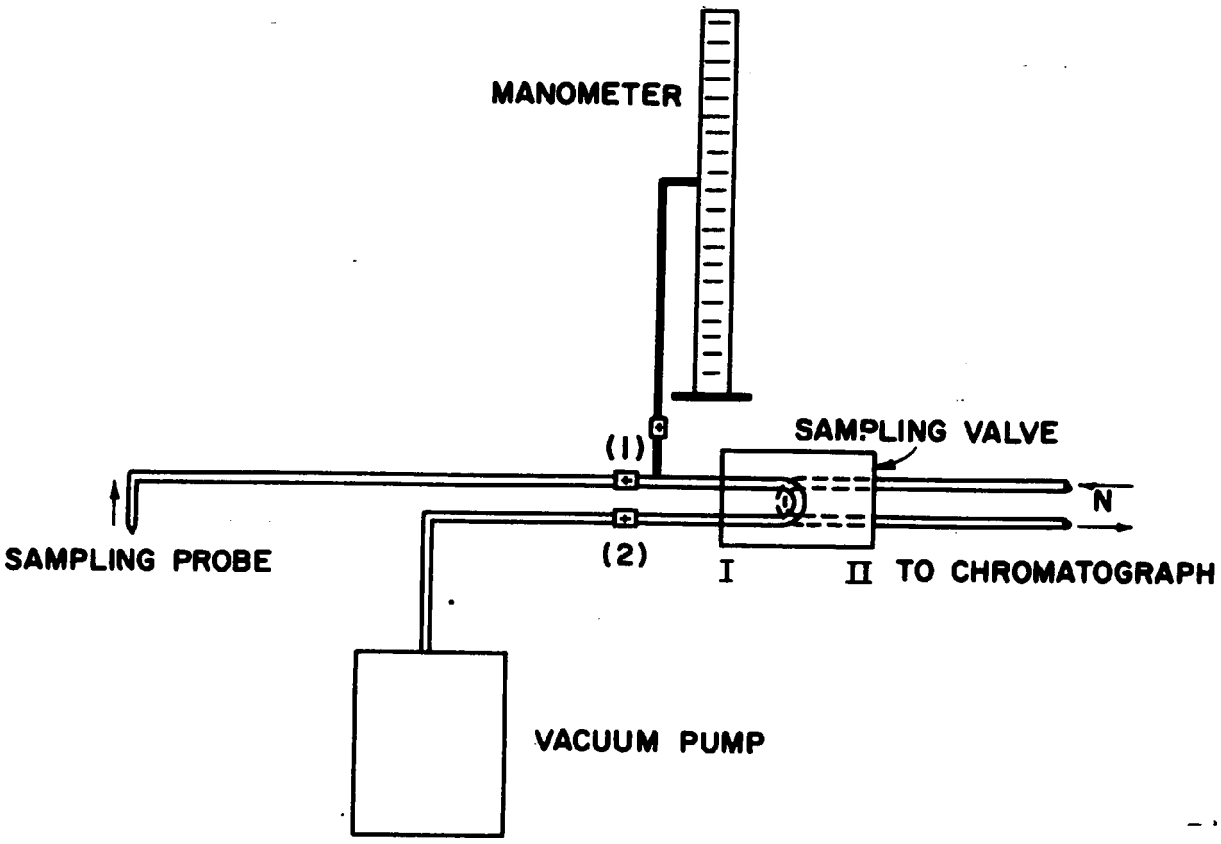


Fig. 10. Schematic diagram for sampling procedure.

8. Open valve (1) and allow to stand for 5 min to flush sampling lines with the gas sample.

9. Shut valve (2).

10. Allow gas samples to fill sampling valve to the required pressure (10 cm Hg) on the manometer.

11. Close valve (1).

12. Allow to stand for 2 min to stabilize gas sample temperature.

13. Read gas sample pressure on the manometer.

14. Start recorder chart.

15. Set required attenuation on chromatograph.

16. Rotate sampling valve to position II.

17. Record output of the chromatograph.

This concluded the procedure for one gas sample. Subsequent samples for the same flame condition were taken by repeating the procedure. Samples were taken at distances from near the plate to a point where there were no detectable hydrocarbons. The lowest concentration measured during these tests was for methane, 0.2×10^{-6} lbm/ft^3 or 30 ppm.

2. Temperature Measurement

The flame temperature thermocouple was mounted solidly in the chamber with its bead at the same level as the probe tip. While the gas sample was being processed in the chromatograph, the flame temperature for that sample was measured by the following procedure.

1. Turn potentiometer on.
2. Adjust the zero on the potentiometer.
3. Measure reference junction temperature.
4. Adjust the reference junction compensator.
5. Set potentiometer to read the output from thermocouple.

In addition to the temperatures at the various levels of the samples, other flame temperatures were taken through the entire flame at increments as small as 0.002 in. to better define the temperature profile and to indicate the spread of the temperature measurements.

3. Location of the Luminous Zone

Location of the luminous zone of the flame with respect to the

plate was determined by measuring the distance between the top of the porous plate and the upper and lower levels of the luminous zone with the Kueffel and Esser optical micrometer.

Although the borders of the luminous part are not sharply defined and cannot be precisely determined, the range of error is no more than 0.001-0.002 in. (luminous zone thickness from 0.015-0.035 in.). From the observations made during the test, the location of the luminous zone with respect to the plate remained constant during a given run.

C. DATA CORRECTIONS

1. Flame Temperature

To get the flame temperature it was necessary to correct the thermocouple temperature for radiation loss. The following method was used.

Because the thermocouple wires adjacent to the thermocouple junction were exposed to the same temperature region in the flame, conduction losses from the junction were minimized. The energy balance equation could then be written as:

Heat transferred to thermocouple from flame

= Heat radiated from the thermocouple to surroundings

Assuming that heat is transferred from the flame to the thermocouple by convection only, then

$$h\,A(T_f - T_c) = \sigma\,A\,F\,\epsilon(T_c^4 - T_w^4) \qquad (4.1)$$

as $T_c^4 \gg T_w^4$, T_w^4 can be neglected.

$F = 1.0$

ϵ for NBS A418 coating was taken as 0.5 (value given for green ceramic)

$$h(T_f - T_c) = 0.5\,\sigma\,T_c^4$$

For the thermocouple bead, assumed to be a sphere, the Nusselt Number can be taken equal to 2.0 when the Reynolds Number is less than 3.0.[28,30]

$$Nu = 2.0$$

$$\frac{hd}{k} = 2.0 \qquad (4.2)$$

Substituting the value of "h" from Eqn. (4.2) into Eqn. (4.1) gives

$$\frac{2k}{d}(T_f - T_c) = 0.5\,\sigma\,T_c^4$$

$$T_f = T_c + \frac{\sigma d}{4k}T_c^4 \quad .$$

The correction factor becomes,

$$C.F. = \frac{\sigma d}{4k}T_c^4 \quad .$$

Figure 11 gives the value of the correction factor at various temperature readings.

2. Hydrocarbon Concentration

Due to the change in the sample density from the flame to the sampling valve, it was necessary to compute actual hydrocarbon concentrations in the flame. From the calibration curves for the gas chromato-

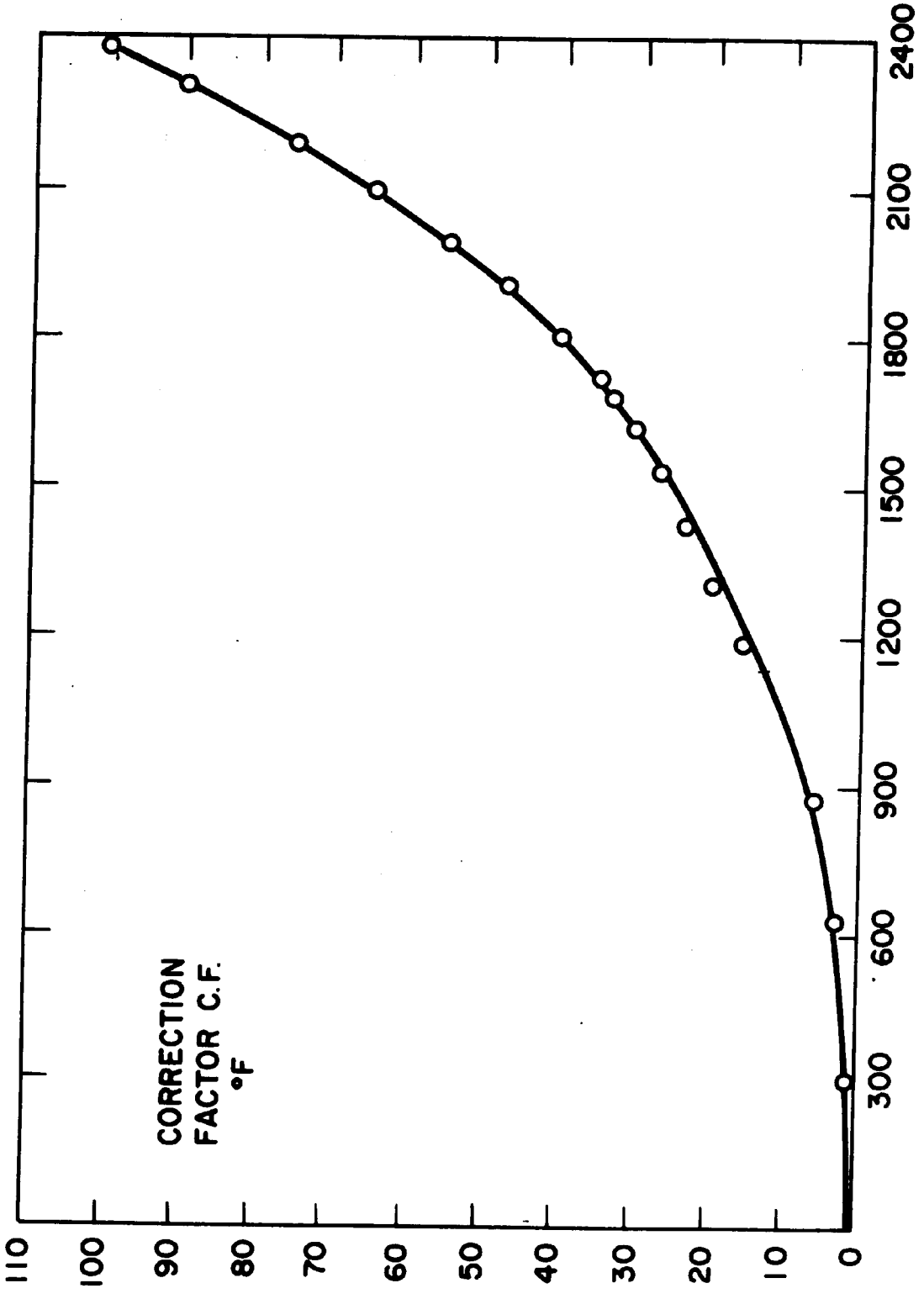


Fig. 11. Temperature correction factor for radiation losses.

graph, the concentrations of the different hydrocarbons were obtained in pounds per cubic feet at the sampling valve pressure and temperature for the measured peak heights. Since

$$C_{iv} = \frac{P_{iv}}{R_i T_v} \tag{4.3}$$

and in the flame

$$C_{if} = \frac{P_{if}}{R_i T_f} \tag{4.4}$$

division of Eqn. (4.4) by Eqn. (4.3) gives

$$\frac{C_{if}}{C_{iv}} = \frac{P_{if}}{P_{iv}} \frac{T_v}{T_f} .$$

As

$$\frac{P_{if}}{P_{iv}} = \frac{P_f}{P_v}$$

the concentration of the hydrocarbon in the flame will be given by,

$$C_{if} = C_{iv} \cdot \frac{P_f}{P_v} \cdot \frac{T_v}{T_f} . \tag{4.5}$$

D. DATA PROCESSING

Hydrocarbon concentration profiles were constructed in which the ordinate represented the concentrations of the hydrocarbon species in the flame in pounds per cubic feet and the abscissa the distance of the probe tip from the plate in inches. To process the data for these profiles,

the following procedure was used.

1. Temperatures from the thermocouple at different levels in the flame were corrected for radiation losses.

2. These values were used to construct flame temperature profiles.

3. From calibration curves for the gas chromatograph, concentrations corresponding to peak heights were obtained.

4. These hydrocarbon concentrations were converted to concentrations in the flame by use of Eqn. (4.5).

5. These values were used to construct the concentration profiles.

The area under each concentration profile was integrated to determine the mass per unit of surface area for each hydrocarbon type. These masses were added to obtain the total mass of hydrocarbons in the quench zone per unit area of wall.

CHAPTER V

DATA AND RESULTS

The results are presented under the headings shown below.

A. Flame Structure (Figures 12-35)

   a. Temperature profiles
   b. Hydrocarbon concentration profiles

B. Quench Distance (Figures 36-38)

   Graphs showing effect of wall temperature and equivalence ratio

C. Mass of Unburned Hydrocarbons

   a. Tables for each hydrocarbon species and total hydrocarbons at each condition (Tables II and III)
   b. Graphs of total mass of hydrocarbons for each condition (Figures 39 and 40)

D. Effect of Pressure, Temperature, and Fuel-Air Ratio

   Tables and curves showing these effects (Tables IV, V, and Fig. 41)

A. FLAME STRUCTURE

One of the objectives in the present work was to obtain the data necessary to describe the distribution of the hydrocarbons in the quench zone under various controlled flame and wall conditions.

The propane-air flame structure near the wall, as represented by hydrocarbon concentration profiles and the temperature profile, is presented for various wall temperatures, mixture ratios, and chamber pressures.

Chamber pressures of 1.0 and 2.0 atmospheres were used. At each chamber pressure, four mixture ratios were used while the plate tempera-

ture was varied with approximately 150°F increments from 200° to 600°F. Table I gives the figure number corresponding to each set of conditions.

TABLE I

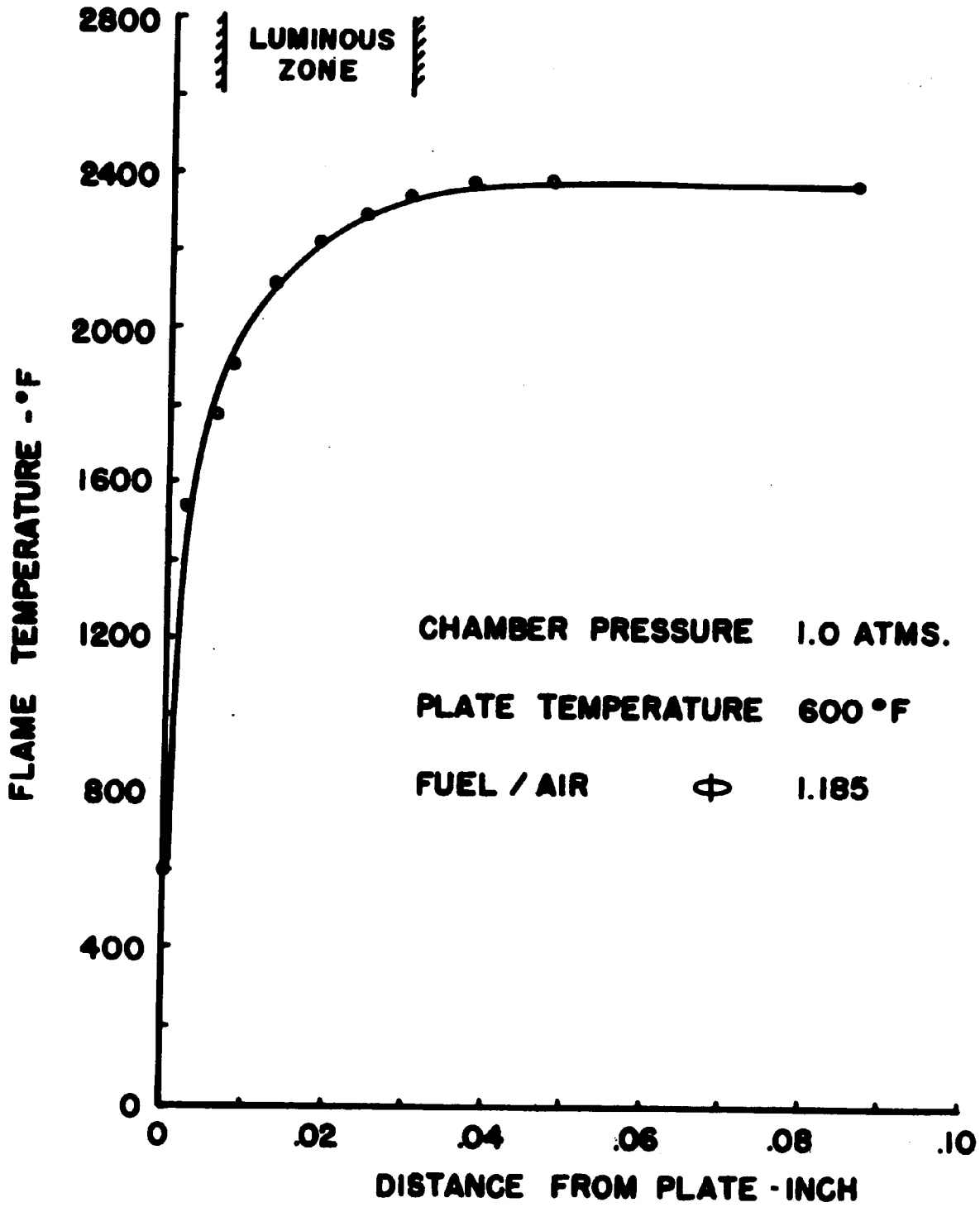
FIGURE NUMBERS CORRESPONDING TO EACH SET OF WALL AND FLAME CONDITIONS

Chamber Pressure, atm	Equivalence Ratio, ϕ	Plate Temperature, T_P °F	Figure Number
1.0	1.185	600	12
		490	13
		265	14
	1.105	585	15
		482	16
		255	17
	1.025	530	18
		420	19
		225	20
	0.945	460	21
		355	22
		190	23
2.0	1.26	565	24
		460	25
		240	26
	1.185	580	27
		435	28
		260	29
	1.105	570	30
		440	31
		255	32
	1.025	485	33
		405	34
		225	35

The temperature profiles show that there was a sharp drop in flame temperature near the wall. In the first few thousandths from the wall, the temperature gradient was as high as 6.0×10^5°F/inch (Fig. 26), and it decreased as the distance from the wall increased. The flame under the test conditions was found to reach its maximum temperature, i.e., equilibrium temperature, at a point near the end of the luminous zone. The equilibrium temperature varied with equivalence ratio; it reached its maximum value of about 2550°F at $\phi = 1.105$ and it was lower for both lean and rich mixtures. Also the equilibrium flame temperature varied with pressure; a drop of about 100°F was noticed as the chamber pressure was increased from 1.0 to 2.0 atmospheres. In general, the wall temperature had a small effect on the equilibrium flame temperature.

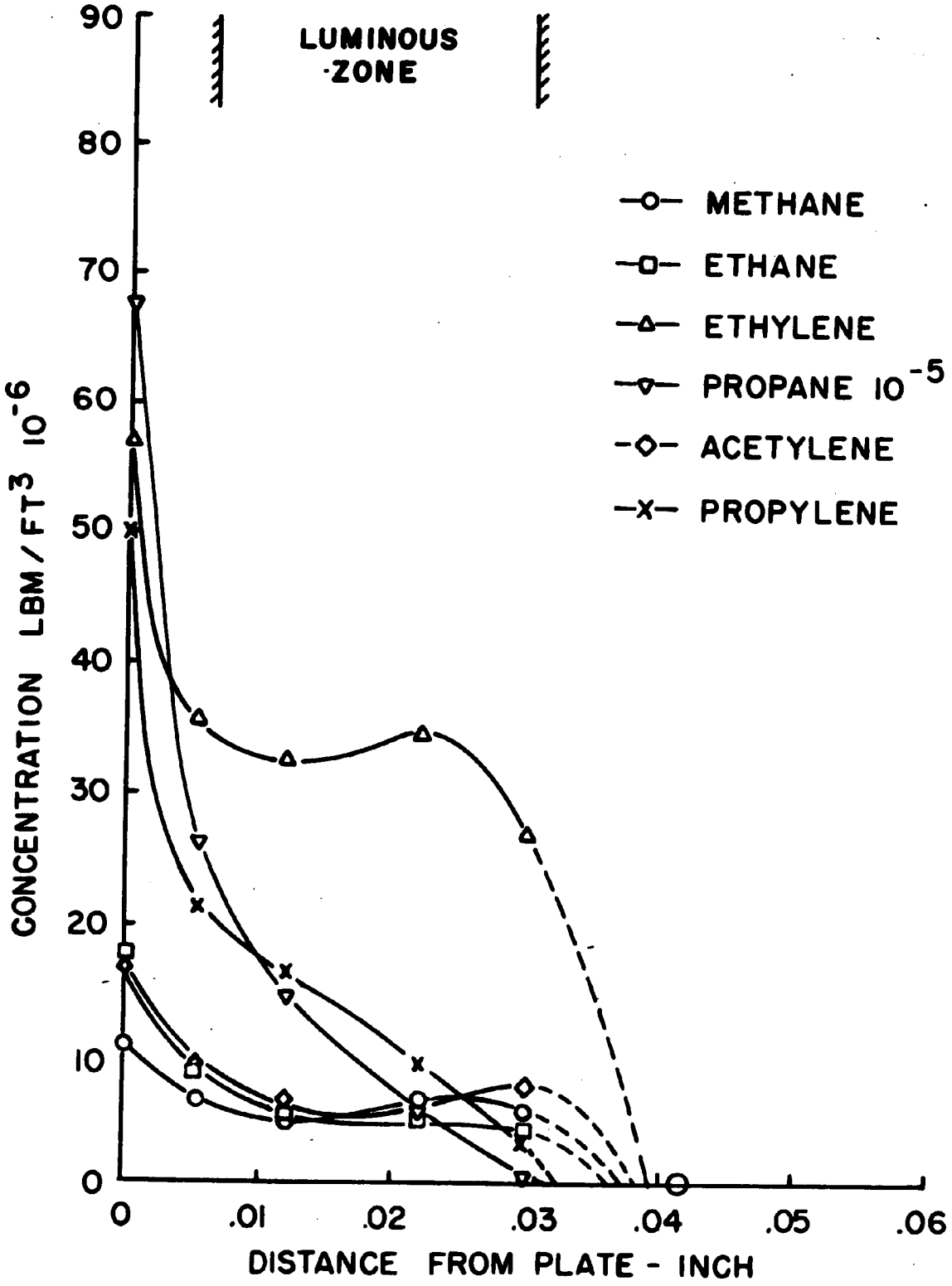
The hydrocarbon concentration profiles show that there were five intermediate hydrocarbon compounds present near the wall, namely, ethylene, propylene, acetylene, methane, and ethane. The order represents the relative magnitude of each with respect to the others. Changing the wall temperature, equivalence ratio, and chamber pressure did not change the number and the specific species of the intermediates. At a chamber pressure of 2.0 atmospheres, tailing of the concentration profiles was noticed near the end of the quench zone.

From the measurements of the luminous zone thickess of the flame it was noticed that the thickness varied with the equivalence ratio; it reached its minimum value at $\phi = 1.105$ and it increased for lean and rich mixtures.



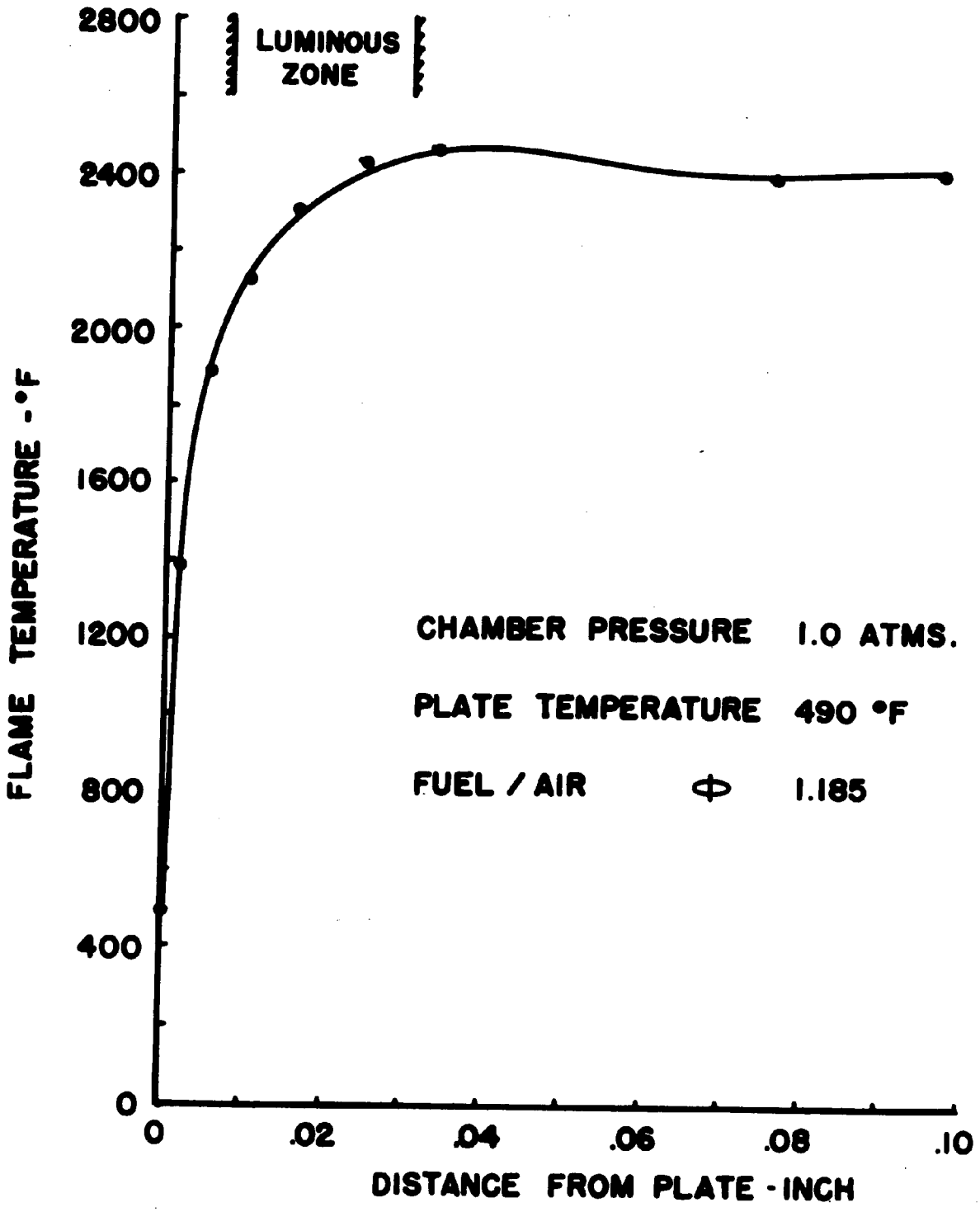
(a) Temperature profile

Fig. 12. Flame structure.



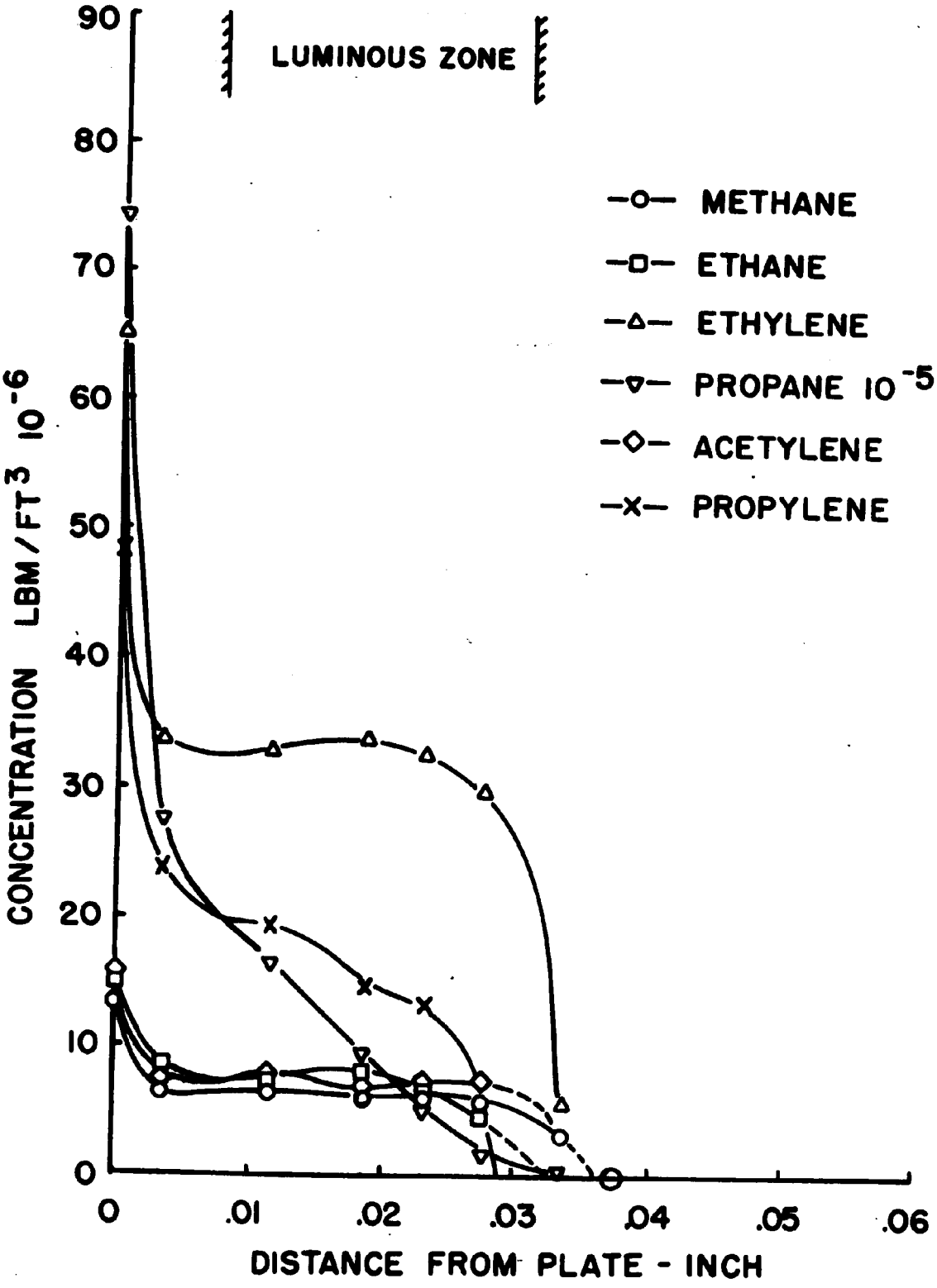
(b) Hydrocarbon concentration profiles

Fig. 12. (Concluded)



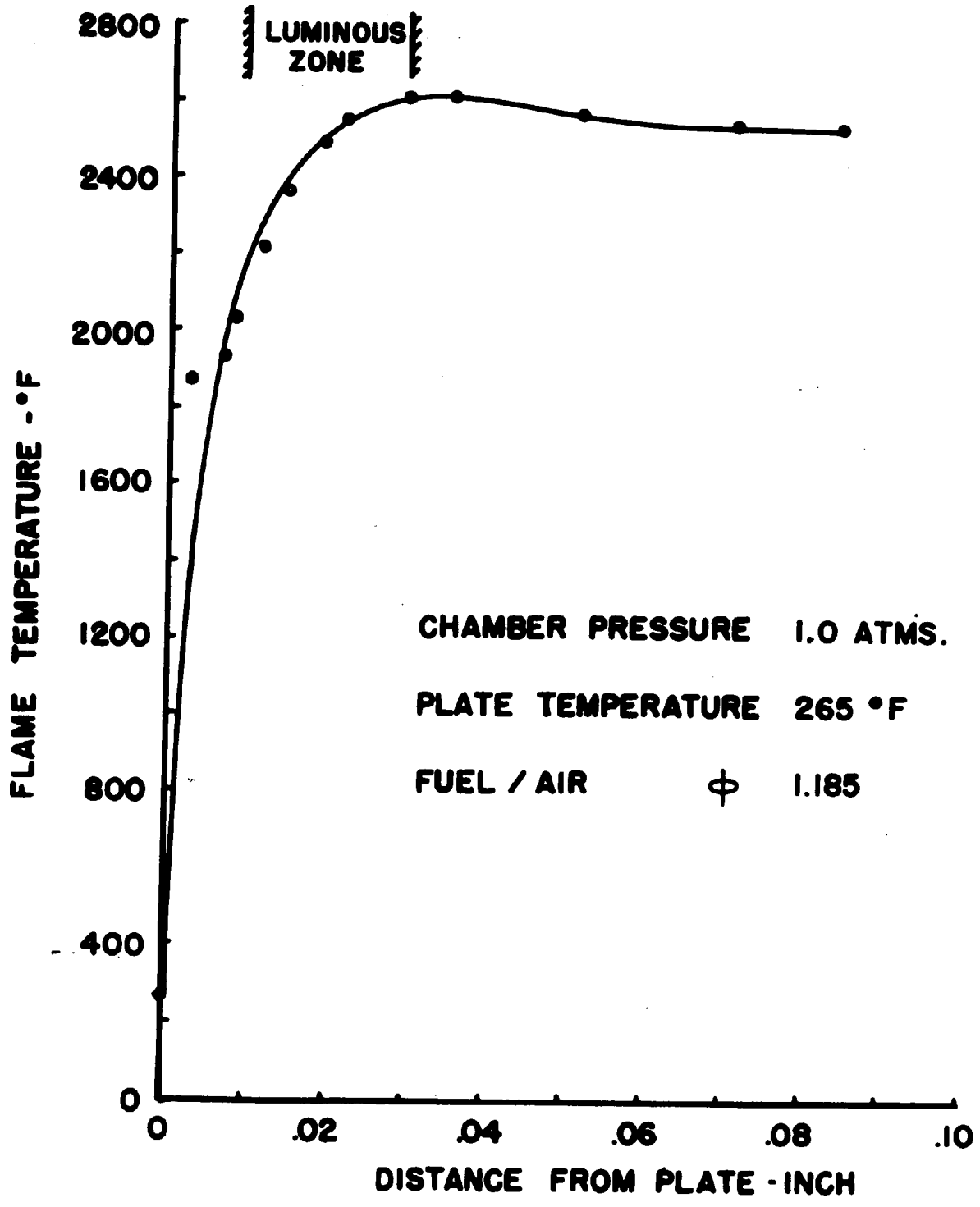
(a) Temperature profile

Fig. 13. Flame structure.



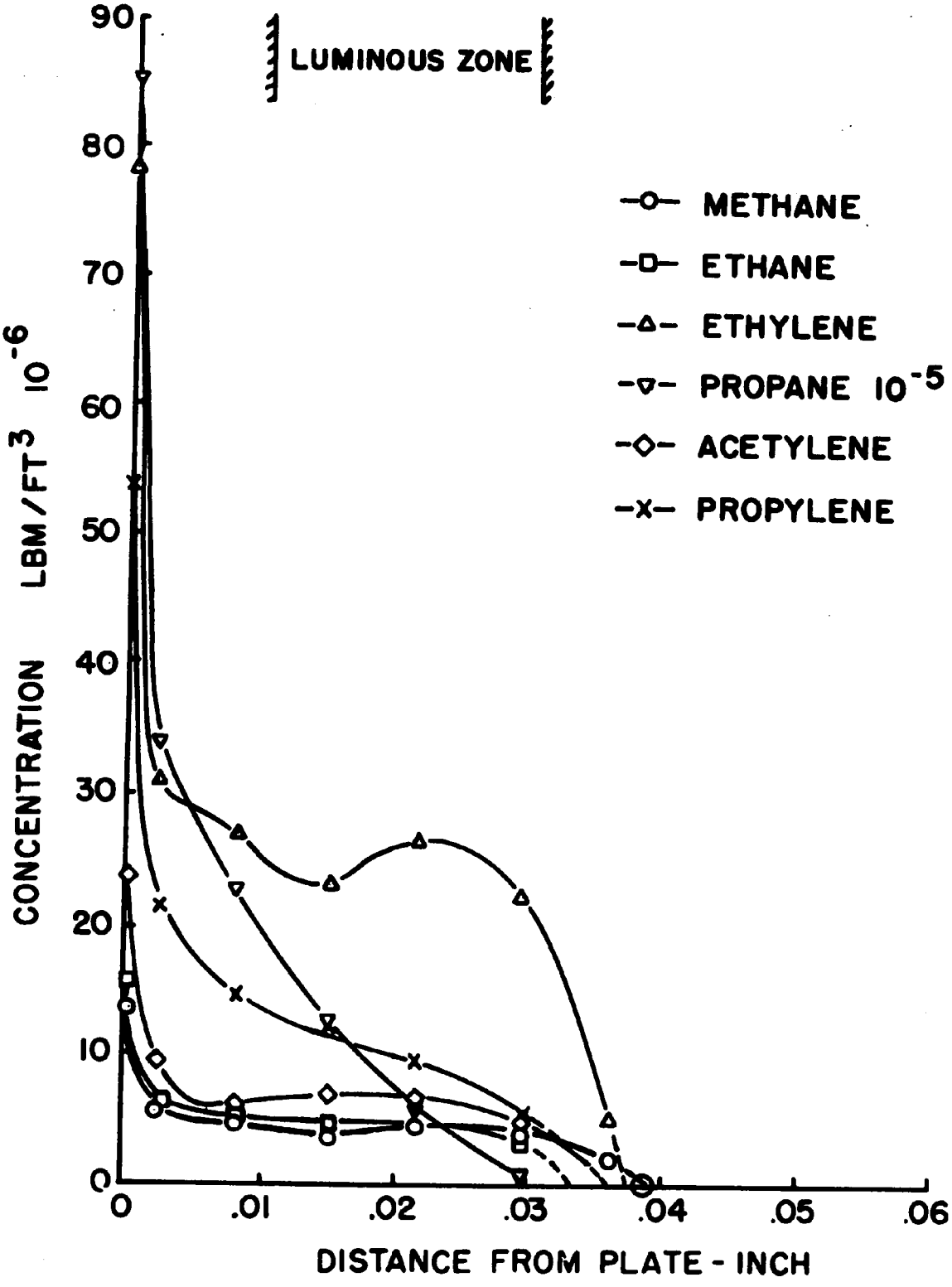
(b) Hydrocarbon concentration profiles

Fig. 13. (Concluded)



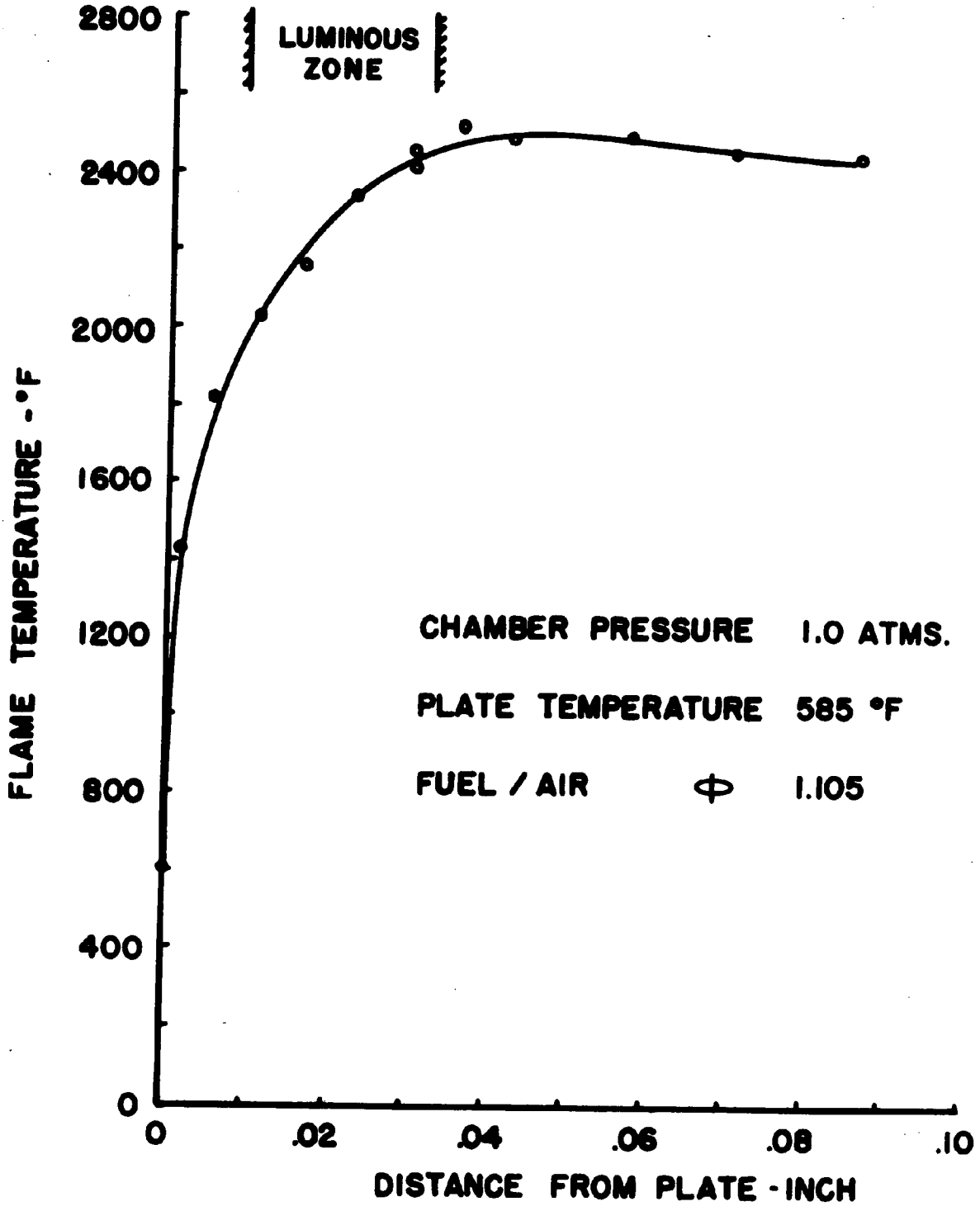
(a) Temperature profile

Fig. 14. Flame structure.



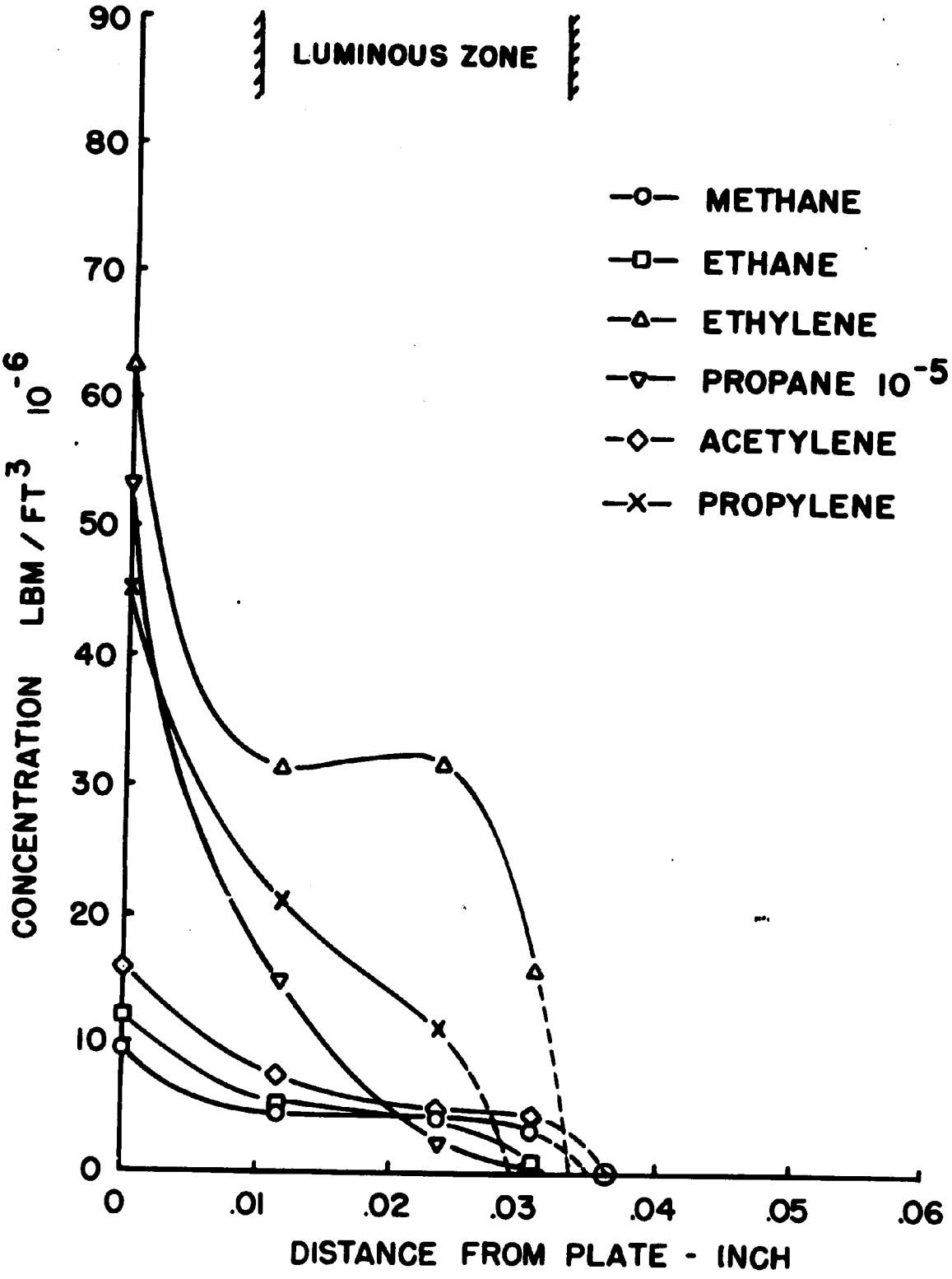
(b) Hydrocarbon concentration profiles

Fig. 14. (Concluded)



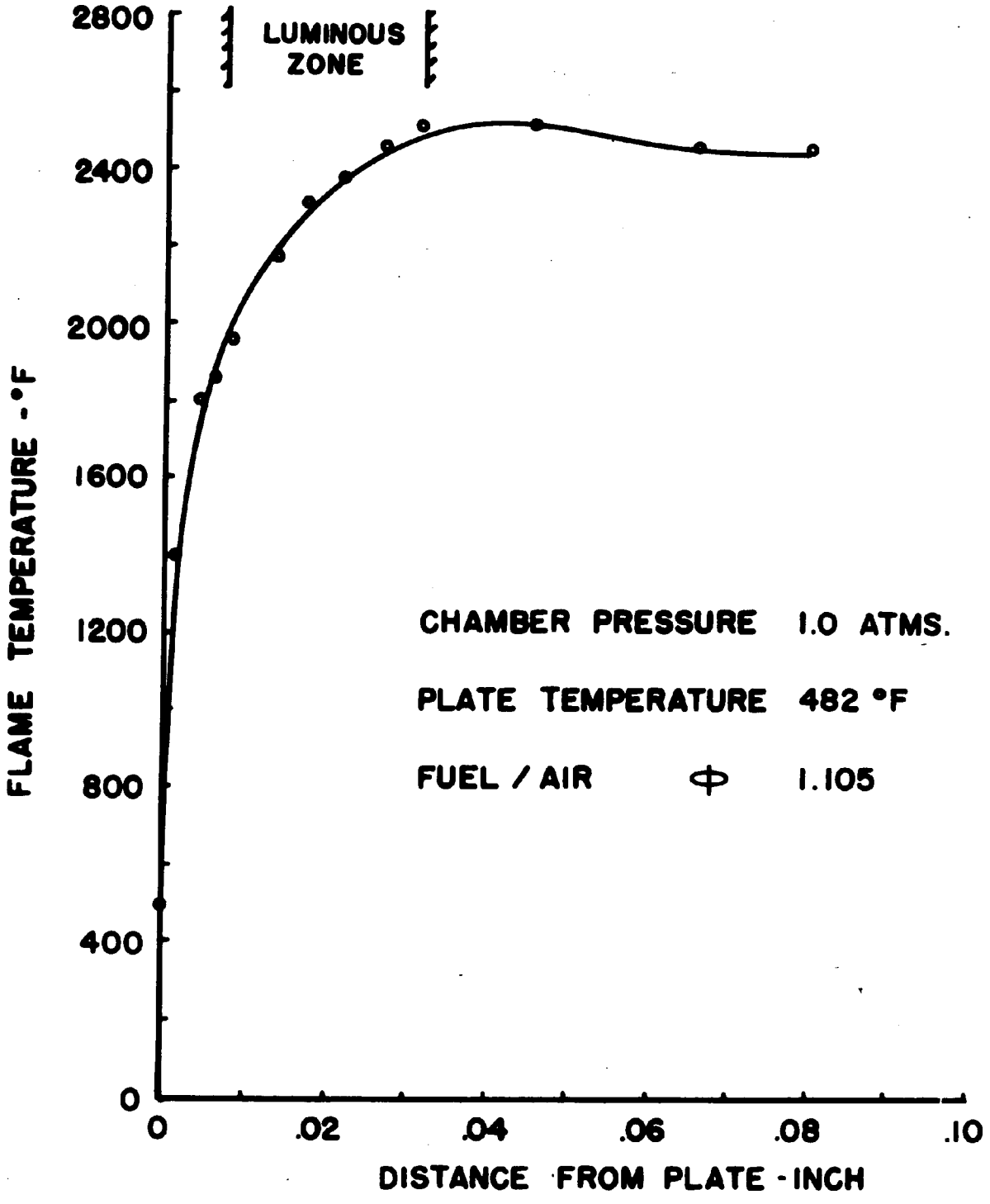
(a) Temperature profile

Fig. 15. Flame structure.



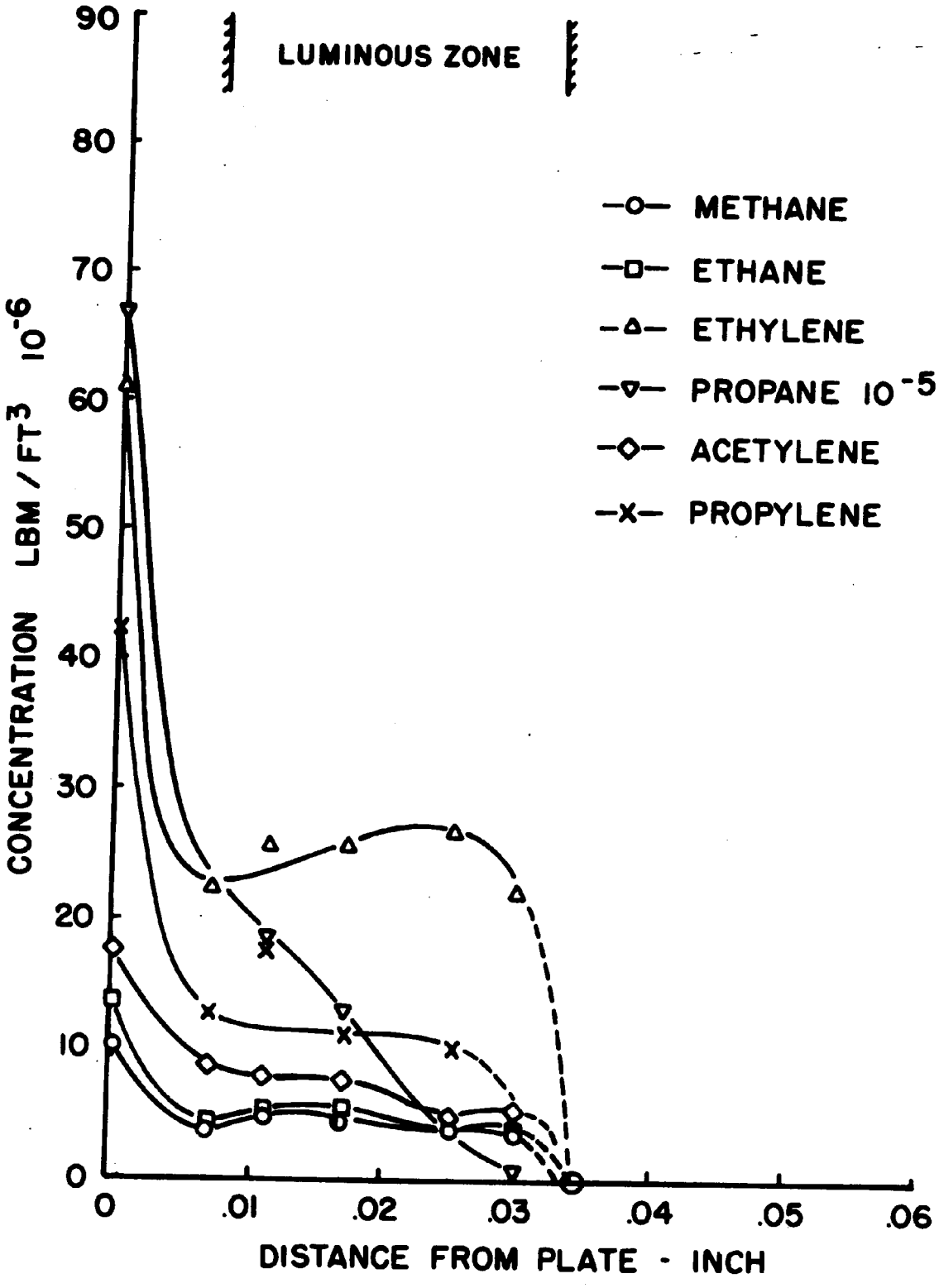
(b) Hydrocarbon concentration profiles

Fig. 15. (Concluded)



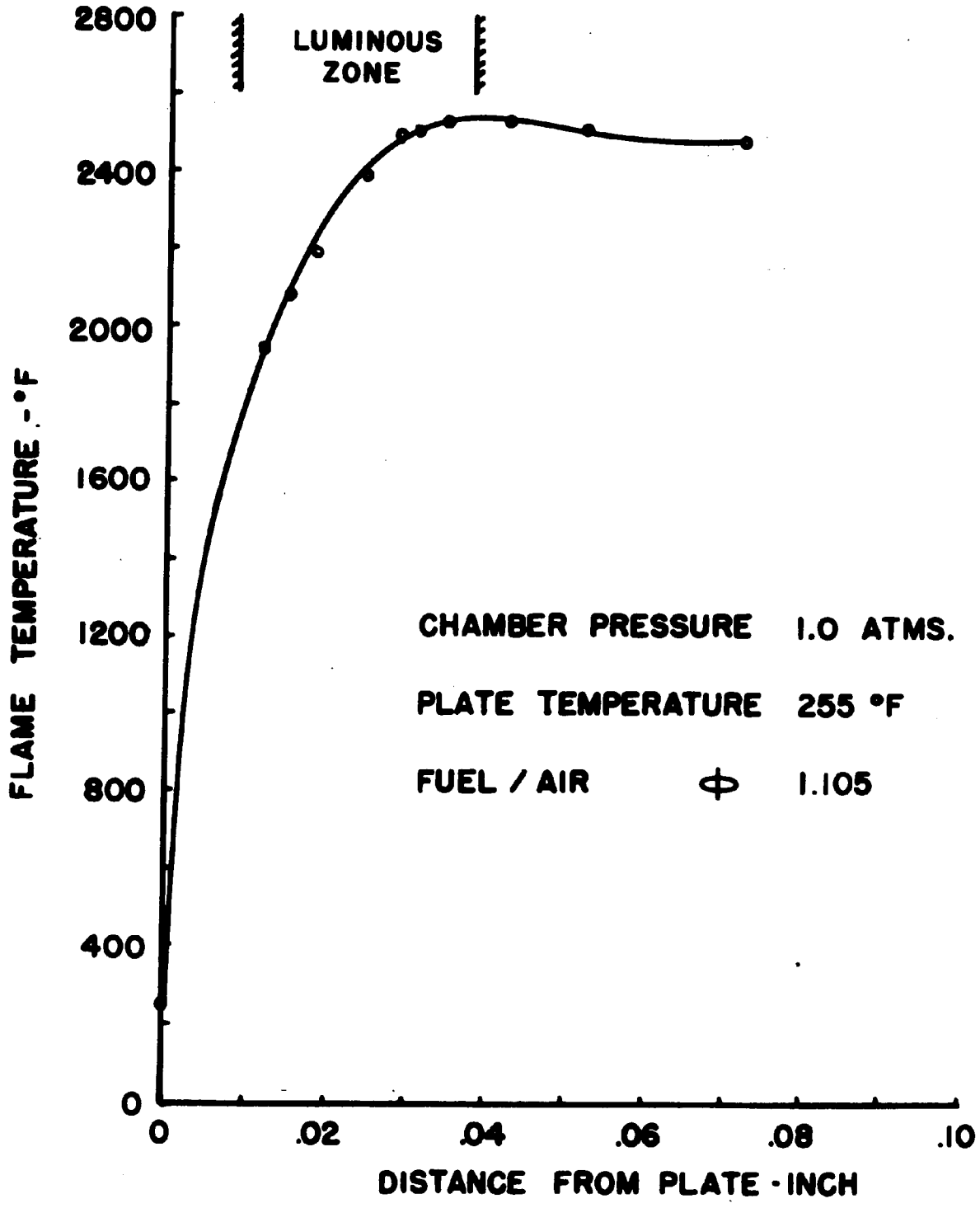
(a) Temperature profile

Fig. 16. Flame structure.



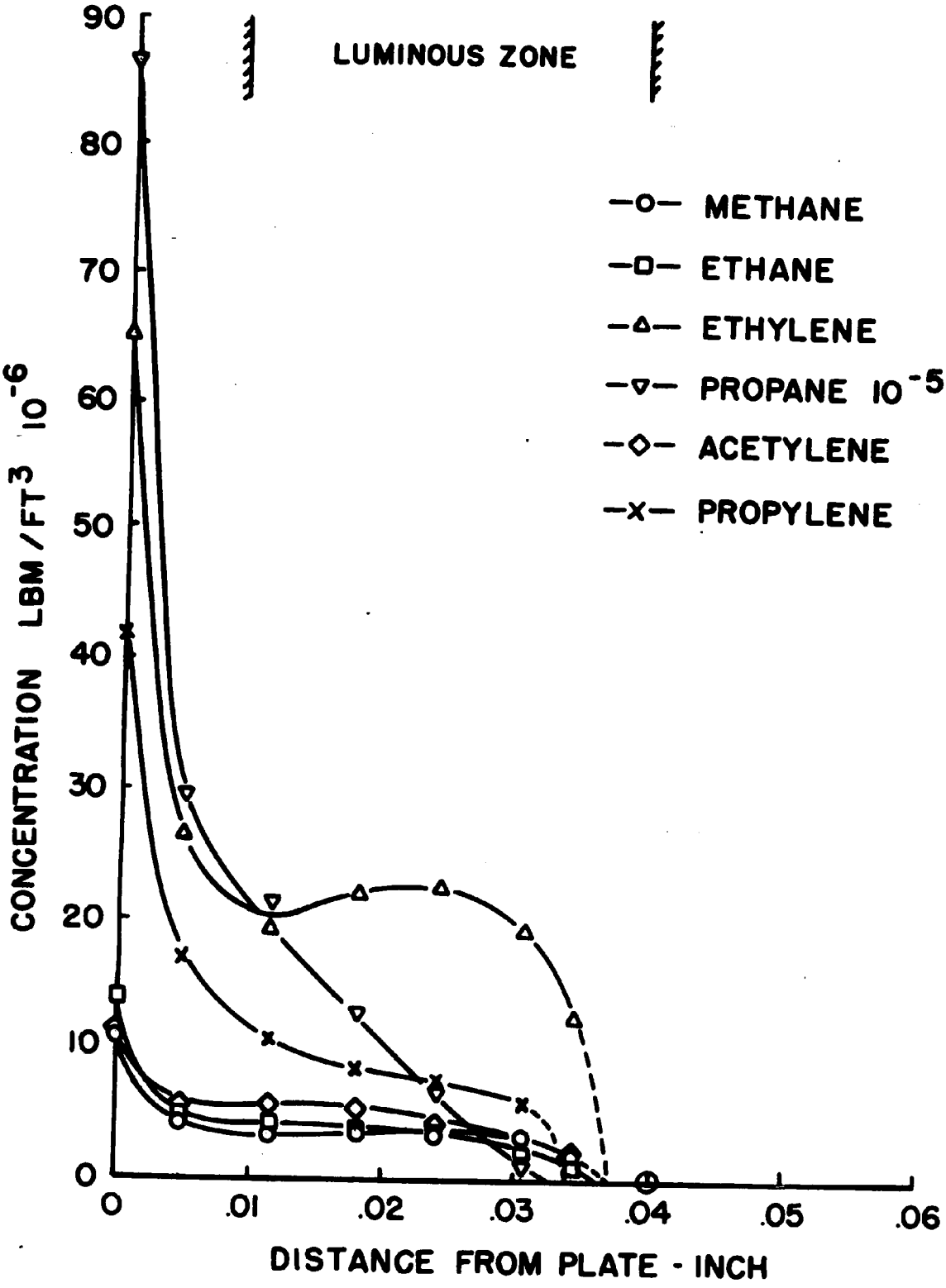
(b) Hydrocarbon concentration profiles

Fig. 16. (Concluded)



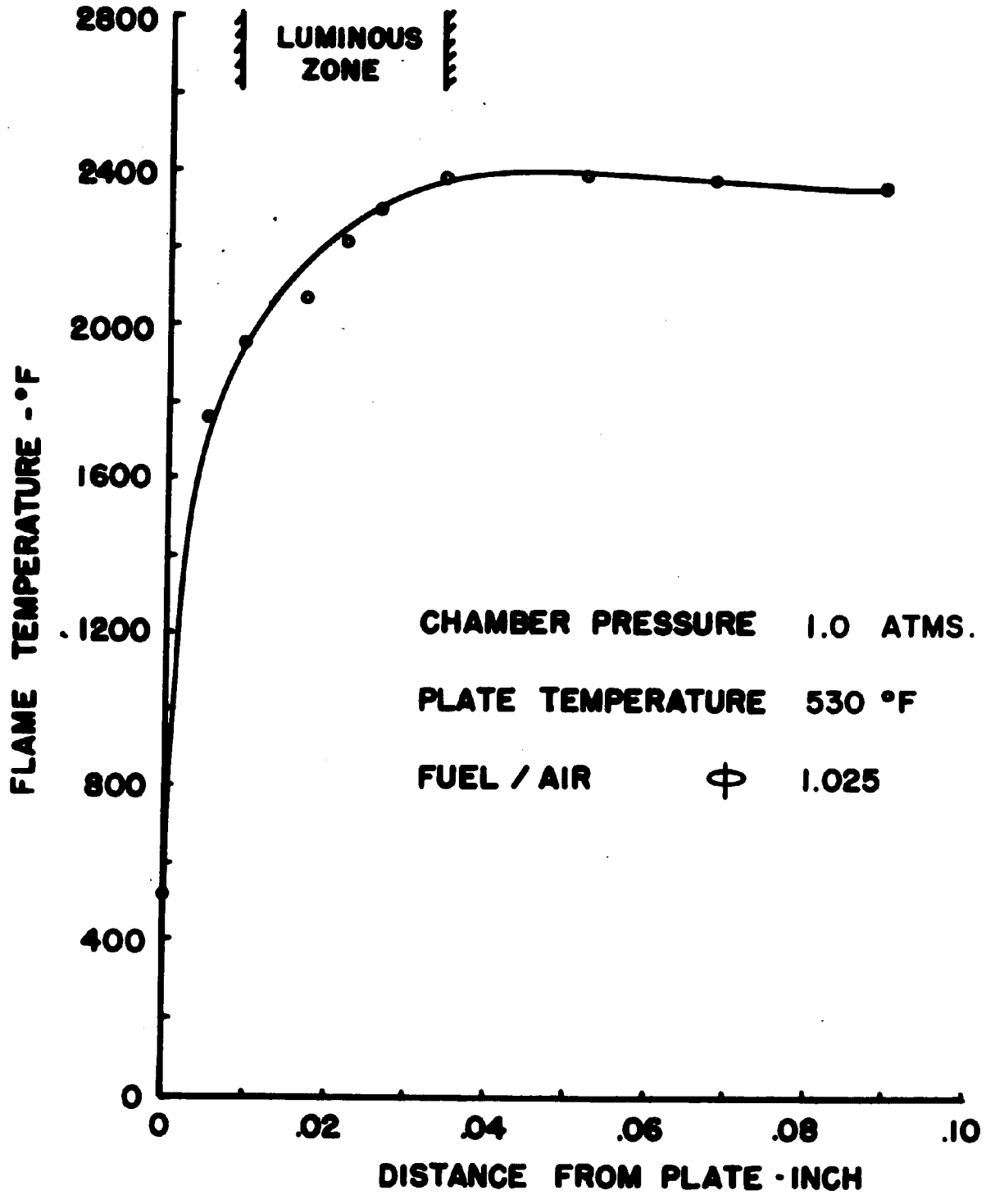
(a) Temperature profile

Fig. 17. Flame structure.



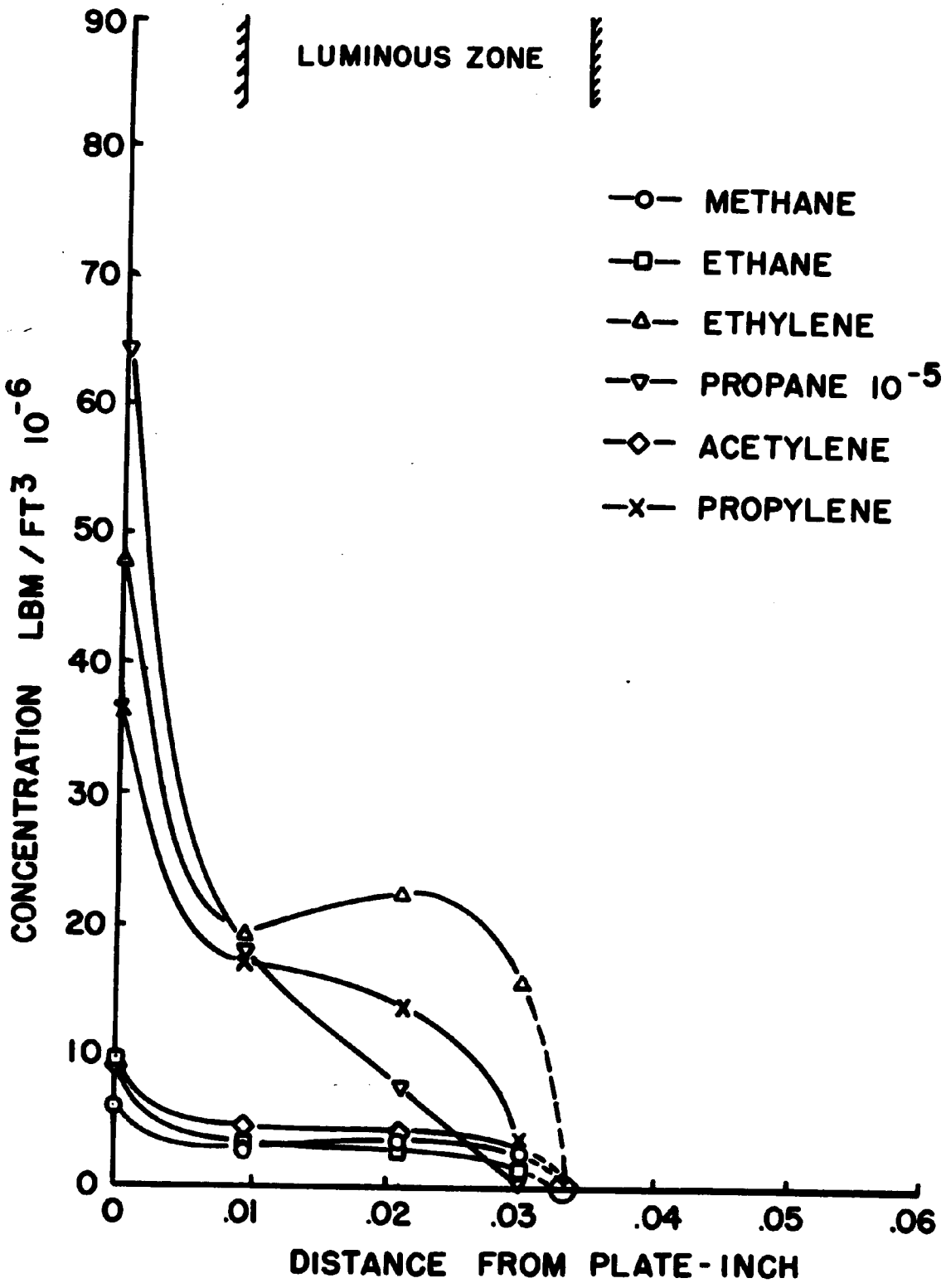
(b) Hydrocarbon concentration profiles

Fig. 17. (Concluded)



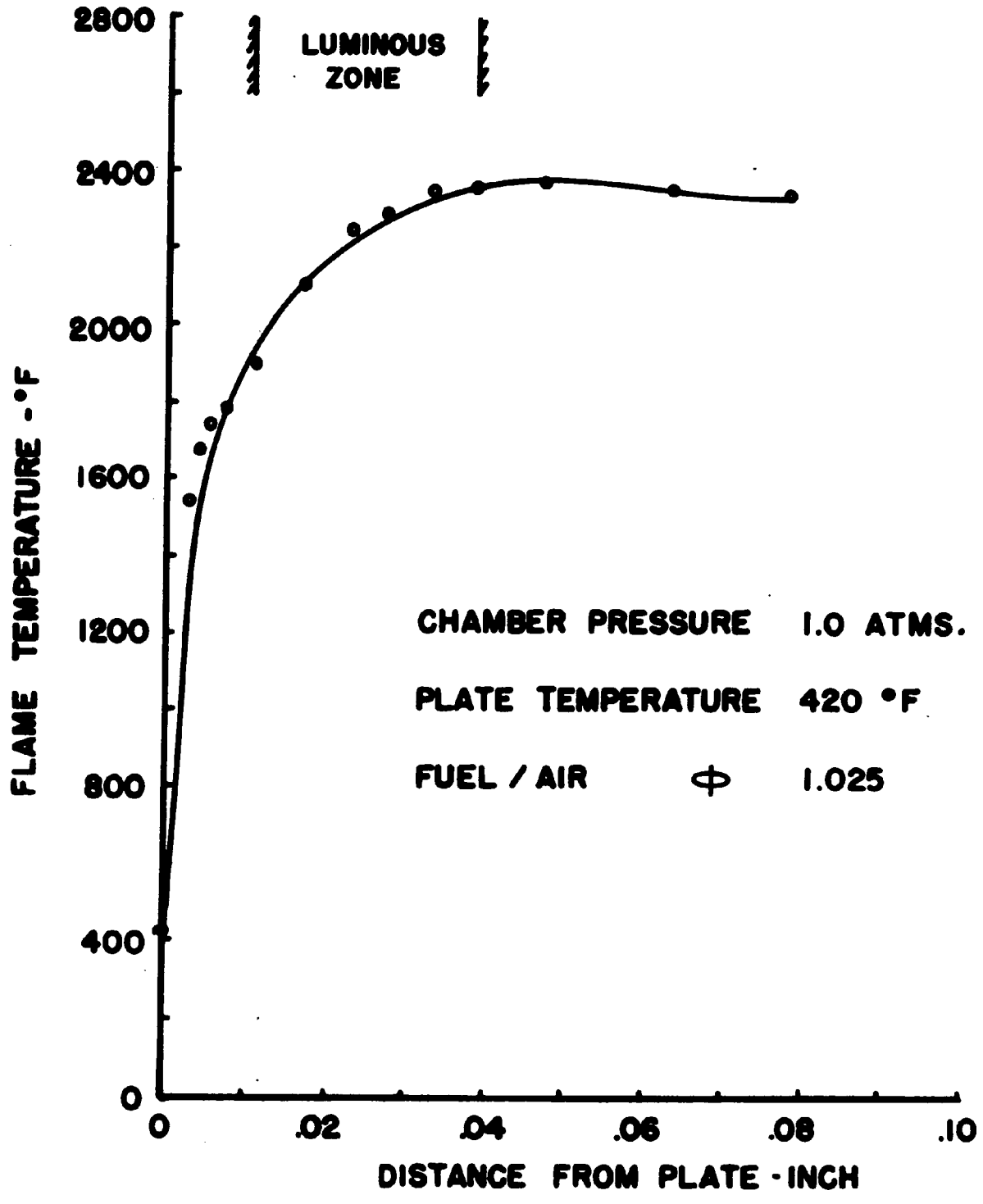
(a) Temperature profile

Fig. 18. Flame structure.



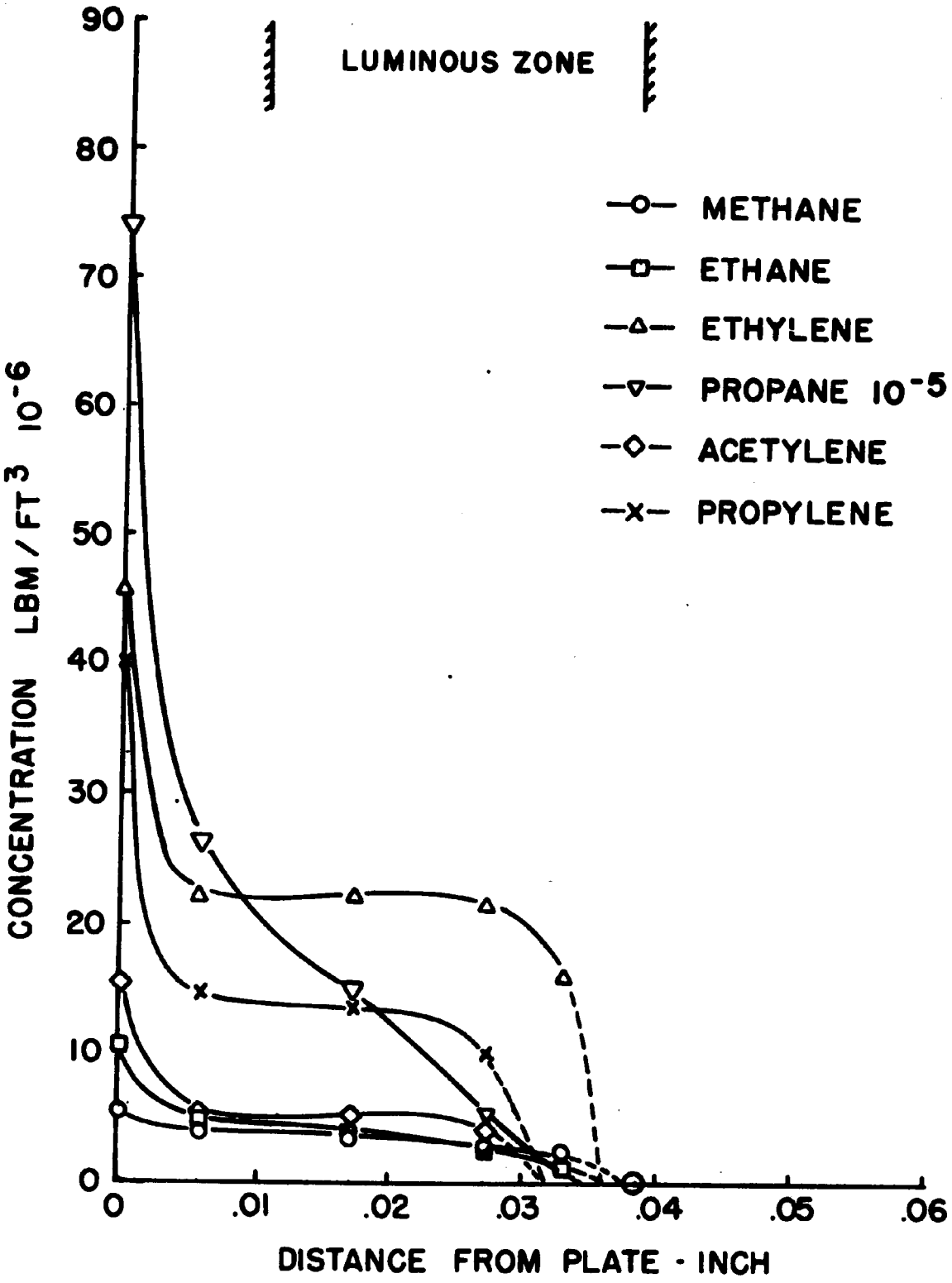
(b) Hydrocarbon concentration profiles

Fig. 18. (Concluded)



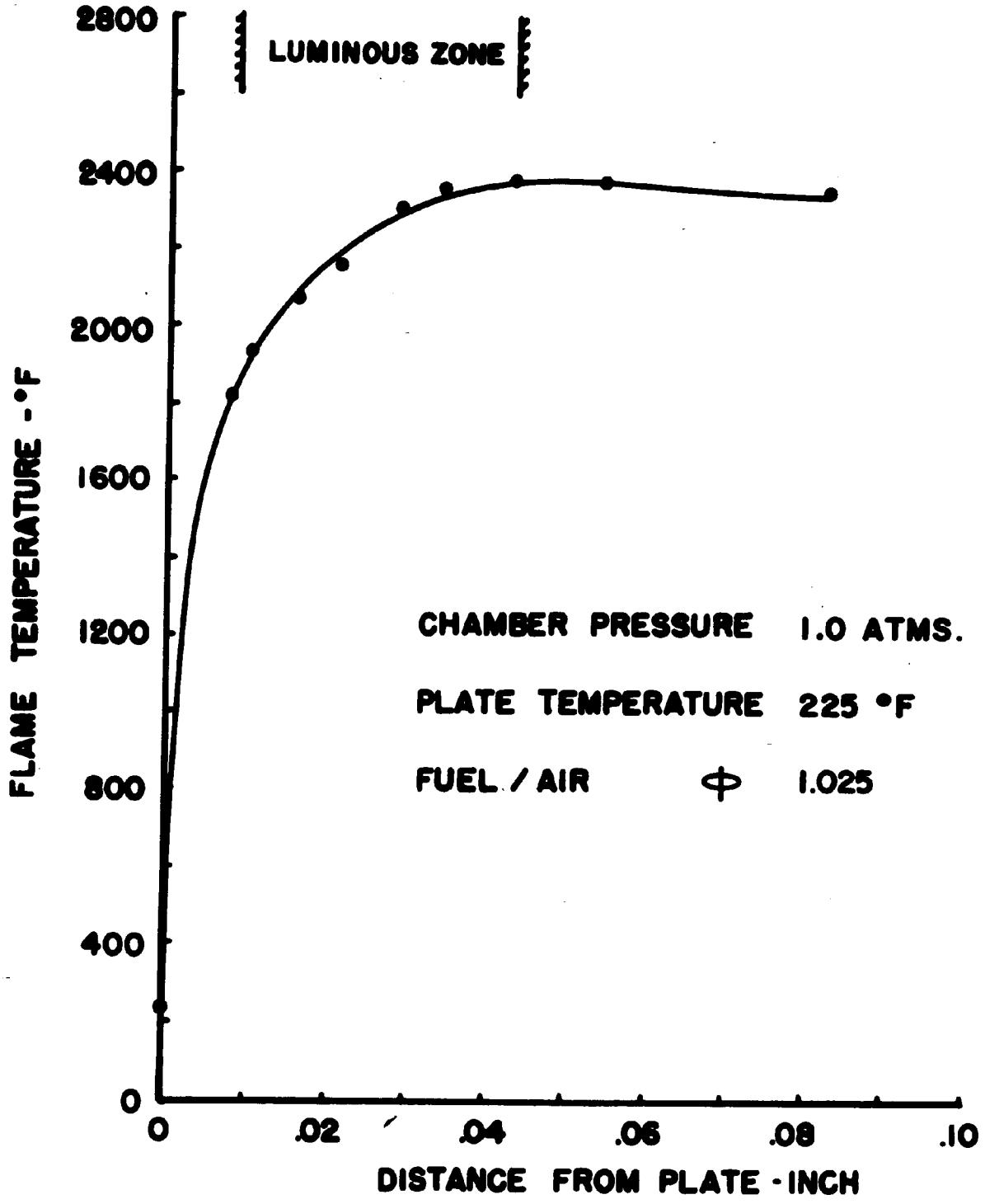
(a) Temperature profile

Fig. 19. Flame structure.



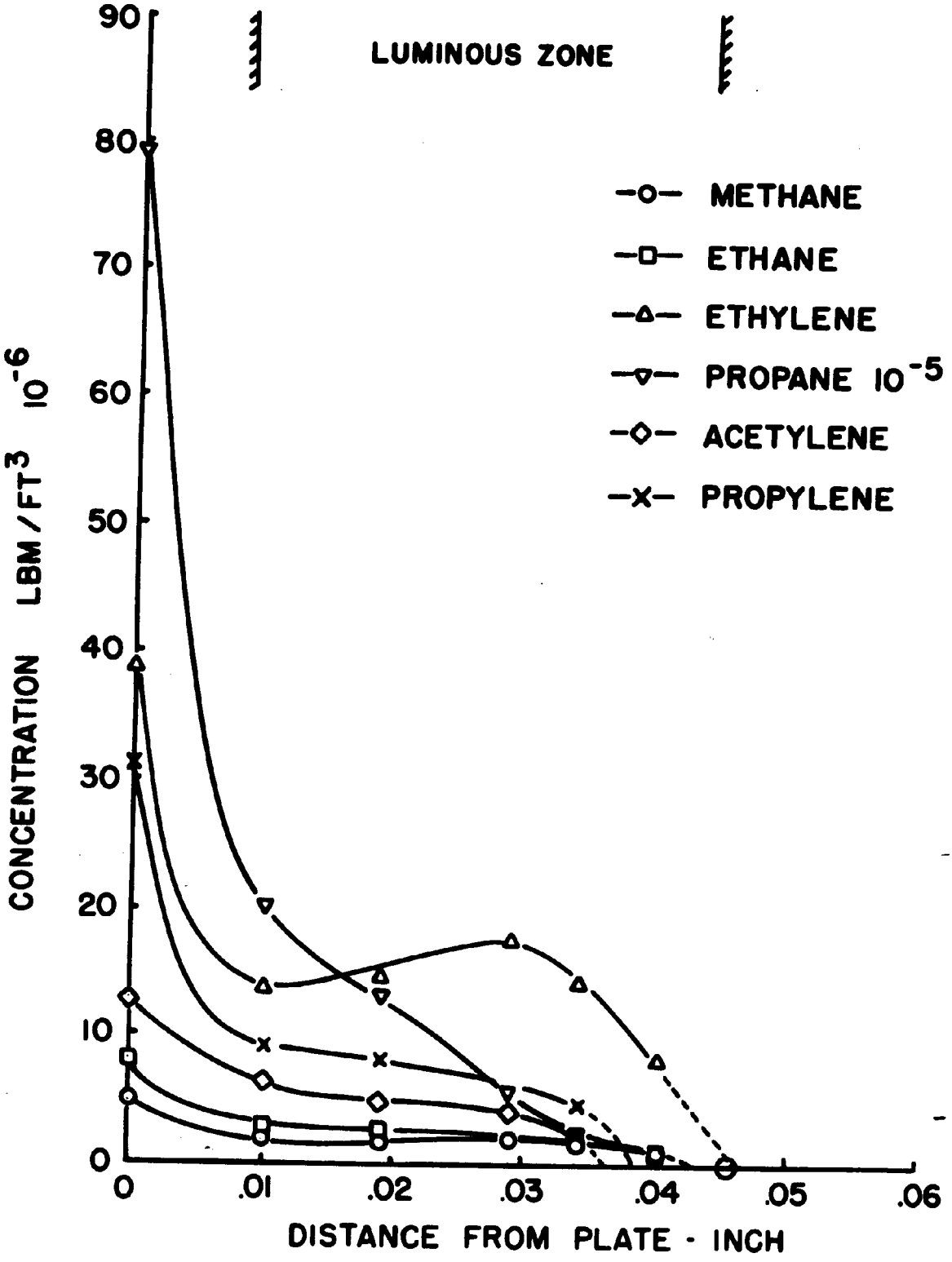
(b) Hydrocarbon concentration profiles

Fig. 19. (Concluded)



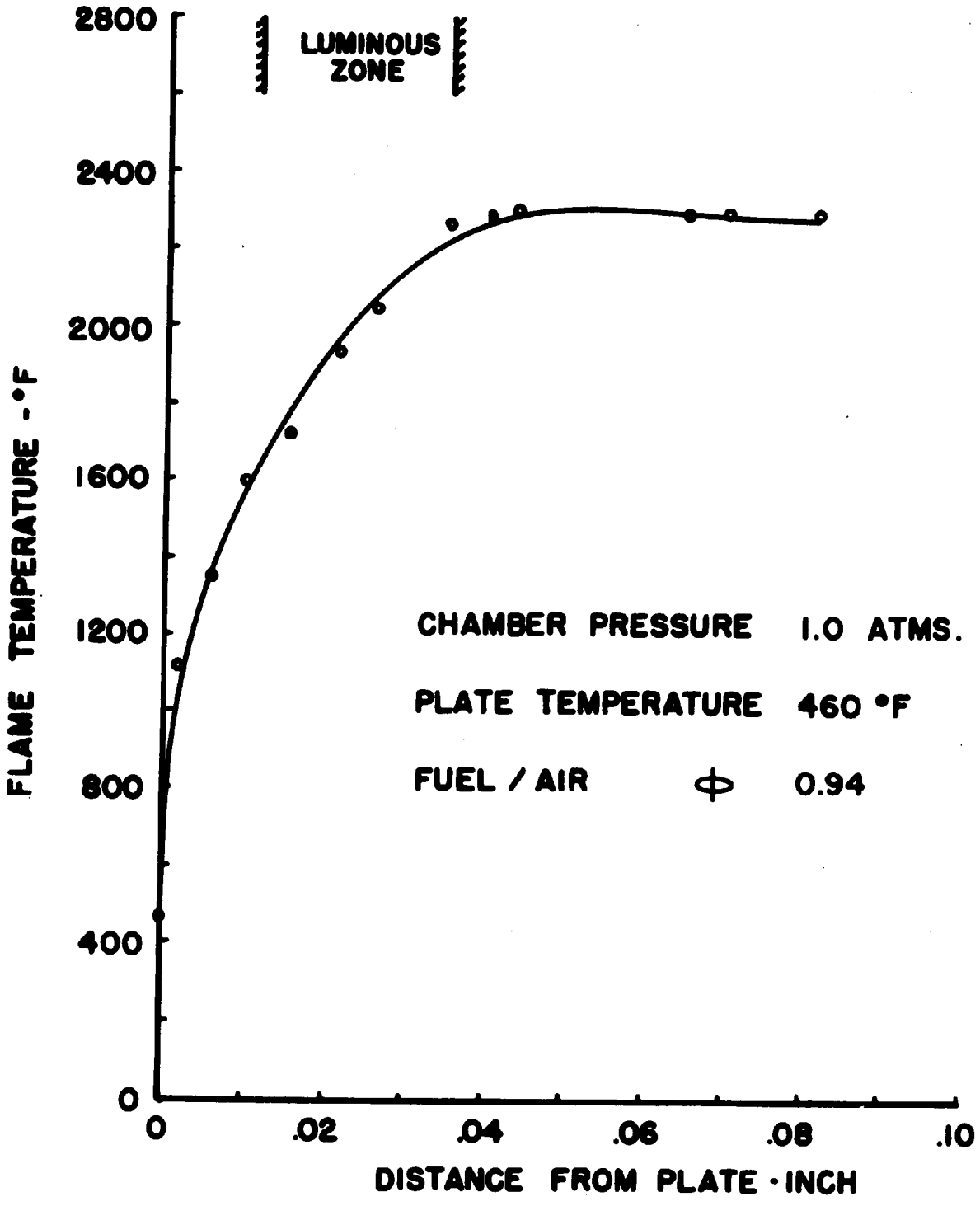
(a) Temperature profile

Fig. 20. Flame structure.



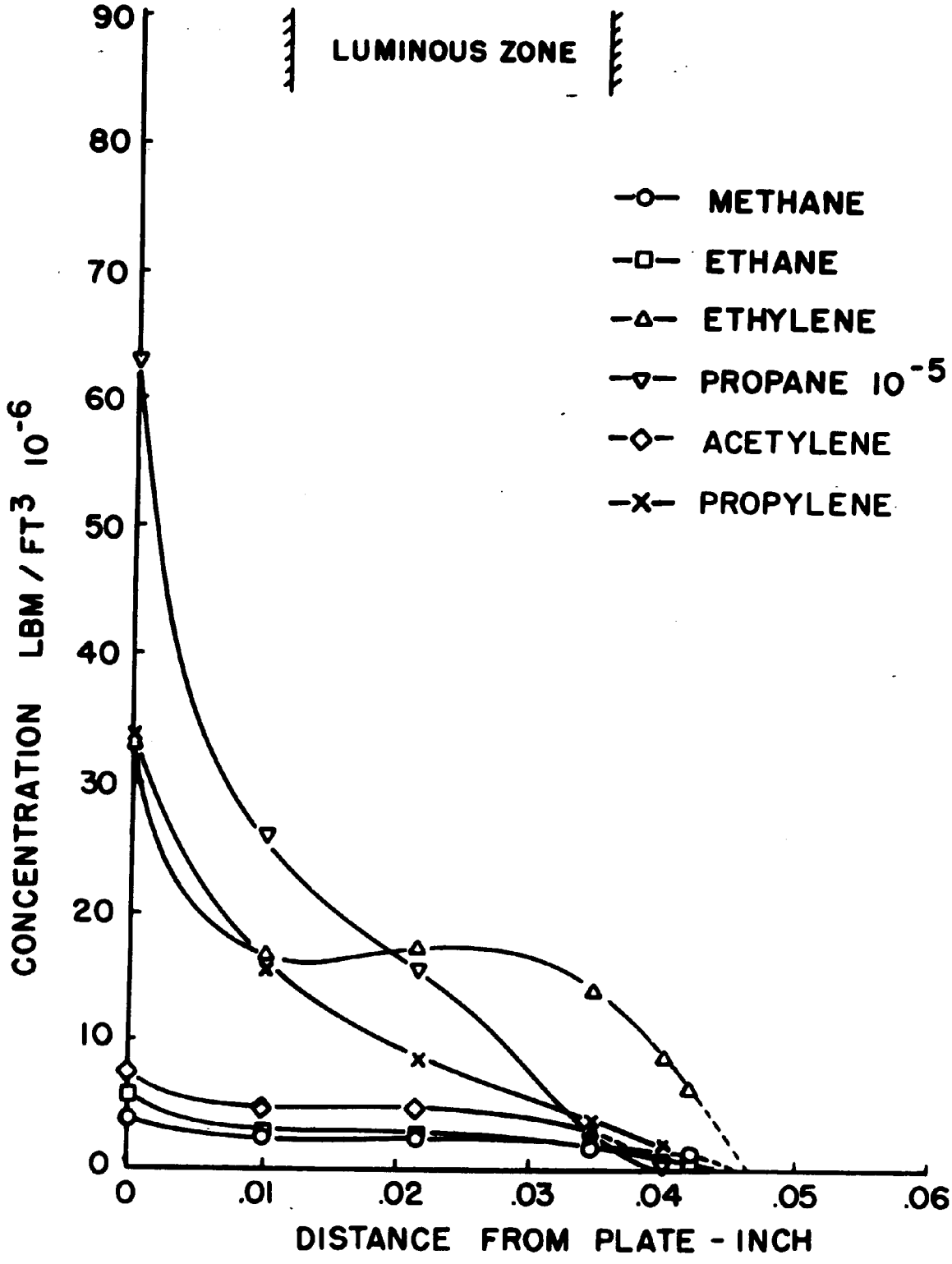
(b) Hydrocarbon concentration profiles

Fig. 20. (Concluded)



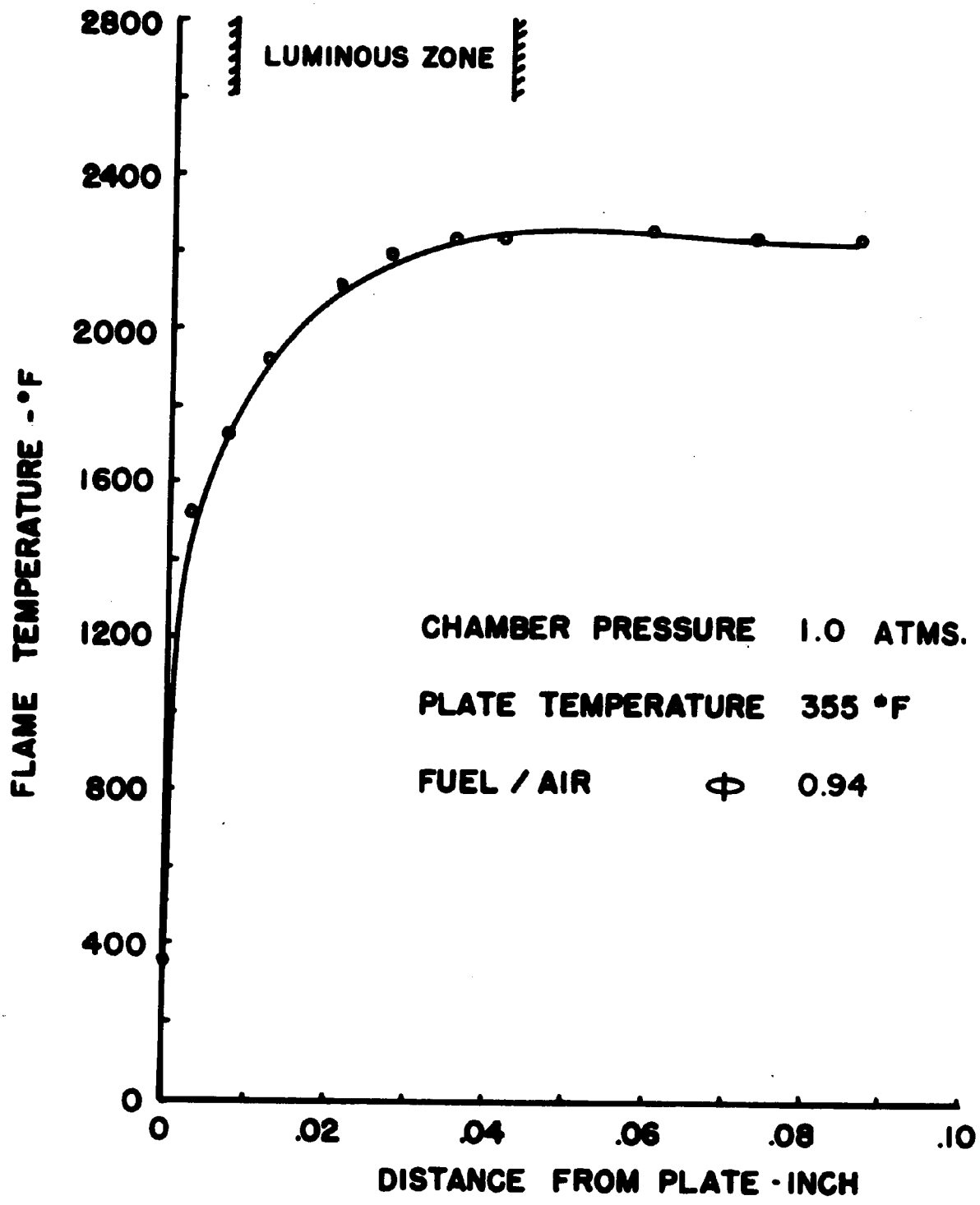
(a) Temperature profile

Fig. 21. Flame structure.



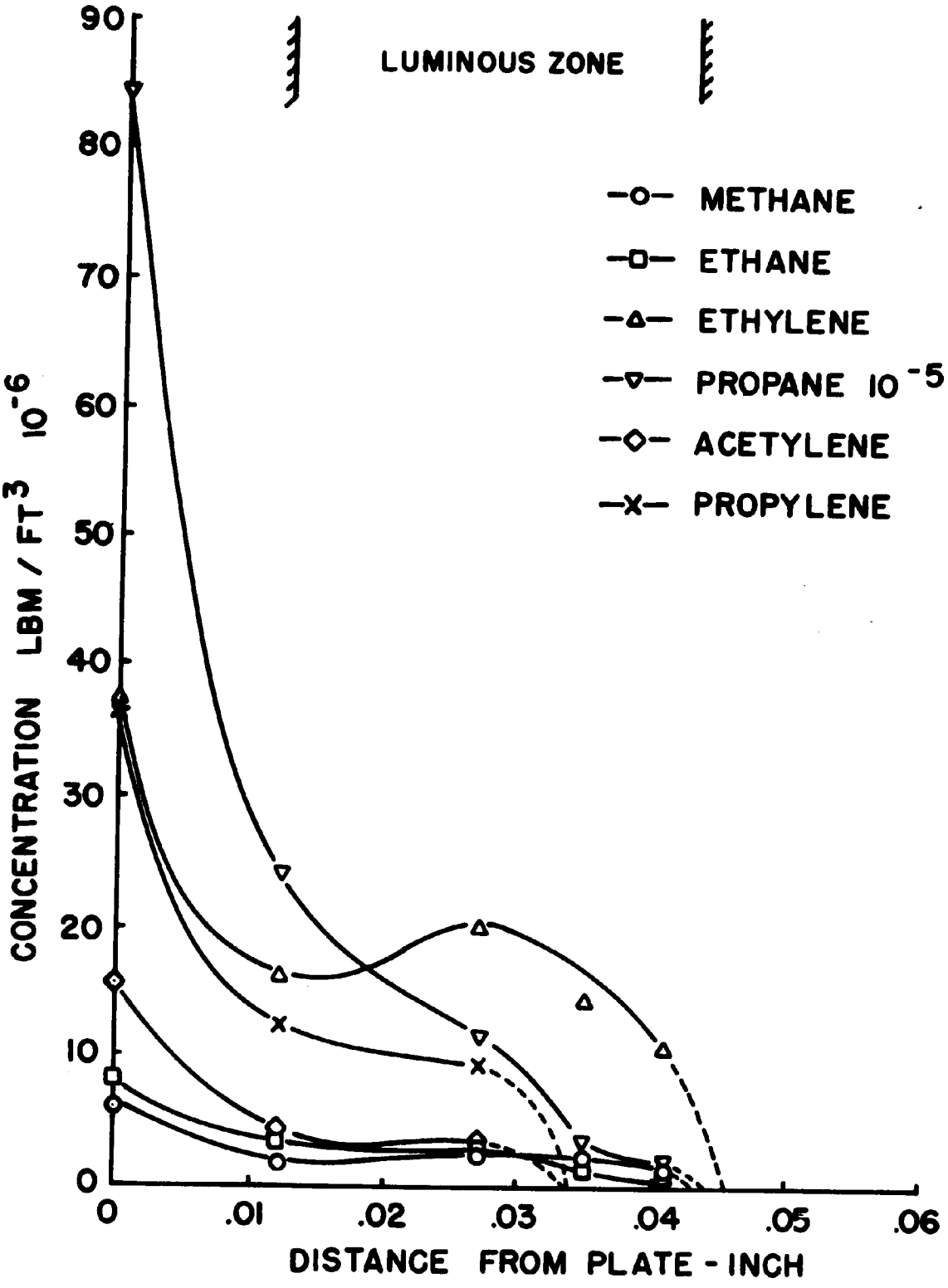
(b) Hydrocarbon concentration profiles

Fig. 21 (Concluded)



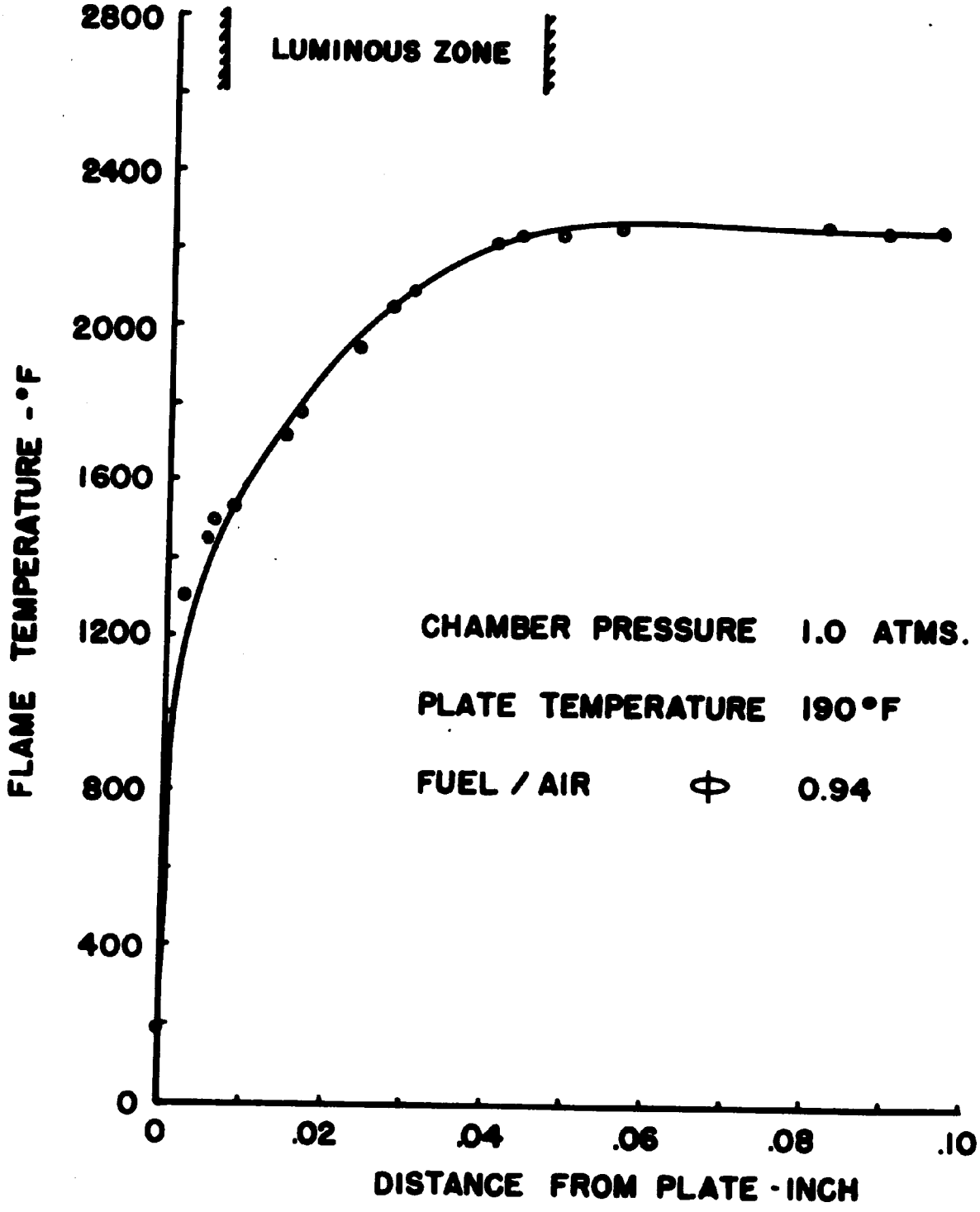
(a) Temperature profile

Fig. 22. Flame structure.



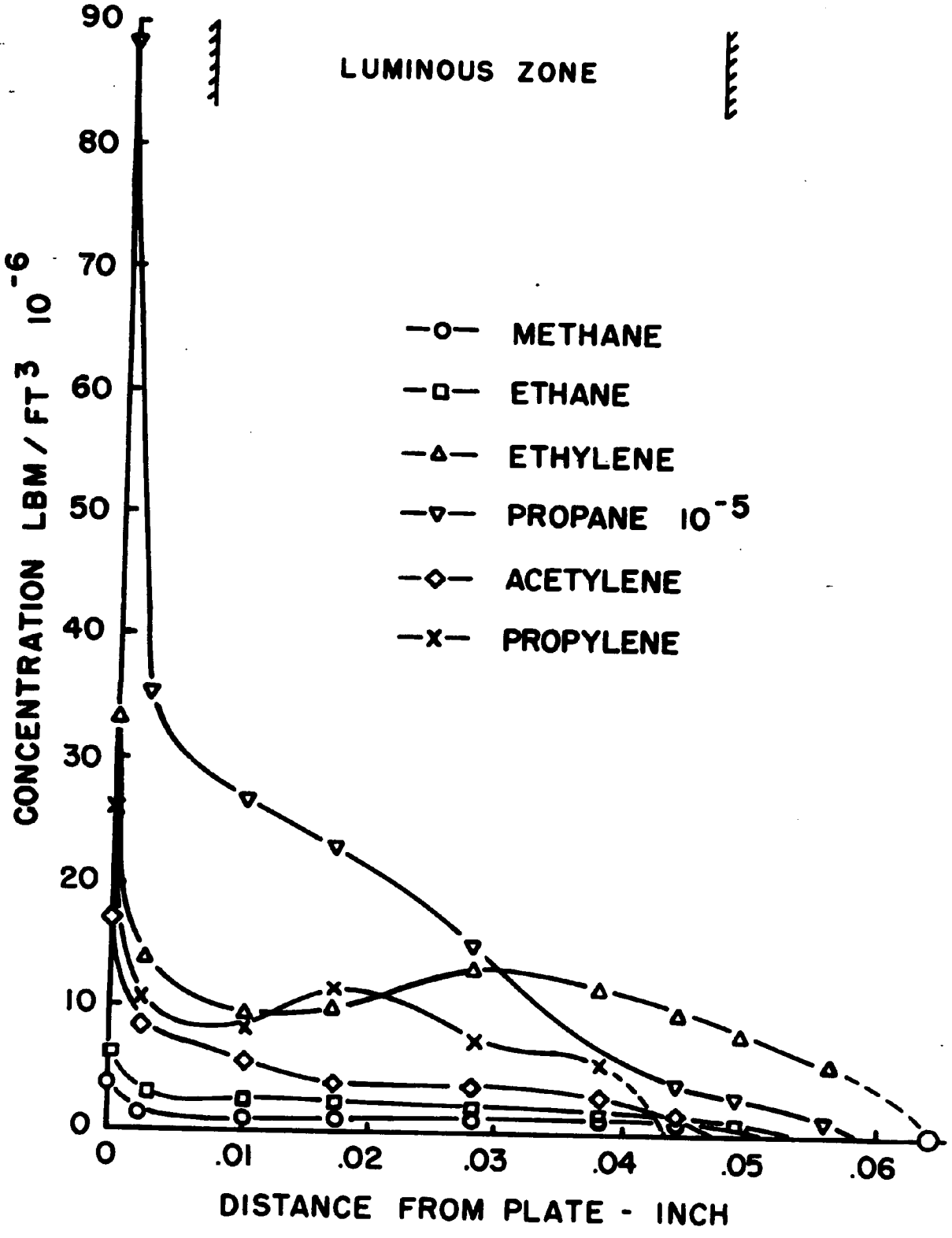
(b) Hydrocarbon concentration profiles

Fig. 22. (Concluded)



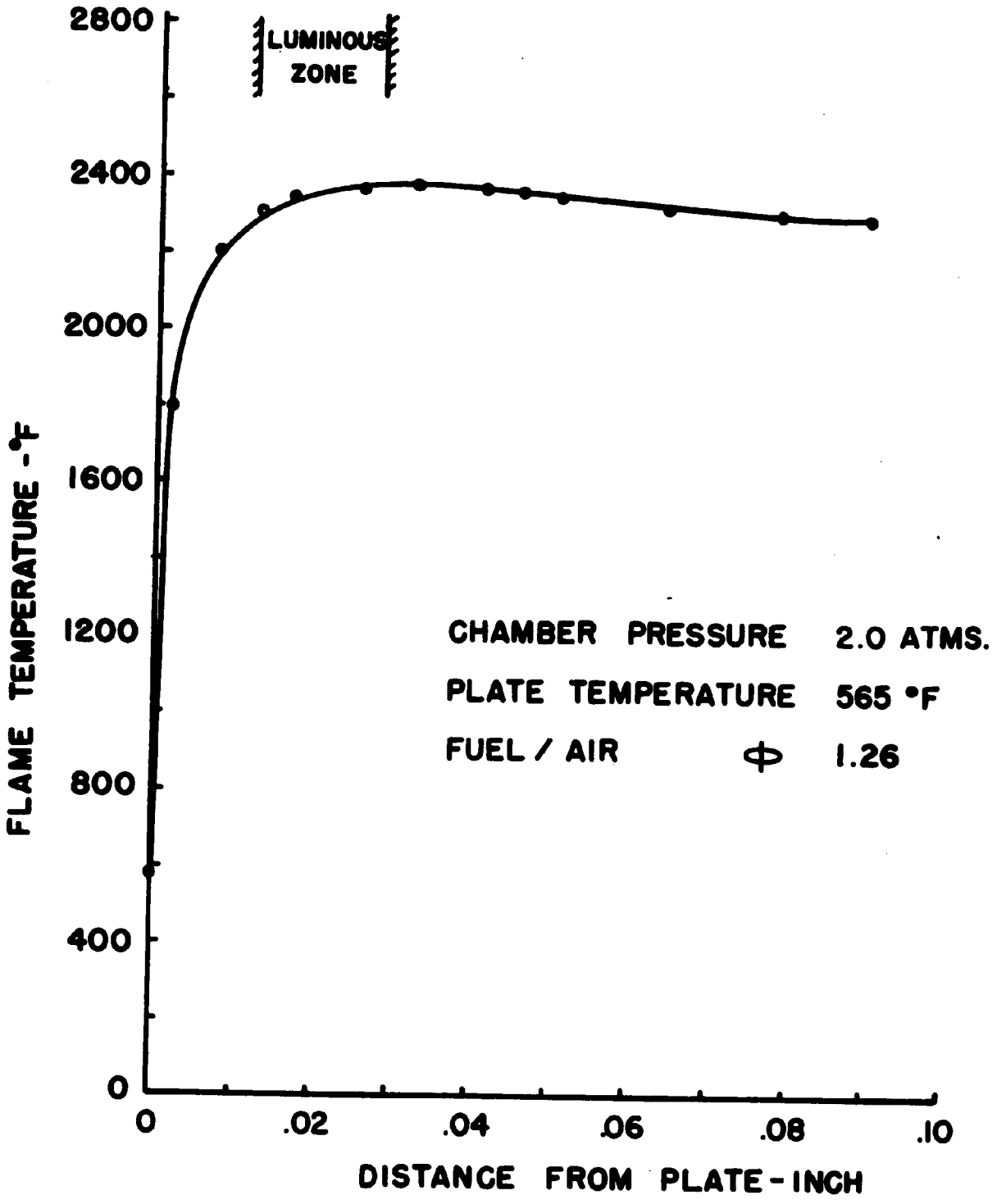
(a) Temperature profile

Fig. 23. Flame structure.



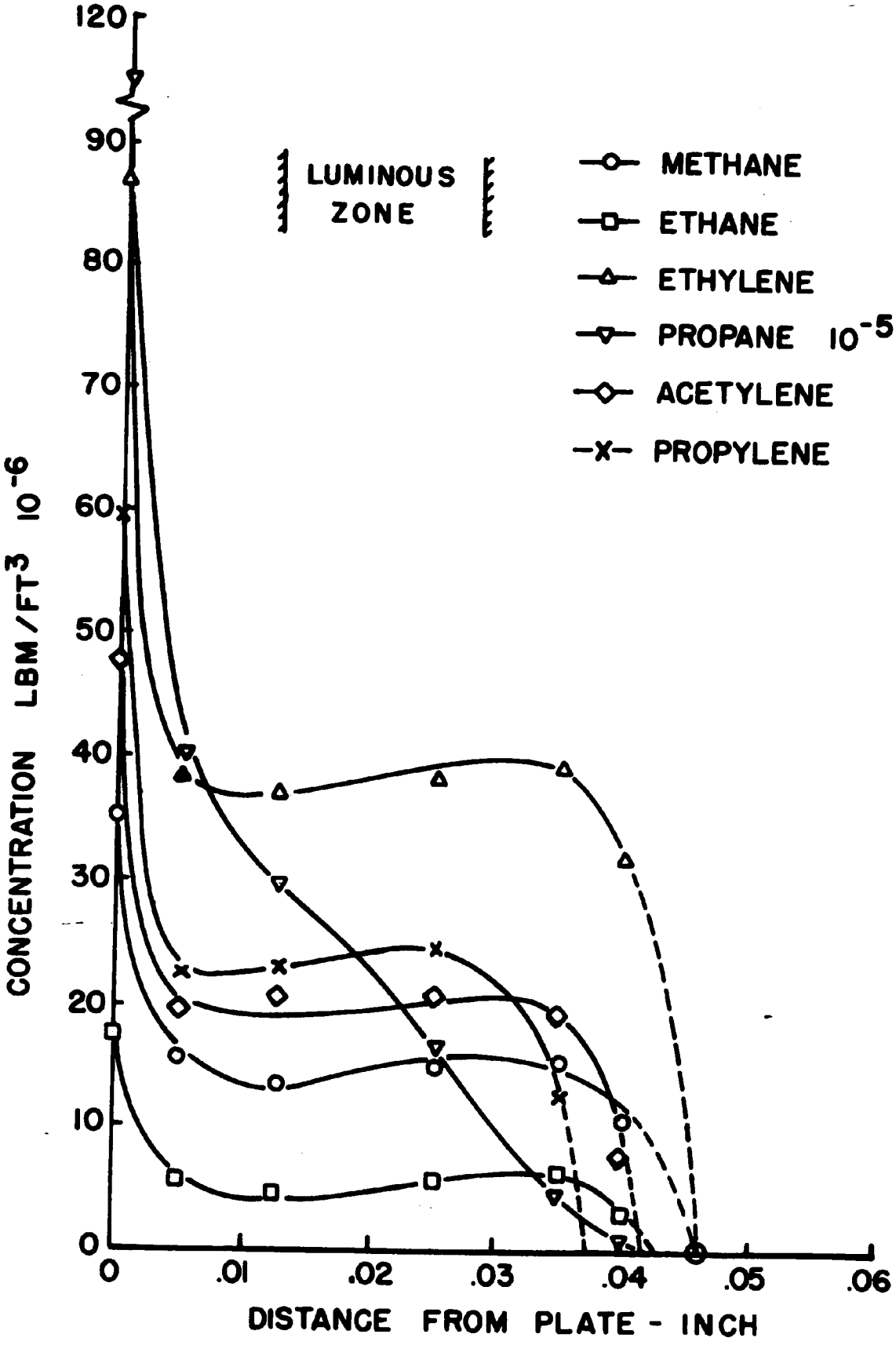
(b) Hydrocarbon concentration profiles

Fig. 23. (Concluded)



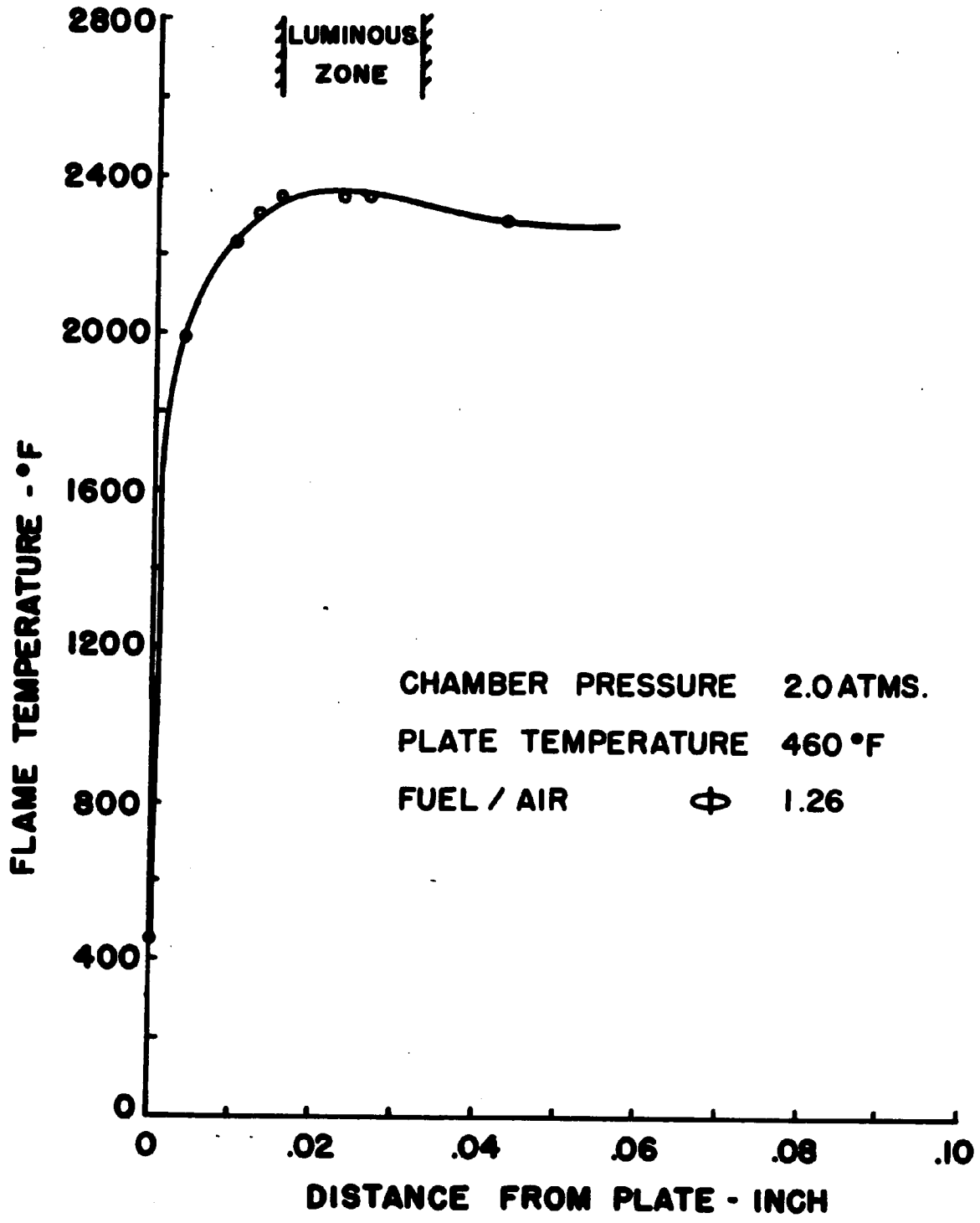
(a) Temperature profile

Fig. 24. Flame structure.



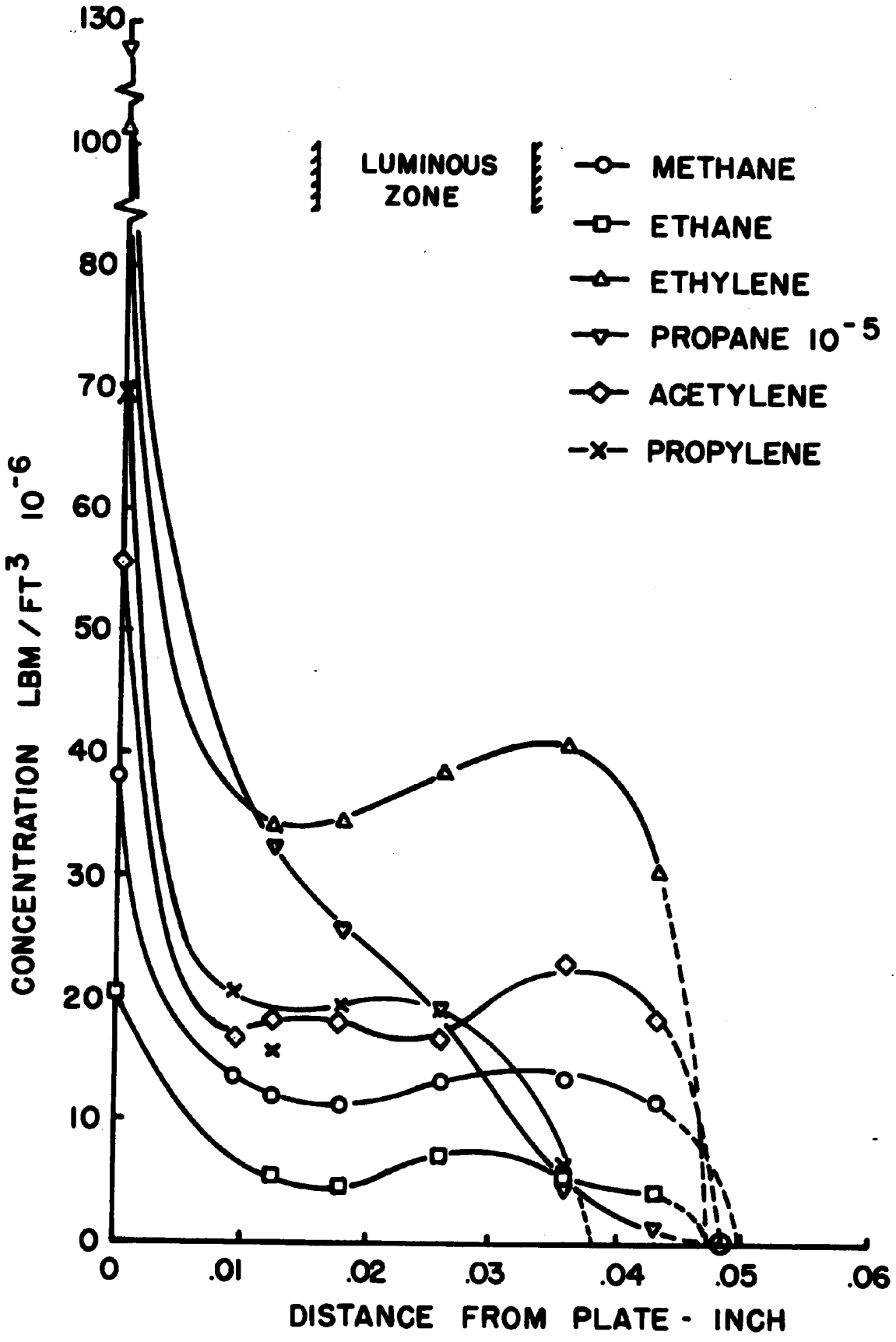
(b) Hydrocarbon concentration profiles

Fig. 24. (Concluded)



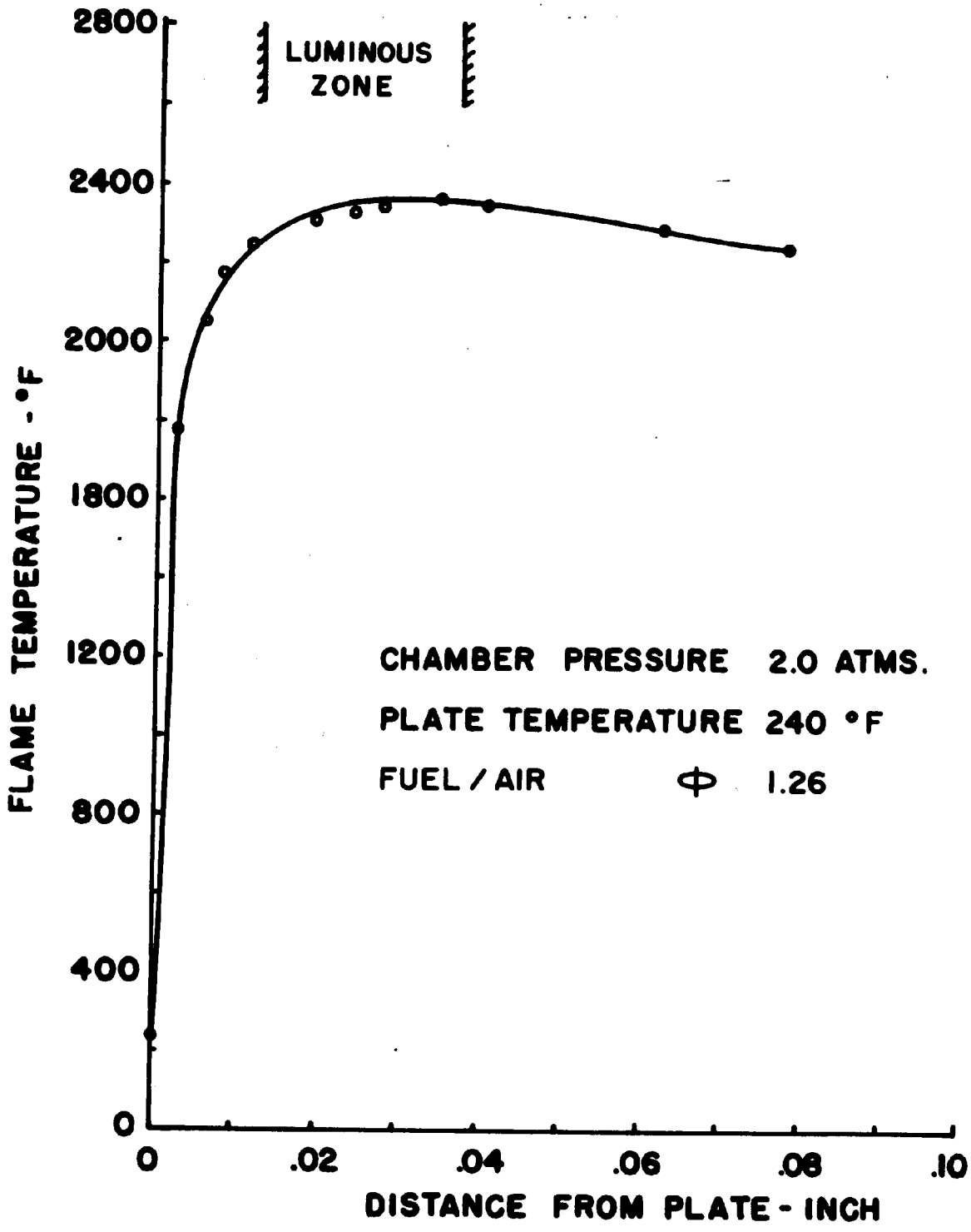
(a) Temperature profile

Fig. 25. Flame structure.



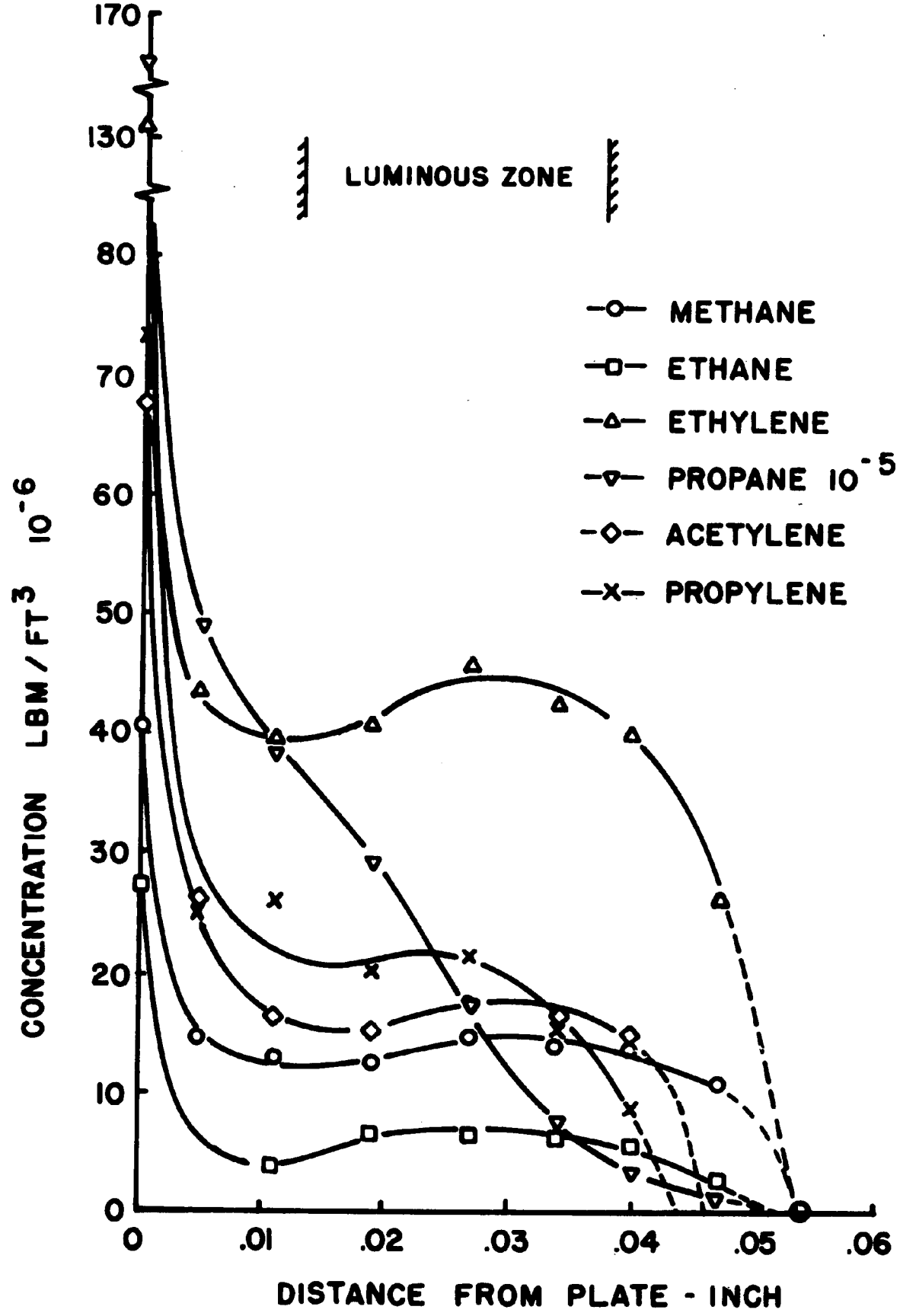
(b) Hydrocarbon concentration profiles

Fig. 25. (Concluded)



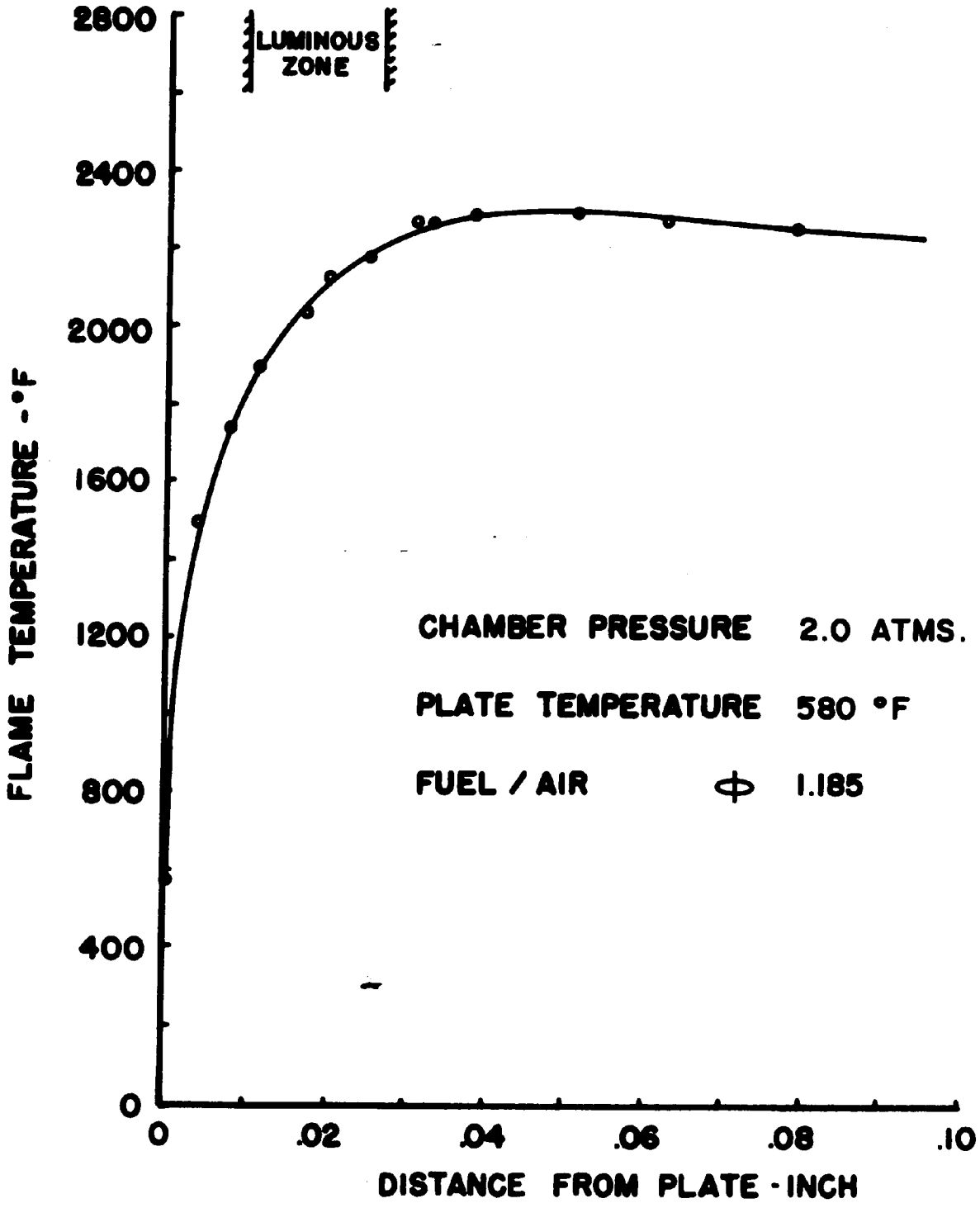
(a) Temperature profile

Fig. 26. Flame structure.



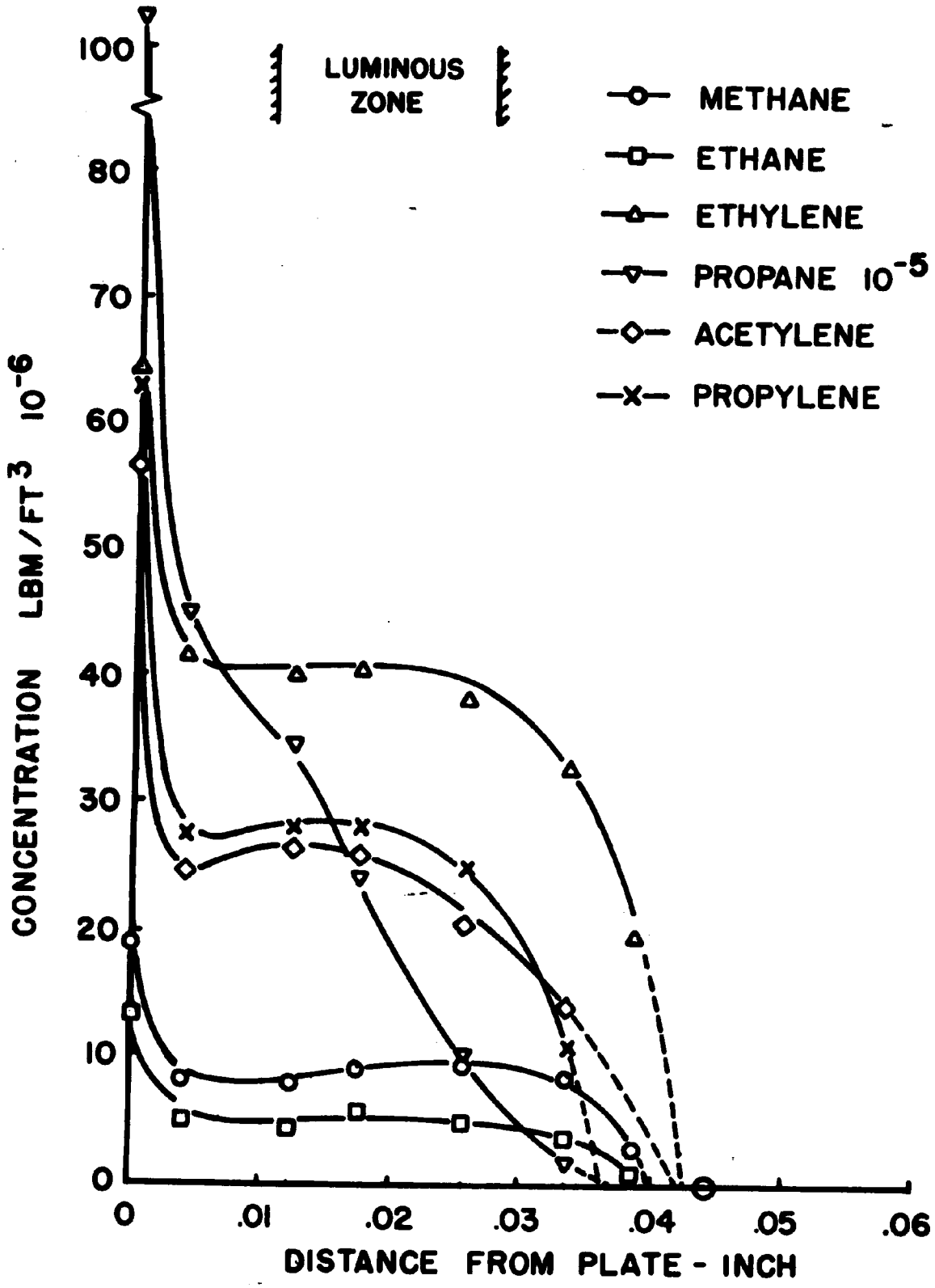
(b) Hydrocarbon concentration profiles

Fig. 26. (Concluded)



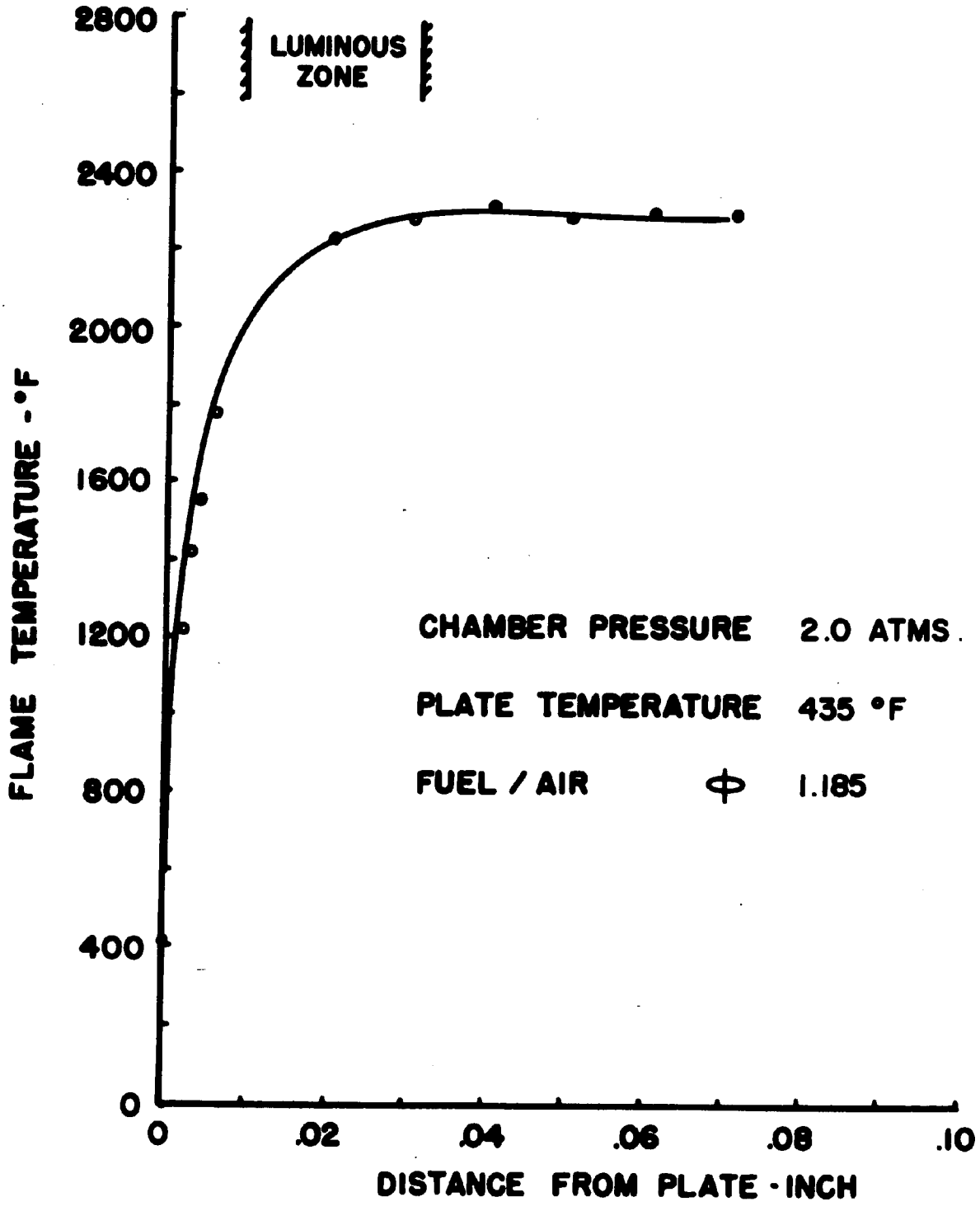
(a) Temperature profile

Fig. 27. Flame structure.



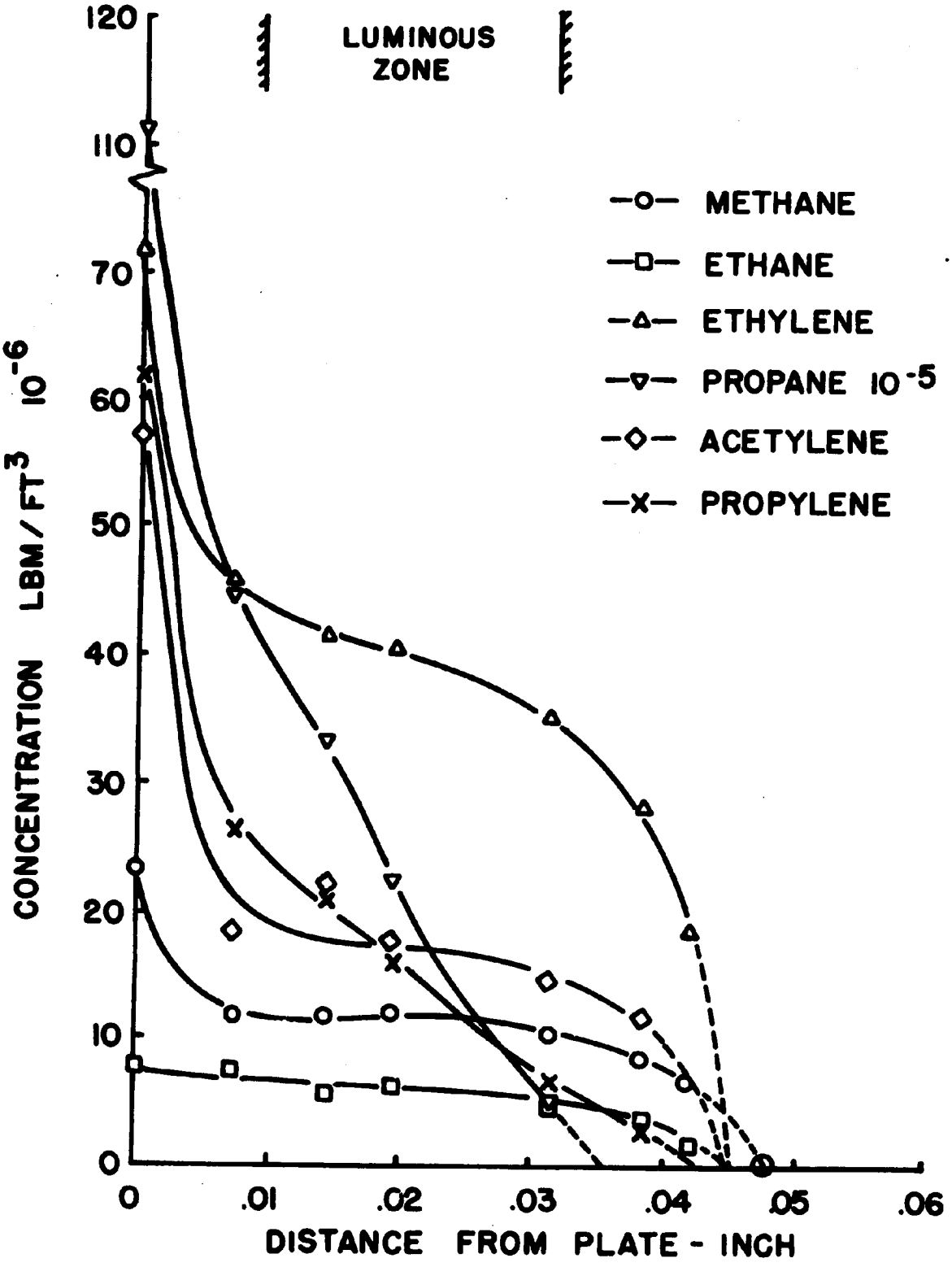
(b) Hydrocarbon concentration profiles

Fig. 27. (Concluded)



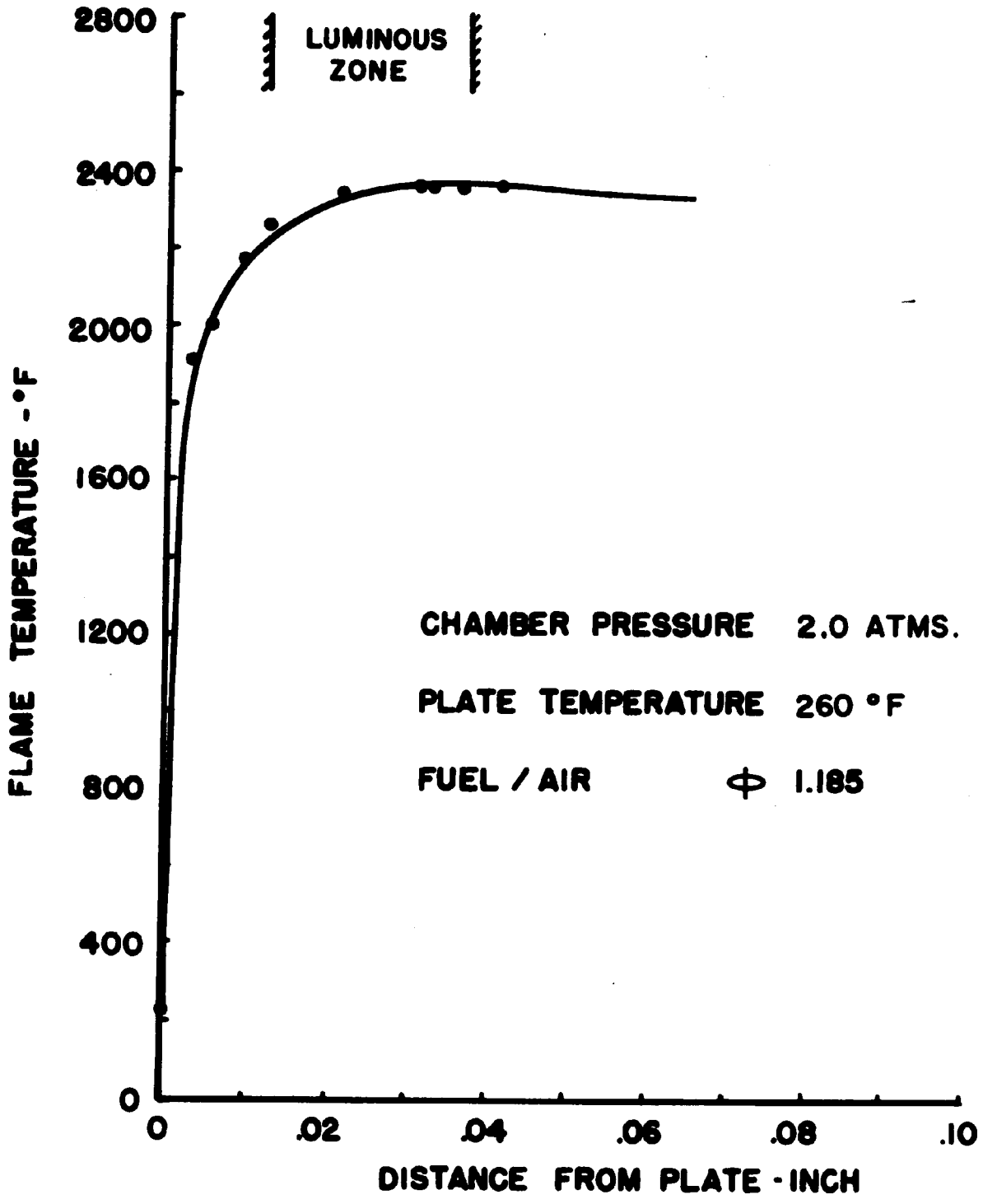
(a) Temperature profile

Fig. 28. Flame structure.



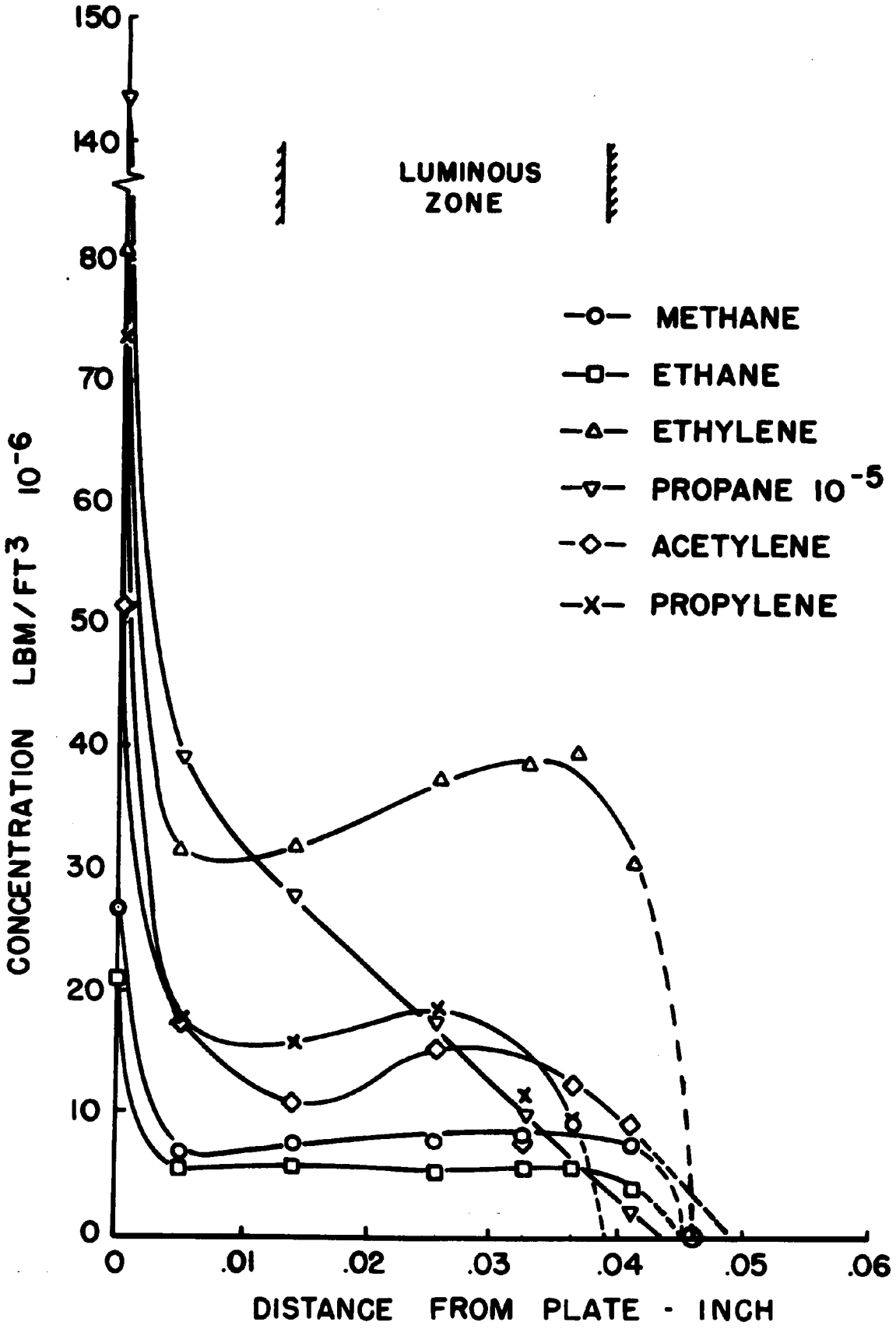
(b) Hydrocarbon concentration profiles

Fig. 28. (Concluded)



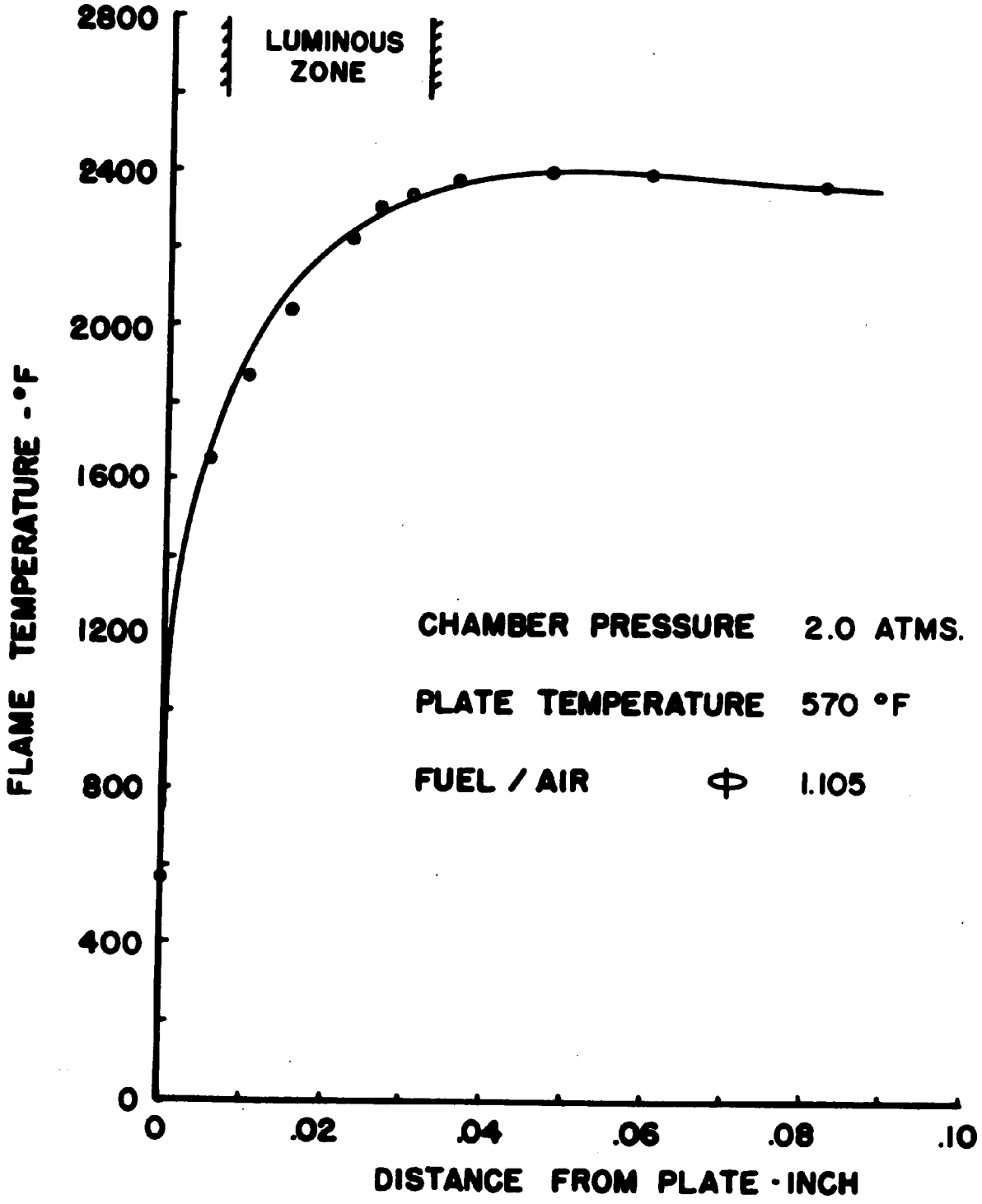
(a) Temperature profile

Fig. 29. Flame structure.



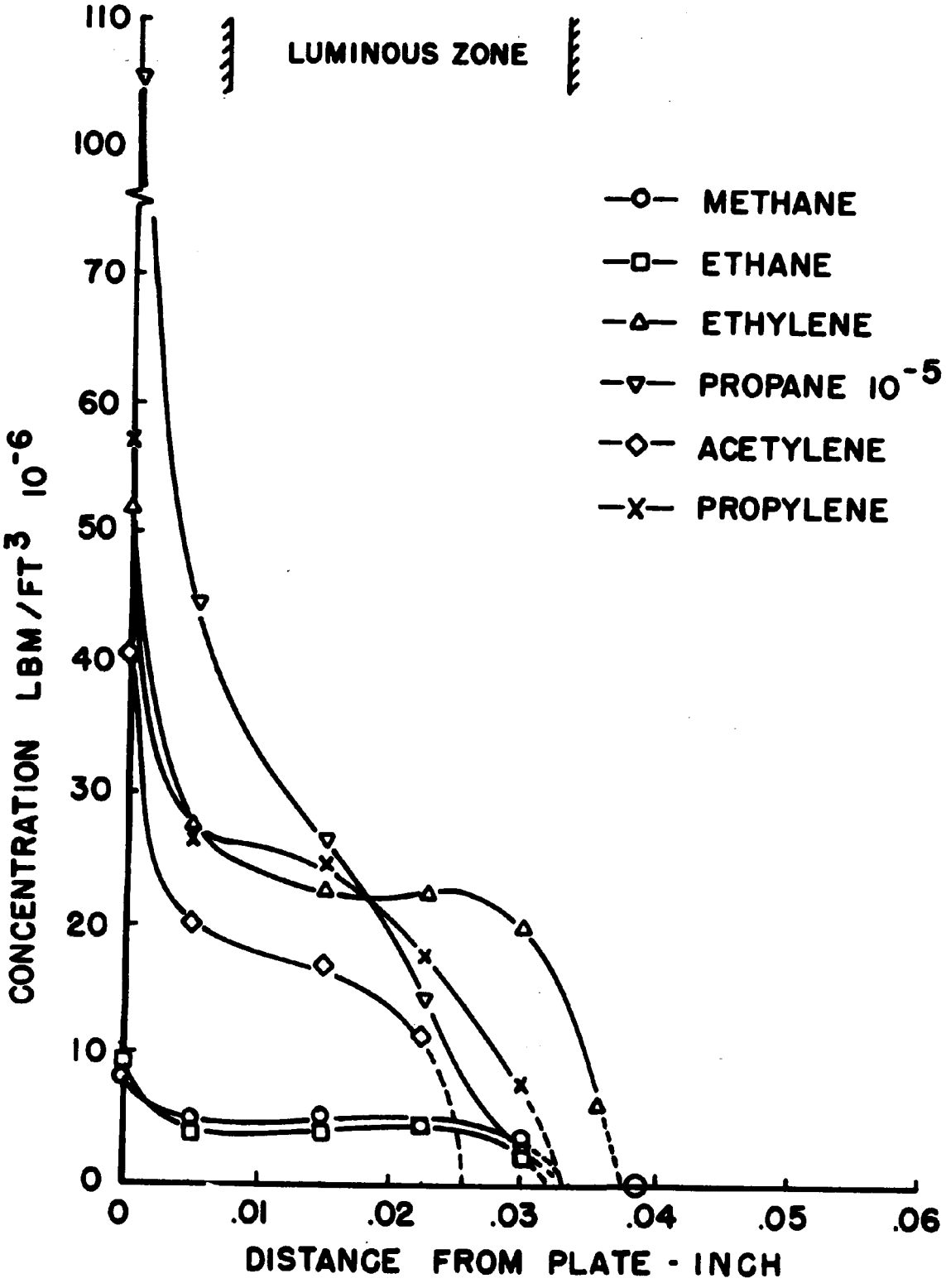
(b) Hydrocarbon concentration profiles

Fig. 29. (Concluded)



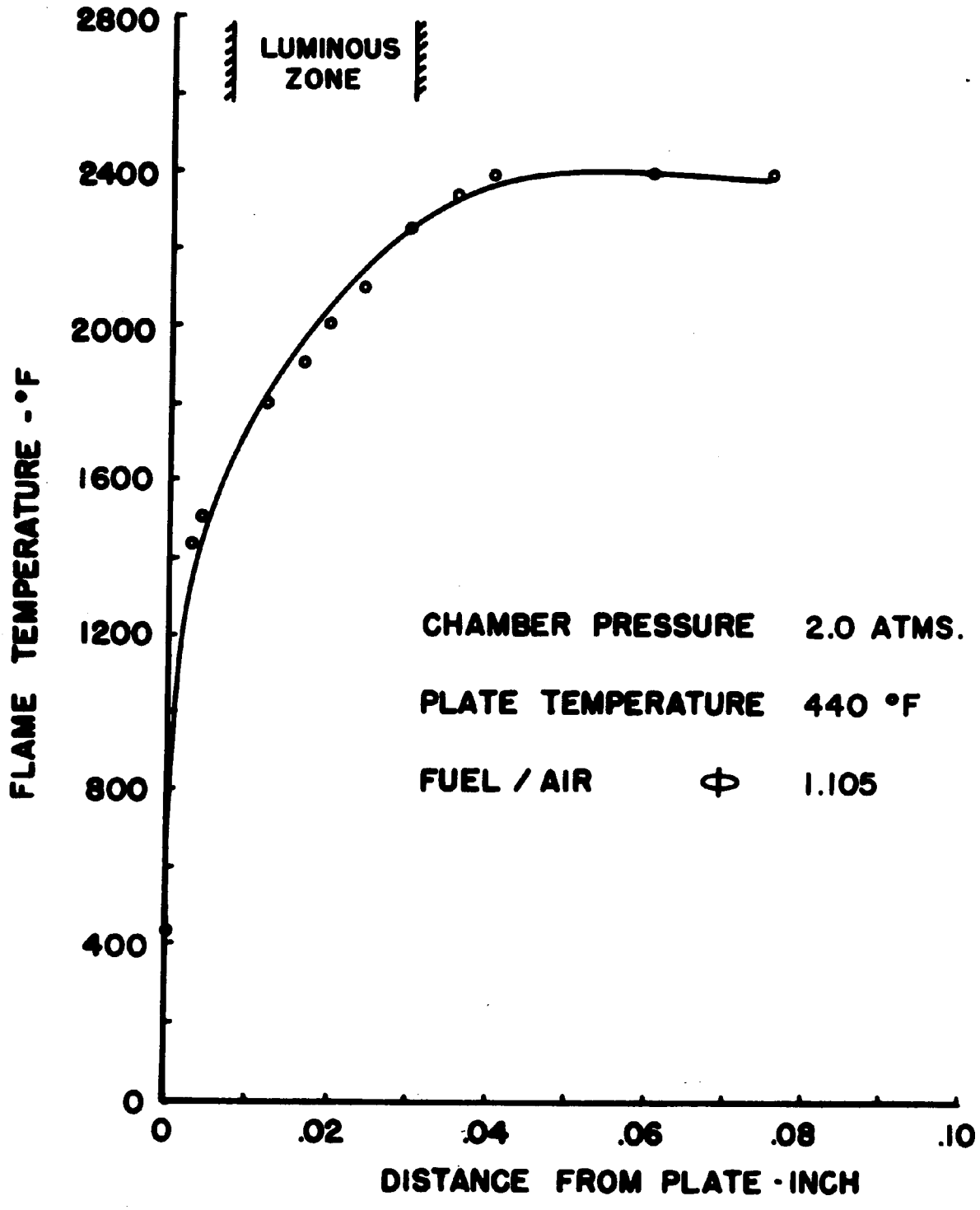
(a) Temperature profile

Fig. 30. Flame structure.



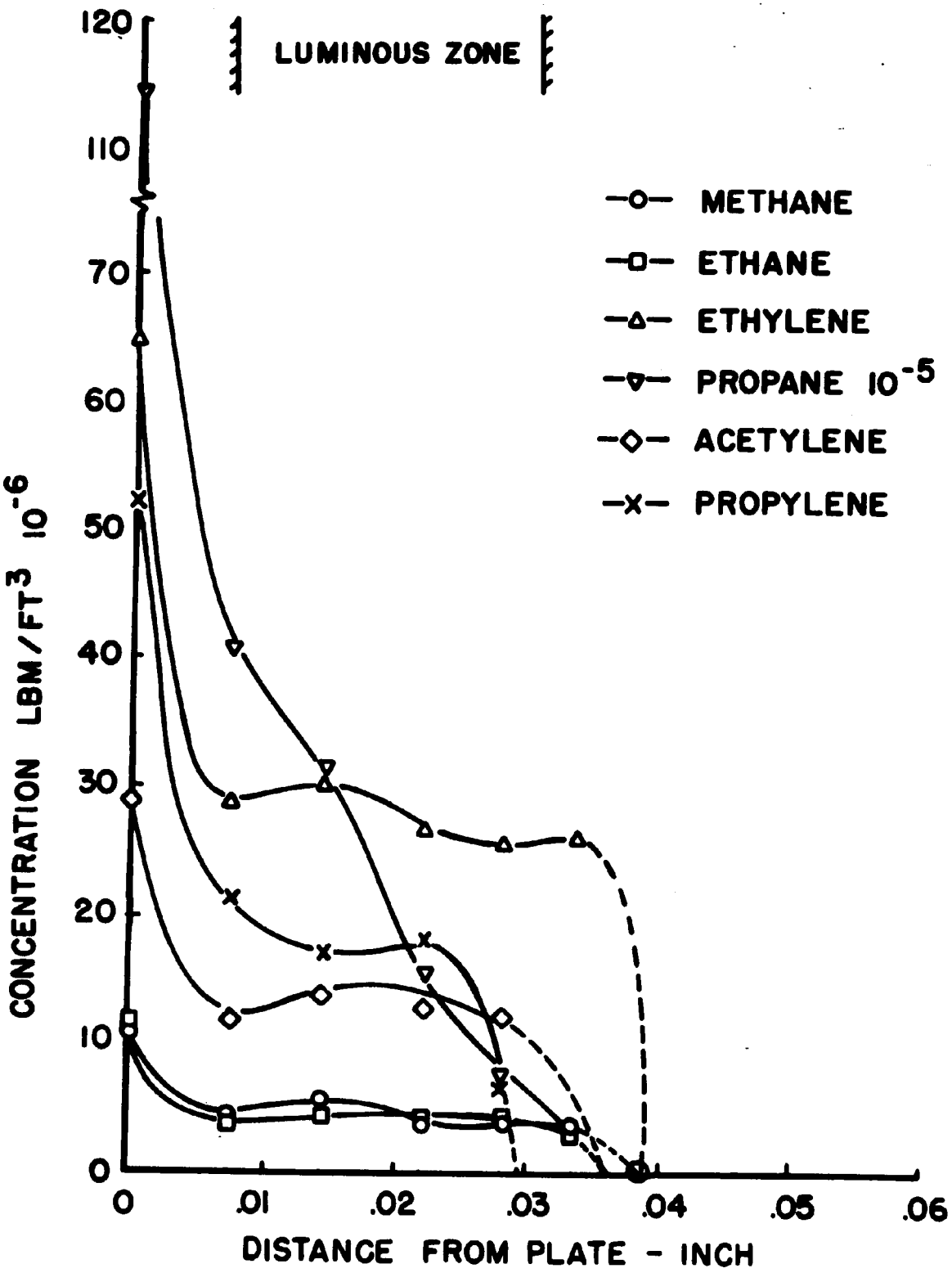
(b) Hydrocarbon concentration profiles

Fig. 30. (Concluded)



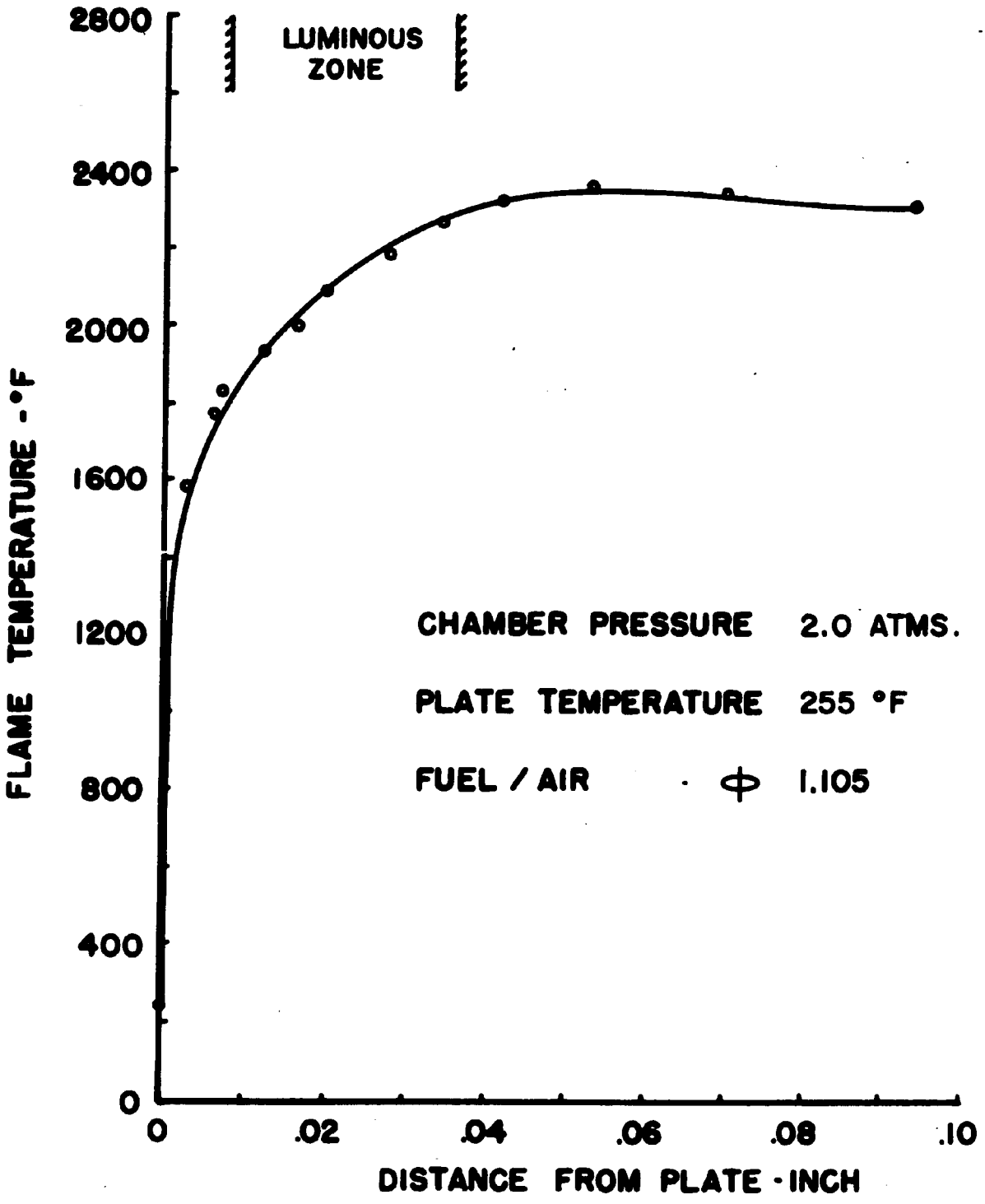
(a) Temperature profile

Fig. 31. Flame structure.



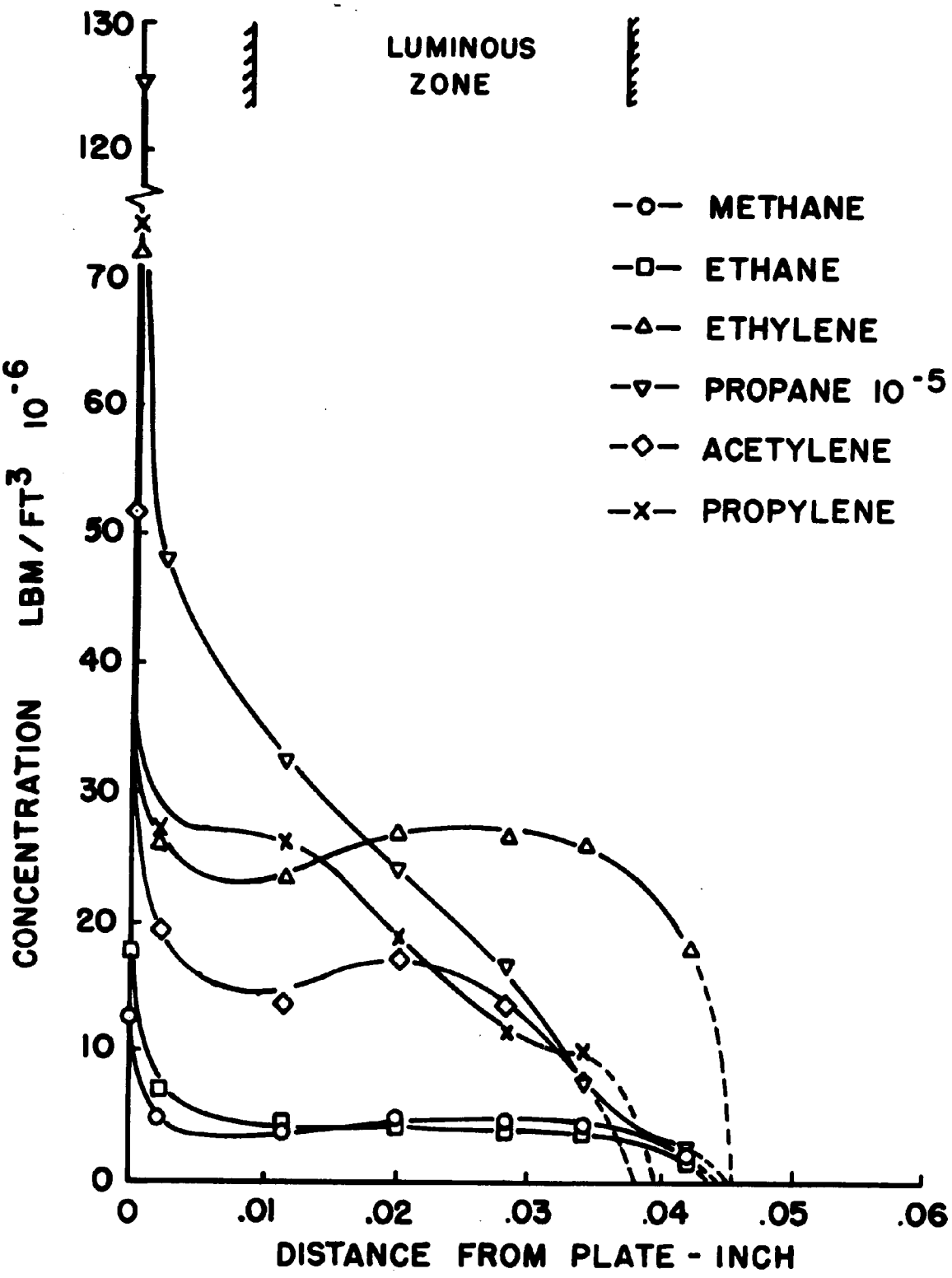
(b) Hydrocarbon concentration profiles

Fig. 31. (Concluded)



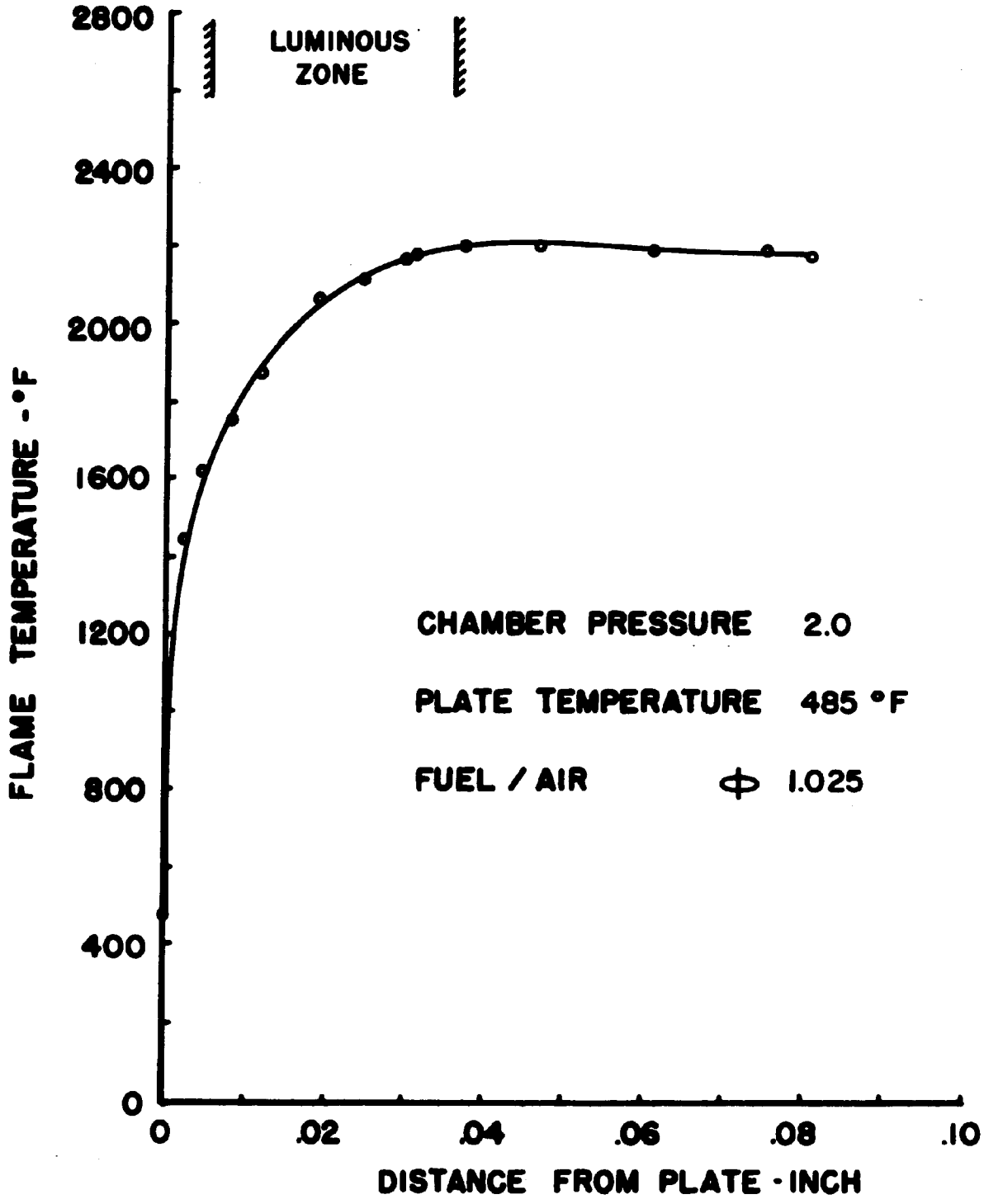
(a) Temperature profile

Fig. 32. Flame structure.



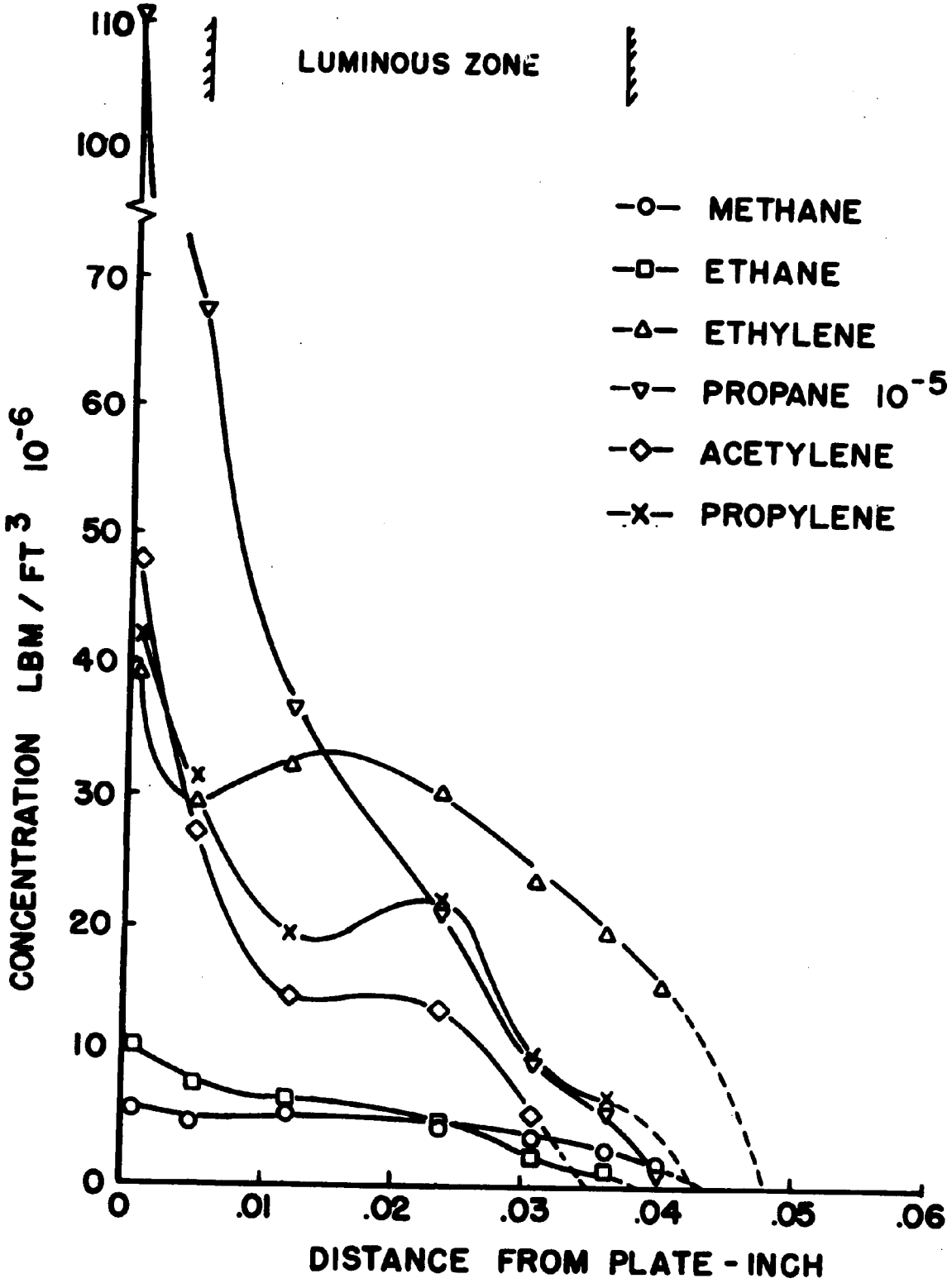
(b) Hydrocarbon concentration profiles

Fig. 32. (Concluded)



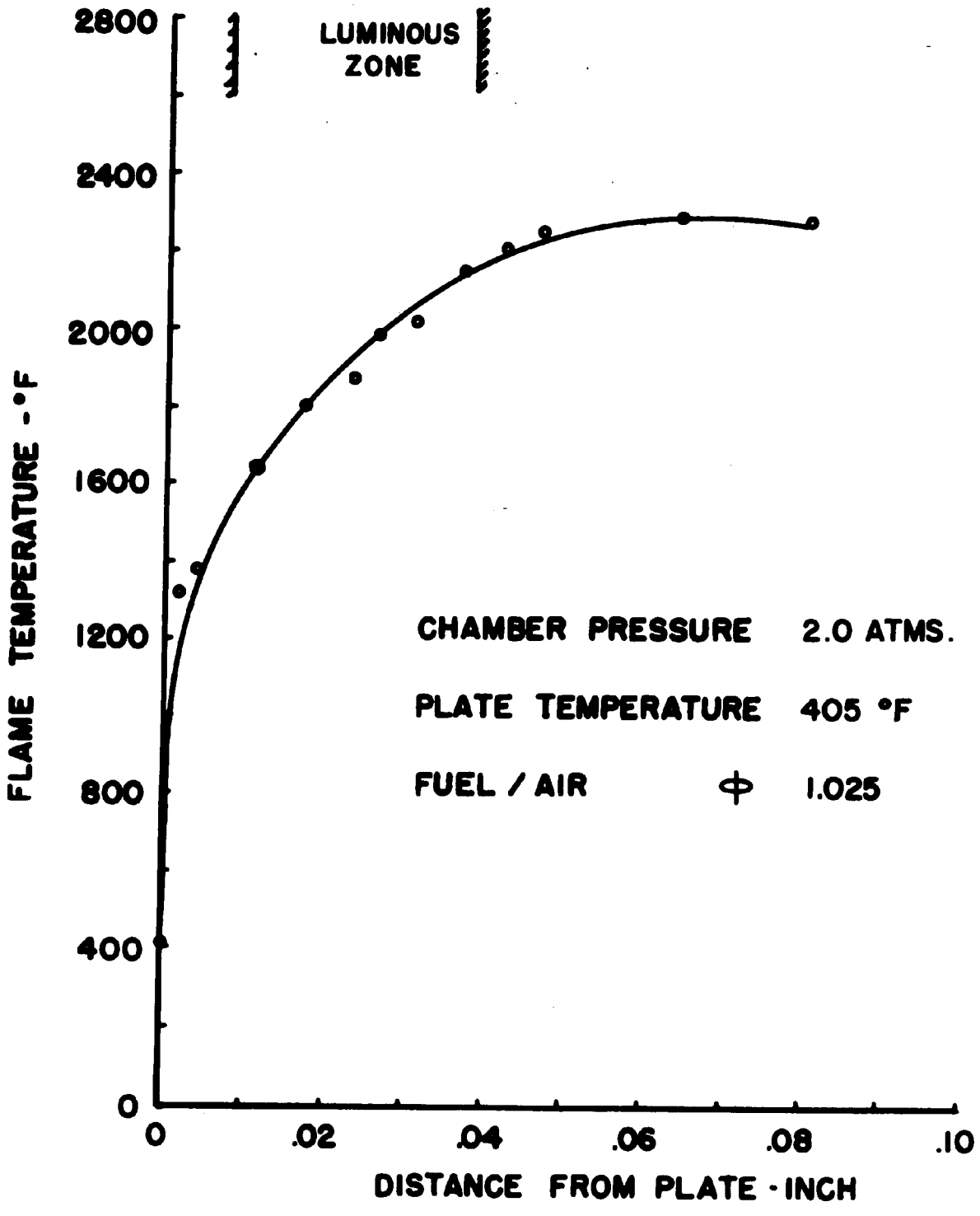
(a) Temperature profile

Fig. 33. Flame structure.



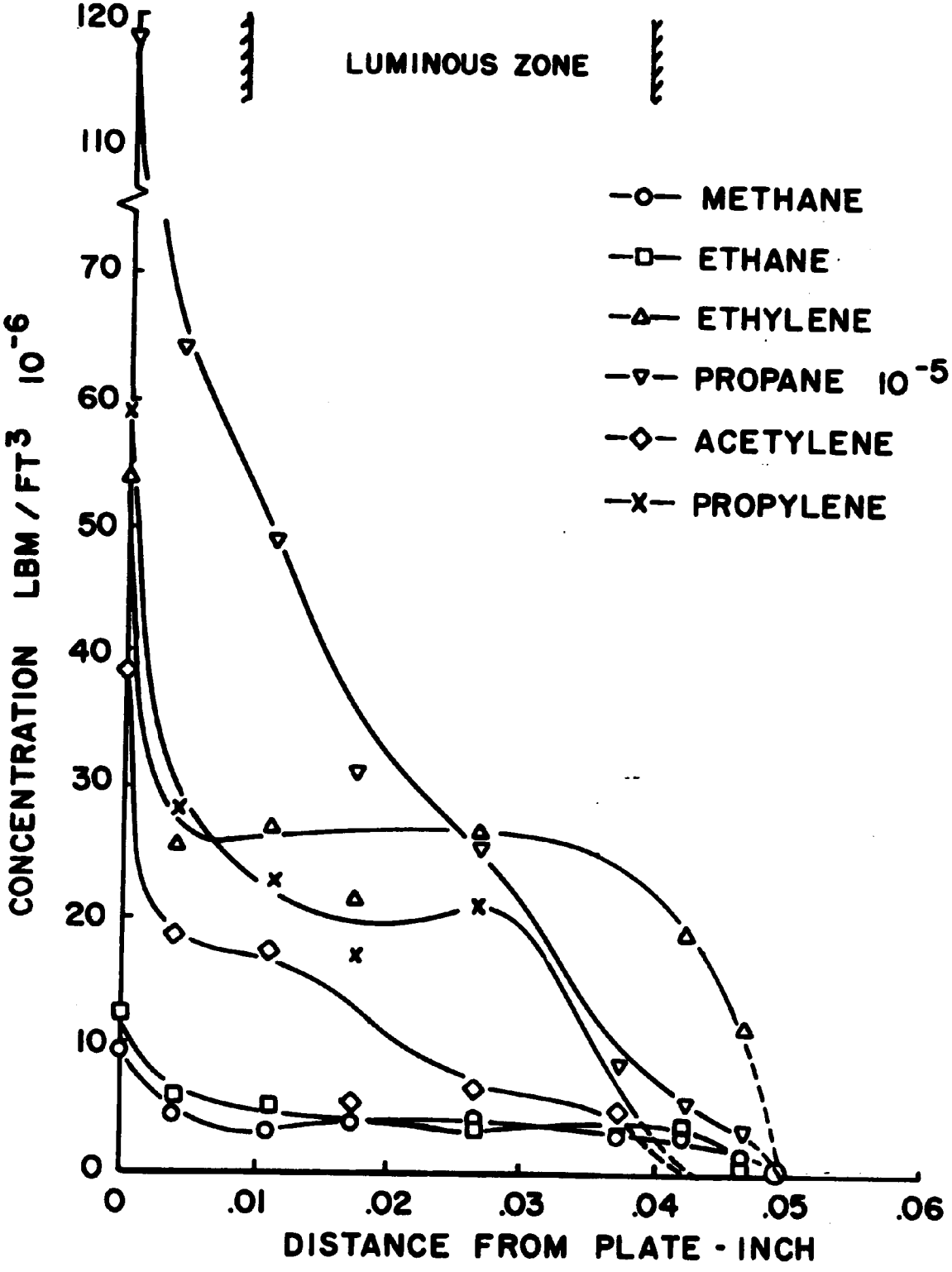
(b) Hydrocarbon concentration profiles

Fig. 33. (Concluded)



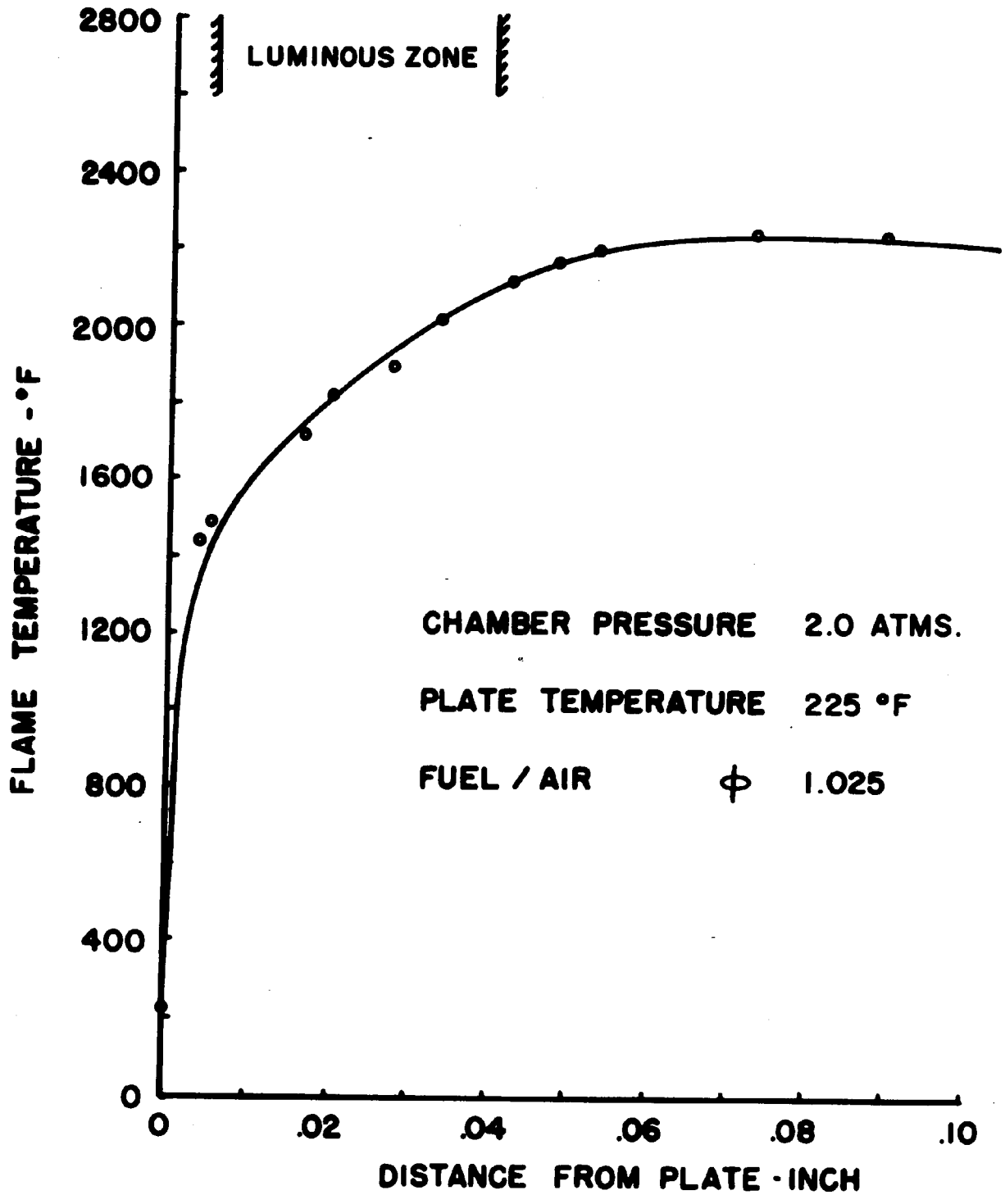
(a) Temperature profile

Fig. 34. Flame structure.



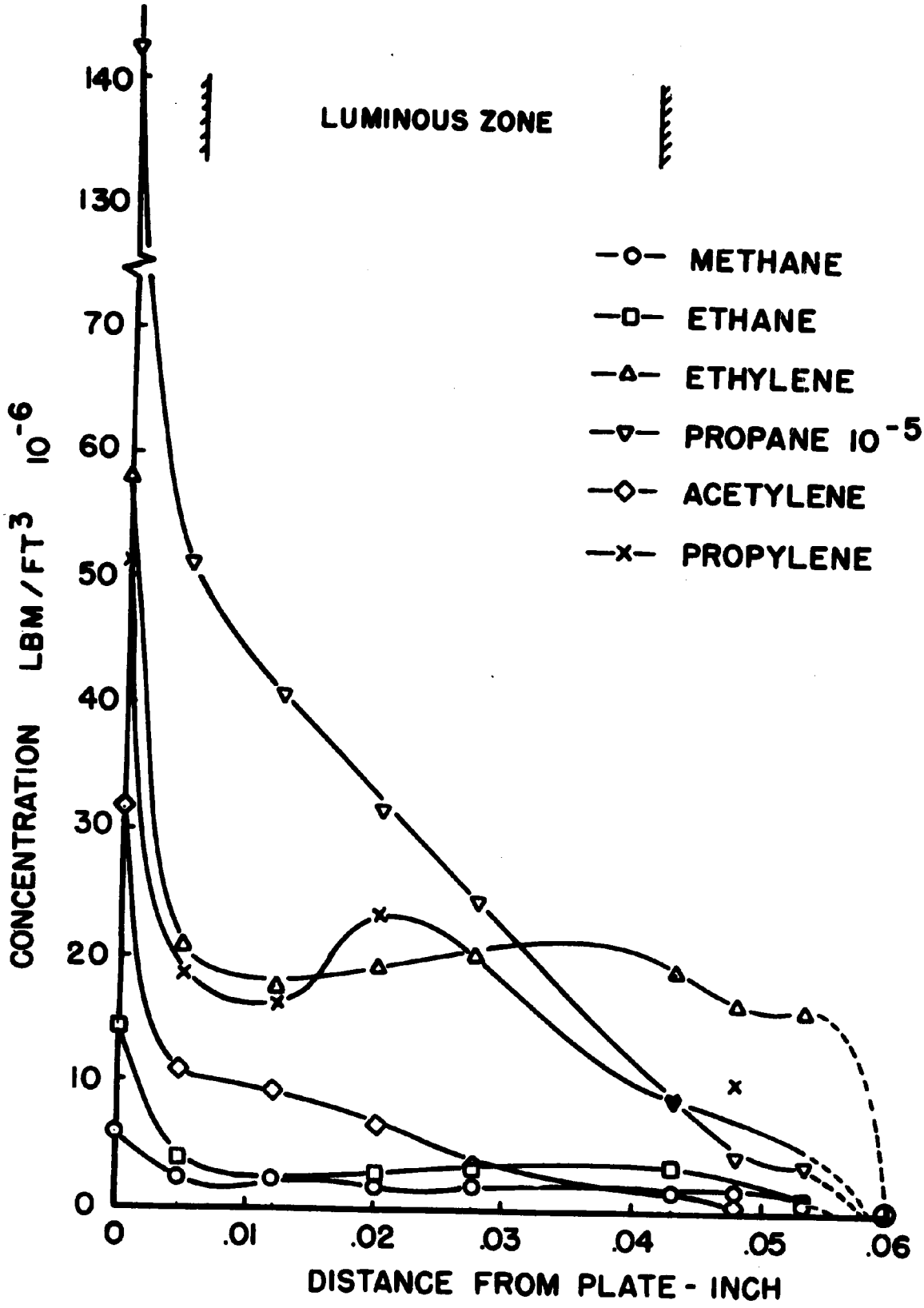
(b) Hydrocarbon concentration profiles

Fig. 34. (Concluded)



(a) Temperature profile

Fig. 35. Flame structure.



(b) Hydrocarbon concentration profiles

Fig. 35. (Concluded)

B. QUENCH DISTANCE

The quench distances used in the accompanying graphs (Figs. 36-38), were taken from the hydrocarbon concentration profiles. They are the distances from the plate to a point in the flame which includes approximately 99% of the unburned hydrocarbons. This point was chosen because of the difficulty of determining accurately the point at which all hydrocarbons were completely burned, this point being somewhere between the last gas sample containing detectable hydrocarbons and the first sample containing none.

Figure 36 shows variations in quench distance at atmospheric pressure for several equivalence ratios at plate temperatures varying between 200° and 600°F.

From this figure it can be seen that the plate temperature had a greater effect on the quench distance at the lean mixture ratios than at the rich. At an equivalence ratio of 0.945 the quench distance was increased from 0.038 to 0.053 in., when the plate temperature was reduced from 460° to 190°F, while at an equivalence ratio of 1.025, the quench distance increased from 0.029 to 0.038 in. when the plate temperature was reduced from 530° to 235°F. At ϕ = 1.185 only a very slight decrease in the quench distance occurred with increasing plate temperature.

Figure 37 shows variations in quench distance at constant plate temperature with equivalence ratios varying from 0.95 to 1.185. This figure replots the data discussed above and shows that for the same mixture ratio the effect of plate temperature on quench distance is not linear.

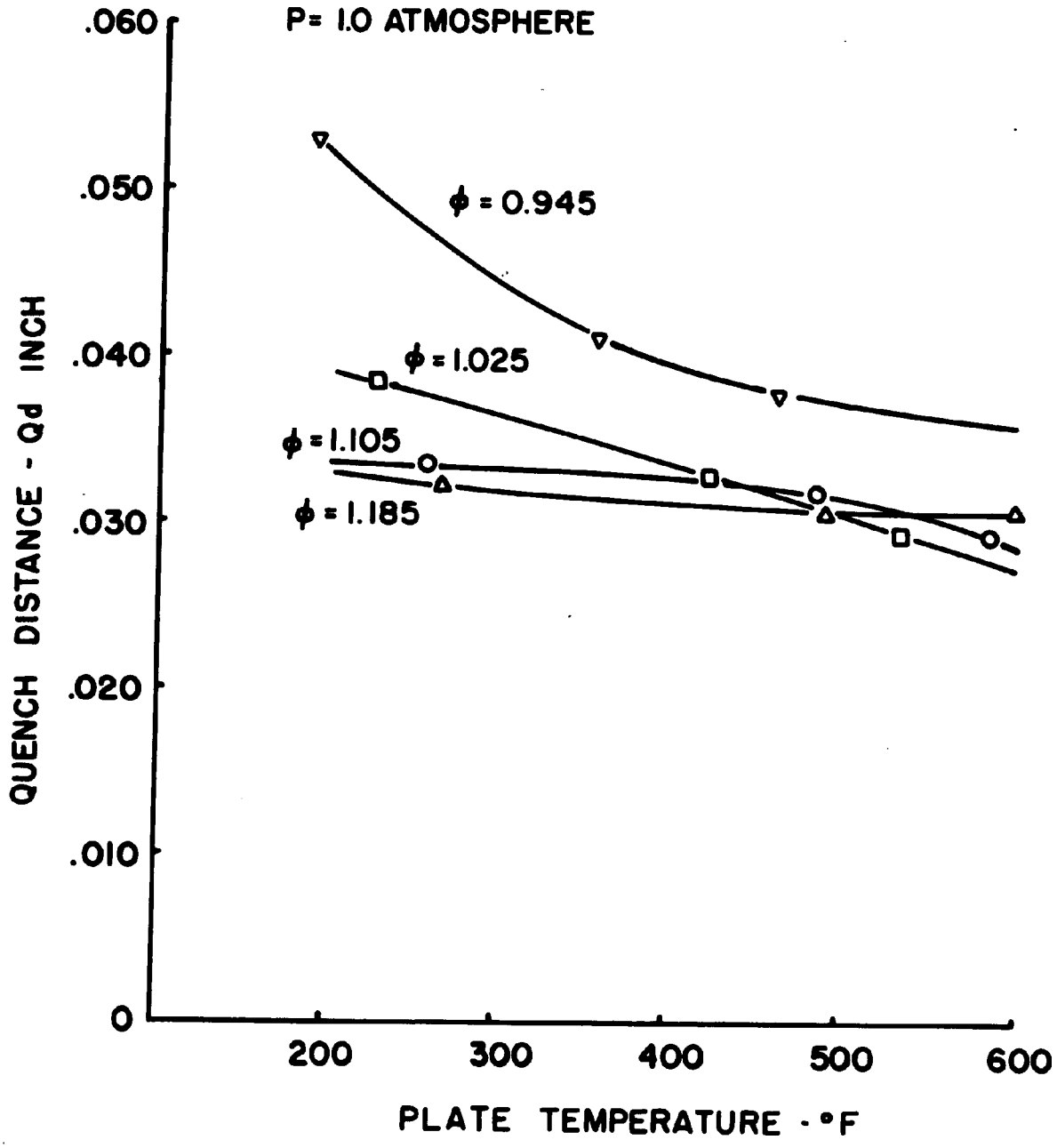


Fig. 36. Effect of wall temperature on quench distance at various mixture ratios at a chamber pressure of 1.0 atm.

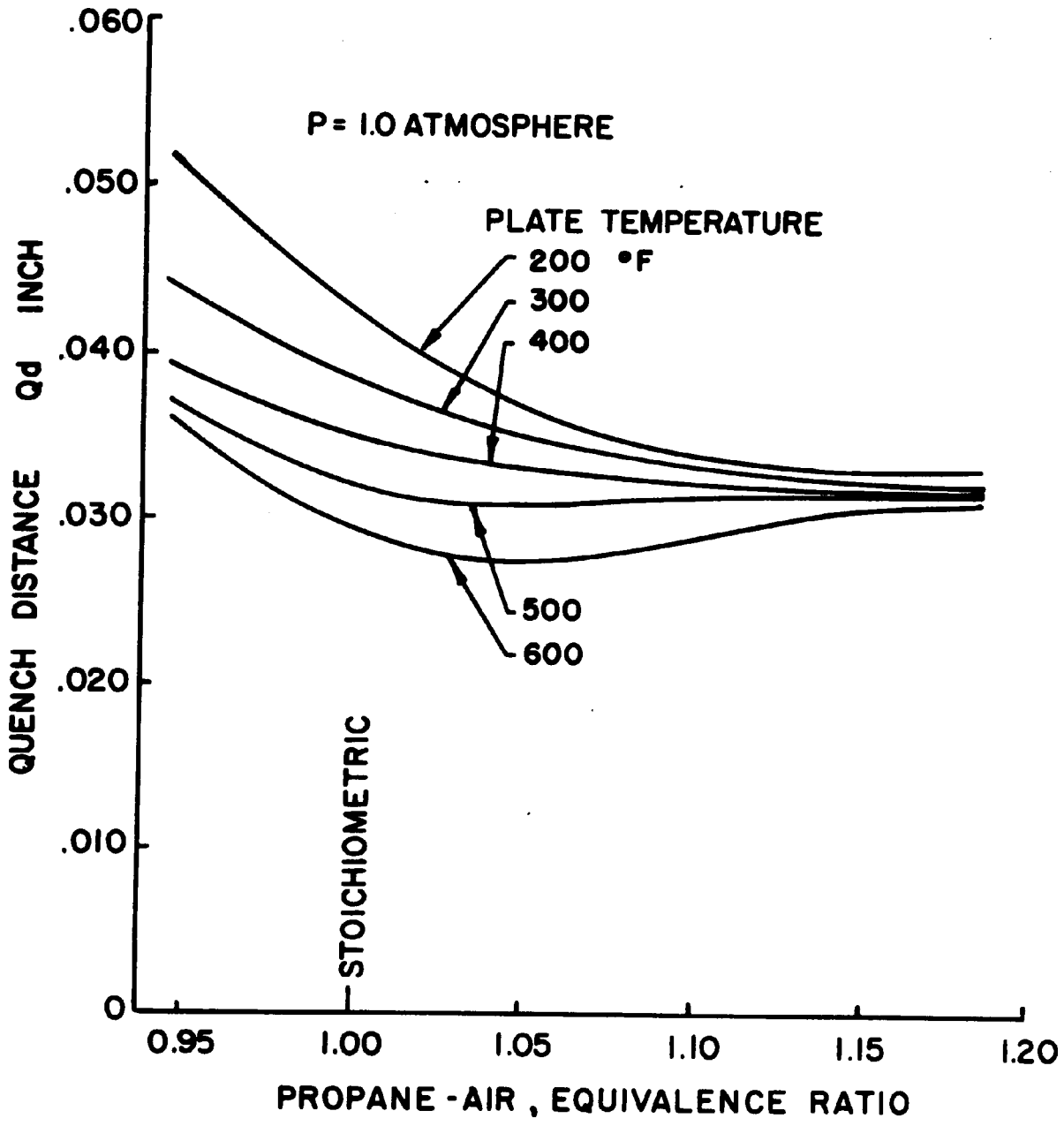


Fig. 37. Effect of mixture ratio and plate temperature on the quench distance at a chamber pressure of 1.0 atm.

Figure 38 is a three-dimensional representation of quench distance at 1.0 atmosphere resulting from variations in both plate temperature and equivalence ratio from which the quench distance can be read for any combination of plate temperature and equivalence ratio when within the ranges used in this test.

The measurement of the quench distance at a chamber pressure of 2.0 atmospheres was offset by tailing of the concentration profiles at the end of the quench zone, which took place in a region of about 0.010 in. (Fig. 35b).

C. MASS OF UNBURNED HYDROCARBONS

The amount of each unburned hydrocarbon in the quench zone is presented in mass per unit area of plate surface. This was obtained by measuring the area under the concentration profile of each hydrocarbon and converting to mass per unit area. The total mass of hydrocarbons is the sum of the masses of the various species.

Hydrocarbon masses for different mixture ratios and plate temperatures are shown in Tables II and III at chamber pressures of 1.0 and 2.0 atmospheres, respectively.

From the data obtained and shown in the tables it was found that there was no apparent consistent trend for the change of the mass of the different intermediates (methane, ethane, ethylene, acetylene, and propylene), due to change in plate temperature.

An increase in the mass of methane, propylene, and ethylene was

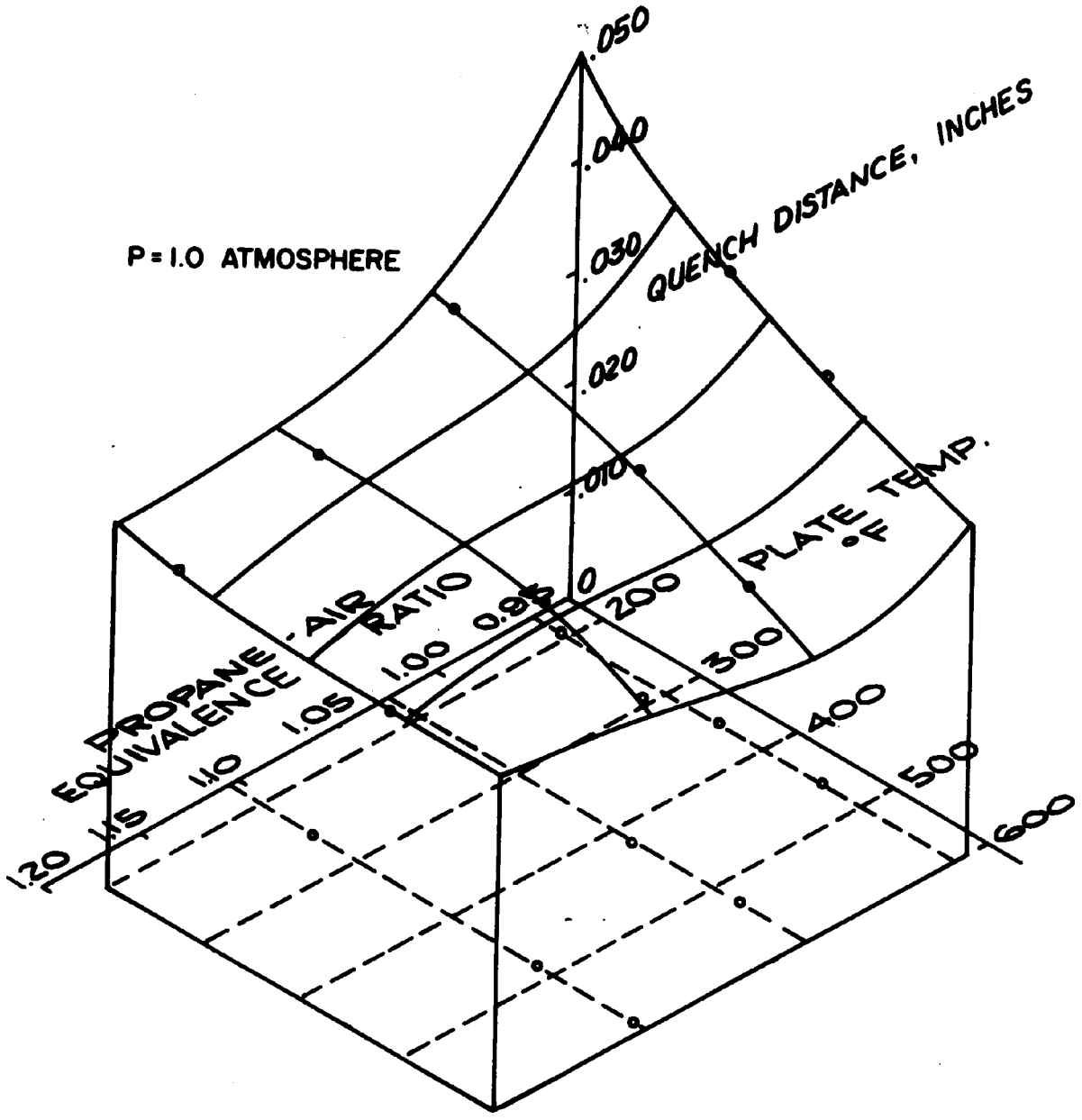


Fig. 38. Three-dimensional representation of quench distance resulting from variations in both plate temperature and mixture ratio at a chamber pressure of 1.0 atm.

TABLE II

MASSES OF UNBURNED HYDROCARBONS PER UNIT SURFACE AREA OF WALL AT VARIOUS MIXTURE RATIOS AND WALL TEMPERATURES AND CHAMBER PRESSURE OF 1.0 ATMOSPHERE

F/A, ϕ	Plate Temperature, °F	Quench Distance, in.	Mass per Unit Surface Area (10^{-8} lbm/ft^2)						
			Methane	Ethane	Ethylene	Propane	Acetylene	Propylene	Total
0.0757	600	0.031	1.67	2.25	9.20	38.8	1.96	3.95	57.83
1.185	490	0.031	1.67	1.67	8.95	38.5	2.00	4.30	57.09
	265	0.032	1.17	1.33	7.85	41.8	1.96	3.60	57.71
0.0708	585	0.029	1.34	1.34	8.20	33.4	1.88	4.42	50.58
1.105	482	0.032	1.08	1.38	7.00	40.5	1.90	3.10	54.96
	255	0.033	1.13	1.17	7.00	48.0	1.50	3.14	61.94
0.0657	530	0.029	0.90	0.92	5.95	41.3	1.34	4.1	54.51
1.025	420	0.033	0.92	1.00	6.43	48.5	1.38	3.6	61.83
	225	0.038	0.67	0.87	5.42	51.5	1.67	2.64	62.77
0.0605	460	0.038	0.88	0.92	5.92	61.0	1.35	3.88	73.95
0.945	355	0.041	0.88	1.13	6.50	66.0	1.54	3.60	79.65
	190	0.053	0.46	0.79	5.19	74.0	1.63	2.97	85.04

TABLE III

MASSES OF UNBURNED HYDROCARBONS PER UNIT SURFACE AREA OF WALL AT VARIOUS MIXTURE RATIOS AND WALL TEMPERATURES AND CHAMBER PRESSURE OF 2.0 ATMOSPHERES

F/A ϕ	Plate Temperature, °F	Quench Distance, in.	Mass per Unit Surface Area (10^{-8} lbm/ft^2)						
			Methane	Ethane	Ethylene	Propane	Acetylene	Propylene	Total
0.0805	565	0.042	5.5	1.92	14.85	79.5	6.85	7.25	115.87
1.26	460	0.044	5.55	2.45	15.00	96.0	7.60	6.70	133.3
	240	0.047	5.85	2.55	17.00	104.0	6.90	7.28	143.58
0.0757	580	0.036	2.67	1.50	12.55	77.0	7.0	7.7	108.42
1.185	435	0.041	2.70	1.84	13.10	79.0	6.1	6.1	108.84
	260	0.041	2.75	1.70	12.20	83.0	5.0	5.2	109.67
0.0708	570	0.031	1.17	1.09	6.80	73.0	3.85	5.85	91.76
1.105	440	0.035	1.35	1.25	9.20	80.0	3.68	4.75	100.23
	255	0.041	1.30	1.26	9.30	91.0	4.45	6.25	113.56
0.0657	485	0.038	1.58	1.58	10.20	106.0	4.85	5.50	129.71
1.025	405	0.045	1.58	1.64	9.90	121.0	4.25	6.43	144.80
	225	0.051	0.83	1.30	9.05	124.0	2.67	6.70	144.57
0.0605									
0.945	425	0.046	0.58	1.38	10.45	146.0	6.42	9.20	174.3

noticed as the equivalence ratio increases, and rose sharply at $\phi > 1.1$. For ethylene an increase of about 25% was noticed as the equivalence ratio was increased from 0.945 to 1.185 at a chamber pressure of 1.0 atmosphere. The mass of all the intermediates except ethane was fonnd to increase with increase in chamber pressure; for ethylene and propylene the mass was almost doubled for the change from 1.0 to 2.0 atmospheres while for methane and acetylene the mass was almost tripled.

Figures 39 and 40 show variations in total mass of hydrocarbons for different mixture ratios and plate temperatures at chamber pressures of 1.0 and 2.0 atmospheres, respectively. From these the total mass for any combination of the above conditions can be read.

Tailing of the hydrocarbon concentration profiles at the end of the quench zone did not affect the mass measurements appreciably; less than 2% of the mass was located in this region.

For the same plate temperature and chamber pressure the minimum mass of hydrocarbons occurred at $\phi = 1.105$ and increased for both lean and rich mixtures. For the same mixture ratio and chamber pressure the mass of the unburned hydrocarbons per unit surface area of the plate increased as the plate temperature decreased. This effect varied from one mixture ratio to another. A maximum increase in mass of about 22% occurred at $\phi = 1.105$ as the plate temperature was decreased from 585° to 255°F, while at $\phi = 1.185$ no noticeable change in mass occurred with change in plate temperature.

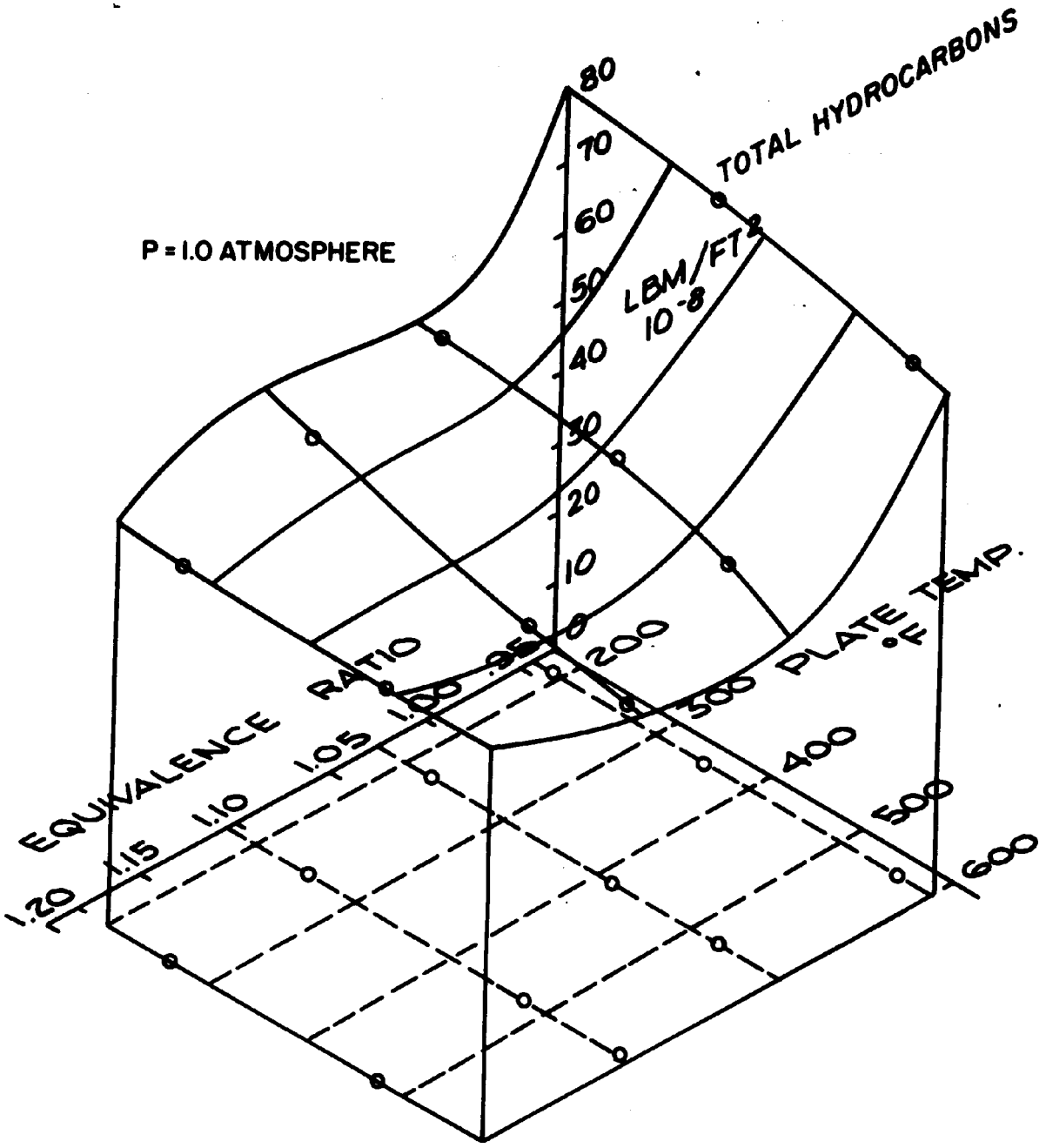


Fig. 39. Three-dimensional representation of mass of unburned hydrocarbons per unit surface area at different plate temperatures and mixture ratios and chamber pressure of 1.0 atm.

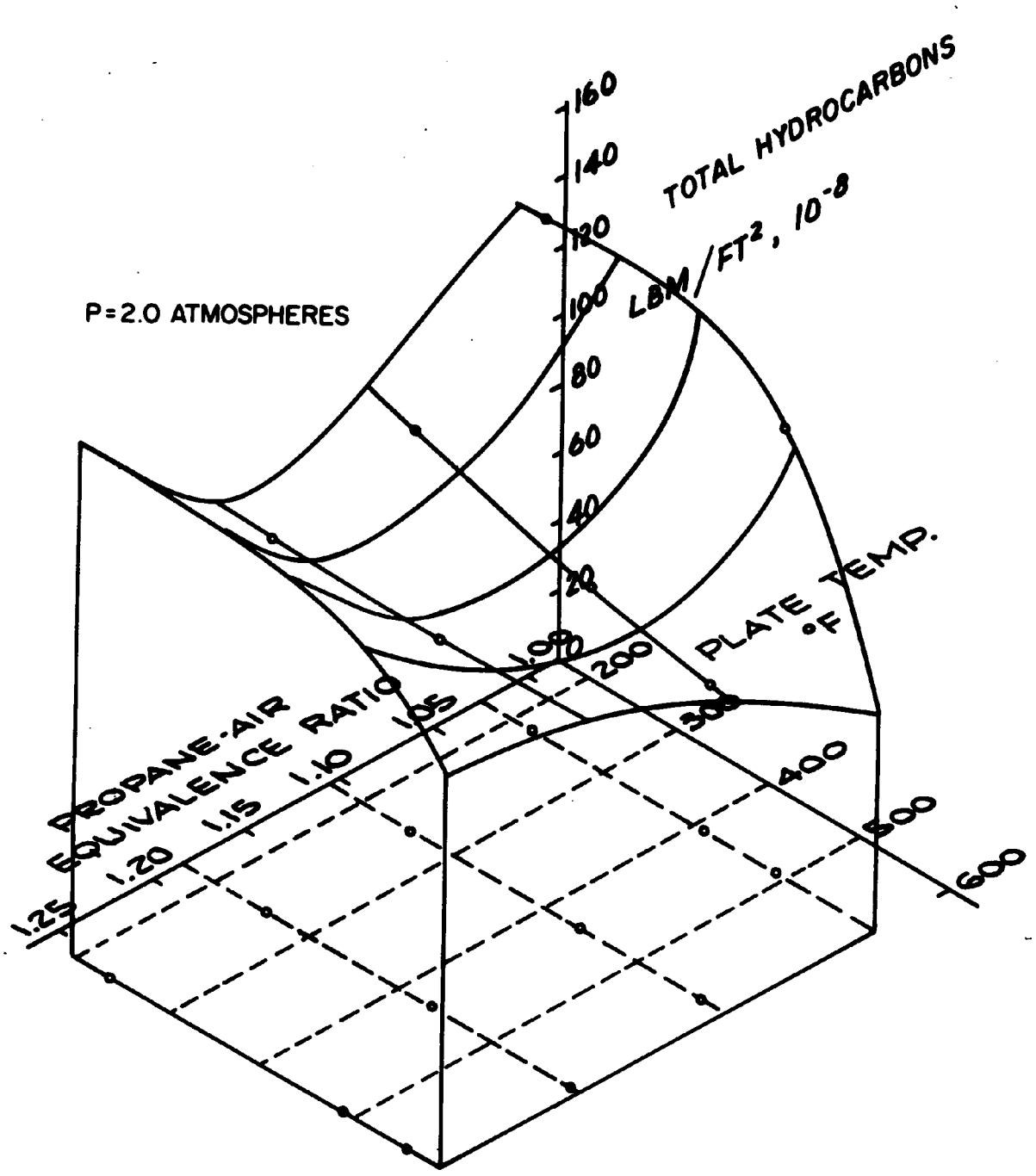


Fig. 40. Three-dimensional representation of mass of unburned hydrocarbons per unit surface area at different plate temperatures and mixture ratios and chamber pressure of 2.0 atm.

D. EFFECT OF PRESSURE, TEMPERATURE, AND MIXTURE RATIO ON THE MASS OF THE UNBURNED HYDROCARBONS

The total masses of hydrocarbons at constant plate temperatures are presented in Table IV for several equivalence ratio and two chamber pressures.

TABLE IV

MASS OF UNBURNED HYDROCARBONS PER UNIT AREA OF WALL AT CONSTANT PLATE TEMPERATURES AND VARIOUS MIXTURE RATIOS AND CHAMBER PRESSURES (lbm/ft^2)

F/A ϕ	Plate Temperature, °F				
	200	300	400	500	600
		Chamber Pressure: 2.0 atm			
1.025	144.0×10^{-8}	144.0×10^{-8}	144.0×10^{-8}	126.0×10^{-8}	100.0×10^{-8}
1.105	118.0	110.0	103.0	96.5	91.0
1.185	109.5	109.0	109.0	108.5	108.0
1.26	143.5	142.0	138.0	127.0	108.0
		Chamber Pressure: 1.0 atm			
0.945	84.8×10^{-8}	82.0×10^{-8}	77.5×10^{-8}	71.7×10^{-8}	64.0×10^{-8}
1.025	63.0	62.5	61.5	57.0	48.0
1.105	62.0	61.0	57.7	54.0	50.0
1.185	57.7	57.7	57.7	57.7	57.7

Figure 41 shows the effect of chamber pressure on the masses of unburned hydrocarbons at different fuel-air ratios and plate temperatures.

From these data, the following relation between the mass of hydrocarbons per unit surface area and chamber pressure, wall temperature, and mixture ratio was obtained.

$$m = K P^{a} T^{-b} \qquad (5.1)$$

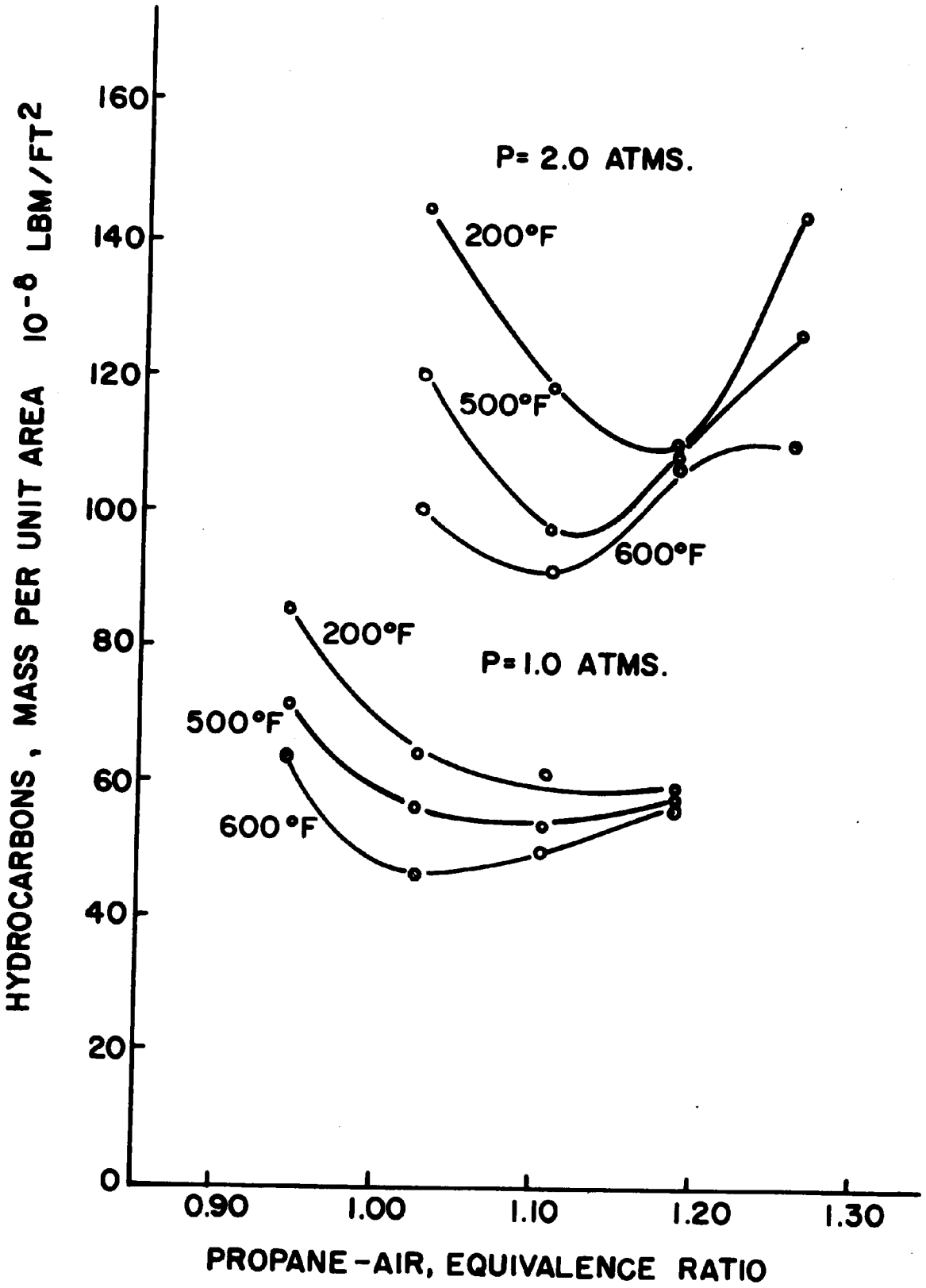


Fig. 41. Effect of chamber pressure on mass of unburned hydrocarbons at various mixture ratios and plate temperatures.

where

m = pounds/ft^2

P = atmospheres

T = degrees Rankine

Table V presents the values of the exponents "a," "b," and constant of proportionality "K" for three equivalence ratios.

TABLE V

VALUES OF CONSTANT OF PROPORTIONALITY AND EXPONENTS USED IN EQN. (5.1)

ϕ	K	a	b
0.945	38.2×10^{-6}	1.0	-0.58
1.0	13.8×10^{-6}	1.0	-0.85
1.105	21.0×10^{-6}	0.93	-0.54

CHAPTER VI

DISCUSSION

A. DISCUSSION OF RESULTS OBTAINED WITH POROUS PLATE BURNER

The results show that the model was suitable for the study of the mass of unburned hydrocarbons resulting from the quenching effect of the plate in the model. Visual observations of the rapid propagation of the flame towards the porous-plate, after the mixture was ignited at a point several inches above the plate, and the readily apparent effect of the plate in suppressing the flame as it approached the plate, demonstrated the influence of the plate in retarding the chemical reaction. The influence of the wall was further demonstrated by the fact that the mass of unburned hydrocarbons varied with changes in plate temperature at constant chamber pressure and fuel-air ratio. It was also observed that the maximum measured temperature of the flame near the wall was about 2550°F (Figs. 15-17) while the adiabatic flame temperature[50] at a similar equivalence ratio and chamber pressure is about 3600°F. This temperature difference indicates that as the flame approached the wall, heat was transferred to the wall at a rate higher than the rate of thermal energy generation in the flame. This loss of heat from the flame retarded the chemical reactions and suppressed flame propagation.

The first assumption that any reaction that would take place in the porous plate are negligible, appears to be reasonable. The intermediates (methane, ethane, ethylene, acetylene, and propylene) found near the

plate surface can be attributed to the propane-air reaction taking place near the wall. The existence of these exothermal reactions is indicated by the fact that the temperature profiles near the plate have a negative second derivative $\frac{\partial^2 T}{\partial x^2} < 0$. Also, the intermediates appeared near the surface of the plate when the plate temperature was as low as 190°F (Fig. 23), a temperature at which reactions in the plate are very unlikely to occur. Although the slope of the concentration profiles of these intermediates near the plate surface may appear to indicate that they originated in the porous plate (Figs. 12-35), the effect is due to the density variation through the flame. When the profiles were corrected to a common density, the maximum concentrations appeared at some distance from the wall as shown in Fig. 42. This indicates that the major source of these intermediates is within the flame itself.

There is a possibility that some fraction of the concentration of these intermediates was due to reactions within the sampling probe itself. This possibility was minimized by choosing a rapidly divergent sampling probe which showed the largest amount of propane near the wall surface, corresponding to samples taken without the flame. This comparison also served as a check on the agreement between the amount of hydrocarbons in the fresh mixture and the amount of the unburned hydrocarbons measured at the wall surface for the same mixture during combustion. Appendix E shows a slight drop in propane concentration when the flame is present, a result of the reactions taking place near the wall.

The second assumption for the model was that the low mixture velocity

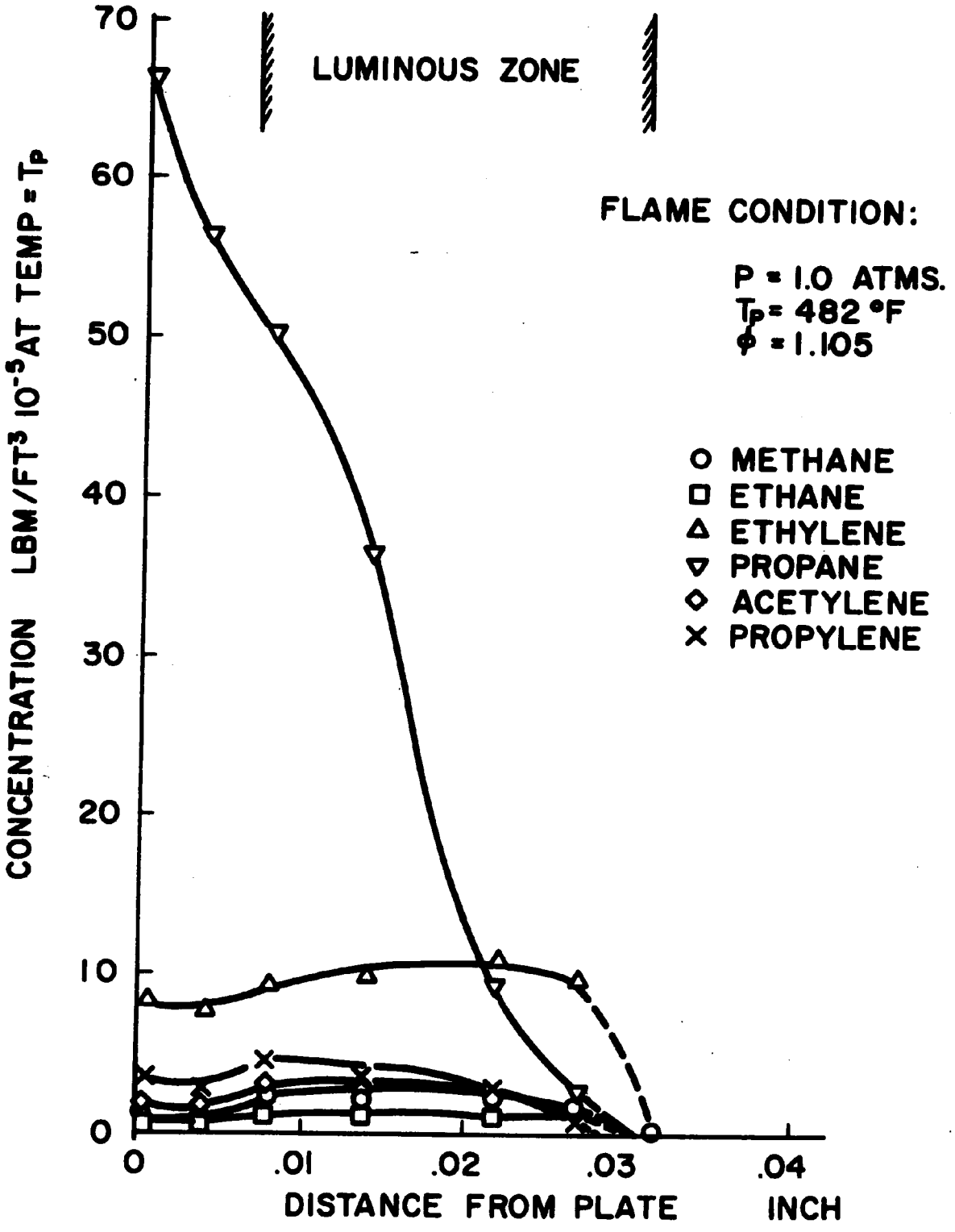


Fig. 42. Hydrocarbon concentration profiles based on a uniform temperature.

used enabled the model to provide a degree of quenching comparable to that for the transient case. The mass flow rate was held constant, giving a mixture velocity of about 5 fpm, as measured by a hot wire anemometer. The flame velocity in the range of conditions used was about 70-90 fpm.[50] With this 16:1 ratio of flame velocity to mixture velocity the degree of quenching, as represented by point A in Fig. 1, approached that for the transient case represented by point B. Furthermore, the fact that the dead space measured in the porous plate model agreed reasonably well with that measured by Kaskan[32] in a model in which the flow was parallel to the wall (Fig. 43), is additional support that the porous plate model is operating in a region close to point B, the point of complete quenching.

The first objective was to develop a method for measuring the quantity and species of unburned hydrocarbons in the quench zone. In Ref. 9 information on the amount of unburned hydrocarbons resulting from wall quenching was obtained by a correlation of dead space to mass of hydrocarbons in the engine exhaust. Measuring the mass from hydrocarbon profiles takes into account the entire hydrocarbon residue in the quench zone whereas mass predictions based on observations of dead space do not. From the measurements in this test it was found that the dead space included only a small part of the total mass of unburned hydrocarbons, e.g., 26% at an equivalence ratio of 1.185, wall temperature of 600°F, and a pressure of 1.0 atmosphere.

The concentration profiles also show that the dead space is not

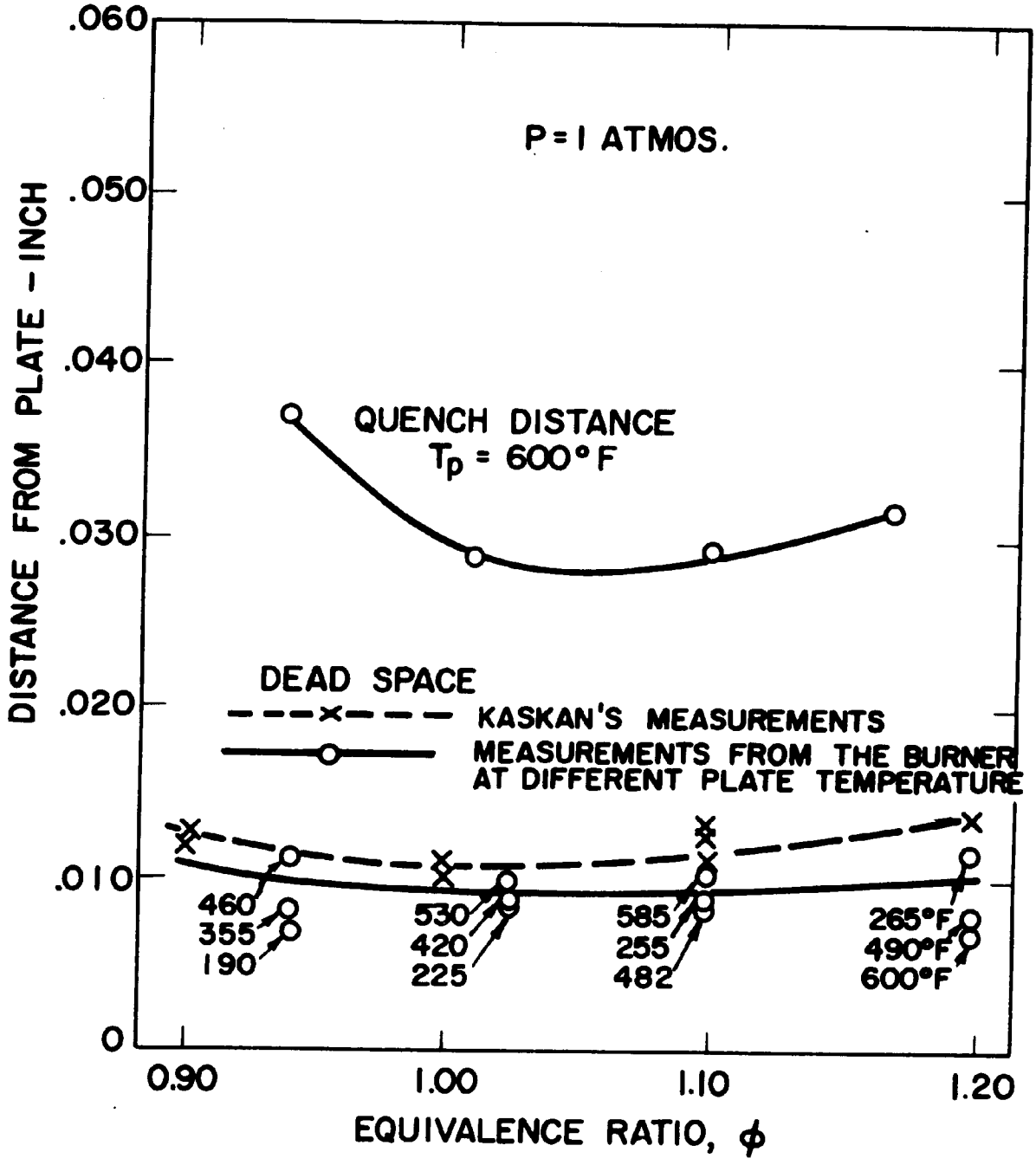


Fig. 43. Comparison of porous plate model quench distance and dead space with dead space measurements by Kaskan.

really "dead." Figure 42 shows that the gas samples taken in the dead space included intermediates and showed a drop in propane concentration indicating that some reaction was taking place.

In the present work the mass per unit wall area for each species of unburned hydrocarbon was determined. It was felt that reporting the different hydrocarbons separately would provide information of interest to those working on the smog problem. Also, the location with respect to the wall of Olifins (ethylene, propylene, and acetylene) and Paraffins (methane, ethane, and propane), can be important in the study of swirl effects on the scrubbing of combustion chamber walls in an engine.

For unit wall area, the total mass of unburned hydrocarbons is equal to the sum of the masses of the various species. At a pressure of 1.0 atmosphere, this total mass ranged from 50×10^{-8} lbm/ft^2 for $\phi = 1.105$ and $T_p = 585°F$ to 85×10^{-8} lbm/ft^2 for $\phi = 0.945$ and $T_p = 190°F$. The minimum mass for a given plate temperature occurred at about $\phi = 1.105$ and increased for both lean and rich mixtures. This was true for the two chamber pressures studied. The mixture that produced the minimum mass also developed the maximum equilibrium flame temperature (Figs. 15-17), and therefore the maximum flame speed. This relation between the mass of the unburned hydrocarbons and flame speed was corroborated by the comparison shown in Fig. 44 between the quench distance, as measured under the definition used in the present study, and the maximum velocities of propane-air flames measured at the same equivalence ratio, chamber pressure, and initial mixture temperature. It can be

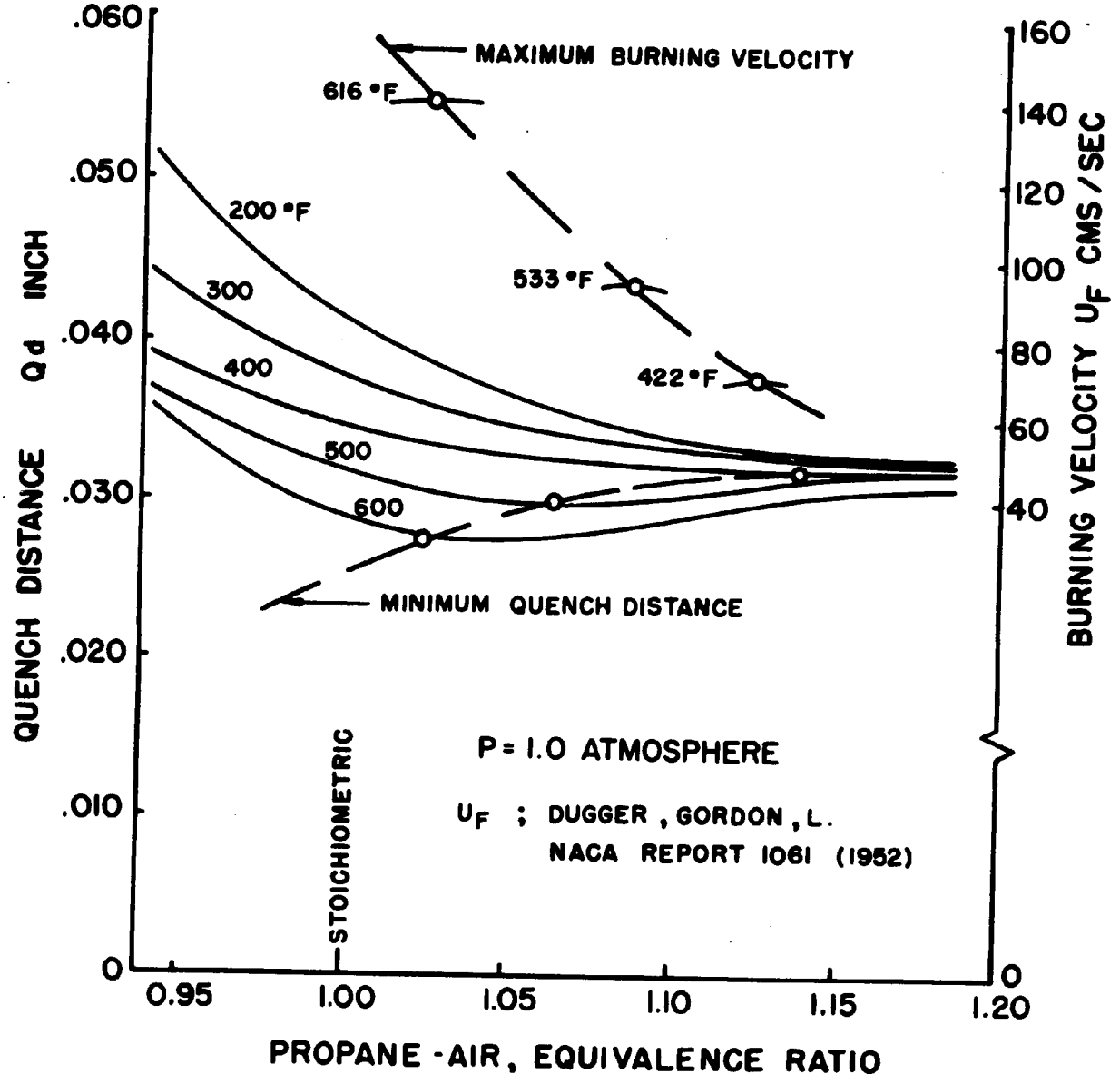


Fig. 44. Relation between quench distance and burning velocity.

seen that the points of maximum velocity have the opposite trend with mixture ratio as that for the points of minimum quench distance.

Also, it has been found in the study of the effect of fuel type on the quench distance[47] that the quench distance decreases in the following order.

Iso octane > n-heptane > propane > benzene

which is the same order as that for the increase in their burning velocities. The comparison between the quench distance equation developed by Simon and Belles[49]

$$d^* = \frac{32\ BP}{N_F \sum_i \frac{P_i}{D_i\ \tau_i\ e_i}} \tag{6.1}$$

and the Tanford and Pease[50] flame velocity equation

$$U_f = \left(\frac{nN_F}{PQ} \sum_i \frac{k_i\ P_i\ D_i}{B_i}\right)^{1/2} \tag{6.2}$$

both of which are based on the diffusion theory, shows that the quench distance is inversely proportional to flame speed.

From the available evidence, then, it appears that the mass of the unburned hydrocarbons is inversely proportional to the flame speed, and we may conclude that the quench effect may be reduced if the flame speed can be increased by inducing a higher reaction rate.

The results shown in Table II show that the total mass varied in-

versely with the plate temperature. At ϕ = 1.105 the mass increased from 50 x 10^{-8} to 62 x 10^{-8} lbm/ft^2, about 24%, when the plate temperature was decreased from 585° to 255°F. It is also shown in Fig. 41 that the cooling effect varies with mixture ratio. The minimum effect of cooling occurred for both pressures at ϕ = 1.185 and it increased for lean mixtures. For flames at a pressure of 2.0 atmospheres the cooling effect also increased for rich mixture.

The reduction of the mass with increase in wall temperature is due to the fact that the higher the wall temperature the less the amount of heat transferred from the flame. Thus reducing the heat transfer to the wall would increase the rate of reaction and thereby reduce the amount of the unburned hydrocarbons. The amount of heat transfer to the wall could be decreased by using materials with lower coefficients of thermal conductivity. Figure 45, taken from Ref. 42, shows that the heat transfer to the wall was reduced by a layer of carbon deposits. It would be expected in a case like this that the hydrocarbon emission from the engine should decrease.

However, published data indicated the opposite. In fact, the apparent increase in hydrocarbon emission can be attributed to factors other than heat transfer to the wall, namely, increase in fuel concentration near the wall due to the absorption of oxygen by the deposits[2] and an increase in surface area due to the irregularity of the deposited surface and also the existence of voids and pits on the surface.

The effect of pressure on the mass is also shown in Fig. 41. It can

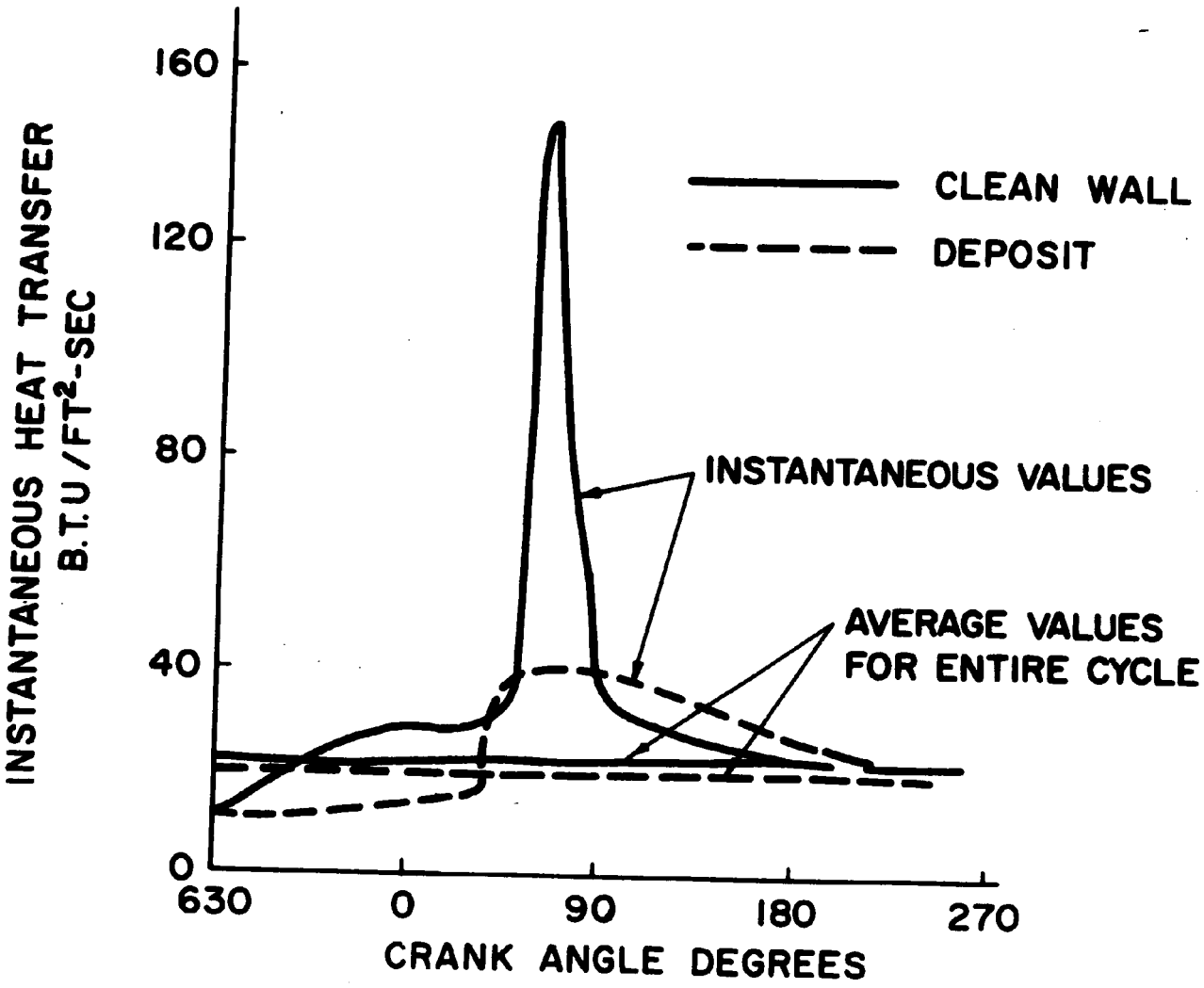


Fig. 45. Effect of engine deposits on instantaneous heat transfer through engine walls.

be seen that the mass varies proportionaly with the pressure. Increase in pressure increases the density. This effect might be partly counteracted by the change in reaction rate in the flame as a result of the change in pressure. This effect is believed to be small since it was reported[4] that there was unnoticeable change in flame speed with increase in pressure from 1.0 to 5.0 atmospheres.

Although the study of the total mass of unburned hydrocarbons under various wall and flame conditions was of importance in this work, it was believed that reporting the masses of the different hydrocarbon species is of equal value especially to researchers in the area of air pollution. The ethylene which is known to be one of the most reactive hydrocarbons showed the highest concentration with respect to the other hydrocarbon intermediates.

The highest percentage of ethylene with respect to total mass amounted to 16% at ϕ = 1.185. This percent decreased for the lean mixtures. Also, the percentage of ethylene decreased with increase in pressure. At ϕ = 1.185, it decreased from 16% to 11.6% as the pressure increased from 1.0 to 2.0 atmospheres. There was no apparent change due to change in wall temperature. The olefins, which have greater smog forming potential than the other hydrocarbons, amount to an average of about 25% of the total hydrocarbon mass. This amount reaches a maximum of 28.4% at ϕ = 1.105 at P = 1.0 atmosphere and decreases for both lean and rich mixtures.

A reduction of 11% is noted at ϕ = 1.105 as the pressure increased

from 1.0 to 2.0 atmospheres. Only 4% reduction is noted at $\phi = 1.025$.

B. COMPARISON OF RESULTS WITH ENGINE DATA

To obtain an indication of the degree of correspondence between the results obtained from this study and those obtained from engine studies, a rough comparison was made. Although admittedly extrapolating the concept of the model and the burner data beyond the point of reasonable confidence, it was felt that an order of magnitude analysis would nevertheless be of interest. The comparison with emission from a single cylinder engine and a multi-cylinder engine is presented in this section.

These amounts were predicted from the test results by using the relation in Eqn. (5.1). To do this it was necessary to have the following data for the engine:

Area of the wall swept by the flame

Wall temperature

Chamber pressure

Mixture equivalence ratio

The area of the wall swept by the flame is taken to be twice the bore area plus the area of the side wall above the piston at top dead center; this assumes that the motion of the piston during combustion is negligible. The wall temperature used is the surface temperature at the instant it is swept by the flame and is taken to be uniform over all parts of the surface. An average chamber pressure for the duration of the combustion process is used. The mixture equivalence ratio is assumed to be constant.

Some essential differences between the test model and an engine can be accounted for. Existing data on the amount of unburned hydrocarbons from an engine are taken from emission measurements; that is, the hydrocarbon content of the exhaust gases was measured. According to Daniel,[10] an estimated 2/3 of the unburned hydrocarbons leave the engine with the other exhaust gases. This gives us a loss factor, but does not account for the possibility that in the engine there are sources of unburned hydrocarbons other than wall quenching. Also, in the existing data, the hydrocarbon concentrations were measured by an infrared analyzer and based on N-hexane. Since these concentrations were roughly half of the concentrations, a correction factor of 2 was used to make them comparable to the concentrations measured by the flame ionization detector.[30]

It should be noted, however, that the pressures used in deriving the relation equation were much lower than those in an engine so that the comparisons between the test model and engines reflects considerable extrapolation.

There may also be other differences between the engine and the model which could affect the quenching process. The difference in wall material could be important, particularly in destroying the chain carriers as described in the diffusion theory. The geometry of the wall and the presence of deposits on its surface could also be factors.

Using the relation equation, the hydrocarbon concentrations found in the present test were compared with those reported in two other tests.

1. Single Cylinder

In a test by Daniel[10] a one-cylinder research engine was used under laboratory conditions. The hydrocarbon concentrations reported were made comparable to those of the present test as follows:

Engine Specifications

CFR Engine	
Bore	3.25 in.
Stroke	4.50 in.
Compression Ratio	8:1

Operating Conditions

Speed	1000 rpm
Air Flow Rate	0.765 lb/min
Fuel-Air Ratio	15.4:1
Fuel Used	Propane
Intake Manifold Pressure	4 in. Hg Gage

The average hydrocarbon concentration reported as measured under the above-mentioned operating conditions was 130 ppm. From the data given the exhaust emis_on in pounds per hour was computed as follows:

$$\text{Mixture Flow Rate} = 0.765 \left(1 + \frac{1}{15.4}\right) = 0.8145 \text{ lb/min}$$

$$\text{Propane Flow Rate} = \frac{\text{Air Flow Rate}}{\text{Fuel-Air Ratio}}$$

$$= \frac{0.765}{15.4} = 0.052 \text{ lb/min}$$

From the ideal gas law, assuming exhaust gas temperature of 2000°R and a gas constant of 53.0 $\frac{\text{ft lbf}}{\text{lbm°R}}$, the exhaust flow rate on a volume base was computed

$$\dot{V} = \frac{0.8145 \times 53 \times 2000}{15 \times 144}$$

$$= 40 \text{ cu ft/min}$$

Corrected hydrocarbons concentration

$= 2 \times 130 = 260$ ppm

Hydrocarbons flow rate in the exhaust manifold

= hydrocarbon concentration x mixture flow rate

$= 260 \times 40 \times 10^{-6}$

$= 10.4 \times 10^{-3}$ cu ft/min

$= 0.625$ cu ft/hr

Hydrocarbons mass flow rate, assuming propane only

$$\dot{m} = \frac{P\dot{V}}{RT}$$

$$= \frac{15 \times 144 \times 0.625}{35 \times 2000}$$

$= 0.0193$ lbm/hr

Prediction of mass rate of hydrocarbons from the quench zone data was computed as follows:

Average chamber pressure	15.0 atm	(Ref. 9)
Wall temperature	675°F	(Ref. 9)
Equivalence ratio	0.98	

Area of wall swept by flame

A = 2 x bore area + area of side wall

$= 0.115 + 0.042$

$= 0.157$ ft^2

From relation Eqn. (5.1)

$$m = K P^{a} T^{-b}$$

$$= 13.8 \times 10^{-6} (15)^{1.0} (1135)^{-0.85}$$

$$= 5.2 \times 10^{-6} \text{ lb/ft}^2$$

Total mass of hydrocarbons in the quench zone in one firing cycle

$$M = m \times A$$

$$= 5.2 \times 0.157 \times 10^{-6}$$

$$= 8.15 \times 10^{-5} \text{ lb}$$

Rate of hydrocarbon production from the quench zone

$$\dot{M} = M \times \text{number of firing cycles per hour}$$

$$= 8.15 \times \frac{1000}{2} \times 60 \times 10^{-5}$$

$$= 0.024 \text{ lbm/hr}$$

Hydrocarbon mass flow rate in the exhaust pipe

$$= 2/3 \times 0.024$$

$$= 0.016 \text{ lbm/hr}$$

2. Multicylinder Engine

The hydrocarbon emission from a V-8 production engine under simulated highway conditions was measured in a test conducted by an automotive research center and was obtained by a private communication.

Since the report of this test was not yet published, as of this writing, only the information necessary for this comparison is shown here:

Engine specifications and operating conditions were as follows:

Engine Specifications

Bore	3.50 in.
Stroke	2.80
Compression Ratio	10.25:1

Operating Conditions

Average engine speed	2000 rpm
Fuel-air ratio	13:1
Fuel used	Indolene 30

Reported hydrocarbons emission: 0.31 lbm/hr (based on N-hexane)

0.62 lbm/hr (corrected)

Predicted mass rate of hydrocarbons from the quench zone data:

Average chamber pressure	240 psi
Wall temperature	600°F
Equivalence ratio	1.1

Area swept by the flame

$$A = 2 \times \frac{\pi}{4} \left(\frac{3.50}{12}\right)^2$$

$$= 0.132 \text{ ft}^2$$

From the relation Eqn. (5.1)

$$m = K P^a T^{-b}$$

$$= 21 \times 10^{-6} \left(\frac{240}{14.7}\right)^{0.93} (1060)^{-0.54}$$

$$= 6.5 \times 10^{-6} \text{ lb/ft}^2$$

Total mass of hydrocarbons in the quench zone in one firing cycle

$$M = m \times A$$

$$= 8.6 \times 10^{-7} \text{ lb}$$

Rate of hydrocarbon production from the quench zone in one cylinder

$$\dot{M} = M \times \text{number of firing cycles per hour}$$

$$= 8.6 \times 10^{-7} \times \frac{2000}{2} \times 60$$

$$= 0.051 \text{ lbm/hr}$$

Predicted hydrocarbon mass flow rate in the exhaust pipe

$$= \dot{M} \times 2/3 \times 8 = 0.275 \text{ lbm/hr}$$

3. Summary of Correlations

The amount of hydrocarbons for the two engines as predicted from the results of the present test are shown below in comparison with the amounts actually measured.

	Predicted, lbm/hr	Measured, lbm/hr
Single cylinder engine	0.016	0.019
Multicylinder engine	0.275	0.62

No doubt the close agreement between the predicted and measured hydrocarbon emission rates is fortuitous and should not be used for predicting emissions from engines without additional experimental support. Nevertheless, the fact that the results are of the same order of magnitude indicates some degree of confidence in these results and lends encouragement to further investigations along these lines.

CHAPTER VII

CONCLUSIONS AND RECOMMENDATIONS

A. CONCLUSIONS

From the results the following conclusions may be made:

1. The quenching effect extends beyond the dead space.

2. Some reaction takes place in the dead space.

3. The model provides a means of measuring the mass of unburned hydrocarbons.

4. The mass increases with increase in chamber pressure. Doubling the pressure nearly doubles the mass.

5. The mass decreases with increase in wall temperature.

6. The minimum mass for a given chamber pressure and wall temperature occurred at an equivalence ratio of 1.105.

7. From conclusions 5 and 6, it is clear that the quenching effect is a function of the amount of heat from the flame available to maintain the reaction; therefore, it follows that the quenching effect can be reduced either by reducing the amount of heat lost to the wall or by optimizing flame conditions to give increased heat of reaction, or both.

8. The relation in Eqn. (5.1) can be used to predict the change in mass per unit area for changes in pressure, temperature, and mixture ratio, within the range of conditions used in the model.

B. RECOMMENDATIONS

The results of this work indicate a number of channels for further study of wall quenching and for putting into effect some of the findings of this study.

It is therefore recommended that:

1. The equipment for this work be used to measure the quench effect at pressures comparable to those in an engine.

2. High-speed pictures should be taken to find the difference between the dead space under steady and transient conditions.

3. A study be conducted of the effect of diluent concentrations and reaction promoters on quenching effect.

4. Tests be conducted with other wall materials to determine the effect of materials.

5. That flames having simple reaction mechanisms te studied analytically and the results justified experimentally to gain information on the relative importance of the thermal and diffusion theories.

6. Studies be conducted to find the effect of applying a high-refractory material to reduce the instantaneous heat transfer to the wall on hydrocarbon emission.

7. The effect of increased flame speed on the hydrocarbon emission from engines being studied.

APPENDIX A

CALIBRATION OF GAS CHROMATOGRAPH

1. STANDARD SAMPLE

To get the relation between the concentration of the different hydrocarbon constituents and their corresponding peak heights, a standard sample was prepared in the laboratory.

This standard sample was kept under pressure in a stainless steel tank and was used in calibrating the gas chromatograph before every test.

The concentrations of the different hydrocarbons in the standard sample are in proportion to those sampled from the flame.

a. Method Used in Preparing the Sample

The standard sample consisted of six different gases: nitrogen, methane, ethane, ethylene, propane, and propylene.

The diagram in Fig. 46 shows the system used in preparing this sample.

First, valves (2), (3), and (4) were opened and the system was evacuated (manometer reading was zero).

Second, valve (2) was closed, nitrogen was introduced through valve (1) to the system until a certain pressure on the manometer was maintained. After that the system was left for 15 min in order to be in thermal equilibrium with the surroundings before reading the manometer head.

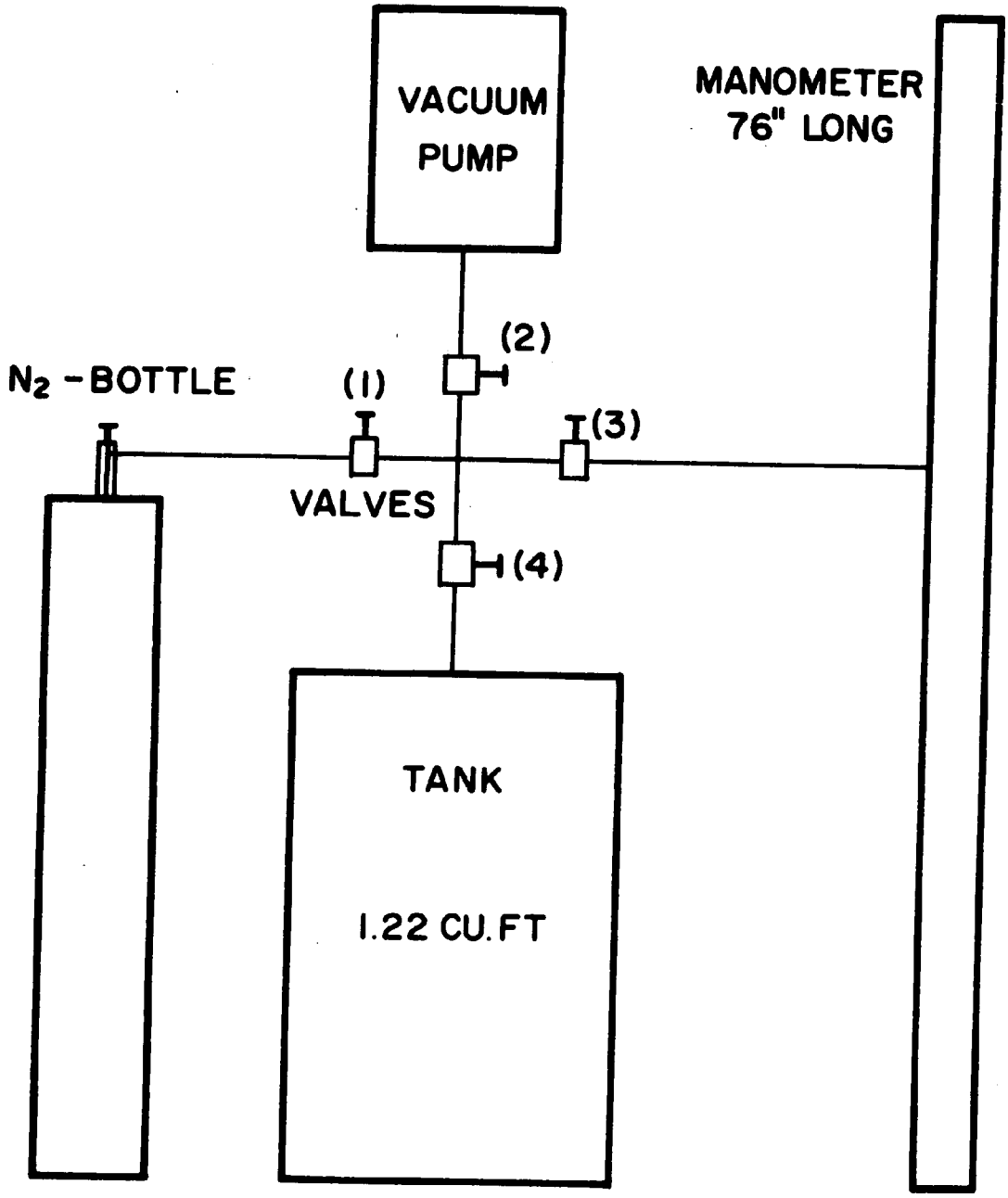


Fig. 46. Schematic diagram showing system for standard sample preparation.

Third, valves (3) and (4) were closed and the nitrogen bottle was replaced by the methane bottle.

Fourth, valve (2) was opened to the vacuum pump and the methane bottle was opened slightly to pass some gas through the pipes.

Fifth, valve (1) was closed, then valve (2).

Sixth, valve (4) was opened and methane was introduced under pressure through valve (1) to the tank.

The system was left for 15 min then valve (3) was opened.

The increasee in the mamometer reading was taken as equal to the partial pressure of methane.

The same procedure was used for the other constituents.

b. Accuracy

The accuracy in determining the concentration of the different constituents in the sample depends on the time allowed for mixing in the tank before reading the pressure on the manometer.

The following example shows that due to the fact that the volume of the lines are very small compared to the volume of the tank, this effect can be negligible.

For the worst case, let us assume that when the methane was introduced in the tank, nitrogen only left the tank to the manometer.

Volume of the Tank 1.22 cu ft

Volume of the Line to the Tank

$$= \frac{\pi}{4} d^2 \cdot L$$

$$= \frac{\pi}{4} \left(\frac{1}{5 \times 12}\right)^2 \times (5)$$

$$= 1.1 \times 10^{-3} \text{ cu ft}$$

Mass of Nitrogen in the Tank

$$M_{N_2} = \frac{54.85 \times 0.49 \times 144 \times 1.22}{55 \times 530}$$

$$= 0.161 \text{ lb}$$

$$M_{CH_4} = \frac{0.45 \times 0.49 \times 144 \times 1.22}{96 \times 530}$$

$$= 0.76 \times 10^{-3} \text{ lb}$$

Mass Fraction of Methane

$$= \frac{0.76 \times 10^{-3}}{0.1617}$$

$$= 4.7 \times 10^{-3}$$

Mass of Nitrogen that Left the Tank

$$M'_{N_2} = \frac{0.45 \times 0.49 \times 144 \times 1 \times 10^{-3}}{55 \times 530}$$

$$= 1.09 \times 10^{-6} \text{ lb}$$

Mass of Nitrogen in the Tank

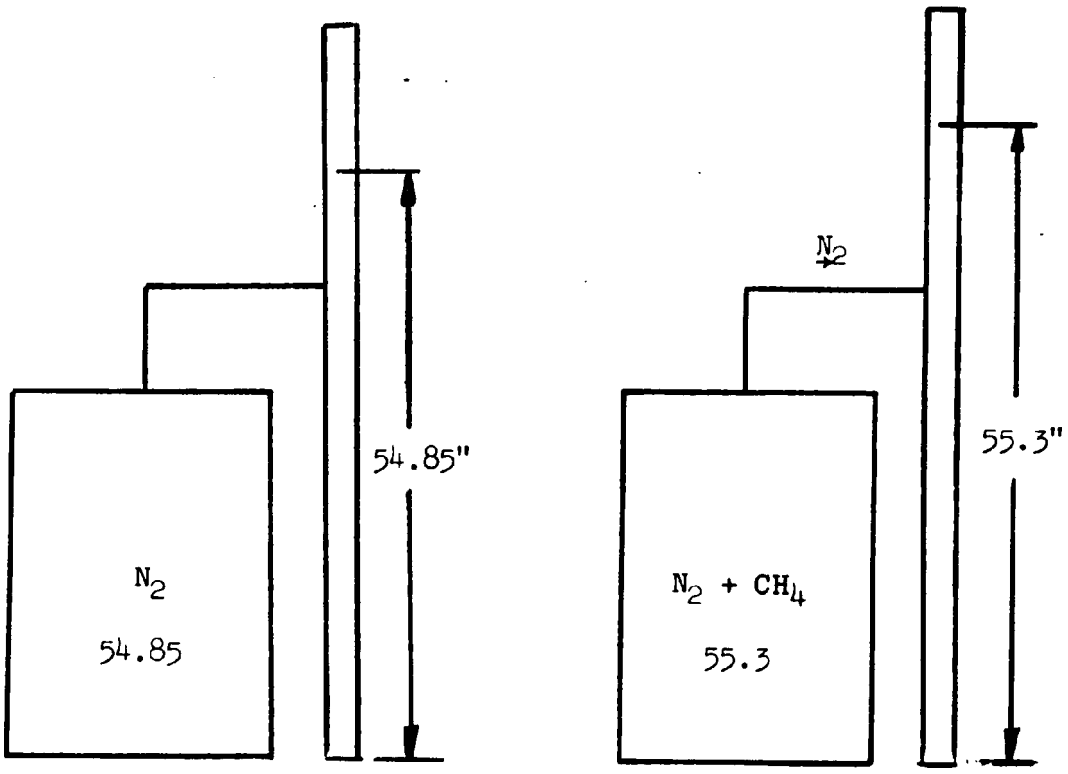
$$M_{N_2} = M_{N_2} - M'_{N_2}$$

$$= 1.61 \times 10^{-1} - 1.09 \times 10^{-6}$$

$$= 1.609999 \text{ lb}$$

From that it can be seen that the change in the mass fraction due to incomplete mixing in the tank can be neglected without inducing any major

error.



3. RELATION BETWEEN THE PEAK HEIGHT AND THE CONCENTRATION OF THE DIFFERENT HYDROCARBON SPECIES

A standard sample was prepared in a stainless steel tank of volume 1.22 cu ft.

The composition as well as the mass fractionsof the different species in the sample are presented in Table VI.

The mass of the sample introduced in the gas chromatograph sampling valve is proportional to the pressure in this valve which can be read in centimeters on a mercury manometer.

The sampling valve was kept at room temperature.

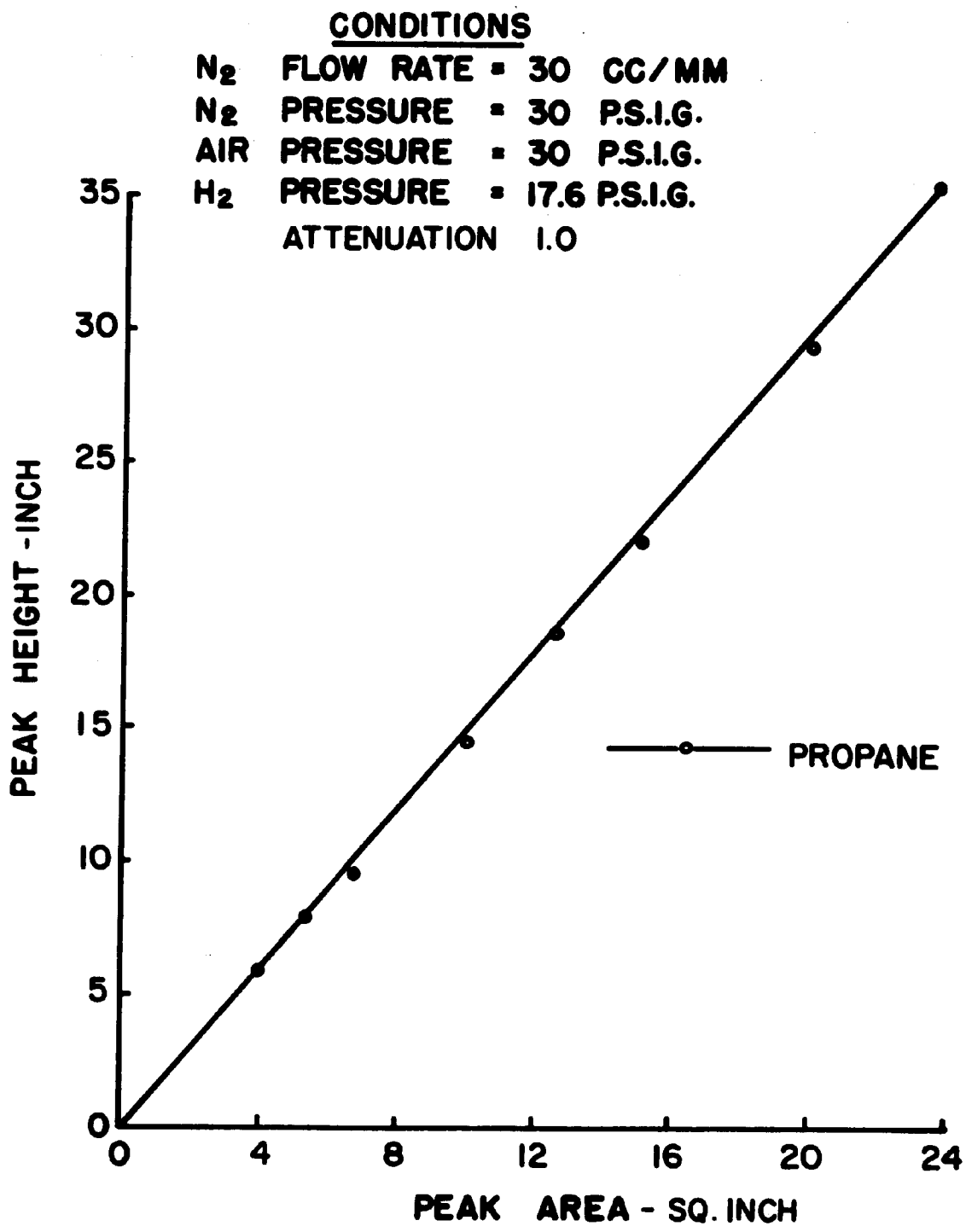


Fig. 47. Relation between peak height and peak area for different hydrocarbon species.

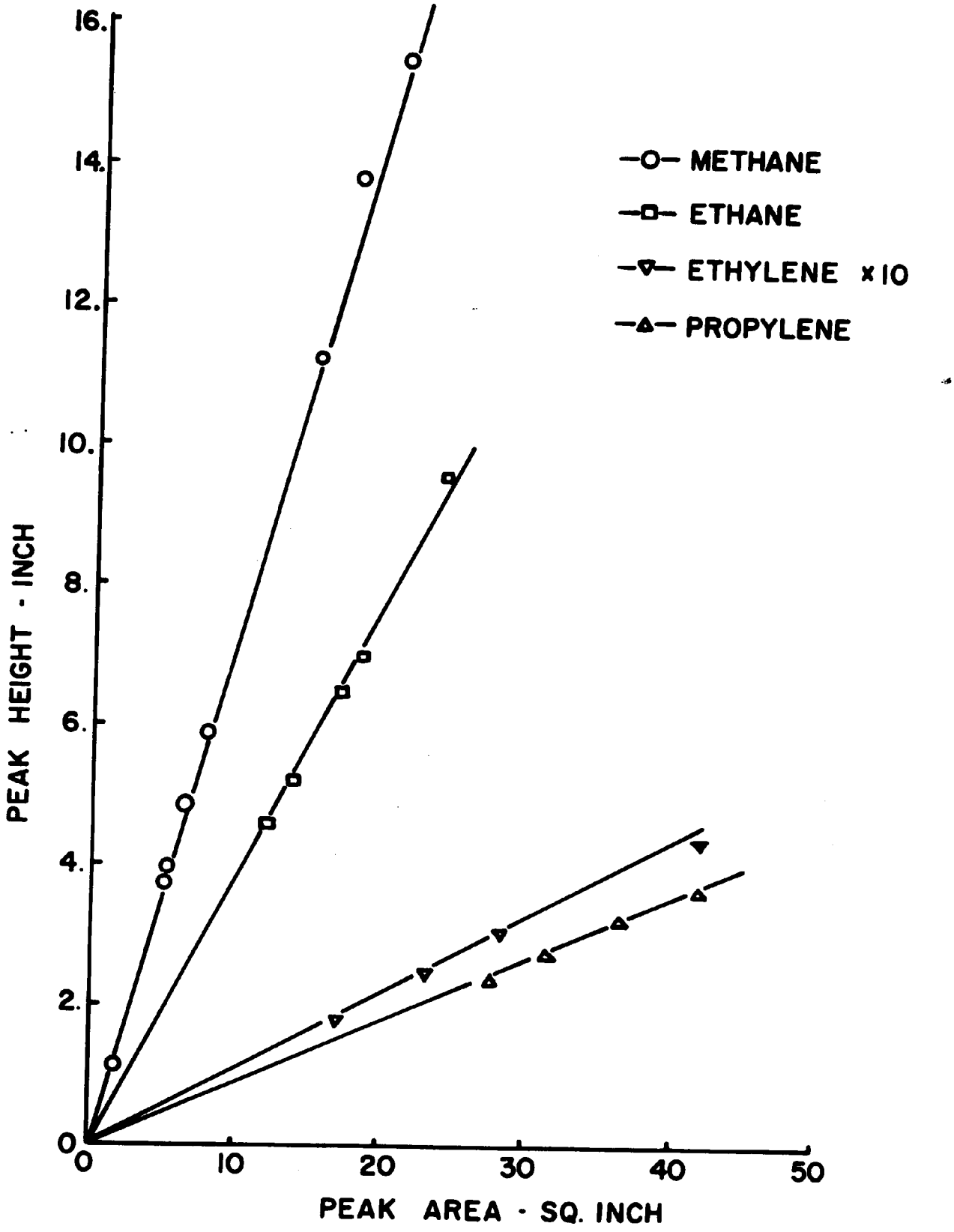


Fig. 47. (Concluded)

TABLE VI

SPECIES AND THEIR MASS FRACTIONS IN THE STANDARD SAMPLE

Species	Partial Pressure, in. Hg	Molecular Fraction, M_F	Molecular Weight, M_W	$M_F \times M_N$	Mass Fraction
N_2	54.85	0.937	28.0	26.20	0.915
CH_4	0.45	0.0076	16.0	0.125	0.0044
C_2H_6	0.60	0.0102	30.0	0.308	0.0107
C_2H_4	0.45	0.0076	28.0	0.215	0.0075
C_3H_8	1.85	0.0316	44.0	1.390	0.0485
C_3H_6	0.40	0.0068	42.0	0.287	0.010
	58.60	1.0008		28.520	0.9940

The concentrations of the different species as a function of the sample pressure is calculated as follows:

$$M_i = \frac{P_i V}{R_i T}$$

$$= M_{F_i} \quad \frac{PV}{R_m T} \qquad \text{(A-1)}$$

where

M_i Mass of species "i" lbm

M_{F_i} Mass fraction of species "i"

P Pressure in the valve lbf/ft^2

V Volume of sampling valve, 0.88×10^{-5} ft^3

R_m Gas constant, 54.2 $\frac{lbf\ ft}{lbm\ °R}$

T Valve temperature, 535°R

From Eqn. (A-1), the masses of the different species in the sampling valve as a function of the valve pressure are:

$$M_{N_2} = 0.915 \times \frac{27.75 \times 0.881 \times 10^{-5}}{54.3 \times 535} P$$

$$= 0.915 \times 0.84 \times 10^{-8} P \quad \text{lb}$$

P is the valve pressure in cm of Hg and the mass in pounds

$$M_{CH_4} = 0.0044 \times 0.84 \times 10^{-8} P = 0.0037 \times 10^{-8} P \quad \text{lbm}$$

$$M_{C_2H_6} = 0.0107 \times 0.84 \times 10^{-8} P = 0.009 \times 10^{-8} \quad \text{lbm}$$

$$M_{C_2H_4} = 0.0075 \times 0.84 \times 10^{-8} P = 0.0063 \times 10^{-8} P \quad \text{lbm}$$

$$M_{C_3H_8} = 0.0485 \times 0.84 \times 10^{-8} P = 0.041 \times 10^{-8} P \quad \text{lbm}$$

$$M_{C_3H_6} = 0.01 \times 0.84 \times 10^{-8} P = 0.0084 \times 10^{-8} P \quad \text{lbm}$$

The relation between the concentration (mass per unit volume) of the different hydrocarbon species in the standard sample and their corresponding peak heights was made by introducing different amounts of samples to the sampling valve and recording the peaks corresponding to the different hydrocarbon species.

The relation between the sample pressure and concentration does not change as long as the pressure in the tank is above atmospheric, but the relation between the sample pressure and the peak height depends on the gas chromatograph condition.

A relation between the concentration and the peak height which is based on attenuation (A-1) is presented in Table VII.

TABLE VII

RELATION BETWEEN HYDROCARBON CONCENTRATIONS AND PEAK HEIGHTS

Experimental Data Conditions:
Nitrogen Pressure: 31.0 psig
Hydrogen Pressure: 17.0 psig
Air Pressure: 30.0 psig
Nitrogen Flow Rate: 30.0 cc/min

Sample Pressure, cm Hg	Methane		Ethane		Ethylene		Propane		Propylene	
	Peak Height, in.	Concentration, lb/ft^3	Peak Height, in.	Concentration, lb/ft^3	Peak Height, in.	Concentration, lb/ft^3	Peak Height, in.	Concentration, lb/ft^3	Peak Height, in.	Concentration, lb/ft^3
10.4	15.2	4.36×10^{-5}	24.25	10.6×10^{-5}	11.75	7.1×10^{-5}	43.75	4.85×10^{-4}	6.25	9.5×10^{-5}
8.0	11.1	3.35	17.75	8.15	8.80	5.4	32.5	3.72	4.70	7.3
6.2	8.7	2.6	13.70	6.3	6.82	4.2	25.0	2.88	3.5	5.65
4.5	6.1	1.89	9.70	4.6	4.70	3.05	10.0	2.10	1.90	4.1
2.6	2.85	1.09	4.40	2.7	2.30	1.88	8.0	1.21	--	2.36

4. CALIBRATION CURVES

This section includes all the calibration curves that had been made for the gas chromatograph during the test period.

The calibration for acetylene was made separately by a technique similar to that used for the other hydrocarbons. This was done because of the slight interference between its peak and the peak corresponding to propane.

The gas chromatograph was checked before every test.

Calibration curves and the corresponding flame condition are given in the following figures.

Calibration Curve Figure No.	Flame Condition Figure No.
49	24, 27, 30
50	33, 12
51	15, 18, 21
52	13, 16, 19, 22
53	14, 17, 20, 23
54	26, 29, 32, 35
55	25, 31, 28, 34

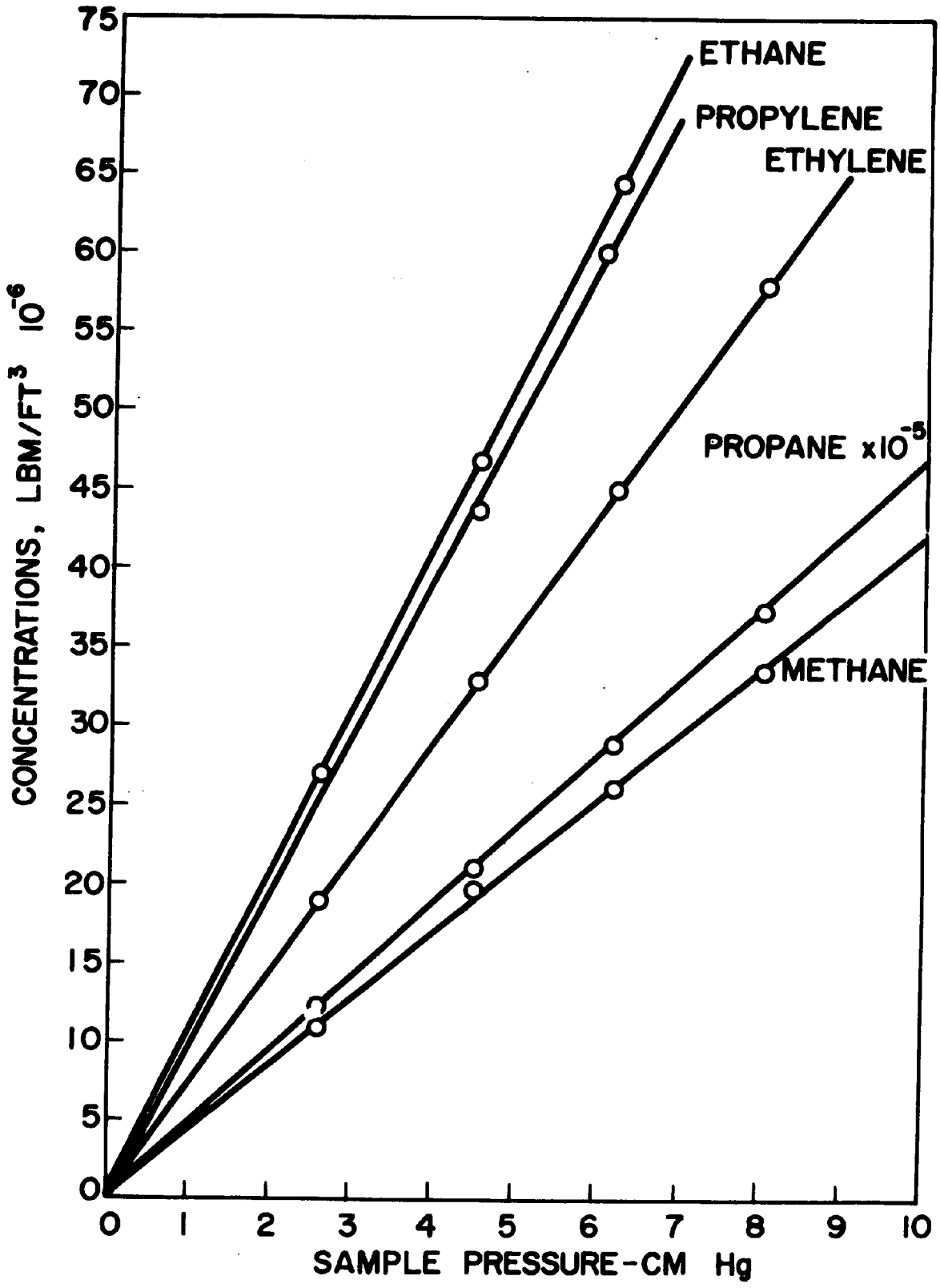


Fig. 48. Relation between sample pressure and concentrations of different hydrocarbon species.

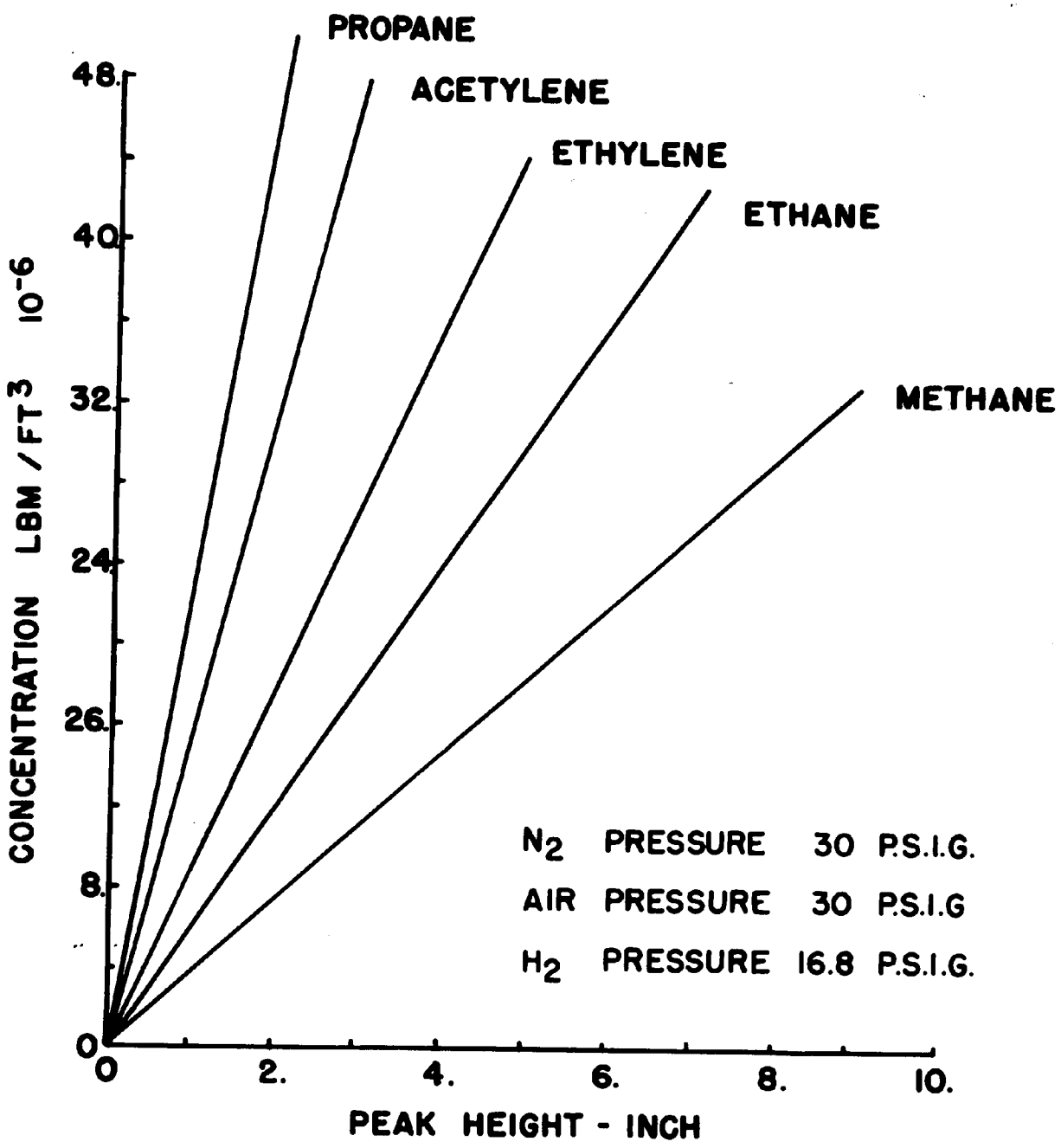


Fig. 49. Calibration curves for gas chromatograph.

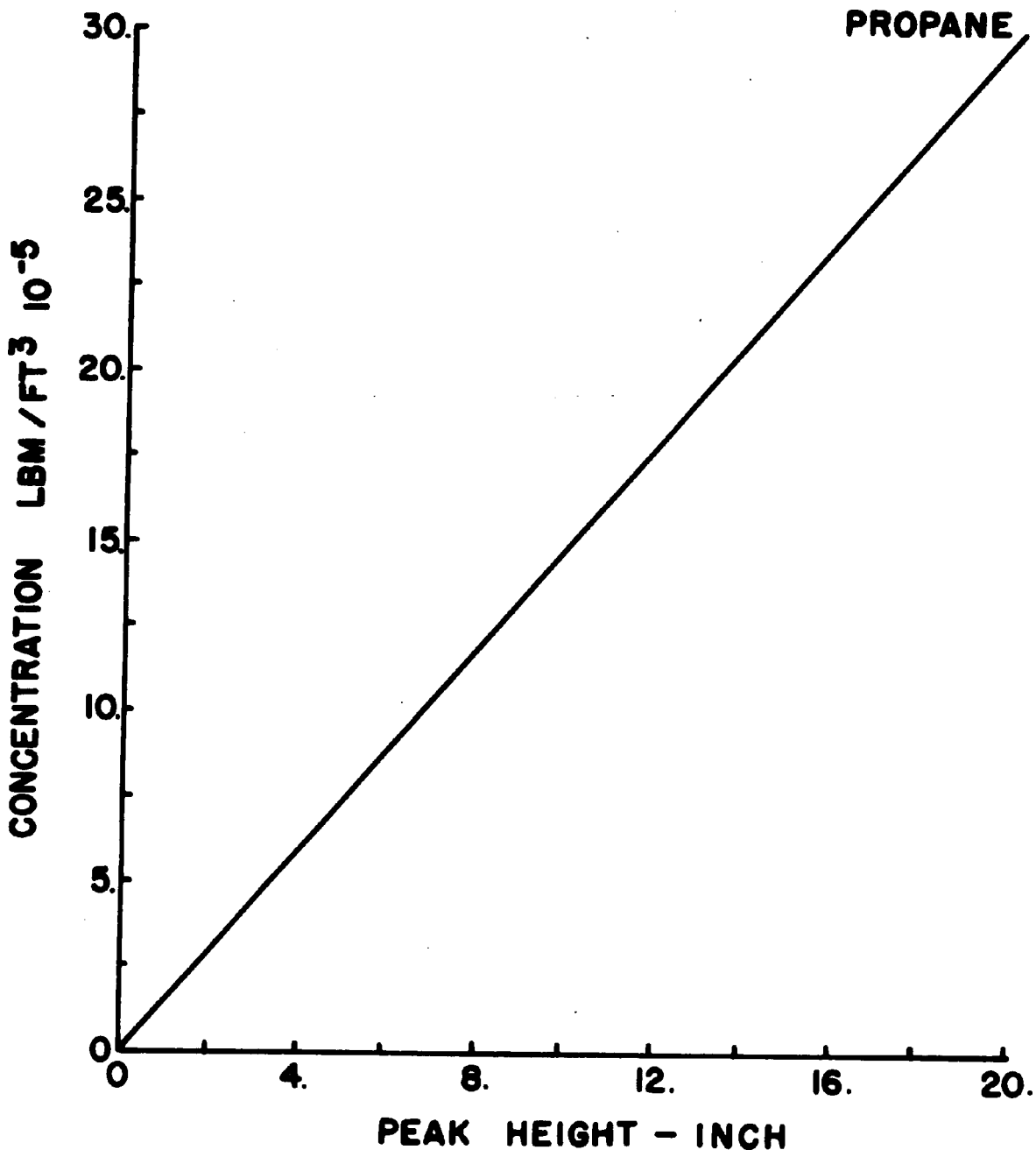


Fig. 49. (Concluded).

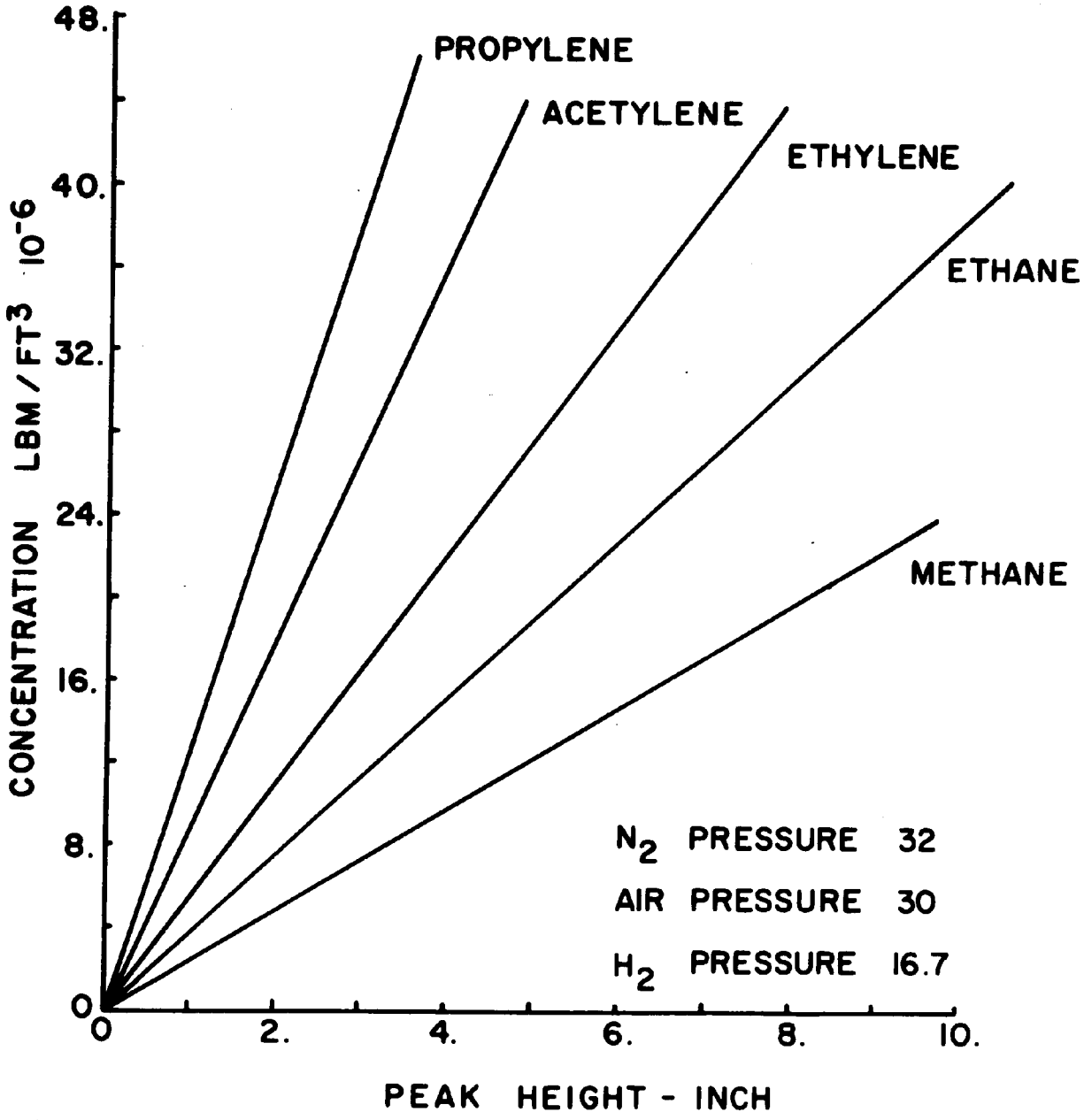


Fig. 50. Calibration curves for gas chromatograph.

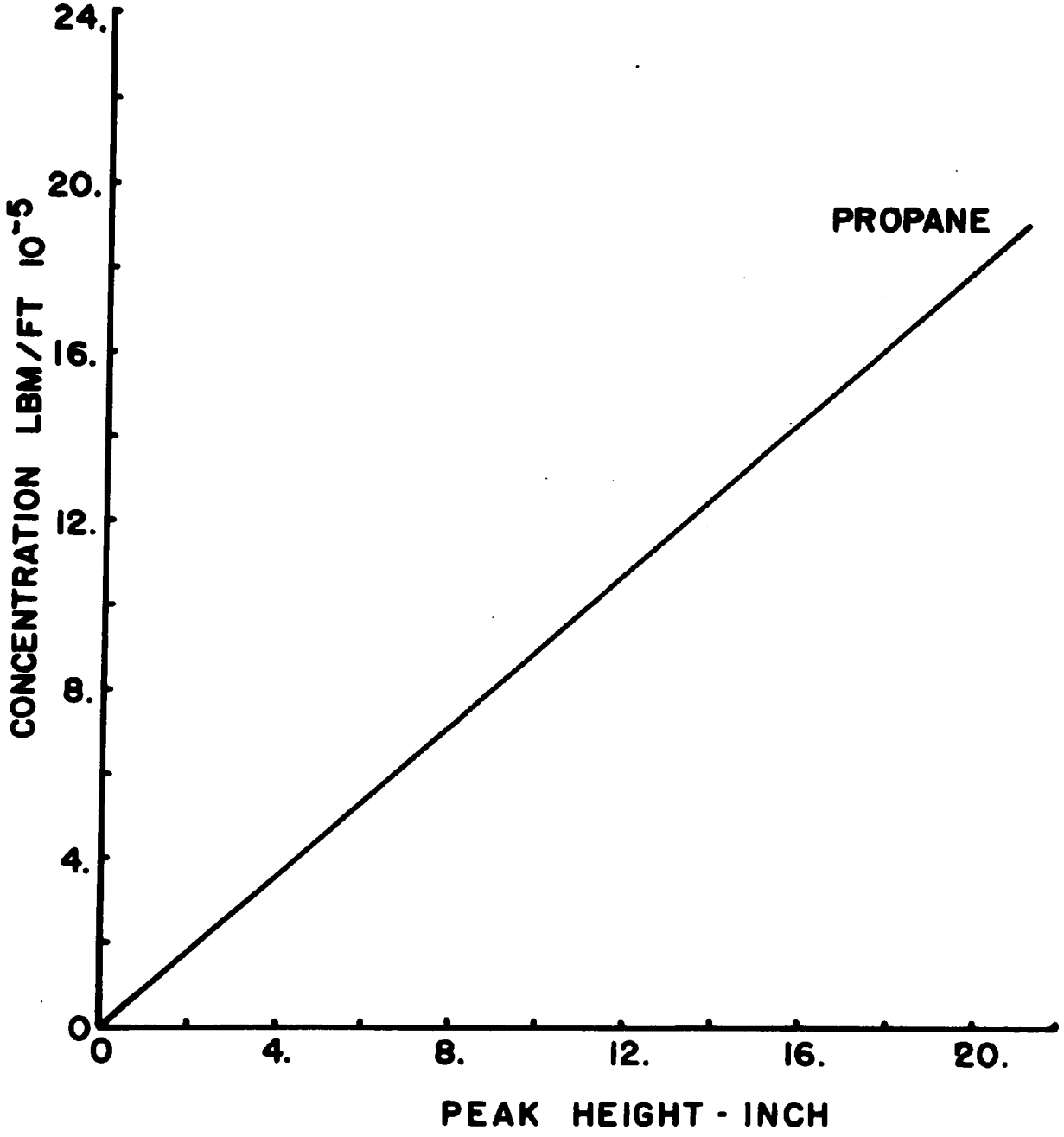


Fig. 50. (Concluded)

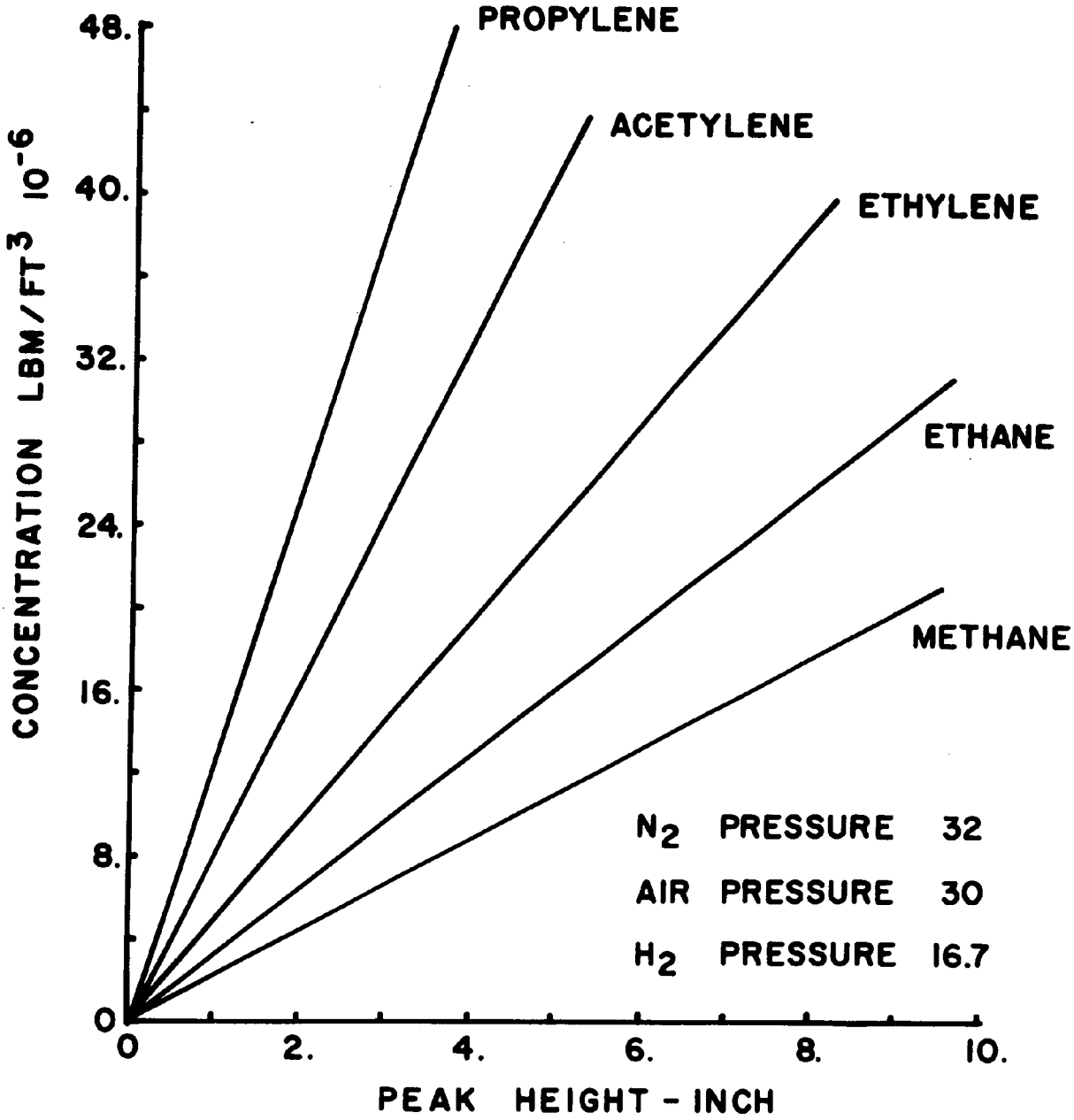


Fig. 51. Calibration curves for gas chromatograph.

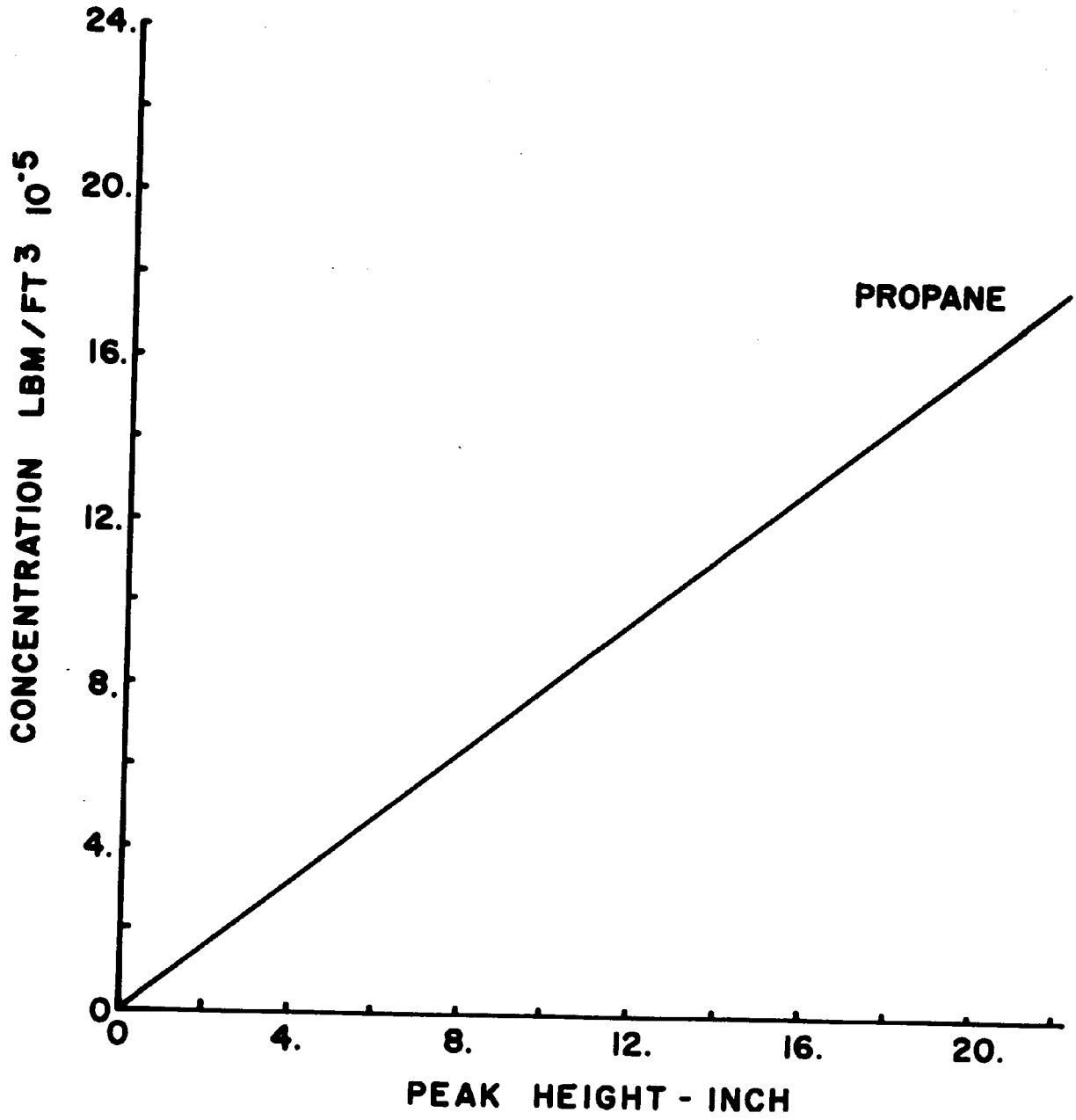


Fig. 51. (Concluded)

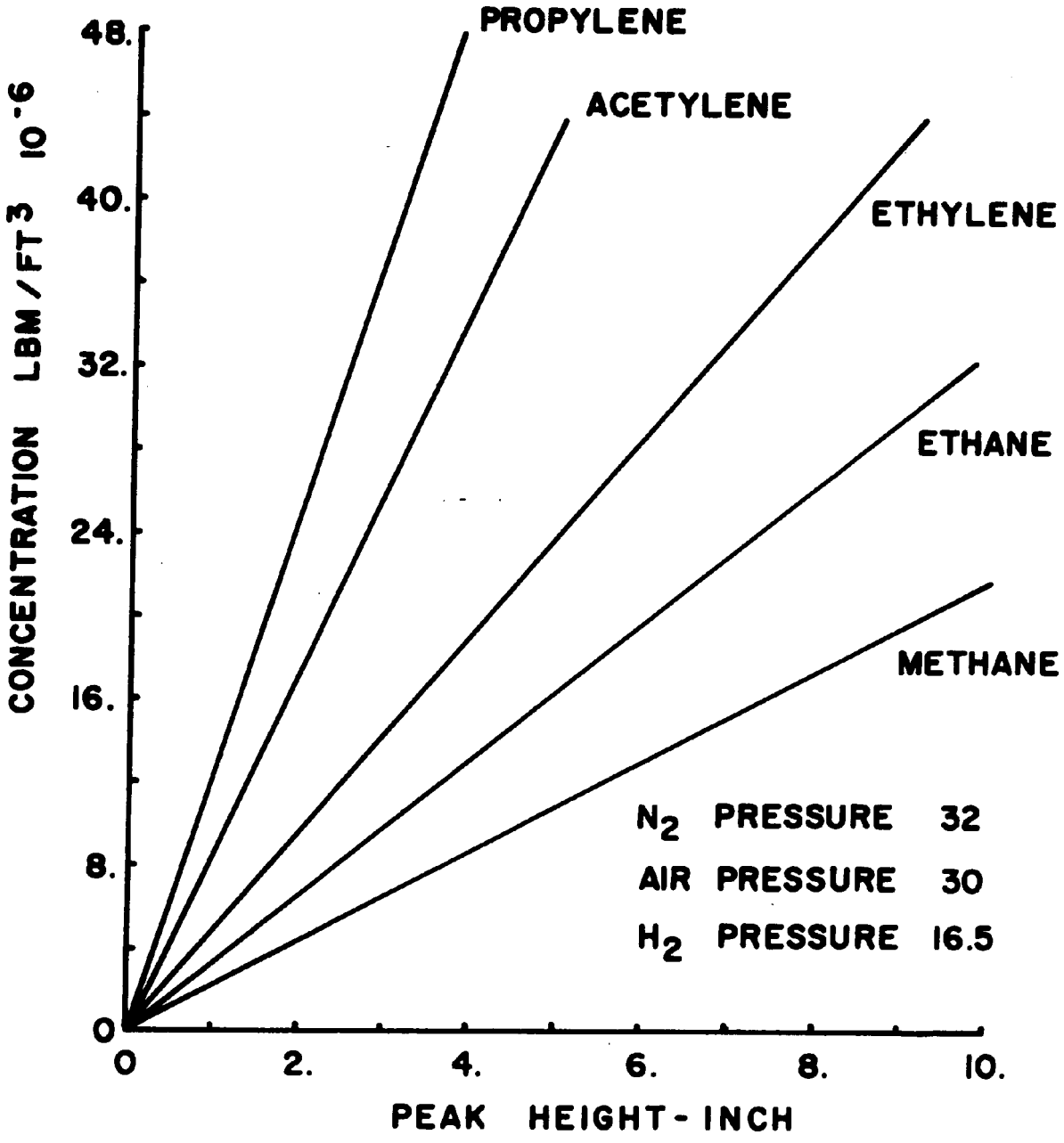


Fig. 52. Calibration curves for gas chromatograph.

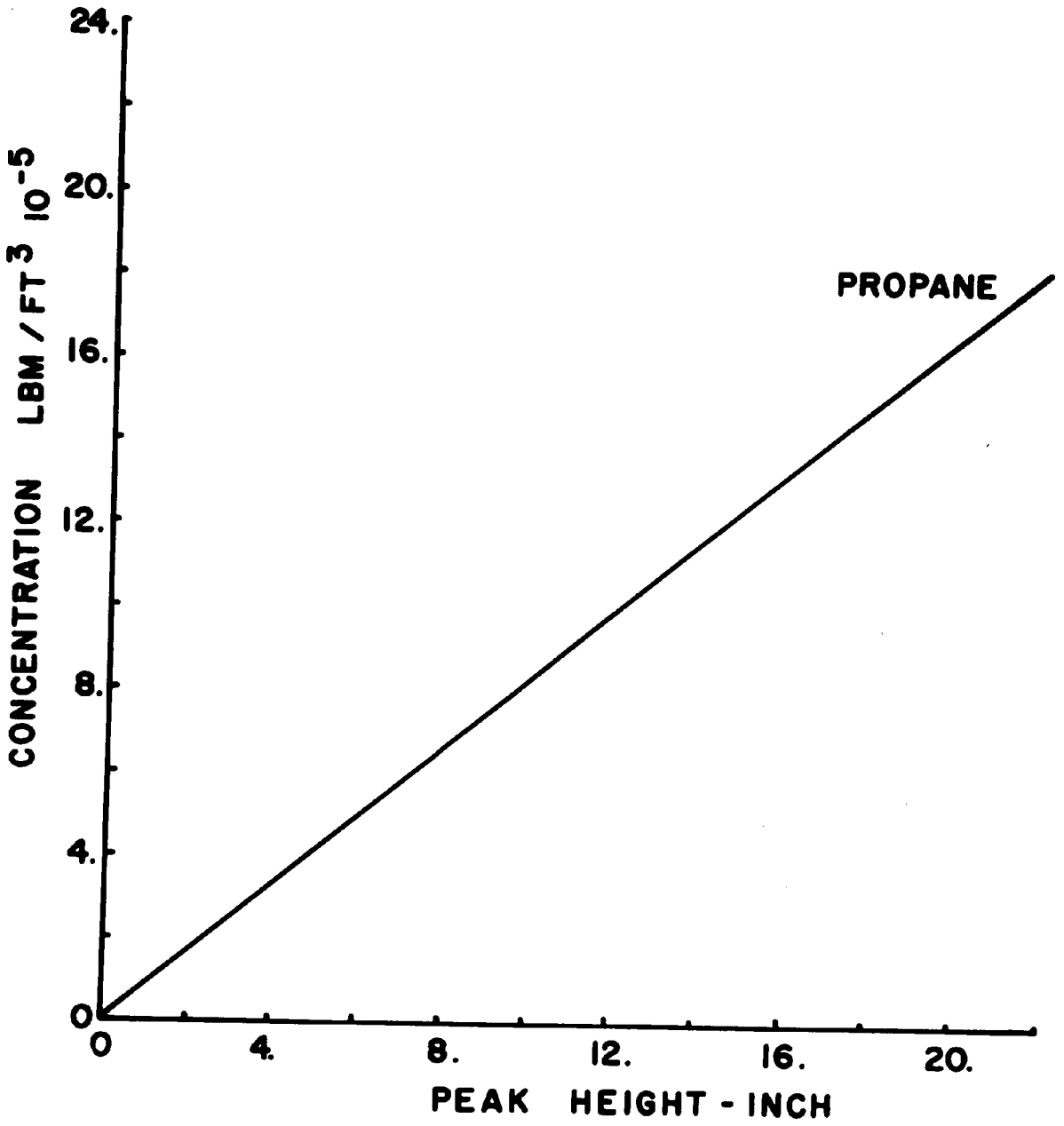


Fig. 52. (Concluded)

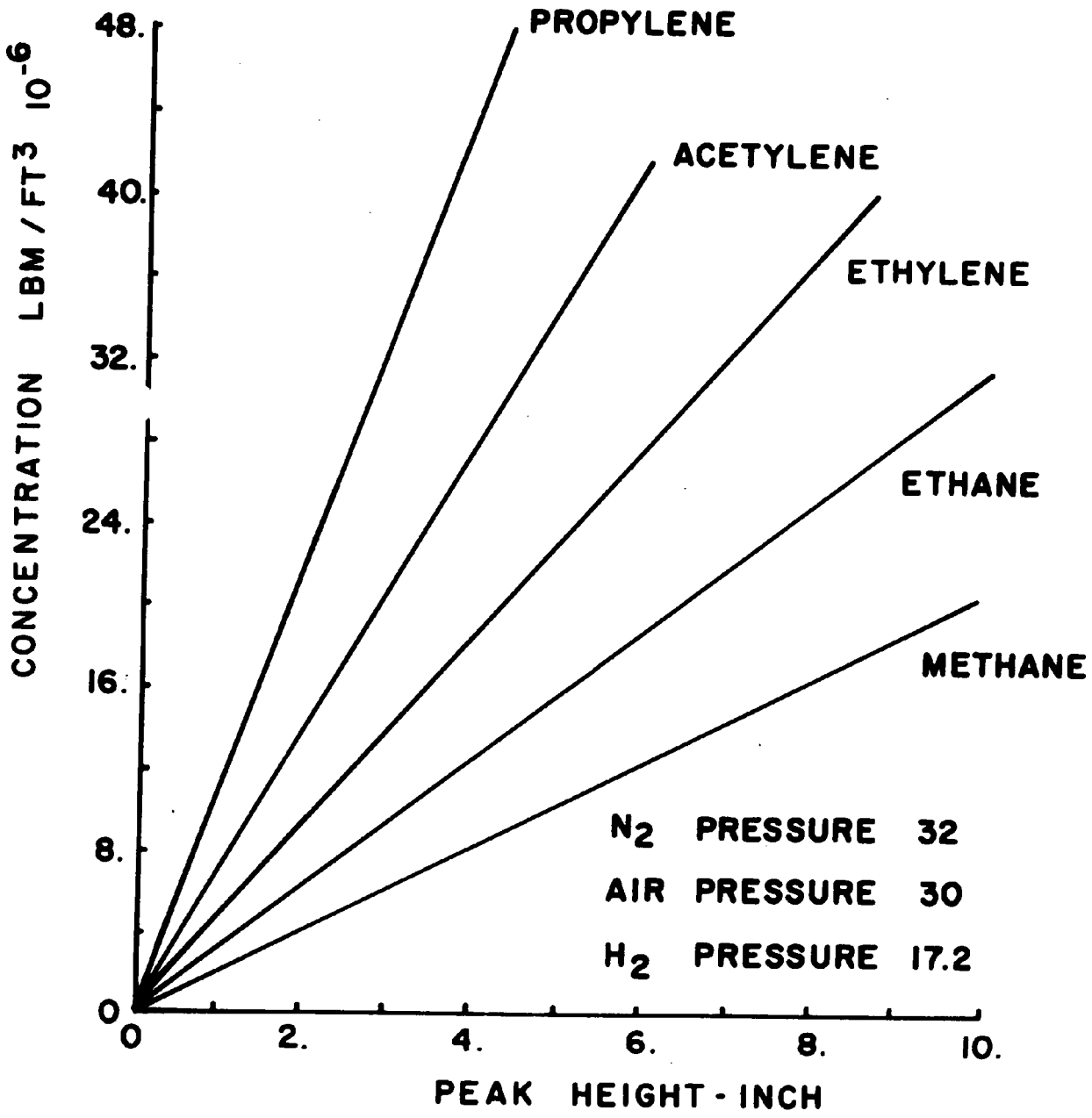


Fig. 53. Calibration curves for gas chromatograph.

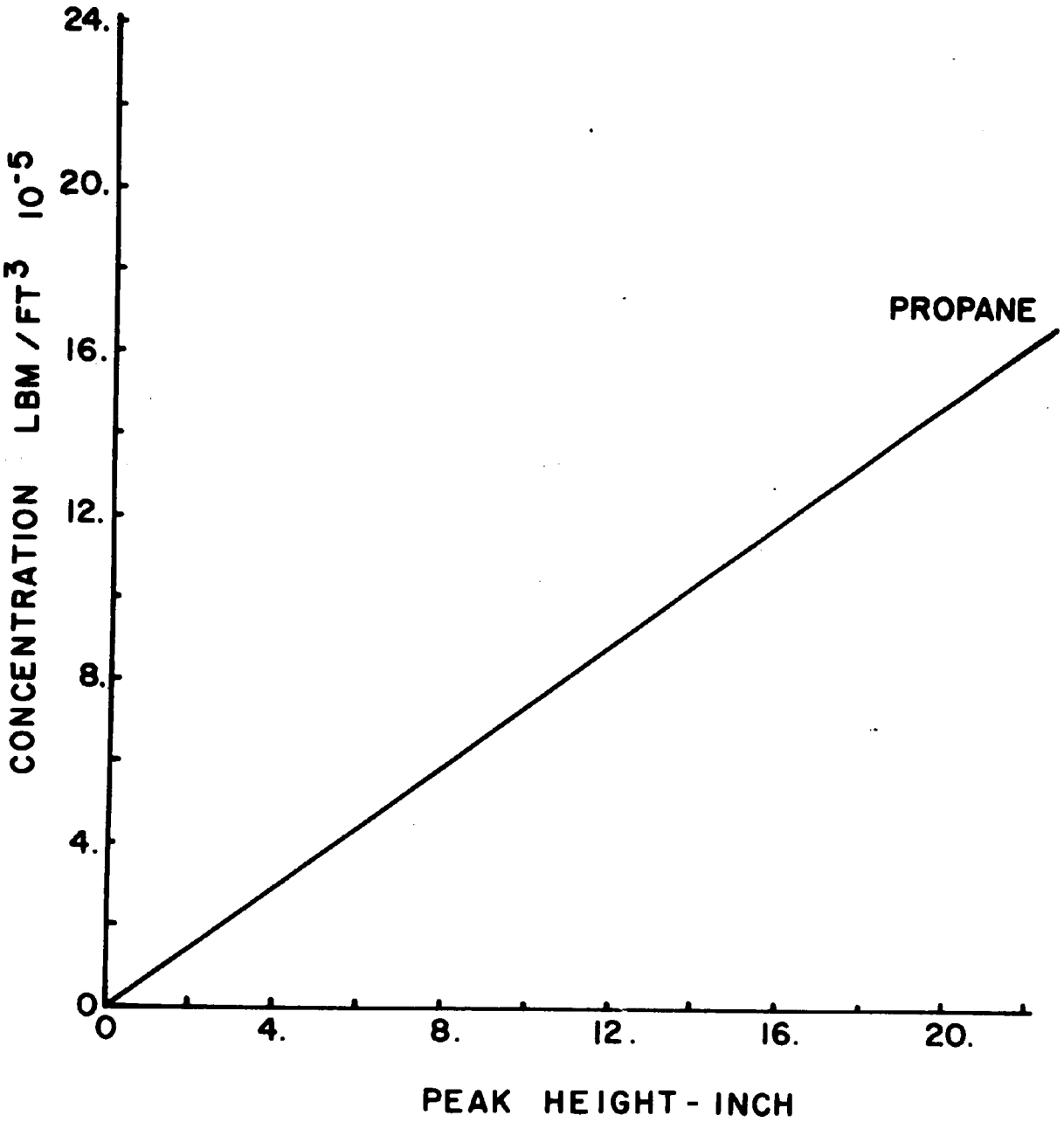


Fig. 53. (Concluded)

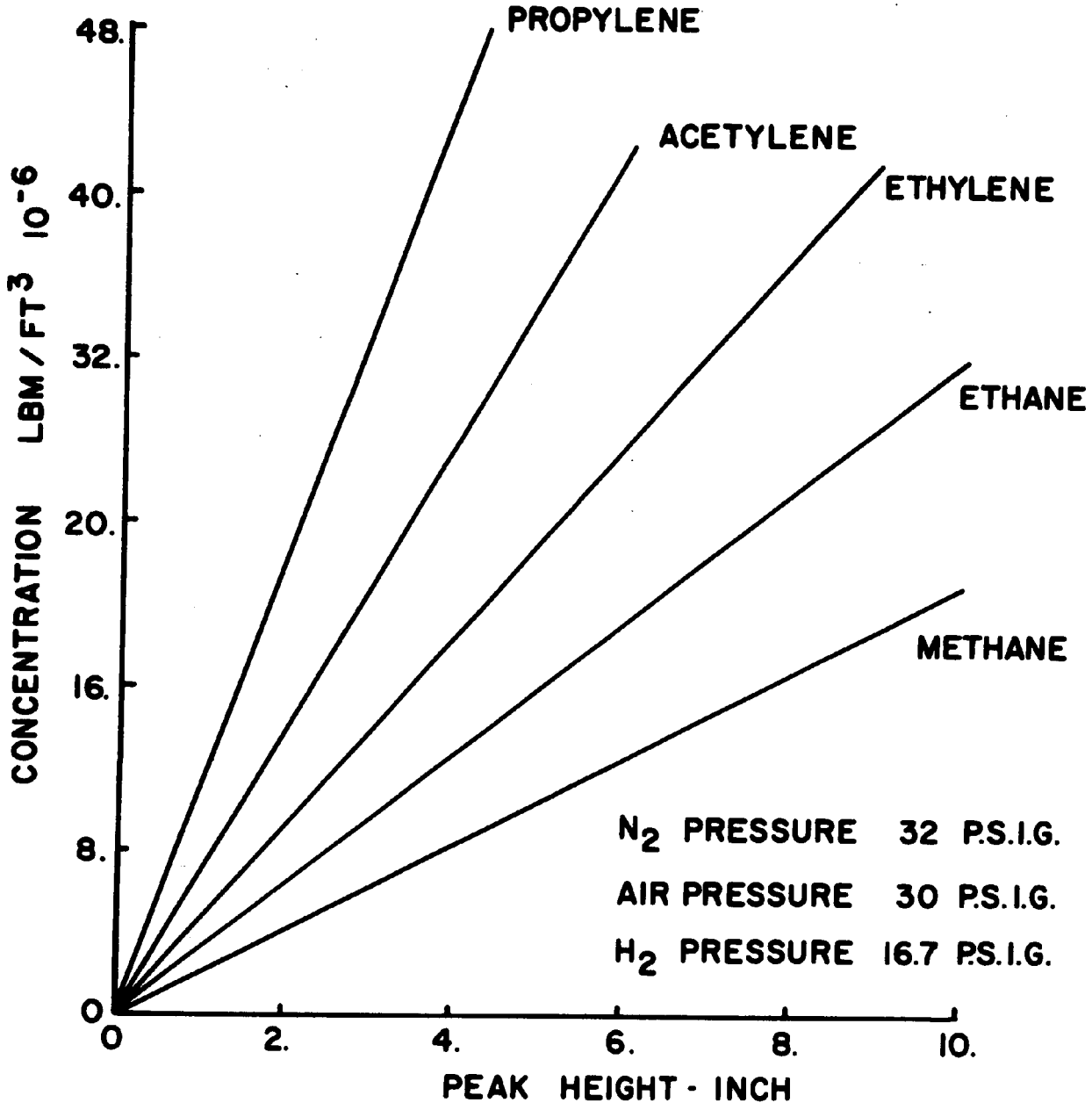


Fig. 54. Calibration curves for gas chromatograph.

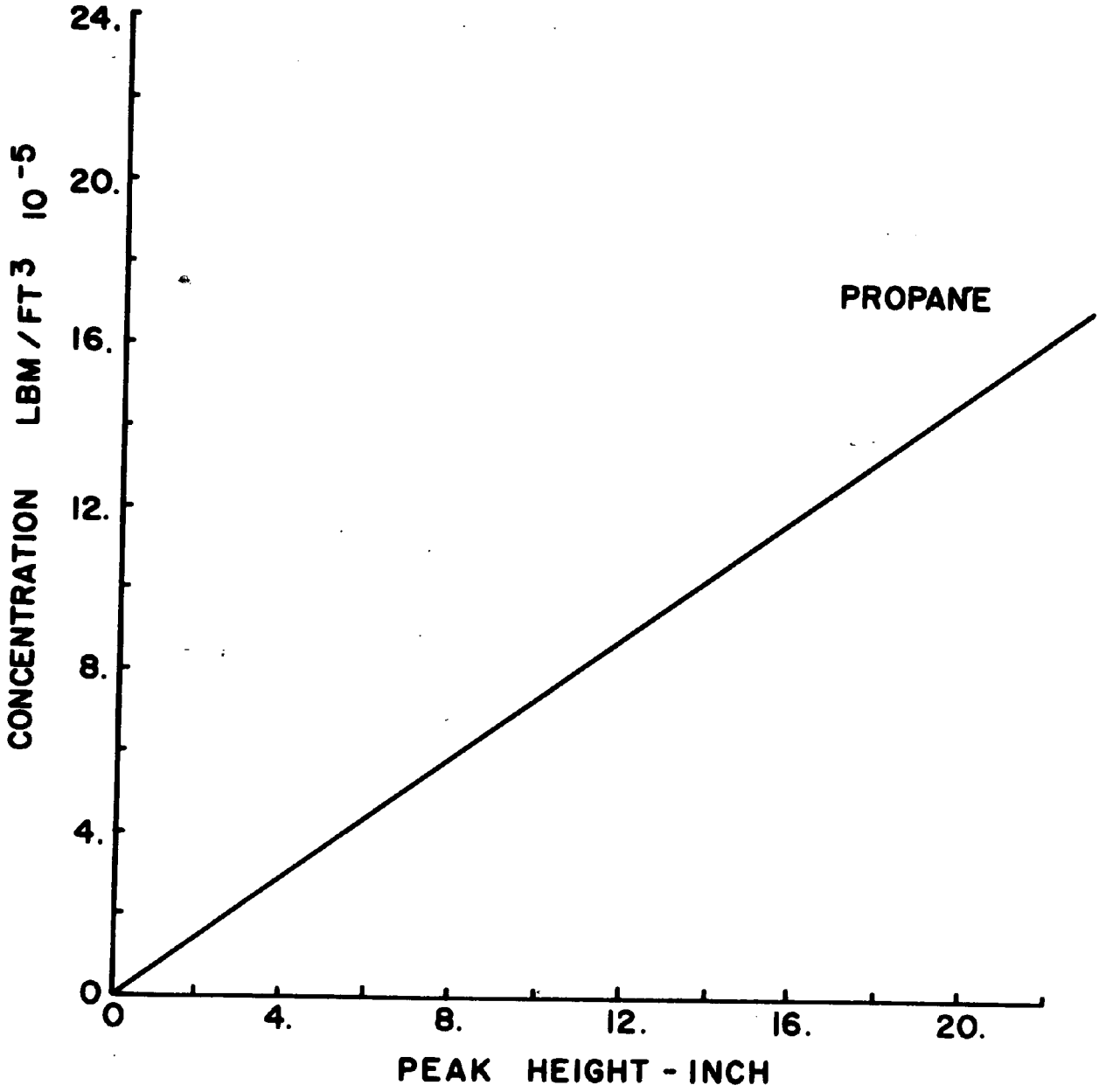


Fig. 54. (Concluded)

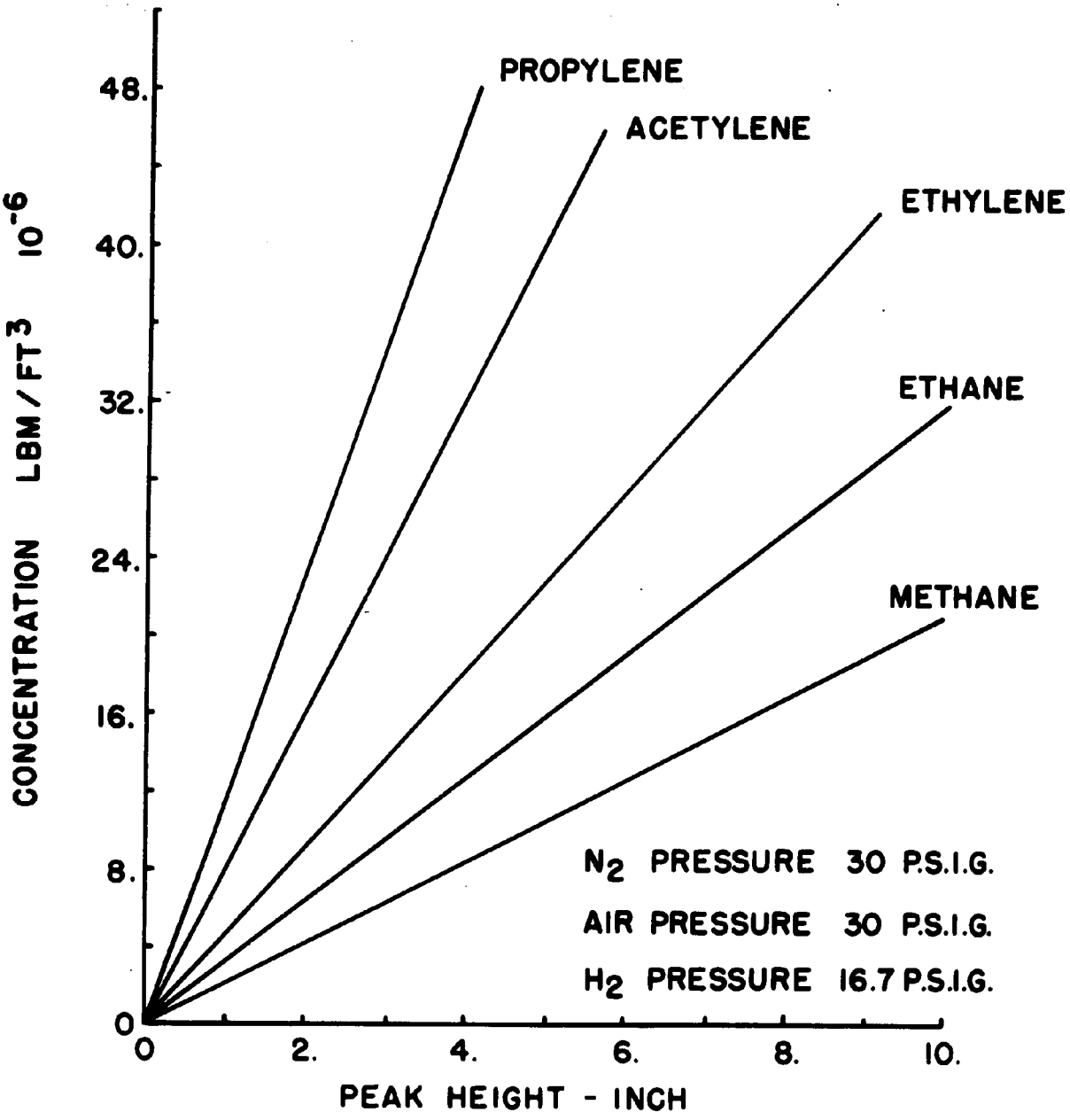


Fig. 55. Calibration curves for gas chromatograph.

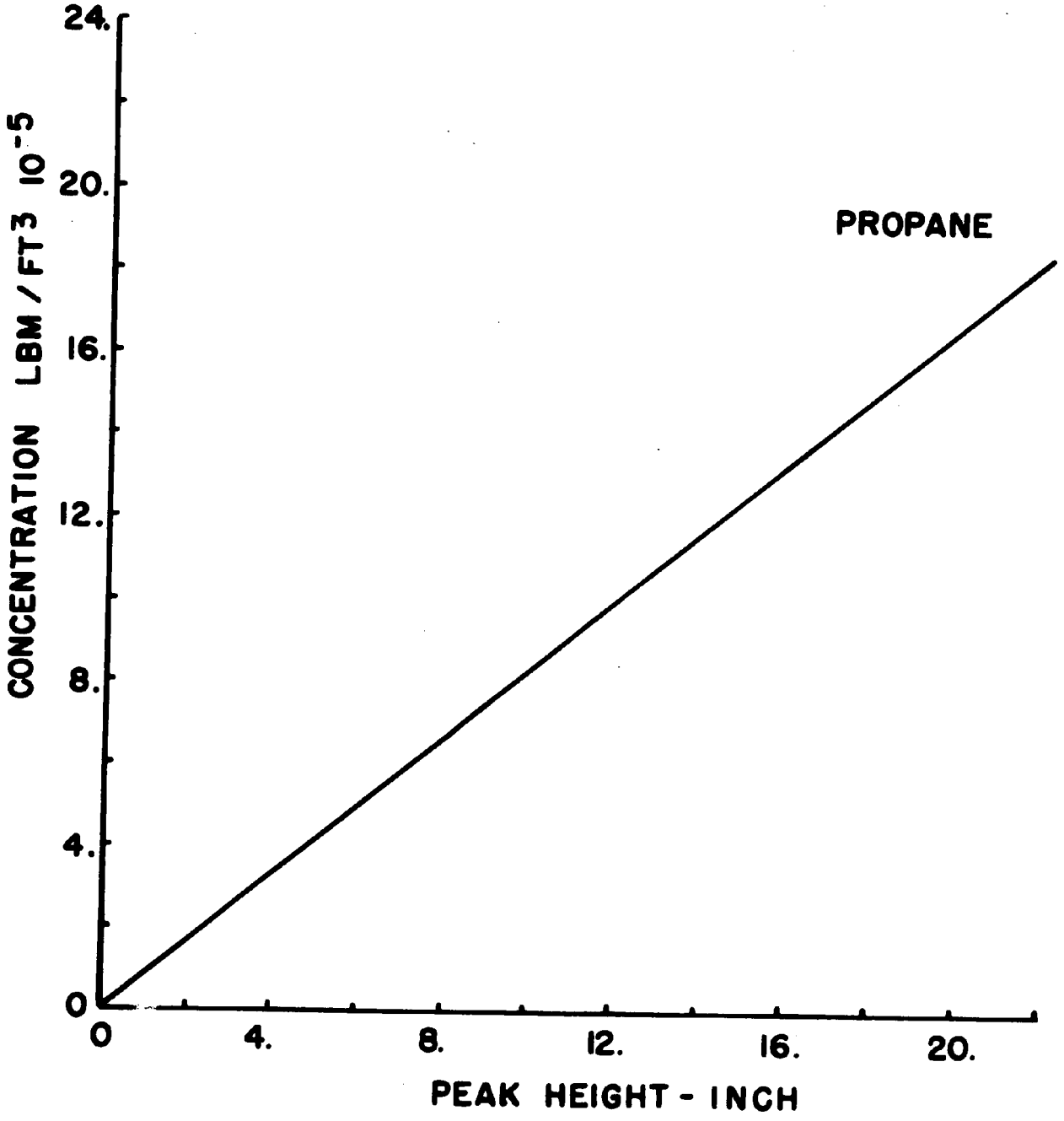


Fig. 55. (Concluded)

APPENDIX B

FLOW RATE MEASUREMENTS AND CALIBRATION OF ORIFICES

Air and propane flow measurements were obtained by using square edged orifices and U-tube manometers. The orifices used throughout the tests had diameters of 0.046 and 0.0135 in. for air and propane, respectively.

Calibrations were made experimentally to compute the discharge coefficient shown in the equation below. By measuring the flow rate with a soap bubble flow meter

$$\text{Mass flow rate} = C_D \sqrt{\frac{P\ \Delta P_{12}}{T}}$$

where

C_D = Orifice discharge coefficient

P = Upstream pressure, psia

T = Upstream temperature, °R

Results obtained are shown in the following tables and figures.

TABLE VIII

DATA FOR ORIFICE CALIBRATION—AIR

(Orifice: 0.046 in.)

Run	T_{UP}, °R	p_B in. Hg	Corr., in. Hg	P_B Corr. in. Hg	P_B Corr. psi	P_{UP} psig	P_{UP} psia	Flow, ml/sec	ρ_{DS}, lbm/ft^3	$\dot{m}$, lbm/sec	$\sqrt{\Delta P_{12} P/T}$	$C_D = \dot{m}/\sqrt{\Delta P_{12} P/T}$
1	535	29.210	0.122	29.078	14.25	44.1	58.35	0.095	0.073	0.245×10^{-3}	0.87	0.282×10^{-3}
2	536	29.210	0.122	29.078	14.25	43.0	57.25	0.115	0.073	0.299	1.03	0.29
3	536	29.210	0.120	29.08	14.25	43.0	57.25	0.128	0.073	0.333	1.14	0.292
4	538	29.210	0.117	29.11	14.32	44.13	58.45	0.103	0.073	0.268	0.930	0.288
5	538	29.210	0.117	29.11	14.32	44.43	58.75	0.090	0.073	0.234	0.80	0.293
6	538	29.210	0.117	29.11	14.32	44.43	58.75	0.0805	0.073	0.210	0.73	0.288
7	538	29.210	0.117	29.11	14.32	44.43	58.75	0.071	0.073	0.185	0.651	0.284
8	538	29.210	0.117	29.11	14.32	44.43	58.75	0.061	0.073	0.159	0.561	0.283
9	538	29.210	0.117	29.11	14.32	44.43	58.75	0.051	0.073	0.130	0.458	0.284

TABLE IX

DATA FOR ORIFICE CALIBRATION—PROPANE

(Orifice: 0.0.35 in.)

Run	T_{UP}, °R	P_P, in. Hg	Corr., in. Hg	P_B Corr. in. Hg	P_B Corr. psi	P_{UP} psig	P_{UP} psia	Flow, ml/sec	ρ_{DS}, lbm/ft^3	$\dot{m}$, lbm/sec	$\sqrt{\Delta P_{12} P/T}$	$C_D = \frac{\dot{m}}{\sqrt{\Delta P_{12} P/T}}$
1	533	29.22	0.117	29.103	14.3	41.8	56.1	6.0	0.11	0.233×10^{-4}	1.235	0.1895×10^{-4}
2	533	29.22	0.117	29.103	14.3	42.7	56.0	5.55	0.11	0.215	1.12	0.192
3	534	29.22	0.117	29.103	14.3	43.0	57.3	5.32	0.11	0.207	1.095	0.189
4	534	29.22	0.117	29.103	14.3	43.2	57.5	5.10	0.11	0.198	1.041	0.190
5	534	29.22	0.117	29.103	14.3	44.0	58.3	4.63	0.11	0.180	0.943	0.191
6	534	29.22	0.117	29.103	14.3	44.1	58.4	3.90	0.11	0.152	0.795	0.192
7	534	29.22	0.117	29.103	14.3	44.2	58.5	3.12	0.11	0.122	0.638	0.191
8	534	29.22	0.117	29.103	14.3	44.9	59.2	2.42	0.11	0.094	0.494	0.190

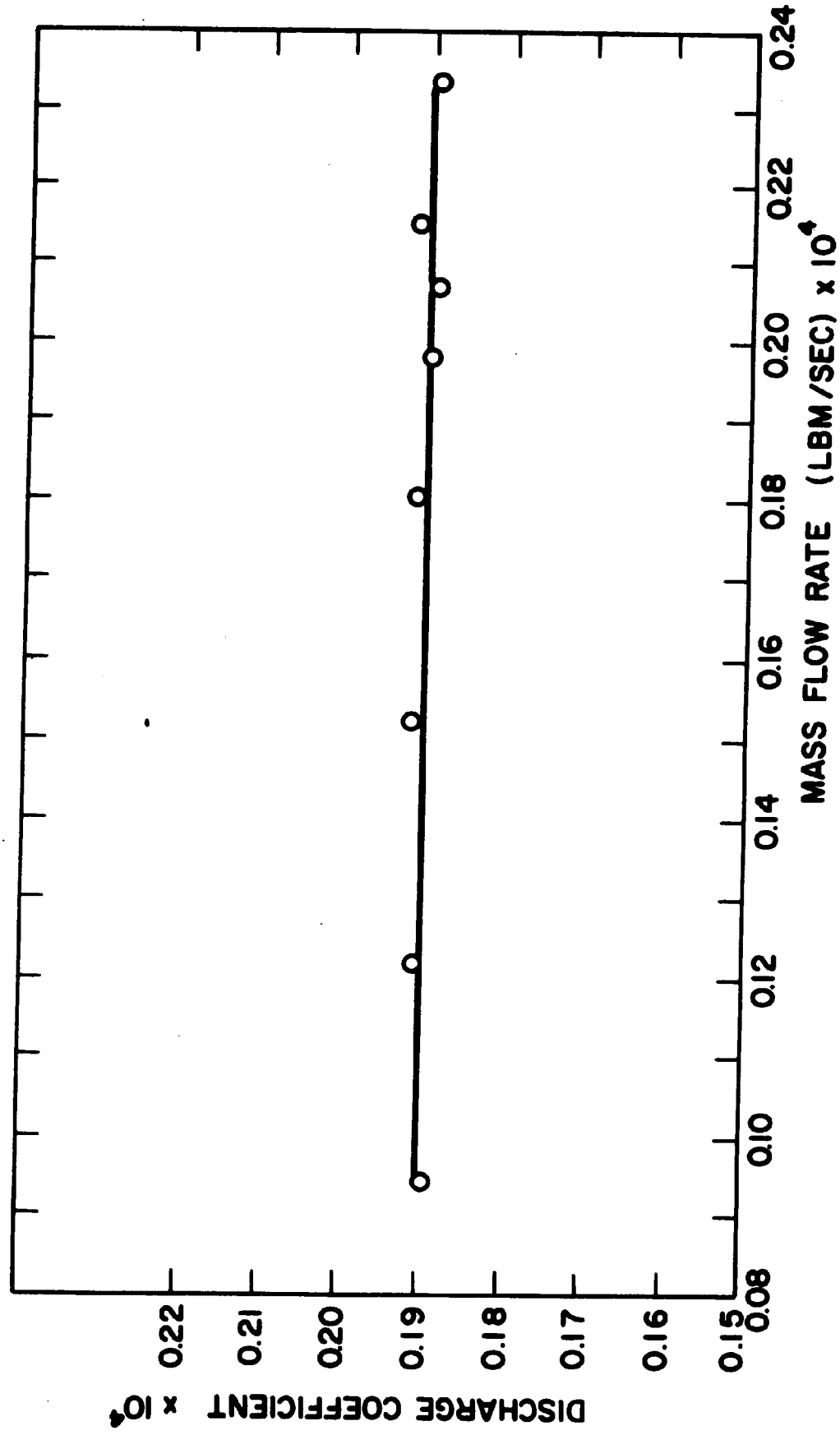


Fig. 56. Discharge coefficient for propane flow.

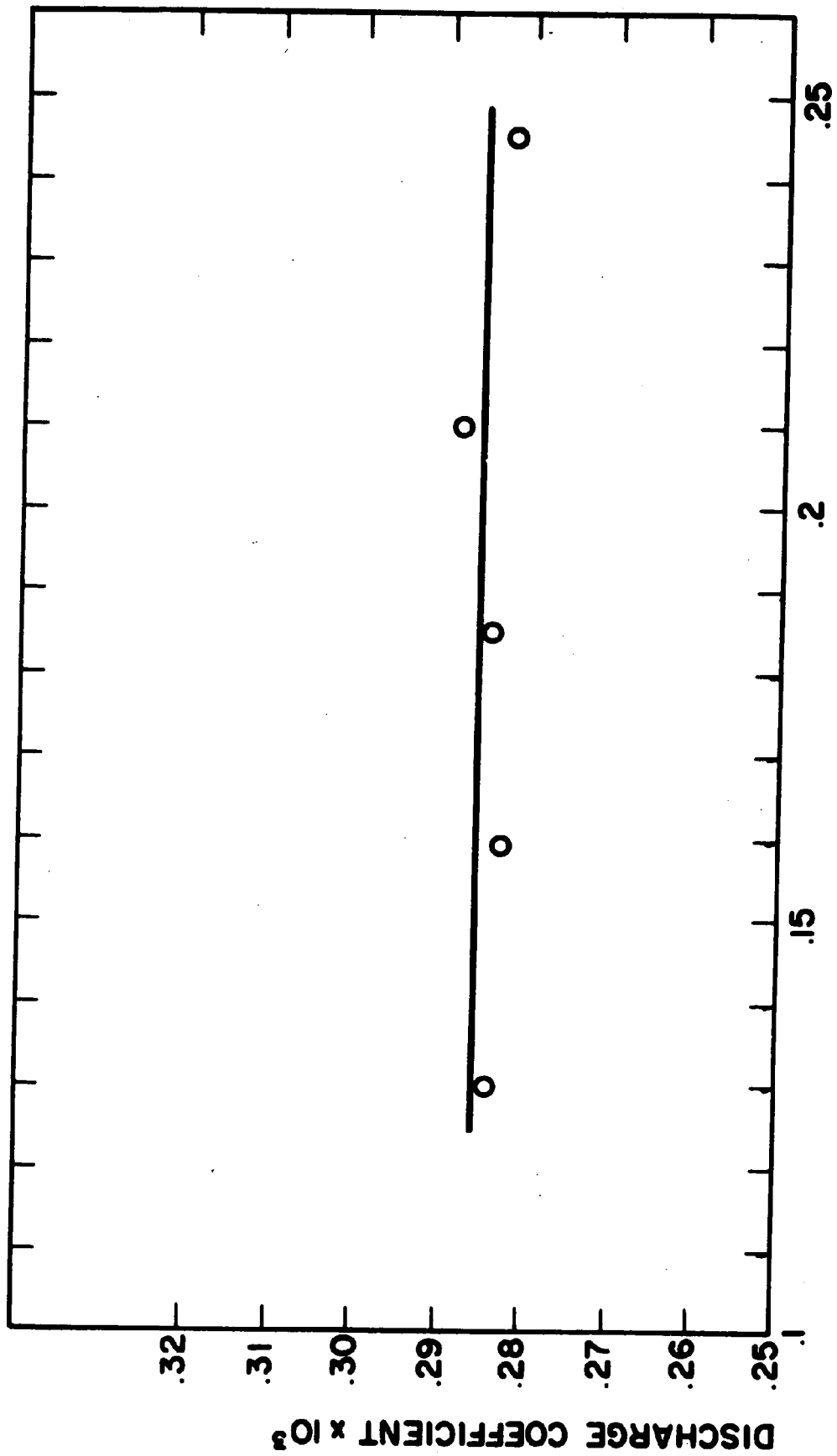


Fig. 57. Discharge coefficient for air flow.

APPENDIX C

CALIBRATION CURVES FOR PRESSURE GAGES, IRON-CONSTANTAN THERMOCOUPLE, AND ROTAMETER

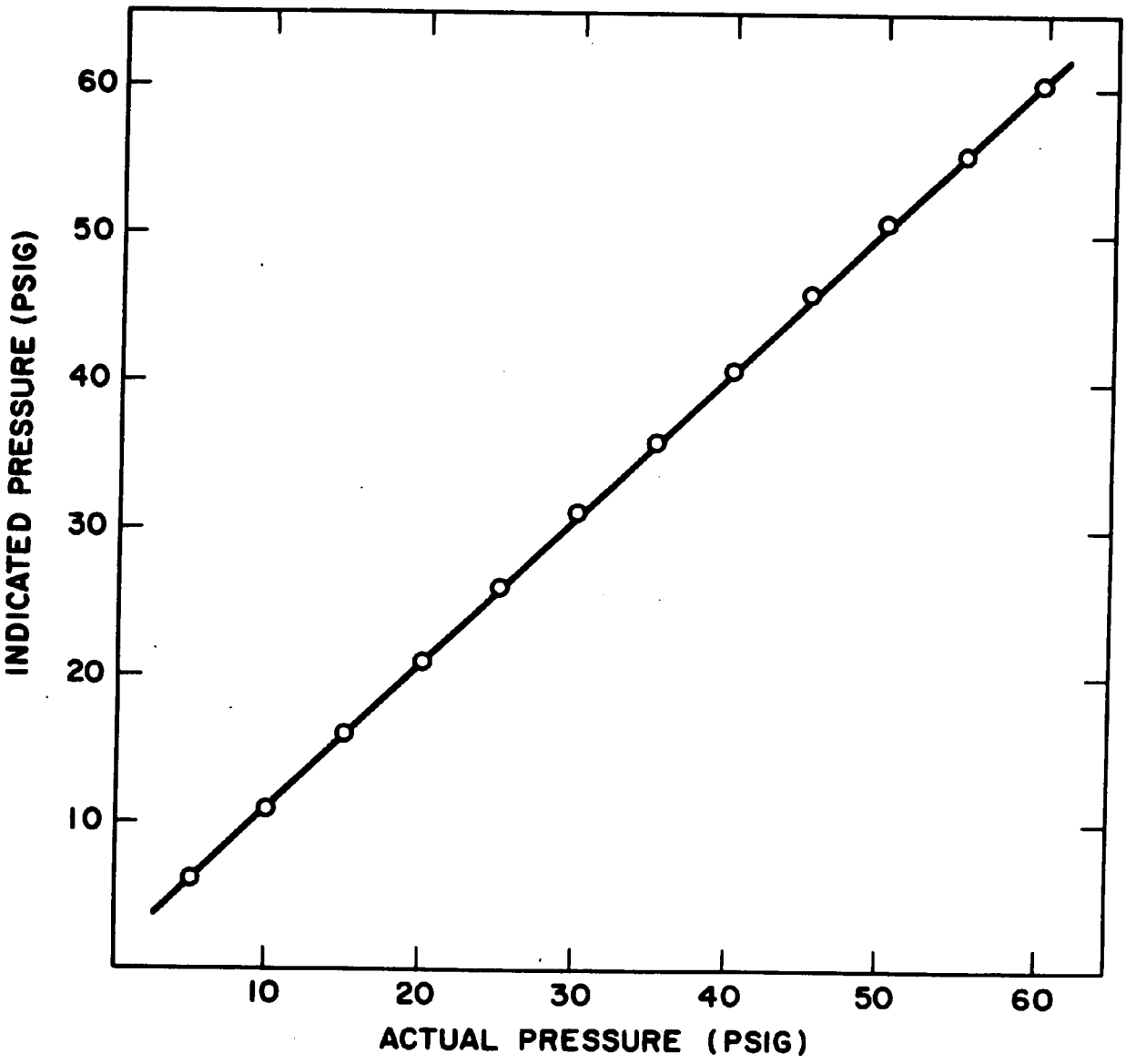


Fig. 58. Calibration curve for pressure gage.

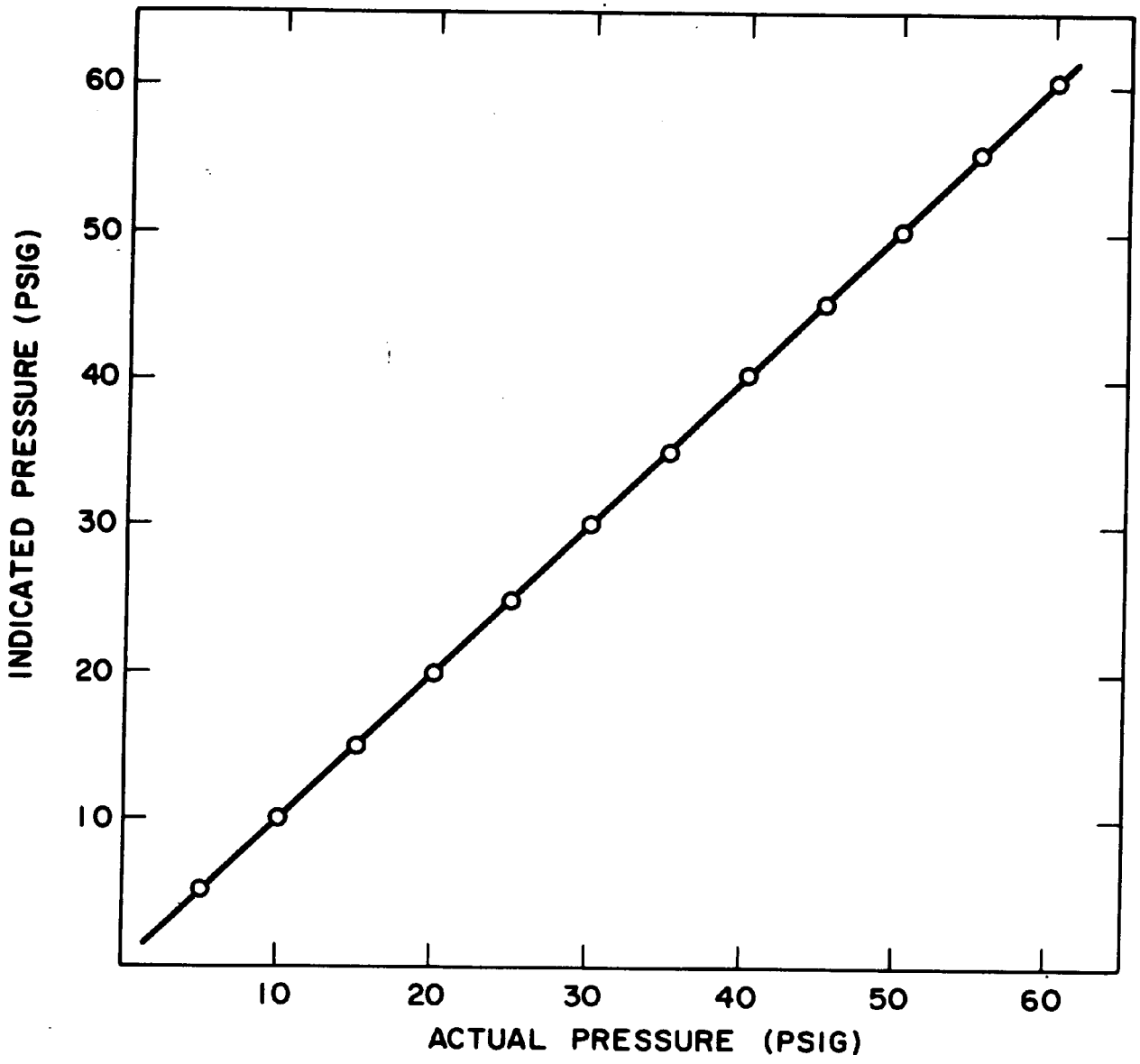


Fig. 59. Calibration curve for pressure gage.

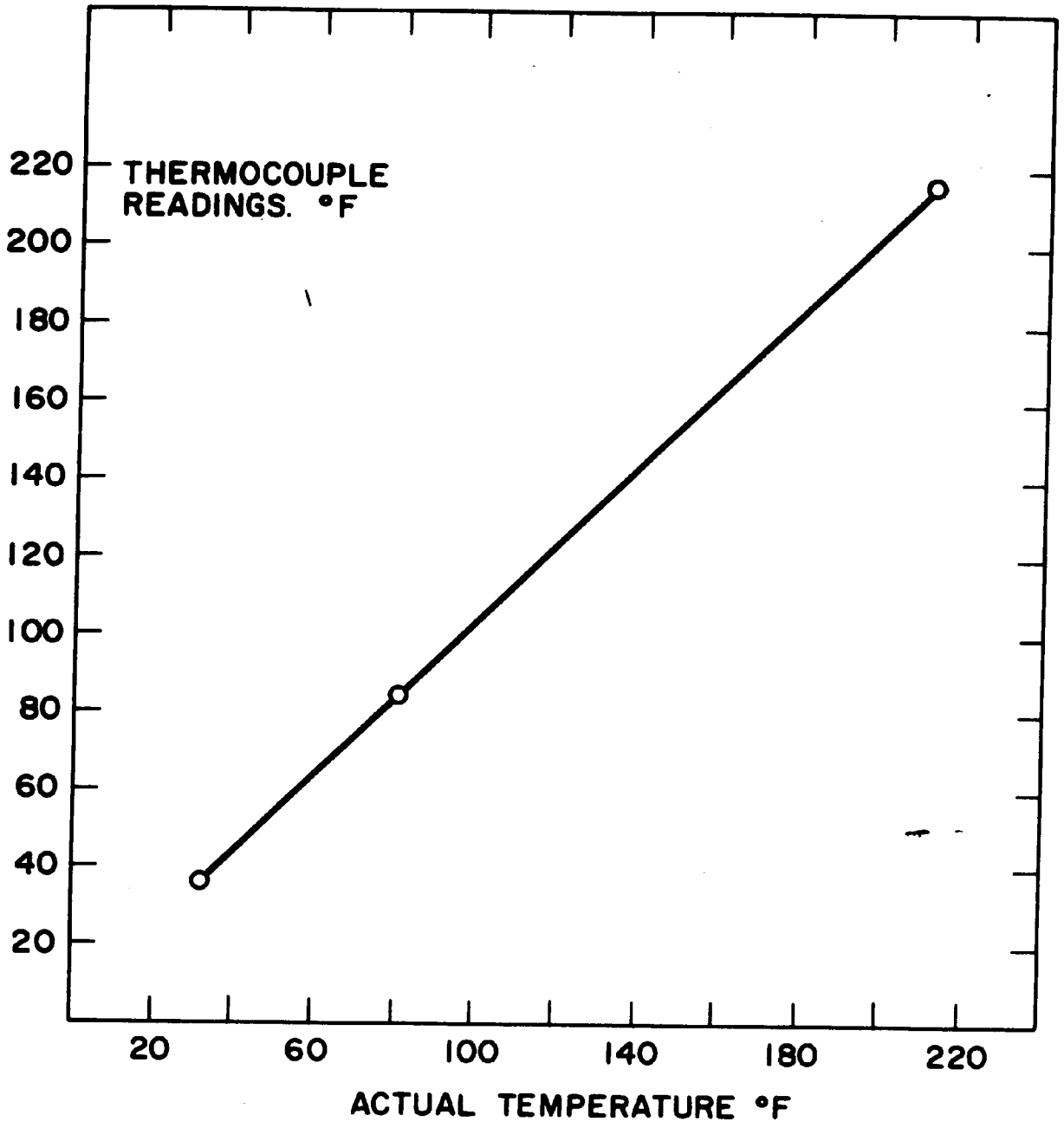


Fig. 60. Calibration curve for iron-constantan thermocouples.

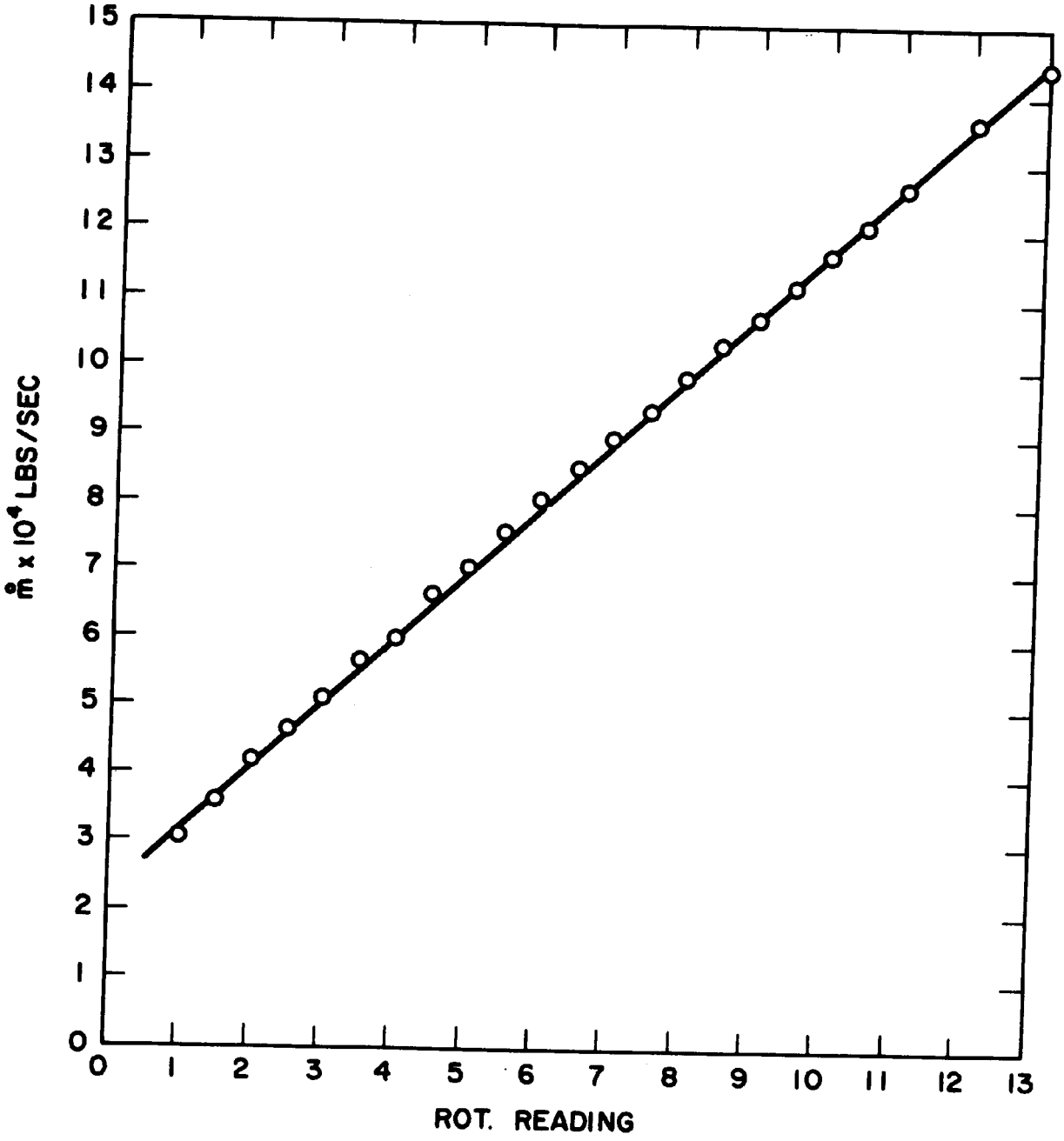


Fig. 61. Calibration curves for rotameter.

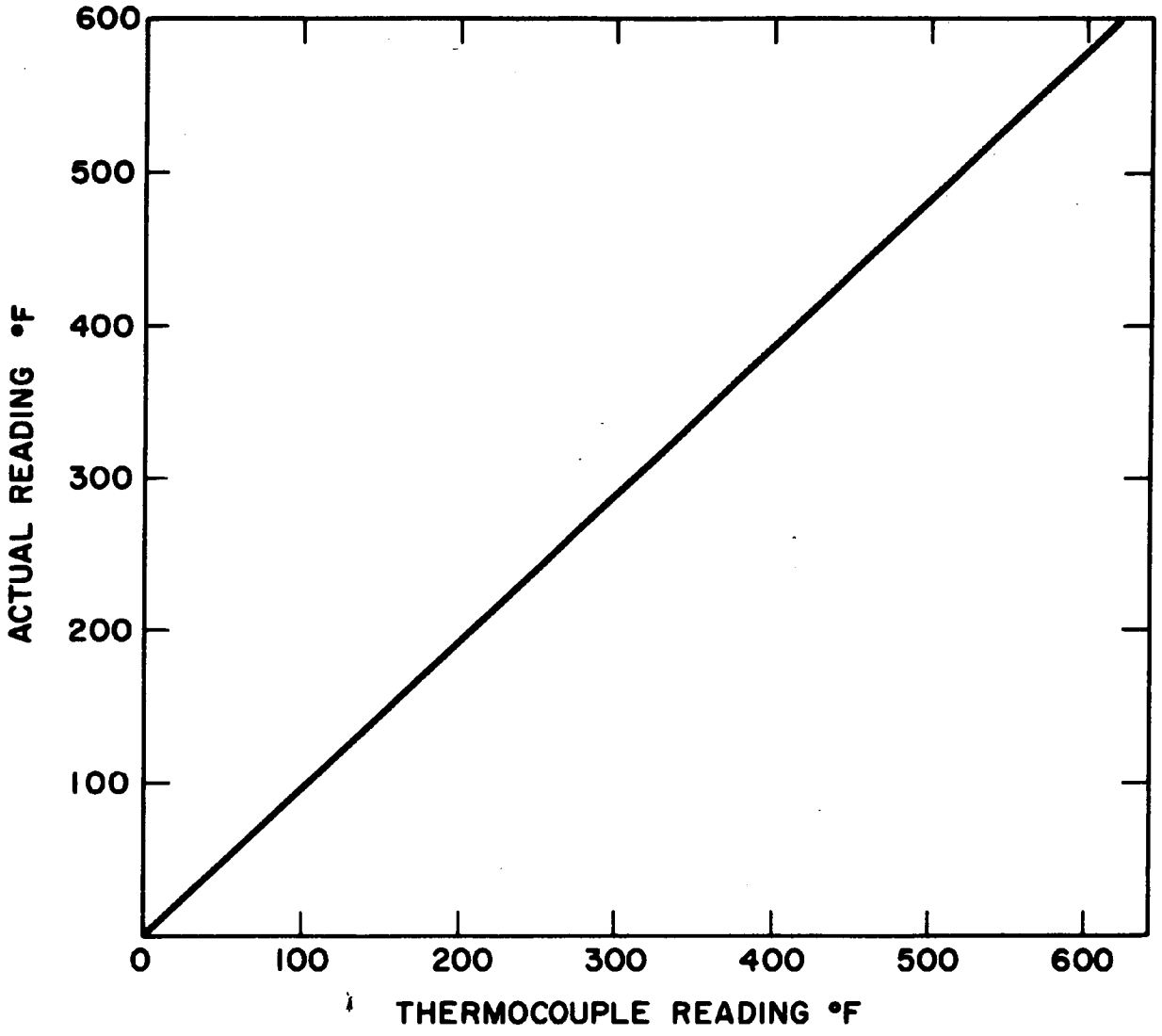
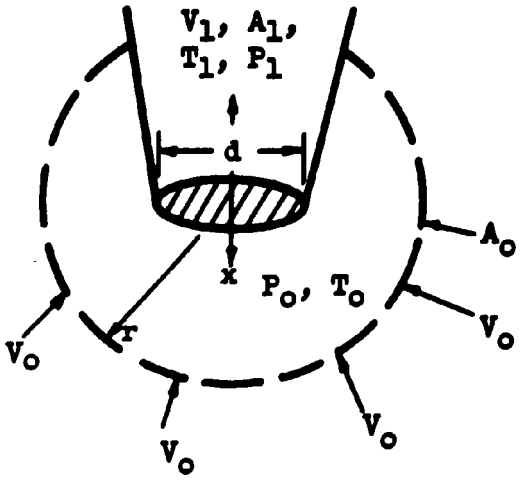


Fig. 62. Calibration curve for iron-constantan thermocouple used to measure plate temperature.

APPENDIX D

LOCATION OF SAMPLING REGION WITH RESPECT TO PROBE TIP

x(mm)	t(sec)	V_1/V_o	P_1/P_o	T
0	0	300	1	T_o
-0.05	-10^{-5}	4	1	T_1



By assuming that the gas sample is collected from a sphere around the probe tip, the relative location of the sampling region can be determined by the use of the values obtained by Fristrom[53] for the velocity, pressure and temperature in this region and tabulated above.

From the continuity equation

$$\rho VA = \text{constant}$$

and the gas law

$$P = \rho RT$$

The area of the sphere will be equal to

$$A_o = \frac{P_1}{P_o} \cdot \frac{T_o}{T_1} \cdot \frac{V_1}{V_o} \cdot A_1$$

Since $T_1 = T_o$,

$$4\pi r^2 = \frac{300}{4} \cdot \frac{\pi}{4} d^2$$

$$r \cong 2d$$

As $d < 0.001$ in.

then, r is about 0.002 in.

This shows that the sample taken by the probe is from a region within a distance of about 0.002 in. from the probe tip.

APPENDIX E

CHOICE OF SAMPLING PROBE

A sampling probe which showed the highest propane concentration near the plate, for a fixed mixture ratio, compared to a sample without the flame was rated best.

For such a test the results are shown below.

	Propane Peak Height, in.	Plate Temperature, °R
No flame	10.2	680
With flame	8.55	805

Since the probe tip was located approximately 0.001 in. from the wall surface, the difference between the peak heights is largely the result of the drop in propane concentration due to the presence of the flame reactions, as indicated in Figs. 12-35.

REFERENCES

1. Andersen, J. W., and R. S. Fein. "Measurements of Normal Burning Velocities and Flame Temperatures in Bunsen Flames." Journal of Chemical Physics, 17, 1949.

2. Becker, J. W., and W. L. Hull. "Mechanism of Surface Ignition in Internal Combustion Engines." SAE, January 11-15, 1965.

3. Belles, F., and A. L. Berlad. "Chain Breaking and Branching in the Active Particle Diffusion Concept of Quenching." NACA TN 3409, 1955.

4. Belles, F., and C. Swett. "Ignition and Flammability of Hydrogen Fuels." NACA Report 1300, 1956.

5. Belles, F. "Chemical Action of Halogenated Agents in Fire Extinquishing." NACA TN 3565, 1955.

6. Berlad, A. L., and A. E. Potter. "Relation of Boundary Velocity Gradient and Flash-back to Burning Velocity and Quench Distance." Combustion and Flame, 1, No. 1, 127+, 1954.

7. Boys, S. F., and J. Corner. "The Structure of the Reaction Zone in a Flame." Proceedings of Royal Society, A197, 1949.

8. Broeze, J. J. "Theories and Phenomena of Flame Propagation." Third Symposium on Combustion, 1949.

9. Daniel, W. "Wall Quenching in an Internal Combustion Engine." Sixth Symposium on Combustion, 1956.

10. Daniel, W. A., and J. T. Wentworth. "Exhaust Gas Hydrocarbons, Genesis, and Exodus." GMC, 1962.

11. Dugger, G. L., D. Simon, and M. Gersten. "Laminar Flame Propagation." NACA Report 1300, 1959.

12. Egerton, A., and D. Sen. "The Influence of Pressure on the Burning Velocities of Flat Flames." Fourth Symposium on Combustion, 1953.

13. Egerton, A., and S. Thabet. "Flat Flame." Proceedings of the Royal Society, A211, 445, 1952.

14. Fine, B. "The Flashback of Laminar and Turbulent Burner Flames at Reduced Pressure." Combustion and Flame, 2, No. 3, 253-266, 1958.

15. Friedman, R. "Quenching of Laminar Oxy-Hydrogen Flames by Solid Surfaces." Third Symposium on Combustion, 1949.

16. Friedman, R. "The Wall-Quenching of Laminar Flames as a Function of Pressure, Temperature, and Air-Fuel Ratio." Journal of Applied Physics, 21, No. 8, 795-797, 1950.

17. Friedman, R. "Measurements of Temperature Profile in a Laminar Flame." Fourth Symposium on Combustion, 1953.

18. Friedman, R.,and R. Cyphers. "Gas Sampling in a Low-Pressure Propane-Air Flame." Journal of Chemical Physics, 23, No. 10, 1875-1880, 1955.

19. Friedman, R., and W. Johnston. "Pressure Dependence of Quenching Distance." Journal of Chemical Physics, 20, No. 5, 1952.

20. Fristrom, R. M., W. H. Avery, and C. Grunfelder. "Reactions of Simple Hydrocarbons in Flame Fronts: Microstructure of C_2 Hydrocarbon-Oxygen Flames." Seventh Symposium on Combustion, 1958.

21. Fristrom, R. M., R. K. Neumann, R. Prescott, and W. H. Avery. "Temperature Profiles in Propane-Air Flame Fronts." Fourth Symposium on Combustion, 1953.

22. Fristrom, R. M. "Chemical Evolution of the Combustion Process." Experimental Methods in Combustion Research. AGARD. Pergamon Press, 1961.

23. Gottenberg, W. G. "Reaction Rate and Surface Area Effect on the Hydrocarbon Content of the Combustion Products of a Spark Ignition Engines." Ph.D. Thesis, Yale University, 1958.

24. Harris, M. W., J. Grumer, G. Von Elbe, and B. Lewis. "Burning Velocities, Quenching and Stability Data on Non-Turbulent Flames of Methane and Propane with Oxygen and Nitrogen." Third Symposium on Combustion, 1949.

25. Hass, G. C. "The California Motor Emission Standards." California Department of Public Health. Berkley, California, 1960.

26. Heaton, W. B., and J. T. Wentworth. "Exhaust Gas Analysis By Gas Chromatography Combined with Infrared Deflection." Analytical Chemistry, 31, 349, 1957.

27. Heimel, S. "Effect of Initial Mixture Temperature on Burning Velocity of Hydrogen-Air Mixtures with Preheating and Stimulated Preburning." NACA TN 4156, 1957.

28. Hilpert, R. Forschung auf dem Gebiete des ingenieur wesens, 1933, p. 215.

29. Hirshfelder, J. O., and C. F. Cortiss. "Theory of Propagation of Flames." Third Symposium on Combustion, 1949.

30. Jackson, M. W. "Analysis for Exhaust Gas Hydrocarbons, Nondispersive Infrared versus Flame Ionization." ISA meeting, New York, October, 1962.

31. Jackson, M. W., W. M. Wiese, and J. T. Wentworth. "The Influence of Air-Fuel Ratio, Spark Timing, and Combustion Chamber Deposits on Exhaust Hydrocarbon Emissions." GMC, 1962.

32. Kaskans, W. Personal contact.

33. Klaukens, H., and H. G. Wolfhard. "Measurements in the Reaction Zone of a Bunsen Flame." Proceedings of the Royal Society (London), A193, 512-524, 1948.

34. Klein, G. "Report on Flame Propagation." Transaction of Royal Society, A249, 389, 1957.

35. Lewis, B. and G. Von Elbe. "Theory of Ignition, Quenching and Stabilization of Flames of Non-Turbulent Gas Mixture." Third Symposium on Combustion, 1953.

36. Linnett, J. W. "Methods of Measuring Burning Velocities." Fourth Symposium on Combustion, 1953.

37. Lowell, W. G. "Relation of Reactive Components of Gasoline to the Production of Photochemical Smog." Los Angeles County Air Pollution Control District, April 8, 1958.

38. Manson, N. "Effect of Pressure on Fundamental Burning Velocity in Gaseous Mixture." Fuel, Vol. XXXII, 186-195, 1953.

39. Minskoff, G. J., and C.F.H. Tipper. "Chemistry of Combustion Reactions." Butterworth Scientific Publications.

40. Mirsky, W., et al. "A Study of the Relation of Combustion to the Emission of Atmospheric Contaminants." Progress Report No. 2, March, 1963, ORA, The University of Michigan.

41. Mirsky, W., G. Van Wylen, and A. Gad El-Hawla. "A Study of the Relation of Combustion to the Emission of Atmospheric Contaminants." Progress Report No. 3, 1964, ORA, The University of Michigan.

42. Myers, P. S., O. A. Uyehara, J. E. Bennethum, and U. D. Overbye. "Unsteady Heat Transfer in Engines." SAE Summer Meeting, June 5-10, 1960.

43. Potter, A. E. and A. L. Berlad. "Effect of Surface Geometry on Quenching Distance." Fifth Symposium on Combustion, 1955.

44. Potter, A. E., and A. L. Berlad. "A Thermal Equation for Flame Quenching." NACA Report 1264, 1956.

45. Potter, A. E., and A. L. Berlad. "A Relation Between Burning Velocity and Quenching Deistance." NACA TN 3882, 1956.

46. Potter, A. E., and A. L. Berlad. "The Quenching of Flames of Propane-Oxygen Argon, Propane-Oxygen-Helium Mixtures." Journal of Physical Chemistry, 97, 1956.

47. Potter, A. E., and A. L. Berlad. "The Effect of Fuel Type and Pressure on Flame Quenching." Sixth Symposium on Combustion, 1957.

48. Shinn, J. N., and D. R. Olson. "Some Factors Affecting Unburned Hydrogens in Combustion Products." SAE Preprint 146, June, 1957.

49. Simon, D. and F. Belles. "An Active Particle Diffusion Theory of Flame Quenching for Laminar Flames." NACA RM E51 L18, 1952.

50. Simon, D. M. "Flame Propagation. III. Theoretical Considerations of the Burning Velocites of Hydrocarbons." Journal of the American Chemical Society, 73, No. 1, 422-425, 1951.

51. Tanford, C. "Theory of Burning Velocity." Journal of Chemical Physics, 15, No. 7, 433-439, 1947.

52. Van Karman, T., and G. Millan. "Thermal Theory of a Laminar Flame Front Near a Cold Wall." Fourth Symposium on Combustion, 1953.

53. Westenberg, A. A., S. P. Raeser, and R. M. Fristrom. "Interpretations of the Sample Taken by a Probe in a Laminary Concentration Gradient." Combustions and Flame, 1, 467-478, 1957.

54. Wohl, Kurt. "Quenching, Flashback, Blow-Off Theory and Experiment." Fourth Symposium on Combustion, 1953.